2007-03-26

Statnamic Lateral Loading Testing of Full-Scale 15 and 9 Group Piles in Clay

Rick Davon Broderick
Brigham Young University - Provo

STATNAMIC LATERAL LOADING TESTING OF FULL-SCALE 15- AND 9- GROUP PILES IN CLAY

by

Rick D. Broderick

A thesis submitted to the faculty of

Brigham Young University

in partial fulfillment of the requirements for the degree of

Master of Science

Department of Civil and Environmental Engineering

Brigham Young University

April 2007

BRIGHAM YOUNG UNIVERSITY

GRADUATE COMMITTEE APPROVAL

of a thesis submitted by

Rick D. Broderick

This thesis has been read by each member of the following graduate committee and by majority vote has been found to be satisfactory.

Date	Kyle M. Rollins, Chair
Date	T. Leslie Youd
Date	Norman L. Jones

BRIGHAM YOUNG UNIVERSITY

As chair of the candidate's graduate committee, I have read the thesis of Rick D. Broderick in its final form and have found that (1) its format, citations, and bibliographical style are consistent and acceptable and fulfill university and department style requirements; (2) its illustrative materials including figures, tables, and charts are in place; and (3) the final manuscript is satisfactory to the graduate committee and is ready for submission to the university library.

Date

Kyle M. Rollins
Chair, Graduate Committee

Accepted for the Department

E. James Nelson
Graduate Coordinator

Accepted for the College

Alan R. Parkinson
Dean, Ira A. Fulton College of Engineering and Technology

ABSTRACT

STATNAMIC LATERAL LOADING TESTING OF FULL-SCALE

15- AND 9- GROUP PILES IN CLAY

Rick D. Broderick

Department of Civil and Environmental Engineering

Master of Science

Studies of seismic and impact loading on foundation piles is an important and a focused interest in the engineering world today. Because of seismic and other natural events are unpredictable, uncontrollable and potentially unsafe it is a vital study to understand the behavior and relationship structures in motion have on there foundation. Statnamic Loading has become a popular method of studying this relationship in a controlled environment.

Two groups of 9 and 15 driven hollow pipe piles were tested in saturated clay at the Salt Lake City Airport in July of 2002. The 9-pile group (3x3 configuration) was separated at 5.65 pile diameters and the 15-pile group (3x5 configuration) was separated at 3.92 pile diameters. The testing consisted of five target deflections. Each target

deflection consisted of 15 cyclic lateral static loadings and a 16th lateral statnamic load. This study focuses on the statnamic loading.

Damping ratios ranged from 23 to 50 percent for the 15-pile group and 29 to 49 percent for the 9-pile group. Both pile groups increased in damping as the deflections increased. The optimized mass in motion for the entire system was found to be roughly 21,000kg for the 15-pile group and 14,000 kg for the 9-pile group. Stiffness for the 15-pile group started at 50kN/mm and ended at 21kN/mm. The 9-pile group ranged from 28kN/mm to 12kN/mm.

ACKNOWLEDGMENTS

I am grateful to Dr. Kyle Rollins for giving me the opportunity to be part of the research project and team. I highly regard Dr. Rollins as patient, insightful, and outgoing. At times when I could not see myself finishing this thesis, Dr. Rollins was there to help me see the end and renew my commitment.

I would like to also give special appreciation to Dave Anderson for his excelling, perfect, and positive support for the equipment setup, testing, and traveling.

I want to also give special thanks to Jeff Snyder, Rob Johnson, Luke Hales, Travis Gerber, and all the rest of the team members, professors, and staff for their friendship, time, incite, photos, and software support. I wish to thank Dr. Youd and Dr. Jones for their willingness to be part of the committee and give insightful suggestions.

I would like to express my gratitude to the National Science Foundation for funding the majority of the Project. Also, a special appreciation to Belcho, Inc., Harper Cement, Inc., Burbridge Cement Pumping and all other companies for donating their time and material in setting up the project. I also give appreciation to the Salt Lake City Airport Authority for providing the site.

Most importantly, I am eternally grateful for my family. My wife, Melinda, definitely deserves this accomplishment more than me. She has been my backbone to obtaining my goals and taking care of my three lovely daughters, Jenna, Mindy and Brittany. I am also grateful to my extended family for always believing in me.

TABLE OF CONTENTS

LIST OF TABLES

LIST OF FIGURES

CHAPTER 1 INTRODUCTION

The world today has been awakened to the importance of structural stability in lateral loads from recent events like 9/11 earthquakes, hurricanes, and other events. Lateral loads are not just impact loads or explosions, but commonly occur as earthquakes, wind, soil instability, and ocean wave loadings. Each loading varies with time. Analyses of structural responses from these lateral loads are significantly improving with the help of measured data from actual events and from research studies. For only the last few decades, piles have been studied with lateral loads under static loads. However, only in the last decade have pile lateral load tests been loaded at the rate of impacts or earthquake loads. By the recent method of STATNAMIC testing, we are now able to study how piles react with dynamic lateral loads.

1.1 Explanation of Statnamic Testing

In October 1994, North Carolina Department of Transportation performed the first lateral Statnamic tests. Since then, Brigham Young University, Auburn University, and other institutions throughout the world have used this innovative method of testing foundation piles (see Figure 1.1)(Johnson, S.R., 2003a).

This new method is rapidly replacing the static lateral load test. Poulos stated that statnamic testing has several advantages, including but not limited to (Poulos, 2000):

1. the test is quick and easily mobilized
2. high loading capacity is available
3. the loading is accurately centered and can be applied to both single piles and pile groups
4. the test does not require any pre-installation of the loading equipment
5. it can be adapted to apply lateral loading
6. the test is quasi-static, and does not involve the development of potentially damaging compressive and tensile stresses in the test pile
7. the test can be carried out on both uninstrumented and instrumented piles
8. the load is measured via a calibrated load cell and does not rely on pile material and cross-section properties.

Figure 1.1: Lateral Statnamic testing (S.R. Johnson, 2003a).

Past investigators have studied how Statnamic testing affect single piles; however, piles are often grouped together to support the column point loadings. It has been

observed that piles that are grouped with six diameter lengths or less apart react differently and with less resistance (Egbert, 2001). Lateral pressures that are normally dissipated through the soil tend to "shadow" each other, thus increasing soil pressures (Olsen, 2001). This shadowing effect reduces the load capacity that a single pile can support (see Figure 1.2).

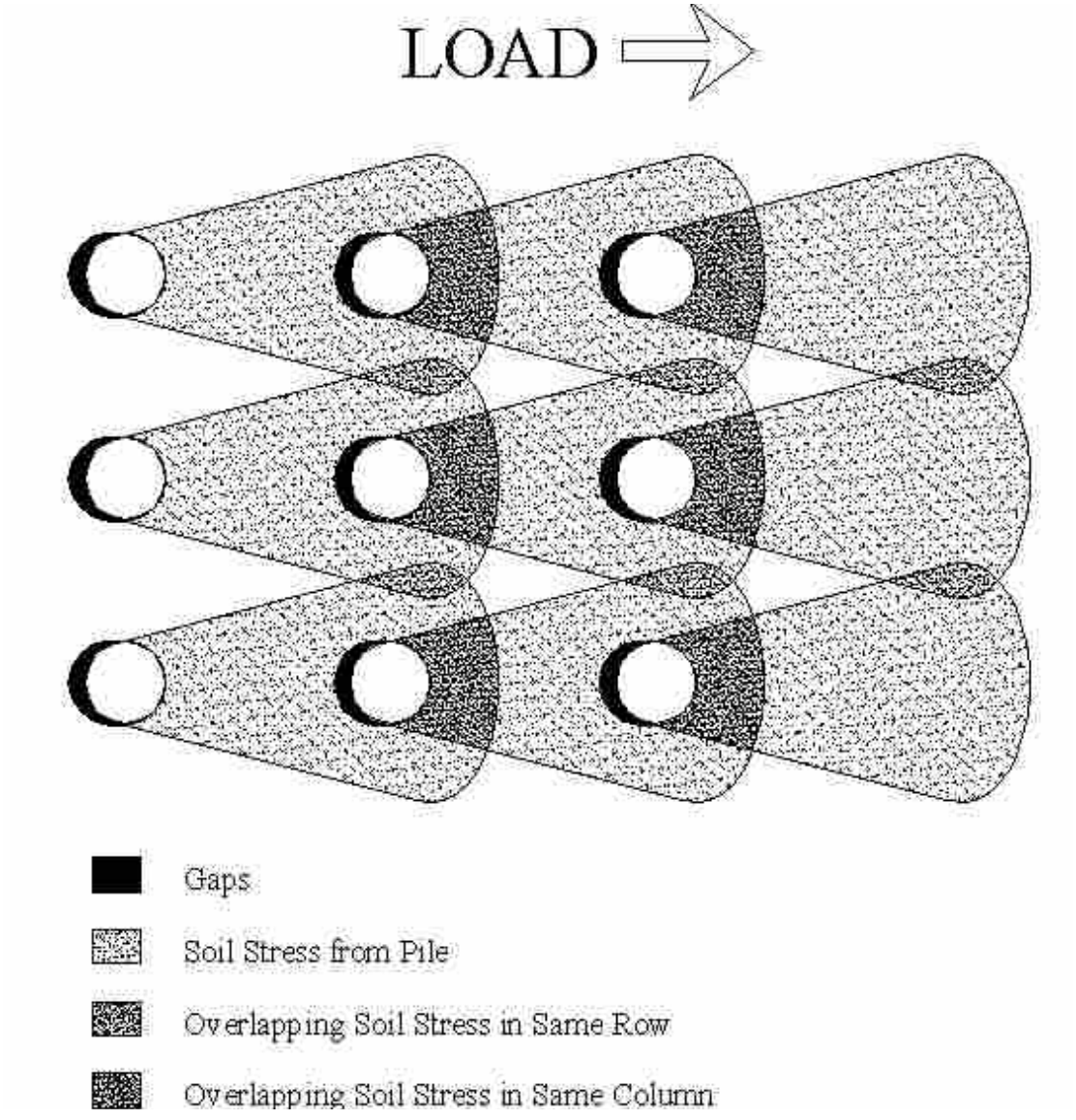

Figure 1.2: Shadow effects.

When the pile rows are close together, the soil stress region and the gaps that form in the leading rows tend to overlap. If the spacing between adjacent piles in a row is too close, the soil stress region will also overlap. Thus, the increase of stress in the overlapped regions reduces soil resistance to each pile. Studies are greatly needed to understand this shadowing affect on soils and how piles deflect when dynamically loaded.

This thesis is part of Dr. Kyle Rollins' research at Brigham Young University of static and statnamic lateral load tests performed in the summer of 2002 at the Salt Lake City Airport (see Figure 1.3)(Johnson, S.R., 2003). The driven foundation piles were closed ended 12 inches in diameter. Two groups of 3 X 5 at 4.2 diameter row spacing and 3 X 3 at 6 diameter row spacing were tested separately. The column spacing for each pile group was 3.5 diameters.

1.2 Objective and Scope of Research

The objectives of this thesis are three fold. First, to create an idealized model that will accurately calculate the response of cyclically loaded pile groups of 3 X 5 and 3 X 3 when under dynamic loads. The Unloading Point Method, Linear Acceleration Method, Central Difference Method, and Force Equilibrium were direct numerical methods used and compared to determine the actual response. In order to accurately model the measured motion these numerical methods require a correct mass, damping coefficient, and static stiffness of the system.

The second objective stems from the first objective; obtain accurate damping ratios for future piles of 3 X 5 at 3.92 diameter row spacing and 3 X 3 at 5.65 diameter row spacing and in clay soil. Without testing, past damping ratio estimates have not been

accurately obtained. With correct and measured damping ratios, future engineering projects in similar will be able to use these ratios to correctly predict the response of the structure.

The third main objective of this study is to be able to predict stiffness coefficients from statnamic testing. The calculated stiffness coefficients will be compared to the stiffness obtained from the last static test performed prior to the dynamic load.

An accurate prediction of mass, stiffness, damping and other properties of the tested 15- and 9-pile groups should be valuable to future analyses. These analyzed structures may be designed using findings from this study to prevent fatigue and other forms of failure.

Figure 1.3: Site location (S.R. Johnson, 2003a).

CHAPTER 2 LITERATURE REVIEW

For statnamic lateral loading effects on piles, several factors should be understood and researched before analyzing or making any conclusions. Some of the factors that are involved include but are not limited to:

1) group effects compared to single pile effects
2) elastic and plastic properties of the pile-soil interaction
3) linearity verses nonlinearity of the system
4) static, statnamic, and dynamic loadings and their differences
5) modeling techniques
6) optimization techniques
7) damping and inertial affects
8) methods to obtain damping ratios

Analysis of dynamic effects of laterally loaded piles may be pursued in several ways. Three common ways are full-scale testing, small-scale testing, and finite element modeling. In this chapter these three testing methods are reviewed and important findings and research are also noted. Before these methods are researched, a brief history and concept of statnamics is given.

2.1 History and Concept of Statnamic

2.1.1 "STATNAMIC: The First Ten Years"—Bermingham, P.D. (2000)

Statnamic testing was developed for several reasons. A large contributing factor was from imperfections in dynamic testing. Dynamic axial load testing has an inability to mobilize a pile or foundation that has been driven to refusal or cast in place. Cost was an additional factor. In 1988, the average cost for static axial testing was 100 dollars per ton. Also in this time era, drilled shafts capacities were increasing to support the large structures being developed. The largest axial test in the United States at the time was a 1200 ton test and only a few axial tests reached 2000 tons throughout the world.

The history of Statnamic testing is very young. The concept began in Hamilton, Canada in 1985 and was proposed for the first time in 1986. In 1988, Berminghammer and TNO improved the concept and created the first small model. Instead of dropping a large mass onto the foundation and risking damage to the pile, a mass reacted with the foundation by pushing the mass off and upward. This small model was able to develop a peak load of 5 tons in 30 ms.

Berminghammer and TNO studied this new loading method for several years, Statnamic axial load tests and Static axial load tests were performed on the same pile or adjacent piles and compared. Predictions were avoided for these first several tests until a wide rage of test results were obtained. The loading sequence was noticed to have an affect on test results. It was also observed that the peak deflection would occur after the peak load was reached or when the statnamic device was unloading. This was the case for all soils except for stiff piles on rock. The velocity was zero at the peak deflection and the pile would begin to rebound. These observations led to the Unloading Point

Method by Middendorp in 1992. The Unloading Point Method is a simple method that calculates stiffness of the static resistance of the pile; this method is more fully considered under statnamic lateral loading conditions in Chapter 7.

Statnamic testing entered the market in 1992. With this new testing technique, foundation tests could be performed over water and at angles. This new method allowed accurate testing for conditions where foundations could not be tested previously. The ability to test at different angles led to the idea of performing statnamic lateral load tests on deep foundations. In 1994, the Federal Highways Administration performed the first lateral statnamic loading tests in the United States. Since that year, several institutions have studied this lateral loading method. Most studies have been with single piles and very few tests were performed where group effects were a factor.

2.2.2 Statnamic Concept—"Pyrotechnics and the Accurate Prediction of STATNAMIC Peak Loading and Fuel Charge Size"—Bermingham, P. and White, J. (1995)

Mechanical, fluid, and pyrotechnics are common ways to create dynamic reactions for testing piles. Statnamics is form of pyrotechnic tests. Magnitude of displacement, period, and characteristic shape of preloading curve are the common parameters determined from dynamic reactions. The parameters are determined by the initial volume of the chamber, type of fuel, amount of fuel, projectile mass (reaction mass), and venting distance (muzzle length for a gun). Common pyrotechnic loading methods are blast loading (gun powder), rocket loading, and now statnamic loading.

The control parameters are significantly different between guns, rockets, and statnamics (Figure 2.1).

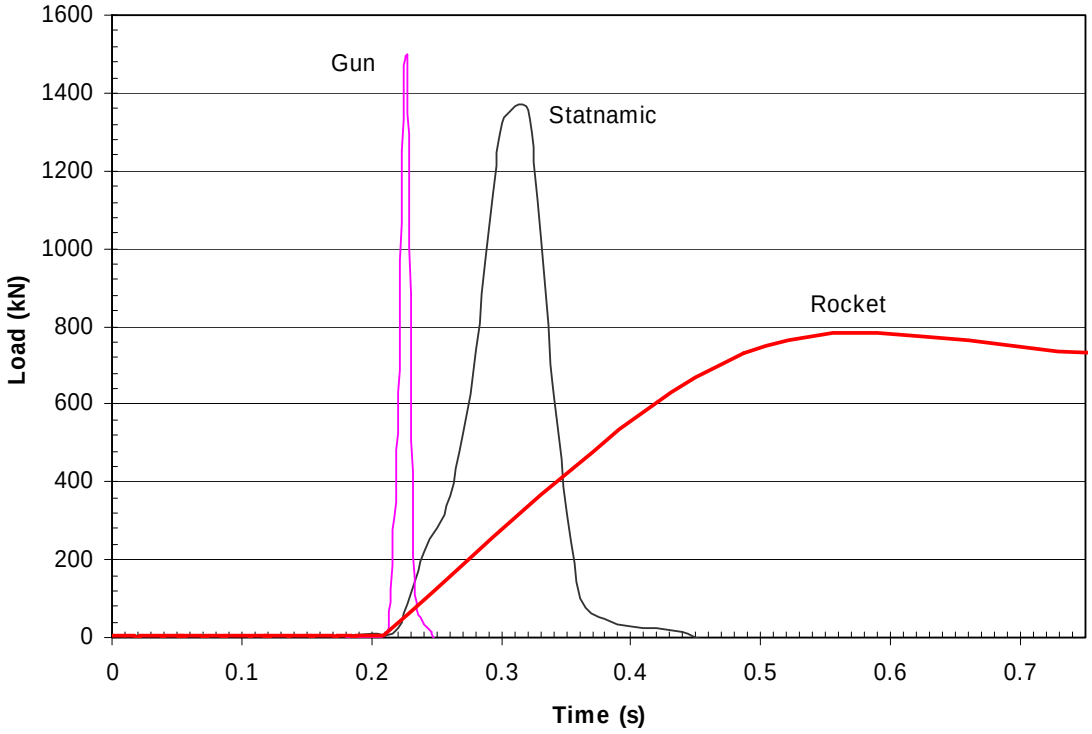

Figure 2.1: Loading rate for a gun, statnamic, and a rocket.

Gun powder has the benefit of creating a pulse force, yet burns too quickly. This method is mainly for blast testing and not for impact or earthquake loading, because the rate of loading is highly unpredictable. Rockets commonly use a fuel of ammonium perchlorate which produces more predictable forces and burns more slowly. The loading characteristic of a rocket can be slower than an impact load or a peak earthquake load. Additionally, the rocket will continue to load until the fuel is entirely burned. Statnamic testing uses the strengths of both the gun and rocket loading characteristics; the load is a pulse load that uses ammonium perchlorate as the fuel.

To use the ammonium perchlorate most effectively, the fuel is made into small pellets (Figure 2.2). Each individual pellet is perforated to allow constant thorough

burning at the exposed surface (Figure 2.3). Because the pellets are small, several pellets are used for a statnamic test, thus imperfections may be averaged out.

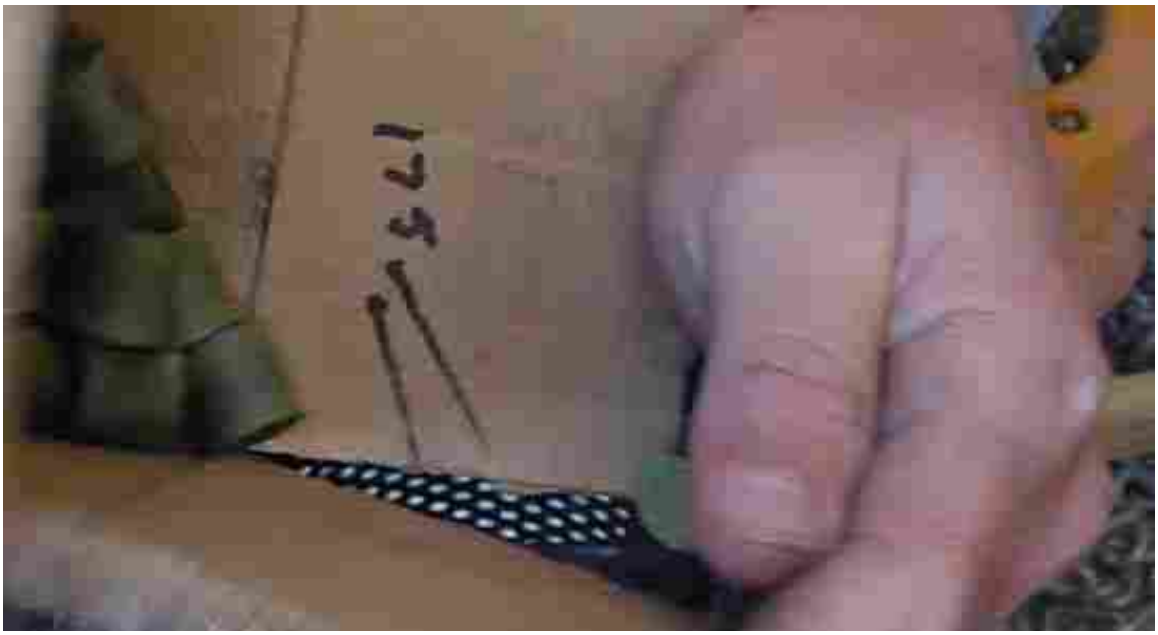

Figure 2.2: Ammonium perchlorate fuel pellets.

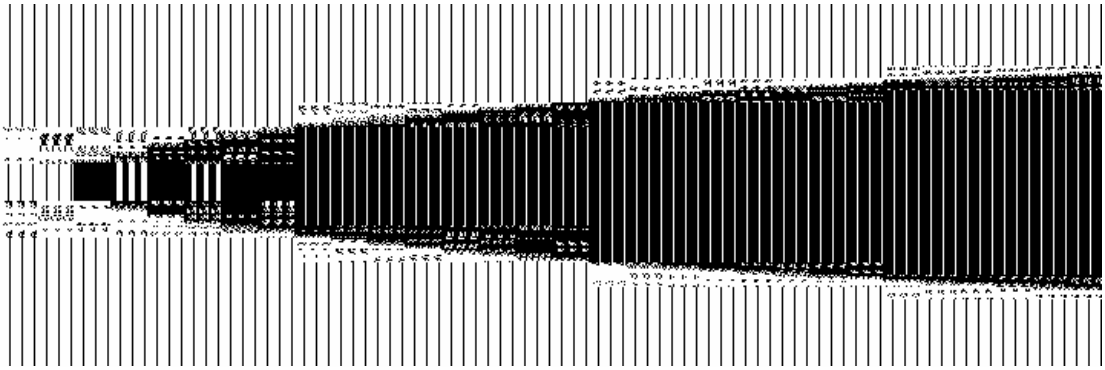

Figure 2.3: Statnamic fuel pellet surface area in burning process.

The fuel pellets also have several safety advantages:

- The pellets will not ignite from a spark, friction, or agitation.
- When the fuel does ignite, it is slow and easily controlled.

- Water may be used to extinguish the ignited fuel.
- The fuel is easily transported.
- The pellets store well for long periods of time.

Prior to testing, a controlled and accurate prediction may be used to target a desired maximum force or displacement. Because initial volume is fixed and fuel pellets are the only type of pellets used, only three major parameters remain to target the desired force:

- amount of fuel
- reaction mass
- venting distance

By principles of physics, these parameters are readily obtainable. This research will not go into the detail of how these parameters are calculated.

2.2 Case Studies in Statnamic and Dynamic Lateral Loading

2.2.1 "An Analytical Study on Statnamic Lateral Pile Testing"—Tsubakihara, Yasumori, et. al. (1995)

A common possible method of analyzing statnamic lateral loads is by Finite Element Modeling (FEM). Tsubakihara et. al. presented a method using three-dimensional FEM for predicting the static load-defection relation from statnamic lateral load test of a single pile. A statnamic lateral load test in October 1994 was used to compare and modify FEM used. The test was part of the Neuse River Bridge foundation load test program at New Bern, North Carolina. The in-situ pile was a concrete pile that was reinforced by a steel casing. The diameter of the pile was 0.61 m (24 in) with a depth to 11.3 m. The soil consisted of sand to a depth of 7 m and porous sandstone

beyond the 7 m depth. The groundwater was at approximately a depth of 1 m. Static lateral load testing and Statnamic *vertical* load testing were performed prior to the statnamic *lateral* load testing. The lateral Statnamic tests were performed in the opposite direction from the static lateral load tests. Three statnamic lateral load tests were performed. The last statnamic test was used for comparing the finite element model. When modeling the pile soil interaction, the pile was treated as elastic and the soil as plasto-elastic. Modifying the shear modulus and shear strength of each soil layer minimized the difference between the calculated and the measured lateral displacement time histories. Tsubakihara suggested that the unloading point method is useful for vertical testing, but not for lateral load testing. This was suggested because the natural period of the pile-soil system is generally longer than the duration of the statnamic loading which makes the stress wave effects important.

Conclusions

Modifying the shear modulus and shear strength of each layer gave fairly accurate results for the calculated static stiffness-deflection curve (Figure 2.4 & 2.5). When removing the tensile stresses in the soil it was found that the ideal model matched better to the measured data.

2.2.2 "STATNAMIC lateral load response of two deep foundations"—Dan A. Brown (1998)

In 1998 Dan A. Brown from Auburn University tested a group of six prestresssed concrete square driven piles and two drilled shafts. The location of the full-scale test was at the Pascagoula River near Pascagoula, Mississippi. The depth of the river at the test site was 5.5 m below the pile head. The soil consisted of alluvial deposits made of soft to

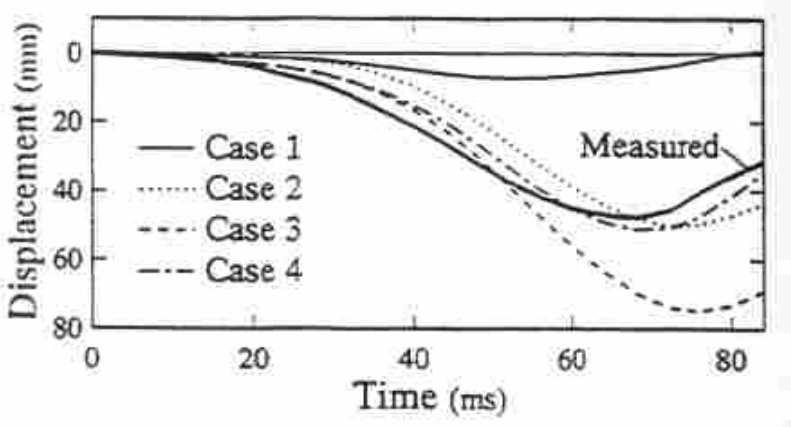

Figure 2.4: Comparison measured and calculated time histories (Tsubakihara, 1995).

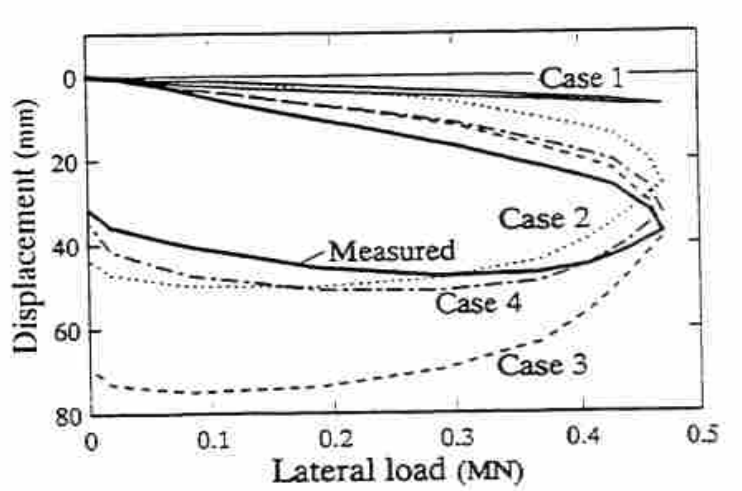

Figure 2.5: Comparison of static stiffness load-deflection curves (Tsubakihara, 1995).

stiff clays to a depth of 18 m and dense sands with layers of stiff clays from 18 to 30 m depth.

The six driven piles were in two rows with a center to center spacing of three pile widths. The sides of the piles were 0.76 m each. The group consisted of two vertical piles and four battered piles. Each corner pile was battered outwardly with a depth to

lateral displacement ratio of 4:1. The two drilled shafts were 2.1 m in diameter and spaced at three pile diameters. A pile cap 2.4 m thick connected the shafts. The shafts were loaded in the strong direction.

After the piles and shafts were loaded in static loadings five times, they were statnamically loaded in the opposite direction in five increasing load tests. The piles and shafts were fully instrumented with potentiometers, load cell, accelerometers, and strain gages.

Using the force data obtained from the load cell, a simple linear modeling of direct numerical methods was used to calculate the motion. To balance the force equilibrium equation, a constant mass, damping coefficient, and static stiffness were determined. The mass was assumed to be the mass of the pile above the ground. The damping coefficient and static stiffness were manually optimized to match a good fit to the measured motion (Figure 2.6). Derived damping ratios were observed by using the following equation:

$$\zeta = \frac{c}{2(km)^{1/2}} \tag{2.1}$$

where:

ζ = damping ratio

c = viscous damping coefficient (optimized)

k = static stiffness constant (optimized)

m = averaged constant mass (assumed)

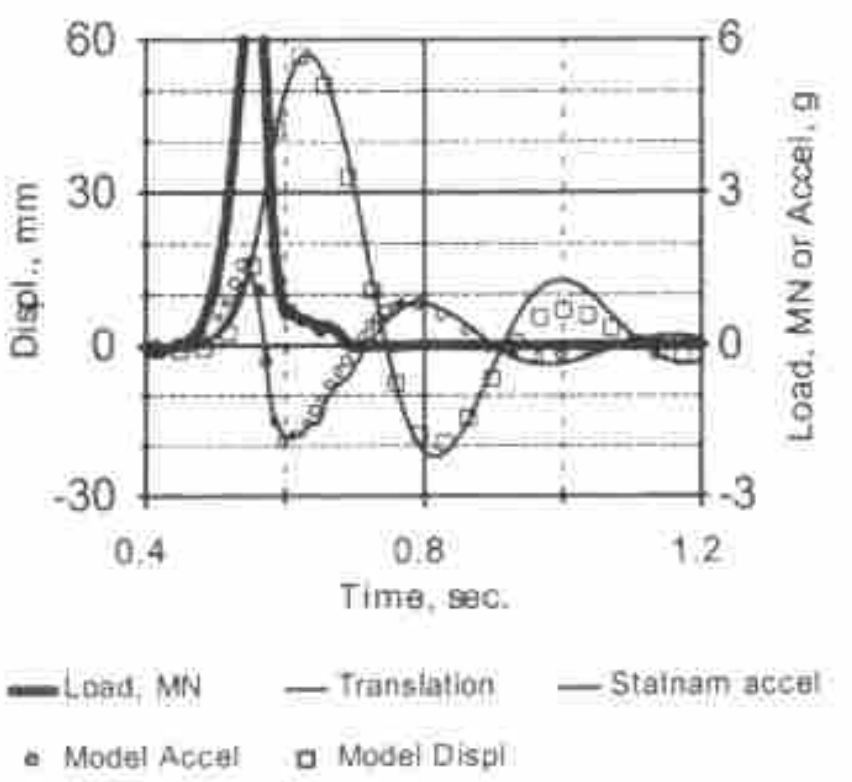

Figure 2.6: Compared measured and derived time histories of deflection and acceleration (Brown, 1998).

Conclusions

The measured motion and calculated motion matched accurately to each other. The derived damping ratios were found to be about 40 percent for the pile group and about 30 percent in the drilled shafts.

2.2.3 "Lateral STATNAMIC load testing of a pile group"—K. M. Rollins, T. J. Weaver, K. T. Peterson (1998)

In 1995 at the Salt Lake City International Airport, a three by three group of closed ended steel pipe driven piles were tested in lateral static and statnamic loadings. The soil at the site consisted of soft to medium-stiff clays and silts that was underlain by

sand. Each pile was instrumented with strain gages and load cells. The group piles were also instrumented with linear variable differential transducers (LVDT's) and accelerometers. The purpose of the test was to determine (1) if the dynamic lateral resistance would be greater or lesser than the static resistance and (2) If the static resistance results could be obtained from the results of the dynamic tests.

In order to predict the static resistance from the dynamic results, the Unloading Point Method (Middendorp, 1992) was used. To understand more about the Unloading Point Method see Chapter 7. To be able to use this method, a constant mass of the system must be determined. After analyzing different masses, the mass of the piles to a depth of five diameters and 30% of the soil weight to that depth was used for the mass of the system.

Conclusions

The results showed that statnamic (dynamic) load tests caused a significant increase of the soil resistance from 30 to 80 percent compared to the static load testing. This increase of soil resistance was caused by the addition of damping and inertial forces. The calculated static force from the Unloading Point Method matched reasonably well with the measured data in four of the five load tests. No damping coefficients were calculated. It was also recommended that additional statnamic lateral tests be performed to increase confidence in determining the static resistance.

2.2.4 "Interpretation of Lateral Statnamic Load and Two Test Results on Single Piles"—El Naggar, M. H. (1998)

Two statnamic lateral load tests at separate locations of single piles were used to optimize the response calculated by the ideal model. Each pile testing consisted of five

statnamic lateral load tests and static load tests. Two objectives were desired: 1) to simulate the pile head time histories with an ideal model and 2) to predict the static load reaction curve.

Modeling

The Modeling was based on the Winkler hypothesis. The soil and piles are divided into several layers. Each layer has two regions, the nonlinear region and the linear region (Figure 2.7). Each region is also assigned a mass (m_1, m_2).

The nonlinear region is adjacent to the pile and consists of a nonlinear spring and dashpot. To find the stiffness constant (K_{NL}), the following equation is used:

$$K_{NL} = \alpha_p K_{NS} \tag{2.2}$$

where:

K_{NL} = nonlinear stiffness constant

α_p = factor accounting for partial slippage

K_{NS} = stiffness of annular zone around the pile

The stiffness of the annular zone is dependent on several parameters. These parameters include the shear modus of the soil (G_m), Poisson's ratio of the soil (ν), inner radius (r_0) and outer radius (r_1) of the annular (nonlinear) zone. To see more about these equations see El Naggar (1998).

The linear region consists of a constant linear spring (K_L) and dashpot (C_L). The stiffness and damping coefficient are dependant on the parameters of Poisson's ratio of the soil, maximum shear modulus (G_{max}), soil shear wave velocity (V_s), frequency dependant coefficients (S_1 and S_2), and the inner radius of the annular zone (r_0).

An additional condition of the pile-soil interface conditions include formations of gaps and separations of the soil and pile while in motion. To correct for this discontinuity of motion, two actions were made to improve the modeling. The models of

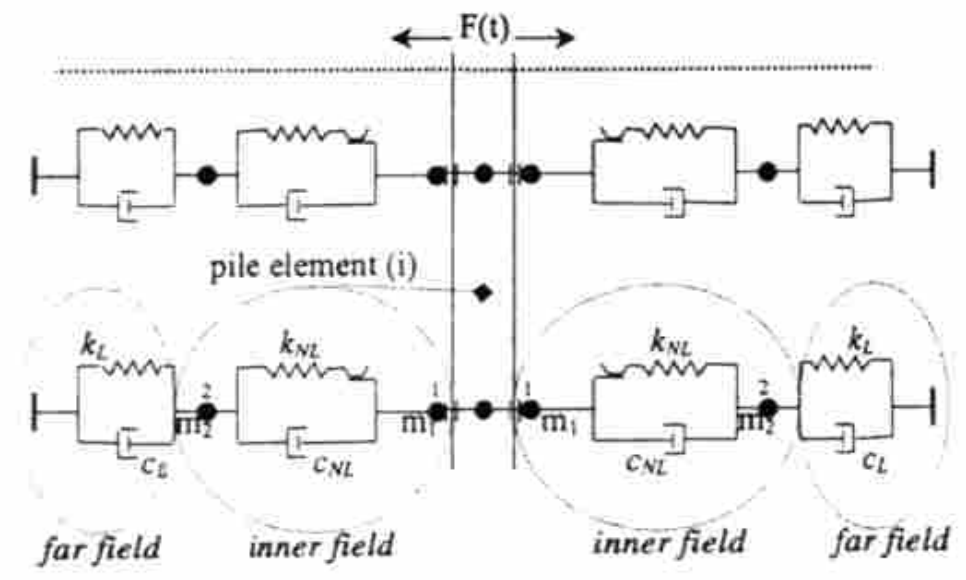

Figure 2.7: El Naggar model for lateral dynamic pile response (El Naggar, 1998).

the nonlinear and linear regions were placed on both sides of the pile. Secondly, the nonlinear springs were connected with a no-tension spring (Figure 3.5). This accounts for gaps and tension stresses that occur to allow a separation of the pile and soil in the model. For noncohesive soils where the soil will tend to fall into the gaps of the piles and soil, a very low stiffness should be implemented at times when tension stresses occur.

Equations of Motion

The linear region used the linear acceleration method and the Newmark β method. The nonlinear region used a modified Newton-Raphson iteration scheme.

To have a correct motion, these equations of motion have parameters optimized to match with the measured test results. The optimization consisted of two stages:

1) Optimization of the deflection time histories. The optimized parameters consist of the shear soil modulus (G), factor accounting for partial slippage (α_p) and the difference of the inner and outer radii of the annular zone (r_1 and r_2).
2) Optimization of the slippage and separation phase of the soil and pile. The strength parameters optimized by the angle of internal friction (ϕ) for sand or the undrained shear strength (c_u) for clay.

This optimization technique was continued until a good match was made from the measured data and the ideal model.

Once the optimization was done, the stiffness of the nonlinear and linear regions were summed and compared with the measured static tests (Figure 2.8).

Conclusions

The modeling of statnamic testing is promising and has significant potential to be useful for testing foundations in the lateral direction. A satisfactory calculated static load-deflection curve was obtained. The lateral capacity of a pile can be estimated using the statnamic test.

2.2.5 "Dynamic Analysis of Laterally Loaded Pile Groups in Sand and Clay"—Mostafa, Y. E. and El Naggar, M. H. (2002)

Three separate tests were performed to analyze the group affects while continuing with the modeling method proposed by El Naggar. The modeling method was in general similar to the single pile modeling El Naggar suggested. An additional consideration of group affects and identifying p-multipliers to compare group affects to a single pile was

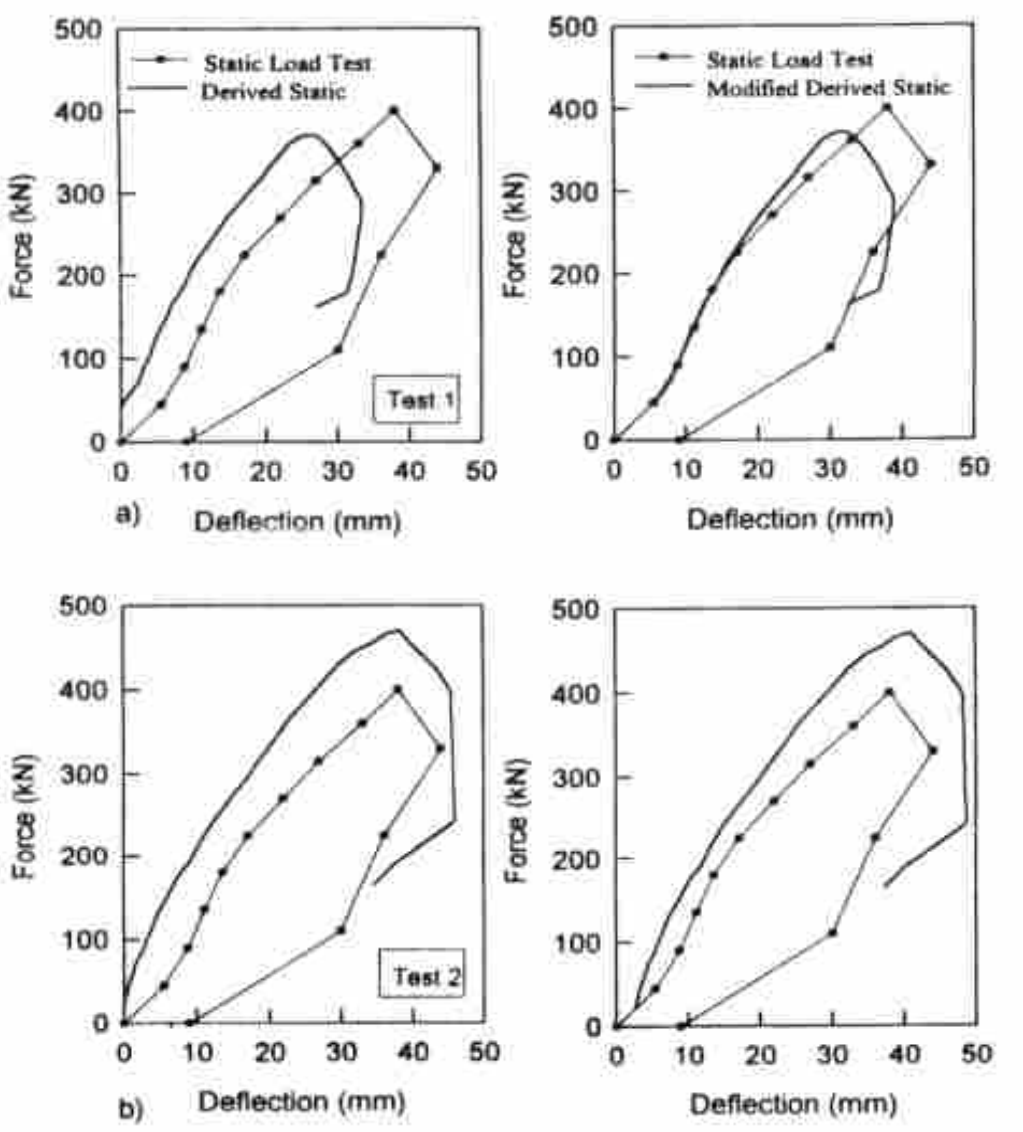

Figure 2.8: El Naggar results of calculated and optimized load-deflection curve (El Naggar, 1998).

added to the modeling method. This additional step was to achieve the goal of obtaining dynamic p-multipliers and did not affect modeling the motion of the piles.

Wilmington, North Carolina

Statnamic lateral load tests were performed on a group of piles in preparation of a proposed bridge over the Northeast Cape Fear River in Washington, North Carolina. A

group of twelve pipe piles of three rows with four piles to each row was tested. The closed ended piles were driven to a depth of 12.2 m into the ground. The outer diameters of the piles were 273 mm with a thickness of 15 mm. The tests consisted of four statnamic lateral load tests and a static test in the opposite direction. Using the same modeling method as before, El Naggar compared modified the ideal model to the measured data. The measured peak loads achieved of tests one through four were 323, 513, 874, and 1209 kN. The calculated peak loads from the model were 371, 641, 1100, 1440 kN (Figures 2.9 & 2.10).

Tests of 9-pile and 12-pile full-scale groups were performed on the Auburn University Campus. These piles sizes and driving technique were the same as the previous test performed in Wilmington, North Carolina.

Spring Villa, Alabama

The 9-pile group was spaced at four pile diameters with three rows and three piles per row. The piles were driven to a depth of 9.7 m. A 3.0 m by 3.0 m pile cap 0.35 m thick was added to the pile group. The soil consisted of stiff and medium-stiff clays. Three statnamic lateral load tests were performed in the opposite direction of the static lateral loading test. The peak measured loads were 470, 1250, and 1950 kN and the peak calculated loads were 531, 1198, and 2310 kN.

The 12-pile group was spaced at three pile diameters. The group consisted of three rows with three piles per row. These piles were also driven to a depth of 9.7 m and had the same soil conditions as the 9-pile group tests mentioned above. Four statnamic lateral load tests were performed in the opposite direction of the static lateral load test. The measured peak loads achieved of tests one through four were 374, 717, 1113, and

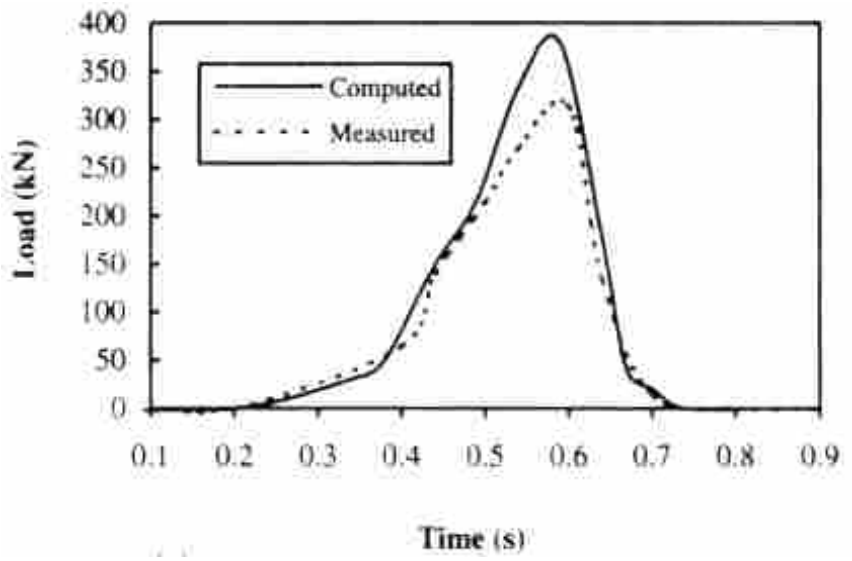

Figure 2.9: Wilmington, North Carolina results, test 1—derived and measured force time histories (El Naggar and M.H., 2002).

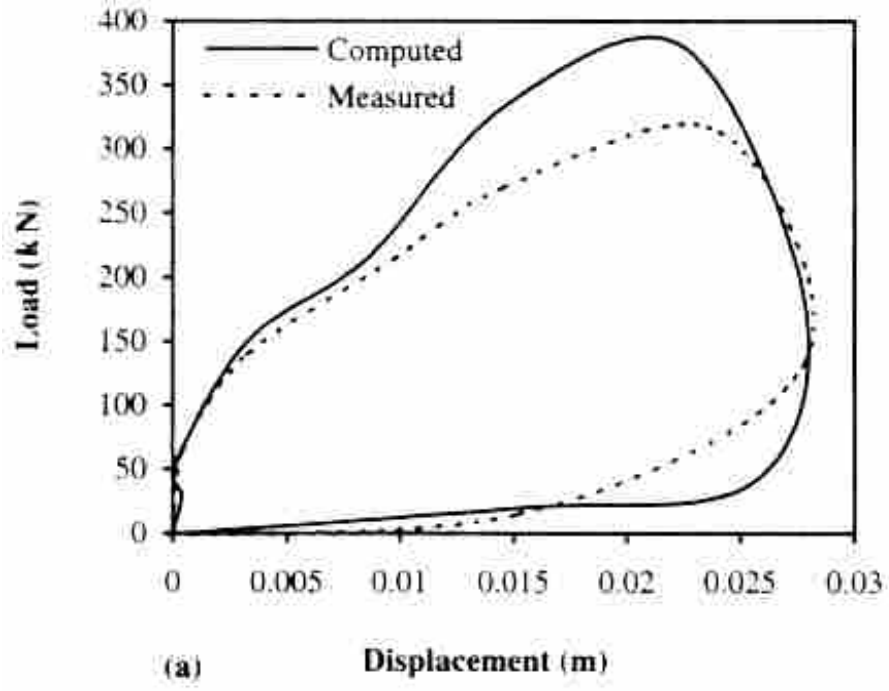

Figure 2.10: Wilmington, North Carolina results, test 1—derived and measured load-deflection curvatures (El Naggar and M.H., 2002).

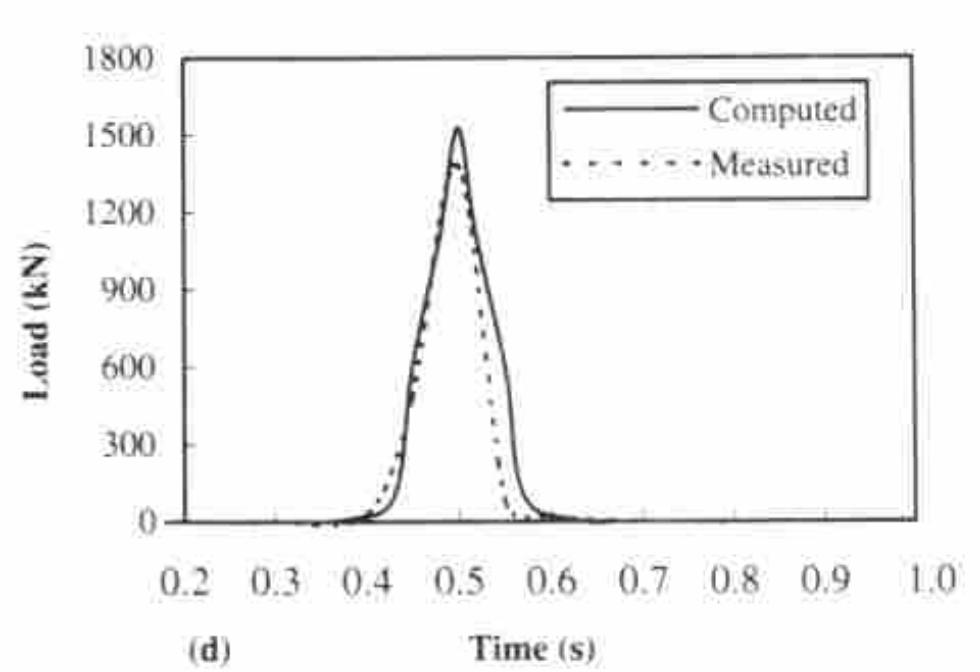

Figure 2.11: Spring Villa, Alabama results, 12 pile group test 4—derived and measured force time histories (El Naggar and M.H., 2002).

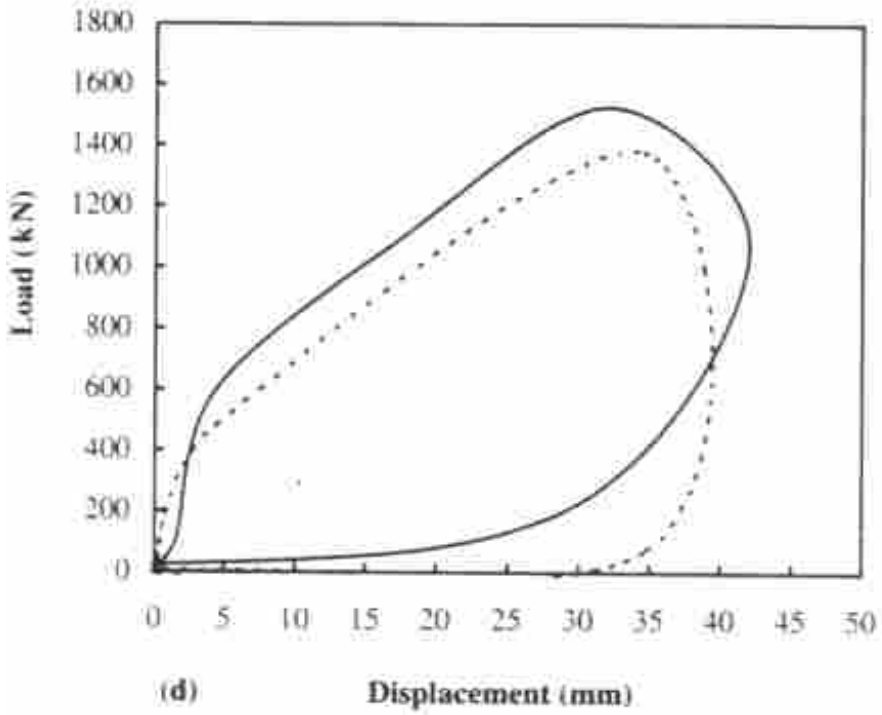

Figure 2.12: Spring Villa, Alabama results, 12 pile group test 4—derived and measured load-deflection curves (El Naggar and M.H., 2002).

1378 kN. The calculated peak loads from the model were 432, 650, 1051, 1527 kN (Figures 2.11 & 2.12).

Conclusions

The ideal model method that was used to compare to the measured motion matched well. P-multipliers are dependent to the diameter spacing. It was also notable that the pile-soil-pile reaction was a great influence in the closely spaced piles.

2.2.6 "Dynamic Response of Laterally Excited Pile Groups"—Burr, James P., Pender, et al. (1997)

Thirteen two-by-two lateral load dynamic tests were performed on small-scale pile groups. Both sites were located within the city of Auckland, New Zealand. The first site was located at Tamaki. The soil consisted of a stiff cohesive volcanic-ash soil to a depth of 2 m. The second site was located at Wairau Park industrial estate. The soil consisted of soft saturated clay to a depth of 4 m. The small-scale piles used were steel tubes 25.4 mm, 38.1 mm, and 51.0 mm diameters. The thicknesses of these piles were 1.2 mm, 1.2 mm, and 1.6 mm, respectively. To simulate a pile cap, the piles to be tested had thick clamps that were bolted to a 10 mm thick plated. The testing procedure consisted of static, "plucking" (i.e. free vibration), and dynamic tests on single piles and pile groups. Then additional mass was added and the tests went in the reverse order (i.e. dynamic, plucking, and static tests). The tests recorded lateral displacement, acceleration, and rotation for each test. Frequency of excitation was measured for the dynamic tests and lateral load was measured for the static tests. The objectives of the research were two fold: 1) to find the spacing to diameter ratios that showed group effects and 2) to create a simple linear elastic theoretical analysis to predict the dynamic

response of the pile groups. See the reference to understand the method used to develop the theoretical response. A damping ratio of 13% was used for each ideal model. The damping ratio found was based on back analyses of soil strains and the peak response.

One can check for validity of the damping ratio of 13% obtained by Burr and Pender, et. al. by using a logarithmic decrement equation with a deflection time history obtained from Burr's research (Figure 2.13). This deflection time history is one test result from "plucking" the group piles.

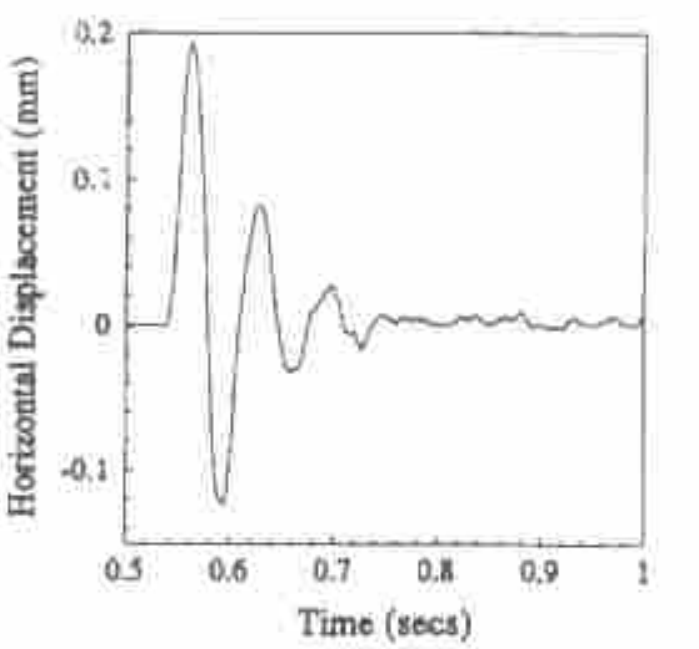

Figure 2.13: Time history of free vibration ("plucking") (Burr, James P., Pender, et al., 1997).

Referring to Figure 2.13, logarithmic decrement gives a damping ratio of about 13.9%. This calculated damping ratio is within 7% of the damping ratio in the research from Burr et. al, which suggests that this is a valid way to find the damping ratio.

Conclusions

Group effects were found to be insignificant at 12 diameter widths and larger for stiff clays and 16 diameter widths and larger for soft clays. The simple linear elastic theoretical analysis showed good estimates of the experimental results. Calculated peak displacements, frequencies, rotations, and accelerations were mostly within +/- 20% error of the measured peaks. An additional observation not in the paper concluded that logarithmic decrement is a valid method to find the damping ratios in the soil.

2.3 Need for additional research

Several significant studies have found that statnamic lateral load testing may be useful to determine the lateral capacity of piles and shafts; however, many more tests must be performed to gain a large data base of satisfactory results. Axial statnamic testing has become well known for testing and is currently going through steps to be adopted into foundation building codes. Similar to the testing and research of several years for axial statnamic tests, lateral load capacity testing may also follow this same direction. To reach this stage, several research ideas and methods need additional testing to gain more confidence and accuracy. If a data base of capacities and damping ratios of piles and shafts are developed depending on their size, diameter spacing (for groups), soil conditions, and etc., deep foundation lateral affects and capacities may be readily available for the engineer in the designing phase. The test data and results of this research will add to the developing data base of statnamic lateral loading affects on group piles. This research will continue studying methods of creating ideal models in order to observe reactions of group piles under lateral impacts and earthquake loads. In doing so, static stiffness constants and damping ratios will be obtained.

CHAPTER 3 GEOTECHNICAL INVESTIGATION

This chapter will briefly describe the available geotechnical testing performed for the test site at the Salt Lake International Airport. The information in this chapter was supported by the in-depth research of Peterson (1996) and Johnson (2003). Additional detailed geotechnical information is available from these sources.

3.1 Site Location

The test site was located approximately 300 m north of the Flight Control Tower at the Salt Lake City International Airport as shown in Figure 3.1. This site was chosen for three main reasons:

1. Extensive Past Geotechnical Investigations—The Flight Control Tower was constructed in 1995 and geotechnical investigations were available at that site. In addition, Peterson and Rollins (1996) conducted a study on the lateral resistance of a 9-pile group (approximately 50 m southeast of test site) and conducted detailed geotechnical investigations. Finally, additional in-situ testing was performed in 1998 and 2003.
2. Soil Profile—For lateral pile testing, the majority of the resistance is provided by soil from the ground surface to a depth of about eight to ten pile diameters. The

Figure 3.1: Test site at Salt Lake City International Airport (USGS).

soil within this depth range consists mainly of silts and soft to medium stiff clays; this is the soil type of primary interest with regard to lateral soil-pile interaction

3. Previous Research—The airport had already given permission to test at this location beginning in 1995 and again in 1999. Research during the initial study in 1995 involved testing of a 3x3 pile group at 3 pile diameter spacing. Testing during the 1999 investigation involved a 3x5 pile group at 4.4 pile diameter spacing and a 3x3 pile group at 5.6 pile diameter spacing. Therefore, research results from the current study could be compared with the research results from the previous studies.

3.2 Geotechnical Investigation

3.2.1 Geologic Setting

The test site is located about 2 miles southeast of the Great Salt Lake. Thirteen thousand years ago this area was completely submerged by an ancient inland lake, Lake Bonneville. Since that time, the lake level has fluctuated within the test site location causing marshy conditions. The ground water level is approximately at the natural ground surface in this vicinity at the present time. The upper 3 to 5 m of the profile likely consists of recent alluvial deposits, which are underlain by lacustrine deposits laid down by Lake Bonneville within the depth range from 5 m to the bottom of the test piles (about 12 m). The site was covered by 1.5m of compacted fill in 1995. For testing the native soils, this fill was removed.

The site is located less than 5 miles from the Wasatch Fault in the Salt Lake Segment that is capable of producing a M_s 7.1 earthquake (See Appendix for calculation of seismic probability). Although the scarp of the fault is five miles away, epicenters

would most likely be closer because the slip direction of the normal fault angles under the Great Salt Lake Valley. Several other small faults are located within a three mile radius. The Granger and Taylorsville Faults are south of the airport in the West Valley Fault Zone. The Warm Springs Fault is a small fault located northwest of the airport, but it is connected to the Weber Segment of the Wasatch Fault. The Weber Segment has the potential of producing a M_s 7.0 earthquake (See Appendix).

Although the site is located beyond the fences defining the secured area around the airport, the site is within an area of future airport expansion. Therefore, a 1.5 m thick layer of compacted sandy gravel fill had been initially compacted by the Salt Lake Dept. of Airports at the location where the piles were to be tested. This fill was removed prior to testing, so that the original cohesive surface layer would be exposed for testing. A 3 x 5 driven pile group with rows spaced at 3.92 diameters was driven with closed ends to a depth of 11.6 m (38 ft). This 15-pile group was located at the south end of the test site (Figure 3.2). A 3 x 3 driven pile group with rows spaced at 5.65 diameters was also driven with closed ends to a depth of 11.6 m (38 ft). This 9-pile group was located at the north end of the test site. A single pile was also driven 1.82 m west of the 15-pile group for comparison tests aimed at developing p-multipliers as a function of spacing in a companion research project. Additionally, two 1.22 m diameter reinforced concrete shafts were cast-in-place 7.92 m on centers from both pile groups to act as a reaction in the static load testing.

3.2.2 Laboratory Testing

Shelby tube samples were taken for undisturbed soil laboratory testing. Other disturbed samples were obtained using a split-spoon sampler and a hand auger. Particle

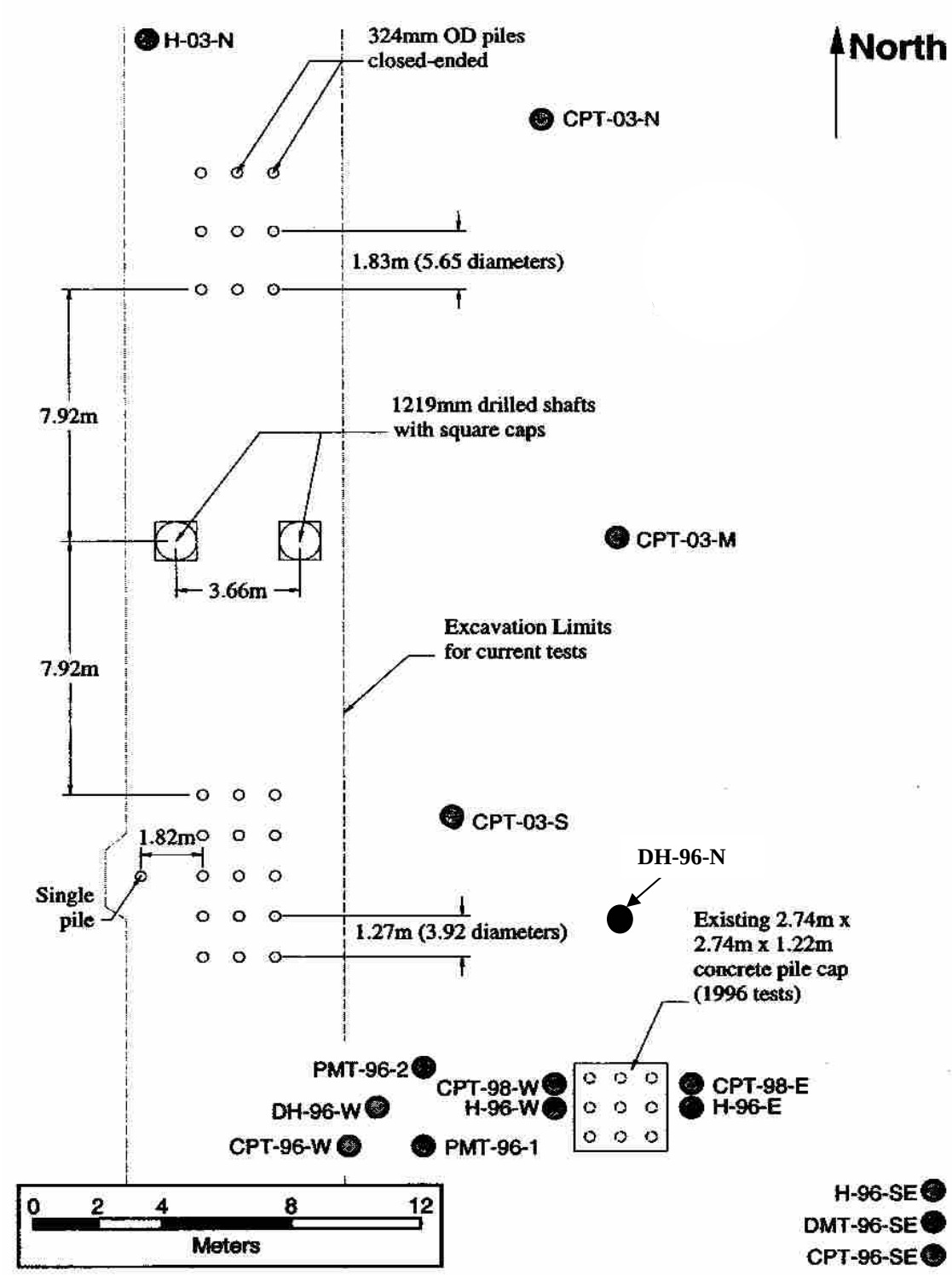

Figure 3.2: Plan view of site with locations of geotechnical testing and sampling (Johnson, S. 2003a).

size distribution, Atterberg limits, consolidation characteristics, and shear strength properties were determined by laboratory tests performed on these samples.

Particle Size Distribution

Mechanical sieve testing defined the distribution of the large particle sizes and hydrometer testing defined the particle distribution for the finer grain samples. The testing was in general accordance with ASTM D-2487. In the upper 4 meters, the soils were mostly fine grained with 50 to 75 percent passing a No. 200 sieve. Clay contents ranged from 10 to 25 percent at the upper depths. Poorly graded medium-grained sand was found between four and six meter depths.

Atterberg Limits

Atterberg limits, defined by the Liquid Limit (LL), Plastic Limit (PL), and Plastic Index (PI) were determined according to ASTM D-4318. The Plastic Index was commonly less then 20 percent indicating that the soils have low to medium plasticity characteristics and are not likely expansive. Natural moisture content (w_n) was generally near the Liquid Limit; however, in a few tests the moisture content was less than and in some cases it was greater than the Liquid Limit indicating high sensitivity.

Soil Classification

The soil was classified using the Unified Soil Classification System (USCS). The fine-grained soil predominated and classified as low-plasticity clays and silts (CL, CL-ML, and ML). The sand layers were classified as poorly-graded sands (SP) and silty sands (SM).

Shear Strength Tests

From the shelby tube test samples three unconsolidated undrained (UU) triaxial tests were performed (one in 1996 and two in 2003) (Figure 3.2). Unconfined compression tests were also performed on the 2003 samples. The undrained shear strengths (s_u) for most of the samples ranged from 25 to 60 kPa. However, the upper cohesive layer (approximately 0.3 m thick), where desiccation had occurred had shear strengths as high as 100 kPa.

Consolidation Tests

Consolidation tests results indicate at the soils were overconsolidated to a depth of about eight meters. The overconsolidation ratio was greatest at 1.7 m depth with a ratio of 2.8 and gradually decreased with depth.

3.2.3 In-situ Tests

Several in-situ tests were performed. These tests include: Cone penetrometer (CPT) tests, standard penetration (SPT) tests, dilatometer (DMT) tests, pressuremeter (PMT) tests, and vane shear (VST) tests. In addition, shear wave velocity was measured using a seismic cone penetrometer and a downhole test. CPT soundings and velocity testing will be discussed in some detail and results from the additional in-situ testing are given by other investigators (Johnson, 2003 and Peterson, 1996).

Cone Penetration Testing (CPT)

Seven CPT soundings were performed within the test site area (Figure 3.2). Two of these tests were performed in 1996. RB&G Engineering performed the first test in 1996 labeled CPT-96-W. Manual readings of tip resistance and sleeve friction were taken every 100 mm. Friction ratios (R_f) were determined by dividing the sleeve friction

by the cone tip resistance. Alta-Geo, Inc. performed the CPT sounding labeled CPT-96-SE. Measurements of tip resistance, sleeve friction, friction ratios (R_f), and pore water pressure (u) were taken automatically every 10 mm. ConeTec Inc performed all other CPT soundings in 1998 and 2003. Tip resistance, sleeve friction, friction ratio, and pore water pressure readings were automatically taken every 50 mm. The test results are given in Figures 3.3 through 3.5 and a comparison of these tests is given in Figure 3.6.

Velocity Profiling

The shear wave velocity profile at the test site was measured using both a conventional downhole approach and with a seismic cone. The downhole test was performed by LGS Geophysics in a 60 m deep borehole drilled immediately north of a pile cap used for load testing by Peterson (1996) as shown in Figure 3.2. A receiver was positioned inside a cased hole at 1.5 to 3 m intervals and a shear wave was generated by striking a wood plank with an instrumented sledge hammer. The arrival times at each depth were then used to define the shear wave velocity profile versus depth. A similar approach was used with the seismic cone during sounding CPT-2003-M. However, in this case velocity measurements were made at 1 m intervals when a new rod was attached.

The two measured shear wave velocity profiles are plotted in Figure 3.7 along with a generalized soil profile. Although both profiles are generally consistent with one another on average, the seismic cone profile, with a finer resolution, appears to better match the characteristics of the soil profile. For example, the seismic cone profile indicates a somewhat higher velocity in the sand layers and a somewhat lower velocity in the cohesive soil layers that is not distinguished by the downhole velocity profile.

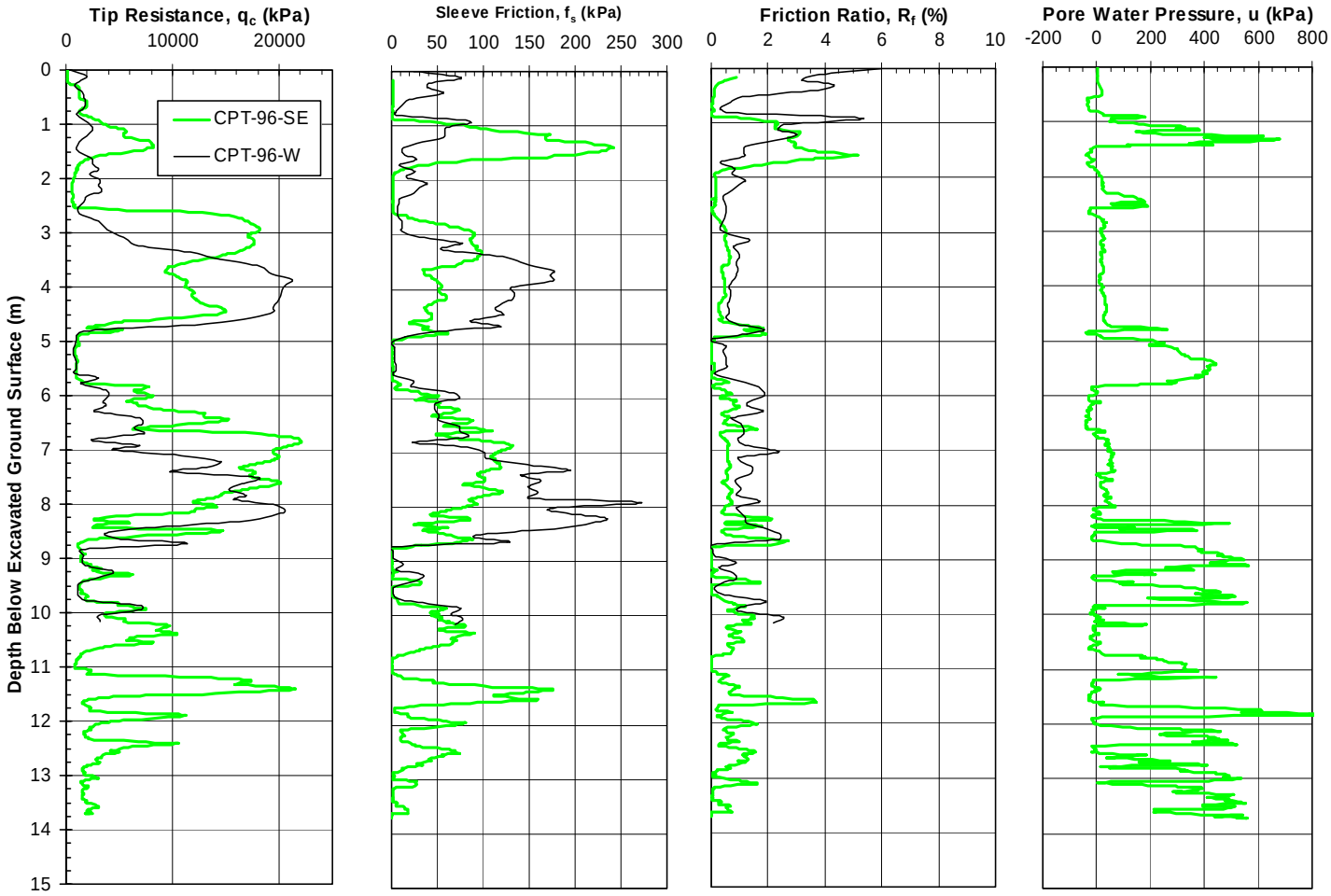

Figure 3.3: Comparison of CPT sounding near test site in 1996.

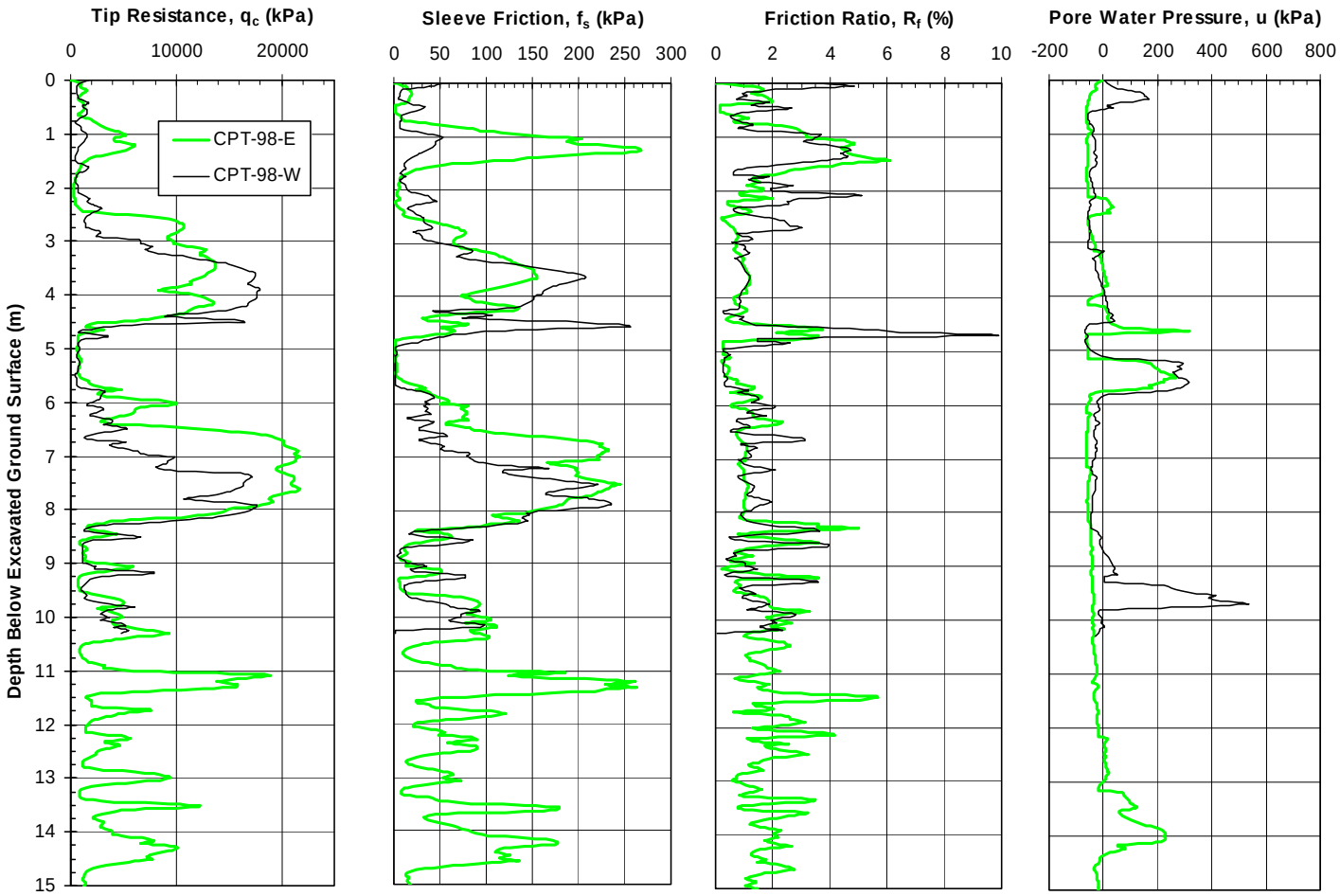

Figure 3.4: Comparison of CPT sounding near test site in 1998.

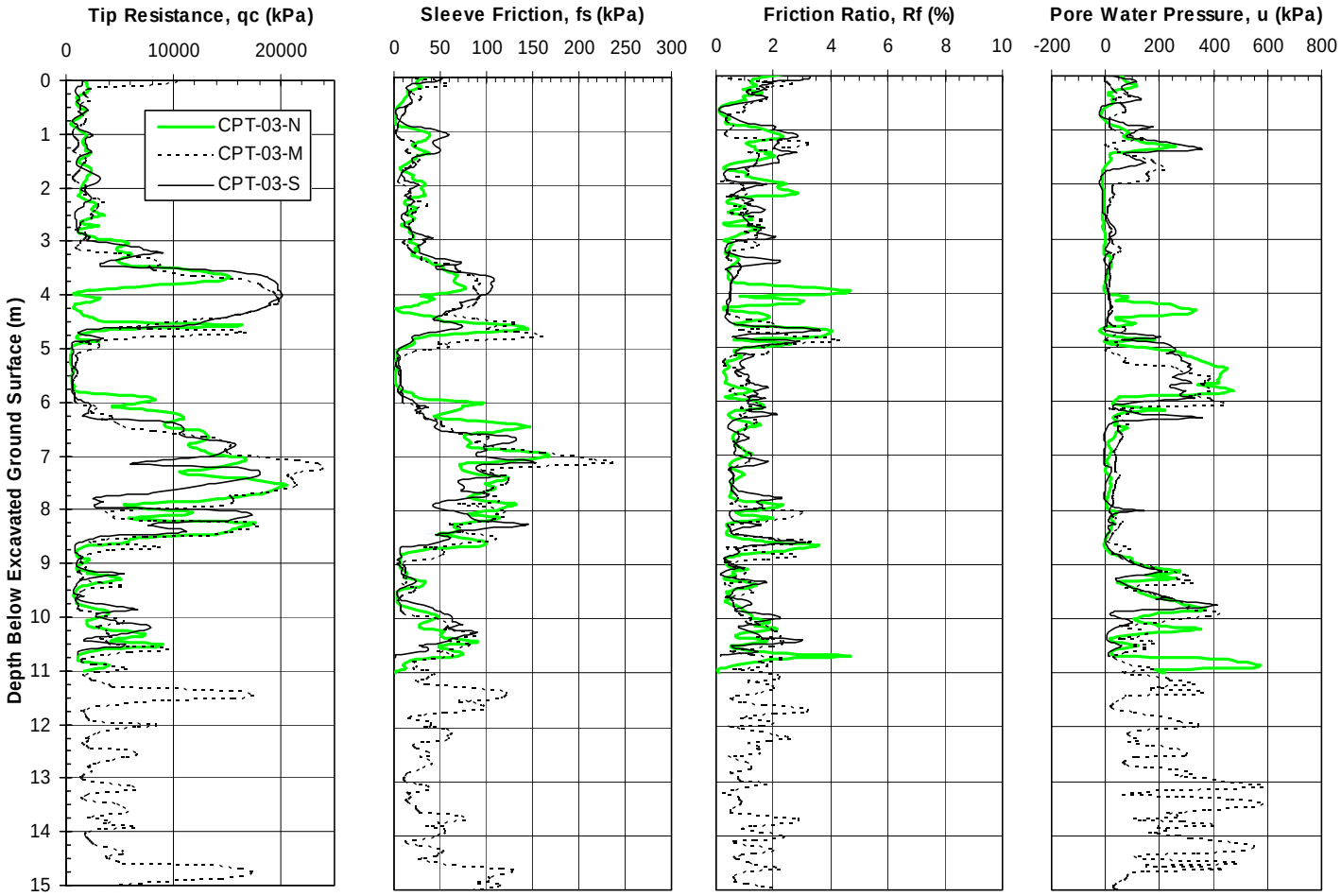

Figure 3.5: Comparison of CPT sounding near pile groups in 2003.

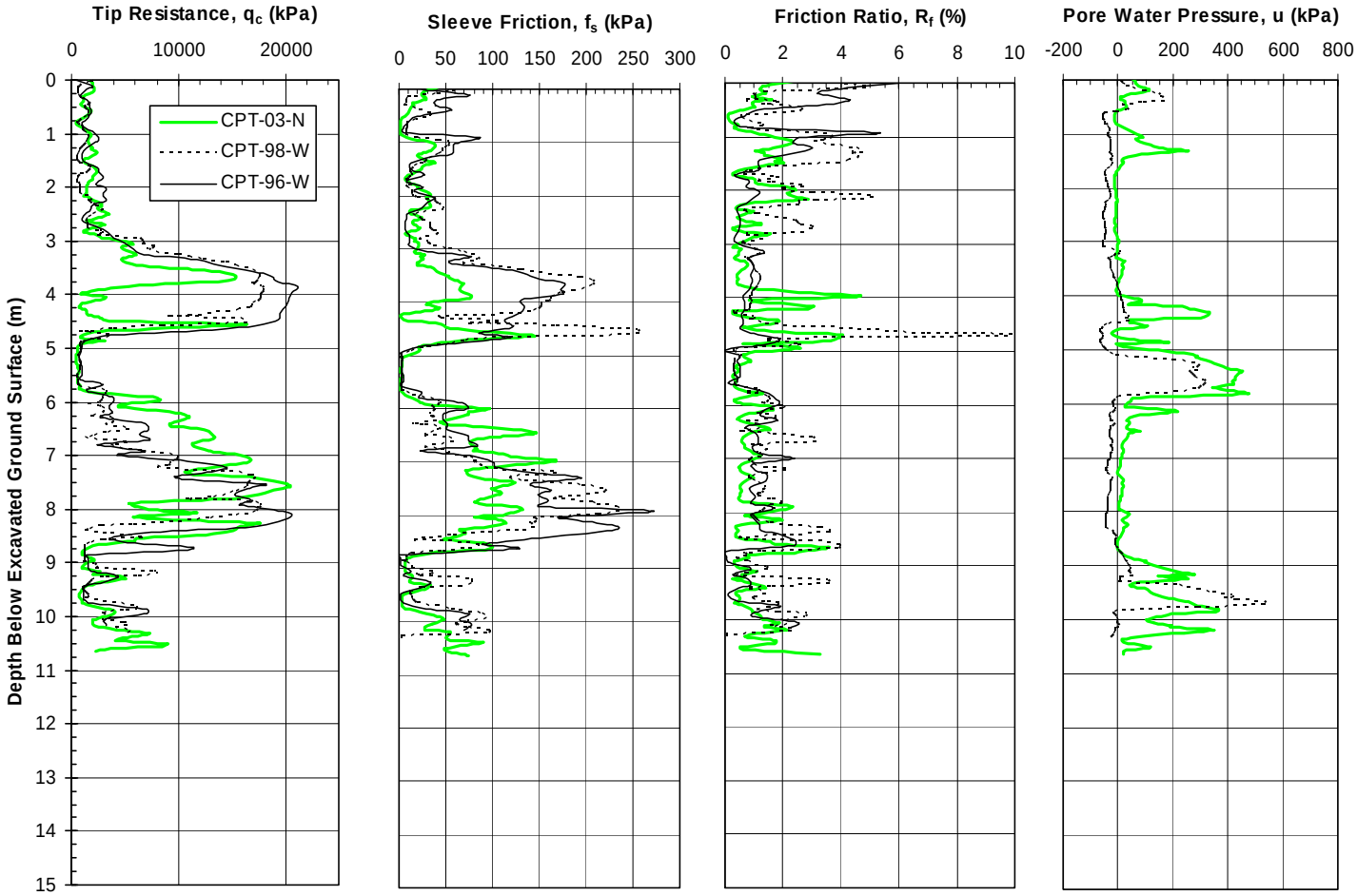

Figure 3.6: Comparison of CPT sounding of CPT-03-N, CPT-98-W, and CPT-96-W.

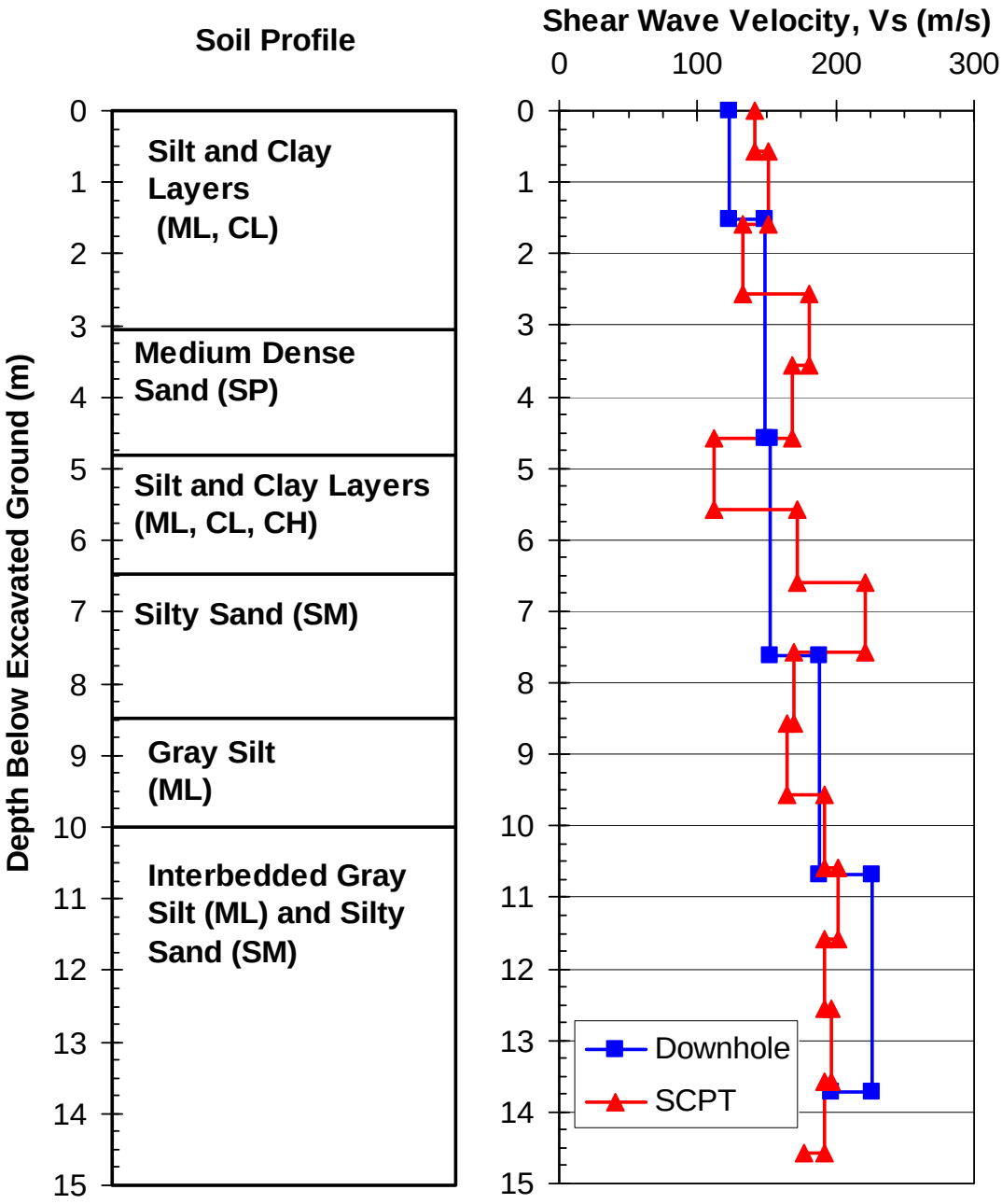

Figure 3.7: Shear wave velocity profile.

A profile of the elastic modulus was obtained from the measured shear wave velocity using the equation

$$E_s = 2\rho V_s^2(1+v) \quad (3.1)$$

where:

v = poisson's ratio assumed to be 0.40

ρ = total mass density (135pcf for gravel and 120pcf for underlying soil

The profile of elastic modulus is plotted in Figure 3.8. The measured increase in elastic modulus has been approximated as a linear increase with depth using the equation:

$$E_s = 0.0924*D - 3.84 \quad (3.2)$$

3.3 Summary of Geotechnical Investigation

Because of the in-depth laboratory and in-situ testing, a reasonably good understanding of the soil properties has been developed. A plot showing the cone tip resistance profiles obtained from all the CPT soundings at the site is presented in Figure 3.9. Although there are variations, the profiles are generally very similar and define the generalized soil profile shown in Figure 3.9. Thus, for analysis purposes it is assumed that the soil profile is essentially the same throughout the testing area.

A somewhat more detailed soil profile interpreted from all the field and laboratory testing is provided in Figure 3.10 along with summaries of field and laboratory testing. The approximate depth of the fill that was excavated was about 1.5 meters. Soils consisted of clay silt with sand, lean clay, and low plasticity sandy silts from 1.5 to 4.5 meter depths. Below this cohesive surface layer, a layer of poorly graded sand was

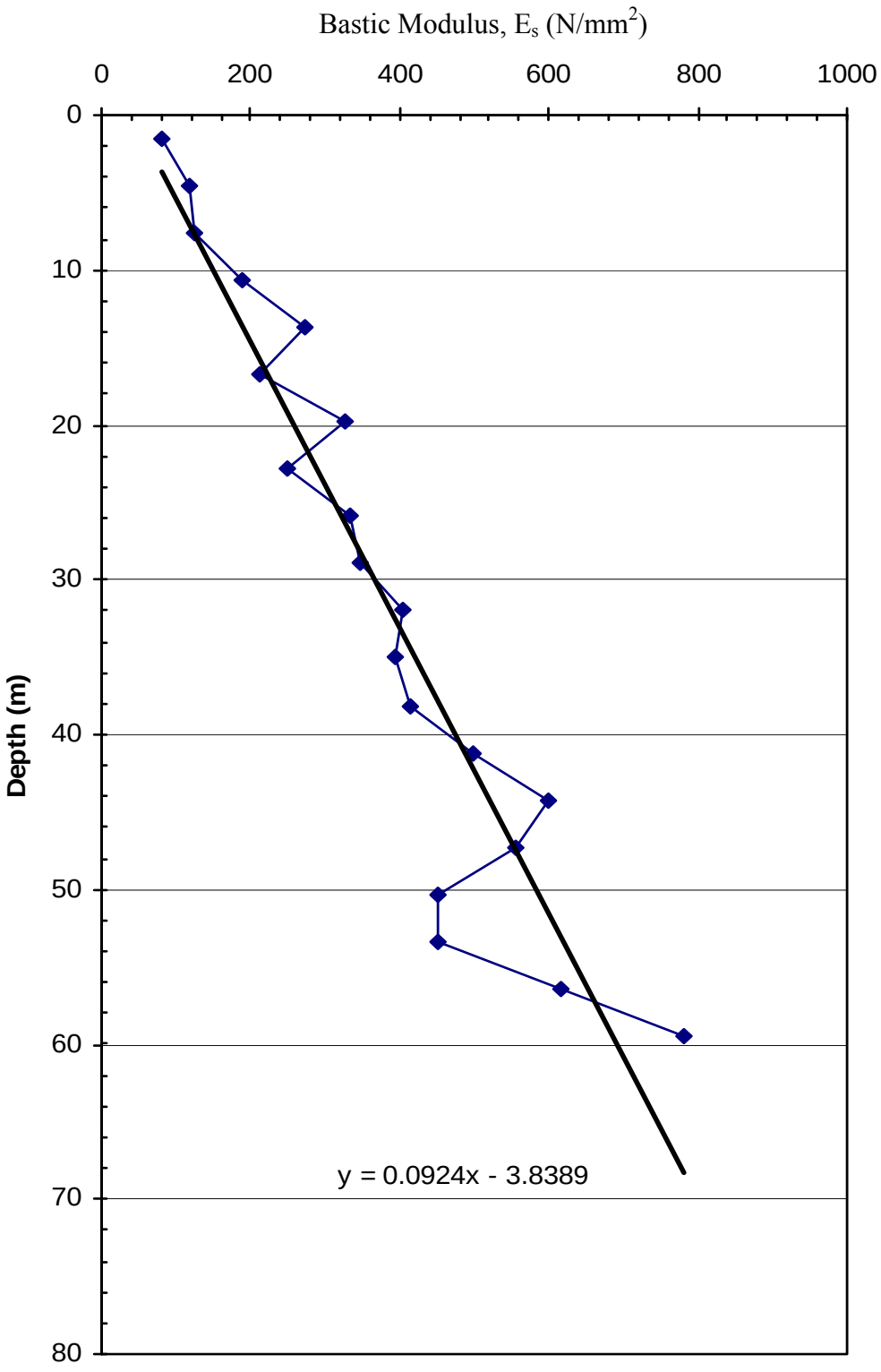

Figure 3.8: Profile of calculated soil modulus from 1996 borehole.

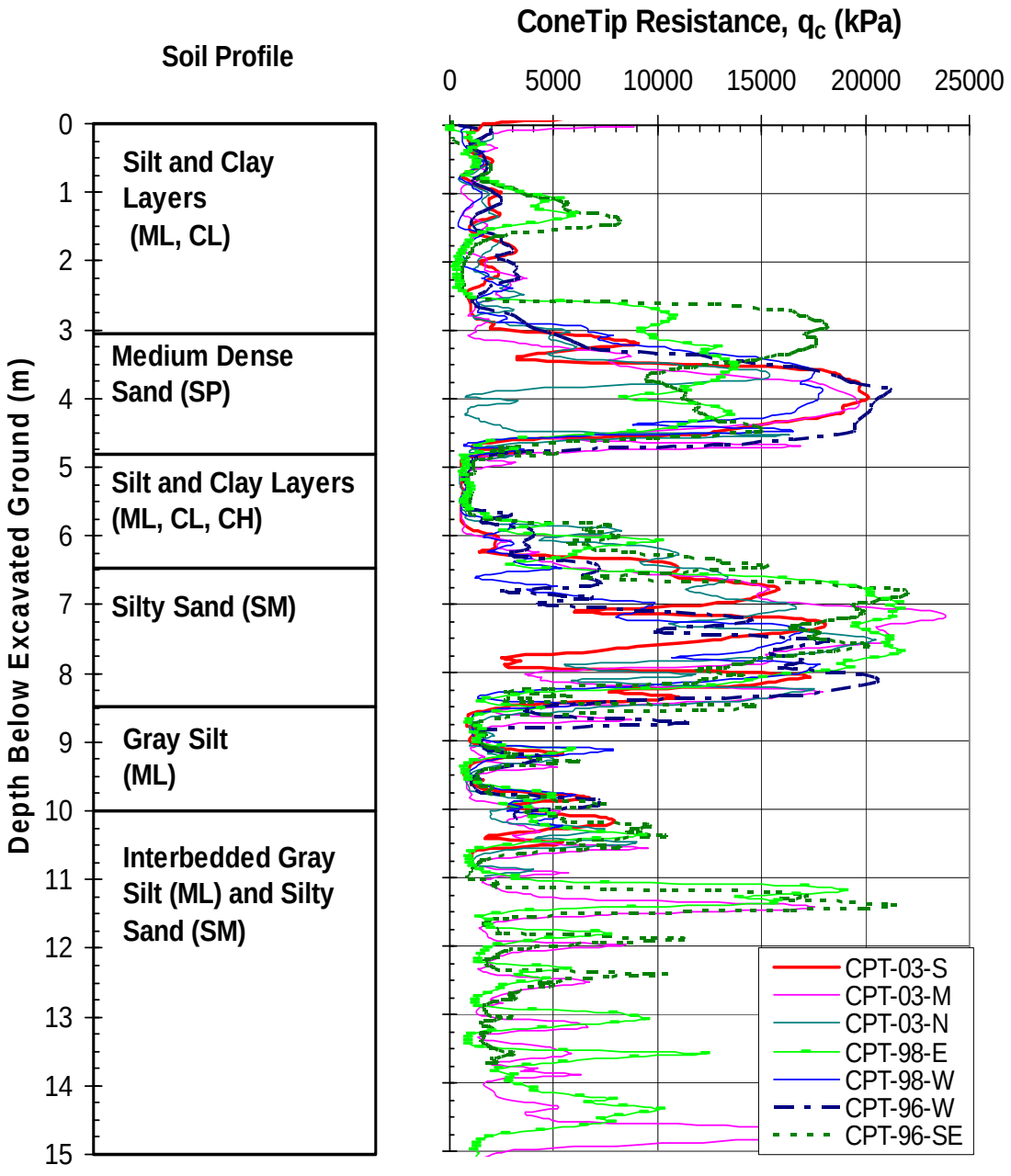

Figure 3.9: Summary of cone penetration tests.

classified for approximately 2.5 meters to a depth of 6.5 meters. A variety of fat and lean clays underlaid the sand layer followed by interbedded silt and silty sand layers to a depth of 15 meters.

The SPT blow counts and the cone tip resistance values in the sand layers generally give ranges of values indicating that the sands are in a medium to dense state.

Moisture content for the most part was greater than the PL and less than the LL, suggesting that the soil is overconsolidated. This is consistent with the result from the consolidation tests that indicate the soil is overconsolidated to a depth of about 8 m but that the overconsolidation ratio decreases with depth. At a few locations the moisture content is greater than the LL, which suggests that high sensitivity could be a concern.

A profile of shear strength tests versus depth for the cohesive soils at the site is plotted in Figure 3.11. Most of the tests were performed from zero to six meters below the compacted fill layer. For most cases, the shear strength ranges from 25 to 60 kPa which places the soil in the medium consistency range defined by Terzaghi and Peck (1952). At a few locations, the undrained strength was under 25 kPa and would be classified as soft clays. Also, a few tests measured shear strengths from 60 to 110 kPa that would be classified as stiff to very stiff clay. These stiff layers, near the ground surface, likely developed due to desiccation from repeated wetting and drying.

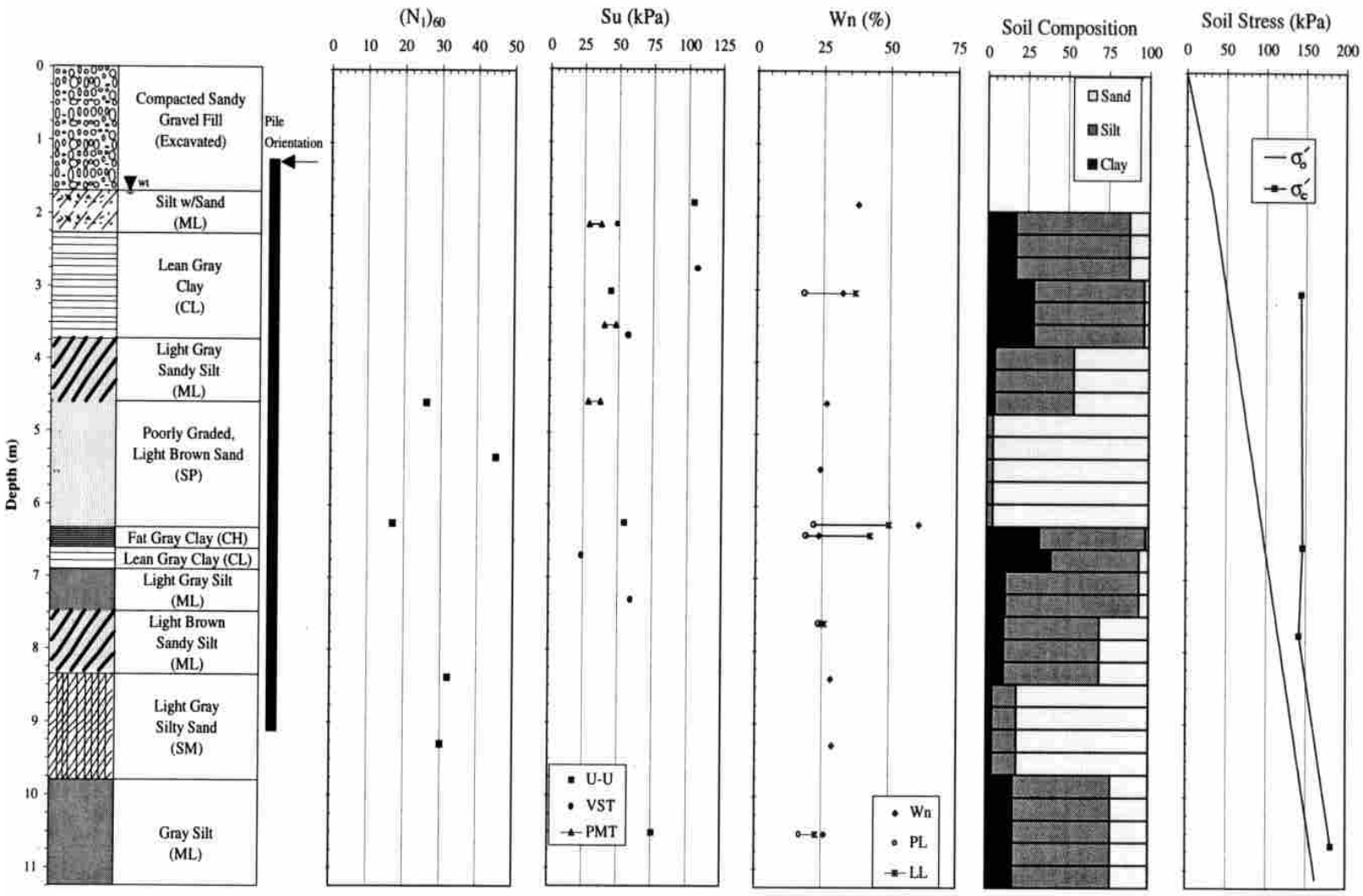

Figure 3.10: Soil profile of test DH-96-W, with VST and PMT strength data (Peterson and Rollins, 1996).

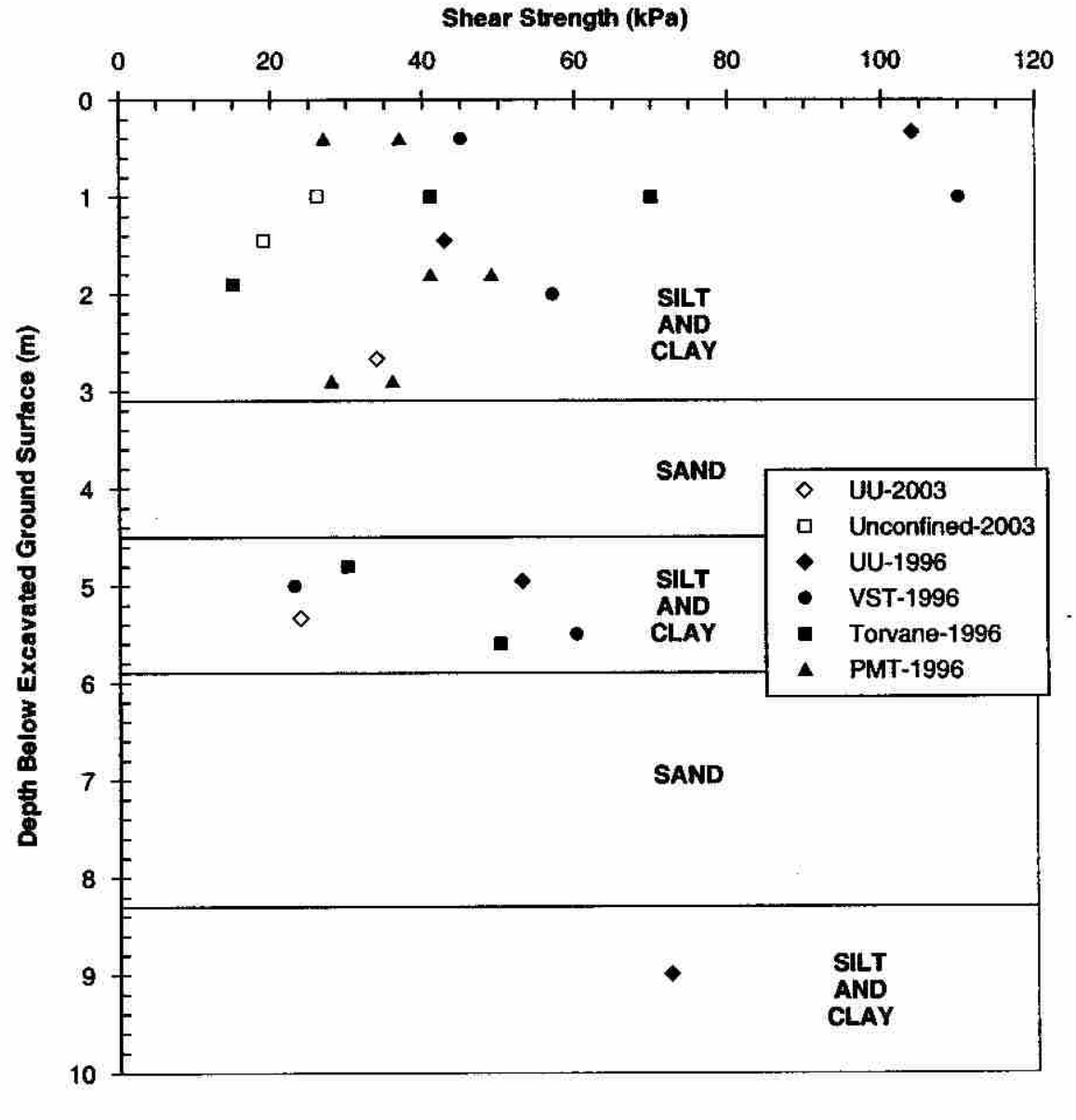

Figure 3.11: Summary of shear strength testing results (S. R. Johnson, 2003b).

CHAPTER 4 15-PILE STATNAMIC LATERAL LOAD TESTING

4.1 Test Setup

4.1.1 Layout

The test piles are 13.7 m (45 ft) long and have an outer diameter of 324 mm (12.75 in) and a thickness of 9.5 mm (0.375 in). At these dimensions, a single pile has a moment of inertia of 1.16 x 10^8 mm^4 (279 in^4). For the purpose of test instrumentation setup, two additional L38x38x5 (L1½x1½x$^3/_{16}$) angle irons were spot welded on the north and south sides of the center pile in each row. Assuming that the angle irons were completely fixed to the piles, the moment of inertia of a single pile would be 1.43 x 10^8 mm^4 (344 in^4). The test piles conformed to the ASTM A252 Grade 3 specifications. As part of the I-15 reconstruction project, Geneva Steel tested 192 steel pipes with the same properties as the driven test piles. Based on these tests, the piles were found to have a mean yield strength of 404,592 kN/m^2 (58.7 ksi) with a standard deviation of 15,168 kN/m^2 (2.2 ksi) based on the 0.2% offset criteria. The mean tensile strength was 584,087 kN/m^2 (84.72 ksi) with a standard deviation of 17,650 kN/m^2 (2.56 ksi),

On June 25, 2002, the 15-pile group was driven by a 102 kN IHC hydraulic hammer. The energy delivered to the driven piles ranged from 7 to 27 kN-m per blow. The piles were driven with row center to center spacing (North/South) of 1.27 m or 3.92 pile diameters and a column center to center spacing (East/West) of 1.1 m or 3.3 pile

diameters as shown in Figure 4.1. This column spacing was chosen, because lateral shadowing effects have no significant effects with 3 pile diameters and greater (Cox et al., 1984) when under static loading. Each pile was numbered for the convenience of identifying individual piles as shown in Figure 4.1.

To distribute the load to each individual pile, a load frame was constructed (Figure 4.1). Each pile was pin connected to the load frame by a 51 mm (2 in) diameter tie rod (Figure 4.4) that was bolted to a plate between two channel sections. The two C250x45 (C10x30) channels were bolted top and bottom to two longitudinal beams W310x67 (W12x45) shown in Figure 4.1. A W760x284 beam was connected at the south end of the load fame and used for the static load testing in which the beam and pile group were pulled to the north. Additional details regarding the static load test set-up are provided by Snyder (2004). The statnamic device as shown in Figure 4.1 loaded the W920x313 beam at the south end of the load frame. These W-Shaped beams were used to ensure uniform motion of the pile group and resist the large bending moments produced by the load application. To reduce friction caused by the load frame, rollers on tracks were connected to the load fame (Figure 4.2). The load reaction occurred at 483 mm (19 in) above the ground level.

A 35-ton statnamic device provided by Applied Foundation Testing, Inc. was placed in contact at the south end of the load frame. In order for the piston of the statnamic device to apply load at the elevation of the tie-rods on the load frame, soil was excavated an additional 0.75 m (2.5 ft) under the statnamic device. To ensure that no excessive moments occurred during the statnamic loading, a swivel plate that was used at the contact location between the statnamic sled and the W910x313 beam.

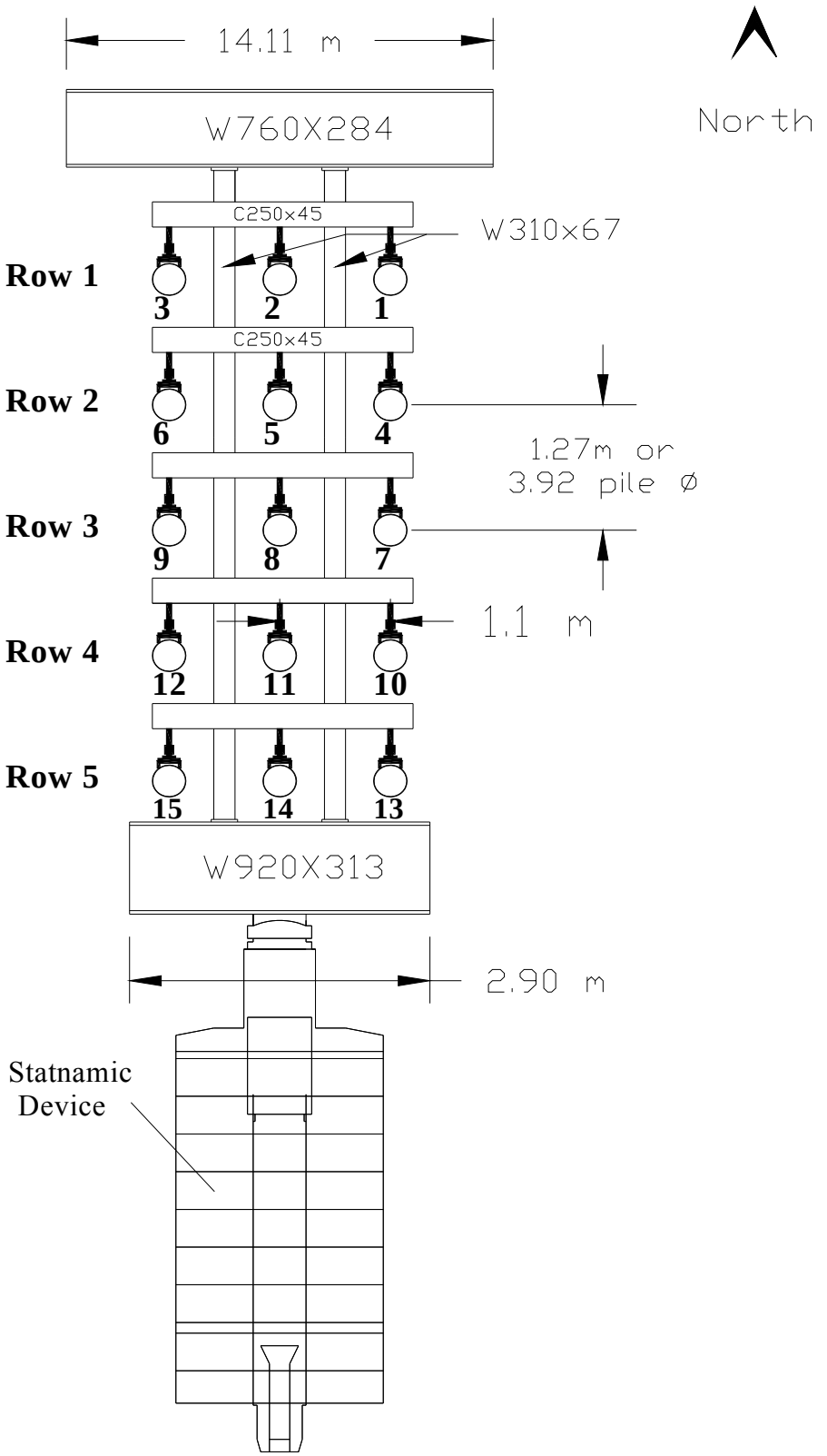

Figure 4.1: Plan view of 15-pile group layout under statnamic testing with pile and row numbering.

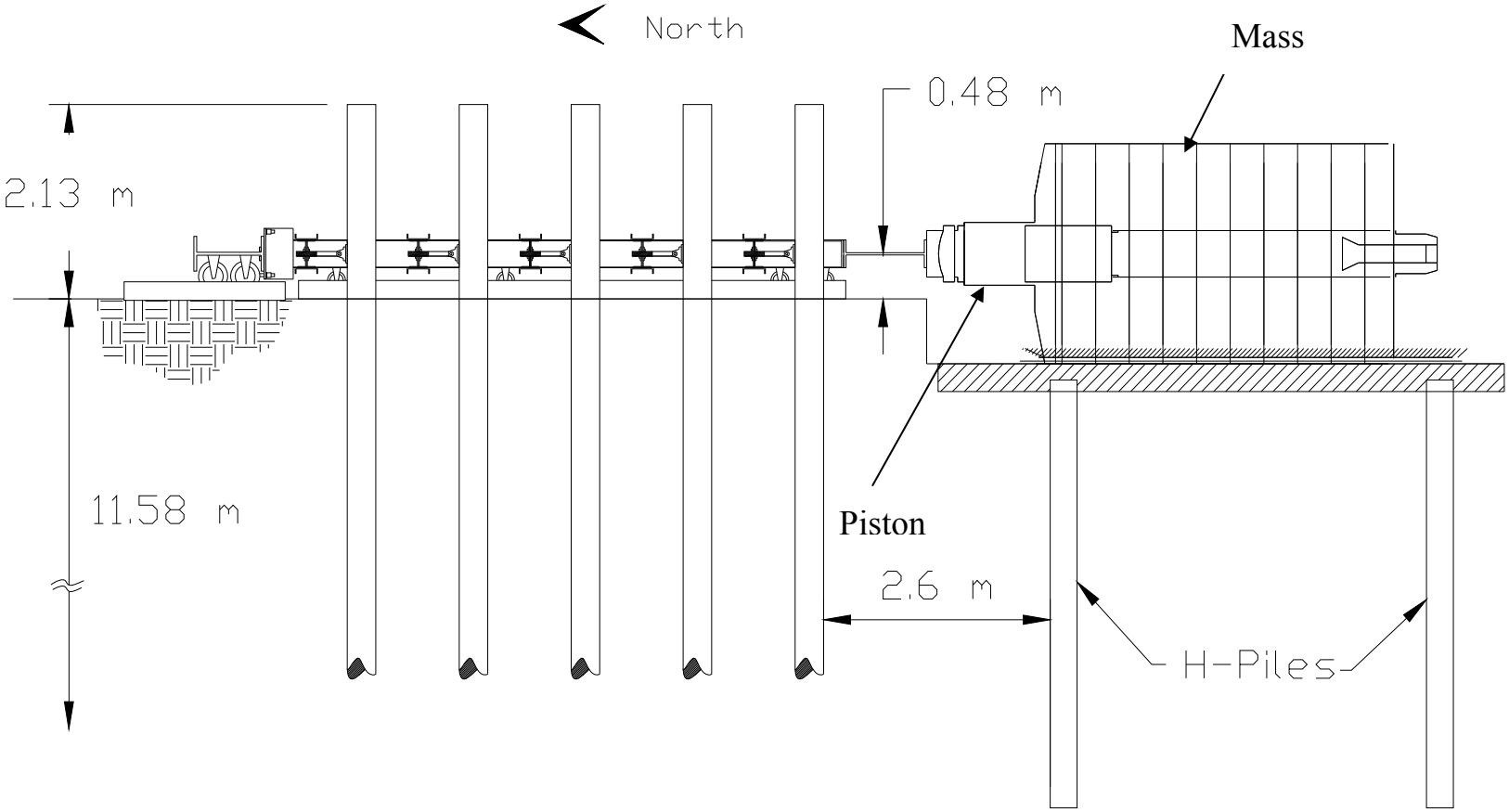

Figure 4.2: Profile of 15-pile group layout under statnamic testing.

The statnamic device consists of a piston and a reaction mass attached to a sled as shown schematically in Figure 4.3. As fuel pellets burn in the combustion chamber located in the piston, gasses are produced which push the piston against the foundation and create an equal and opposite force on the reaction mass and sled. As a result, the foundation deflects in one direction while the reaction mass sled slides off in the opposite direction.

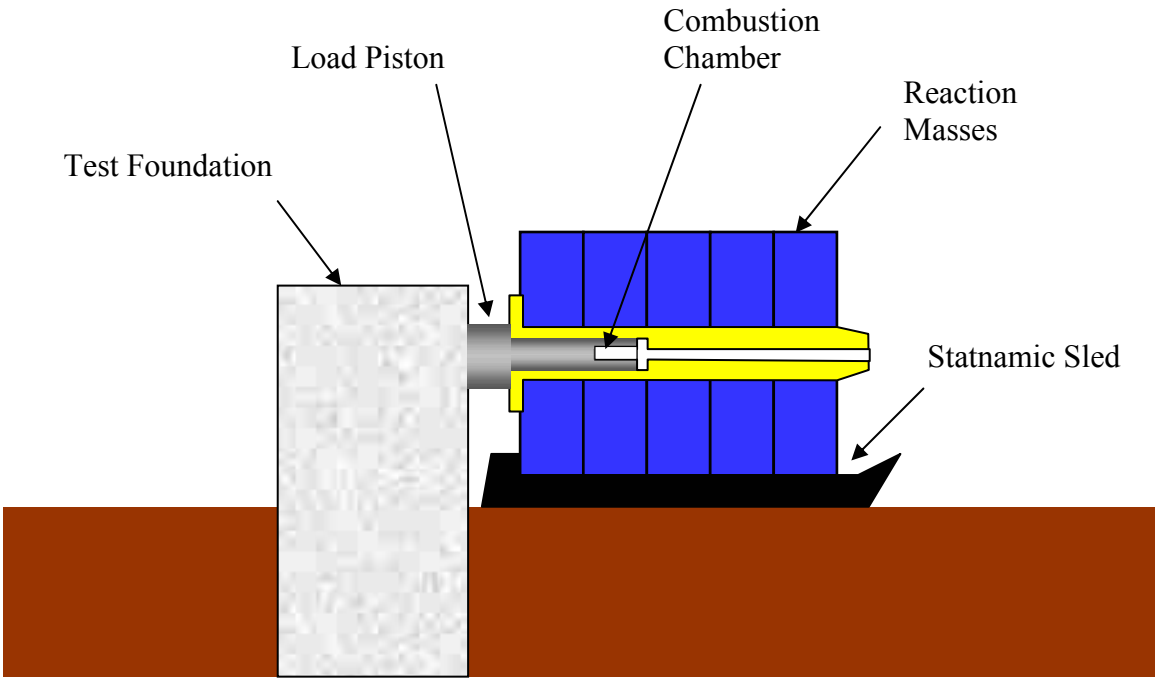

Figure 4.3: Components for statnamic lateral load testing.

Four H-piles were driven 4.6 m (15 ft) into the ground as a foundation for the statnamic device. These H-piles and the surrounding soft clay supported two 7.9 m (26 ft) long W920x233 (W36x150) beams lying on their sides which served as a "runway" for the statnamic sled as shown in Figure 4.2. Railroad ties were placed on top of the webs of these beams to create a level surface for the runway.

4.1.2 Instrumentation

The 15-pile group was instrumented with load cells, linear variable differential transformer (LVDTs) transducers, piezoelectric accelerometers, and electric resistance strain gages. With these instruments, forces, deflections, velocities, accelerations, moments, and rotations could be determined.

Each individual tie rod connecting a pile to the frame contained two strain gages that measured the force on each pile and canceled out bending effects (see Figure 4.4). The sum of the load measured by the tie-rods was found to be within an average of 2.9 % or the load measured by the load cells on the hydraulic jacks during the static load testing (Johnson, 2003). An additional load cell was attached at the head of the piston on the statnamic device to measure the total load applied to the load frame.

Pile head deflection was measured on each pile with an LVDT mounted at the same elevation as the applied load as shown in Figure 4.5. These LVDTs are accurate to 0.13 mm. Two additional LVDTs were located at 1.5 m (5.0 ft) above the loading point on the center piles (piles 2 and 14) on the leading row (row 1) and trailing row (row 5). These LVDTs coupled with those at the load point made it possible to determine the pile head rotation. All LVDTs were connected to a reference frame that would not be influenced by the movement of the group piles.

A total of 14 accelerometers were used for measuring the accelerations produced by the dynamic load testing. Three accelerometers were connected to the outside of piles 1, 2, and 3 on the leading row at the load point. Ten additional accelerometers were magnetically attached to the inside wall of pile 2 as shown in Figure 4.6. The accelerometers were spaced at 0.61 m (2.0 ft) increments, ranging from the ground level (0 m) to a depth of 5.49 m (18.0 ft) below the ground surface. An additional

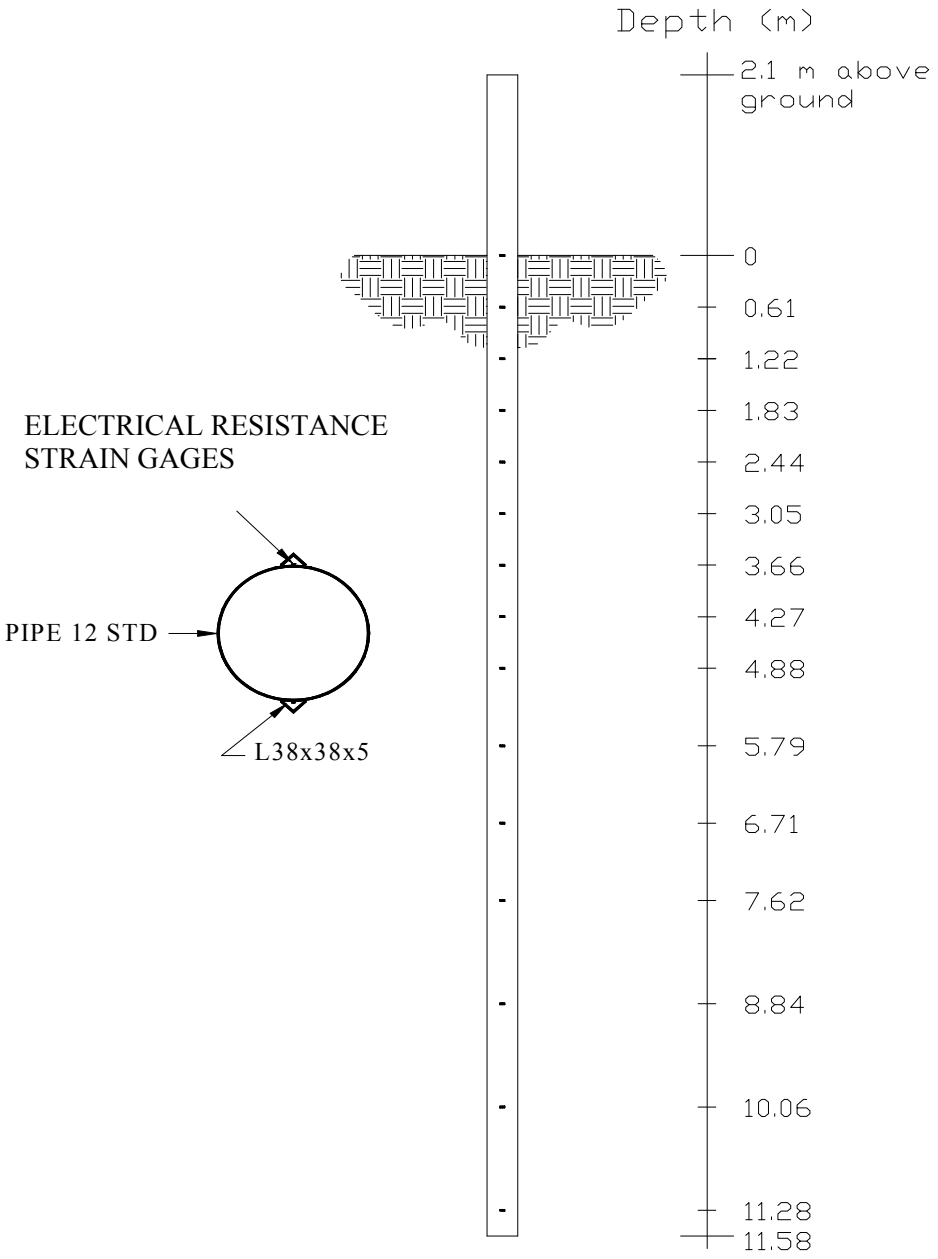

Figure 4.4: Plan and profile of a single pile with strain gage locations.

accelerometer was placed on the reference frame to observe if any excessive deflections occurred. Applied Foundation Testing, Inc. supplied six of the 13 accelerometers and attached all the accelerometers to the pile.

Each center pile (piles 2, 5, 8, 11 and 14) contained quarter-bridge electrical resistance type strain gages. These strain gages were 120 Ω waterproof electrical resistance gauges manufactured by Texas Measurements, Inc. (model WFLA-6-120). Strain gauge pairs were attached at fifteen locations down the outside of each pile as depicted in Figure 4.4. Nine pairs were located at regular intervals of 0.61 m (2.0 ft) from the ground surface to a depth of 4.88 m (16.0 ft). The next three pairs were spaced at 0.91 m (3.0 ft) intervals to a depth of 7.62 (25.0 ft). The last three locations were spaced at 1.22 m (4.0 ft) intervals to a depth of 11.28 m (37.0 ft). Each location contained two strain gages, one on the north and the other on the south. This was done to find the maximum compressive and tensile strains that occurred during the lateral load testing. The strain gages were attached to the outside of the piles with epoxy glue.

To protect the strain gages from any physical damage, angle irons were tack welded to the piles at points between the strain gauges as previously noted. To further protect the gauges, waterproof foam was sprayed into the void space between the angle iron and pile.

Data from the instrumentation was obtained with an Optim Megadac data acquisition system (model 5414AC version 7.4). A total of 197 channels were used; 150 channels for strain data, 14 channels for accelerometer data, 17 channels for LVDT data, 15 channels for the tie rod load data, and one channel for the statnamic load cell. During statnamic testing, the data was obtained every 0.000667 seconds (1500 Hz). A portable electric generator powered the electrical systems.

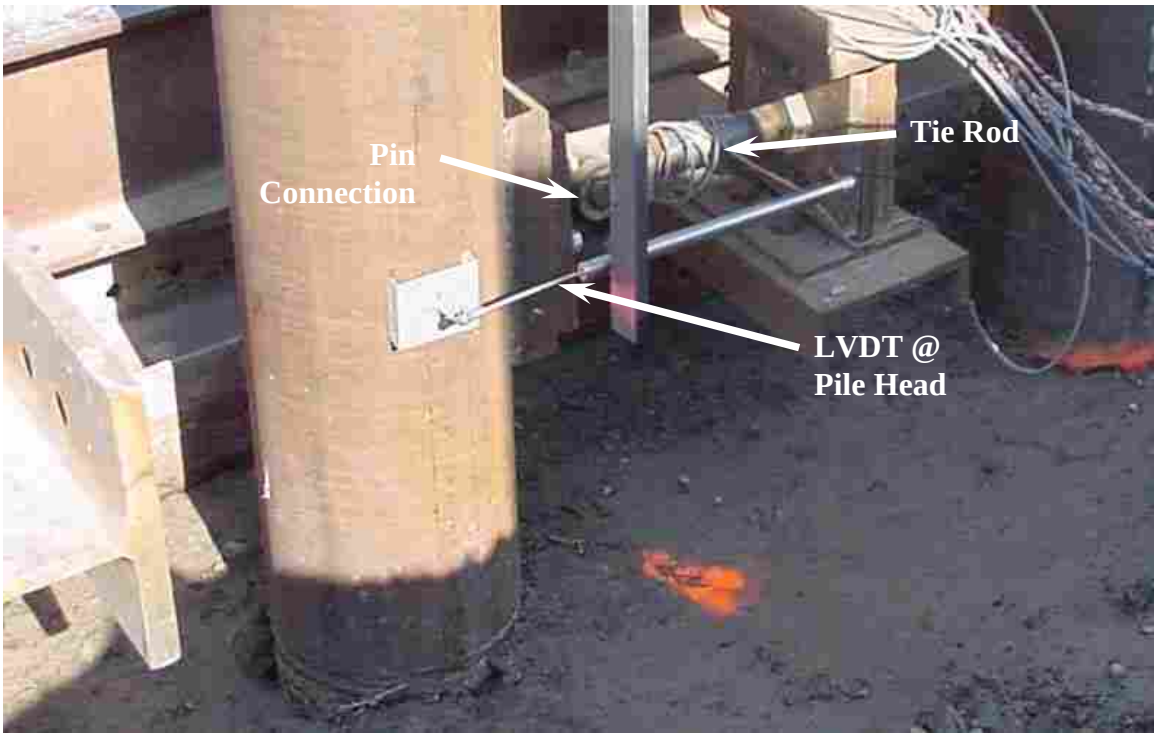

Figure 4.5: LVDT and tie rod connections to individual piles at pile head.

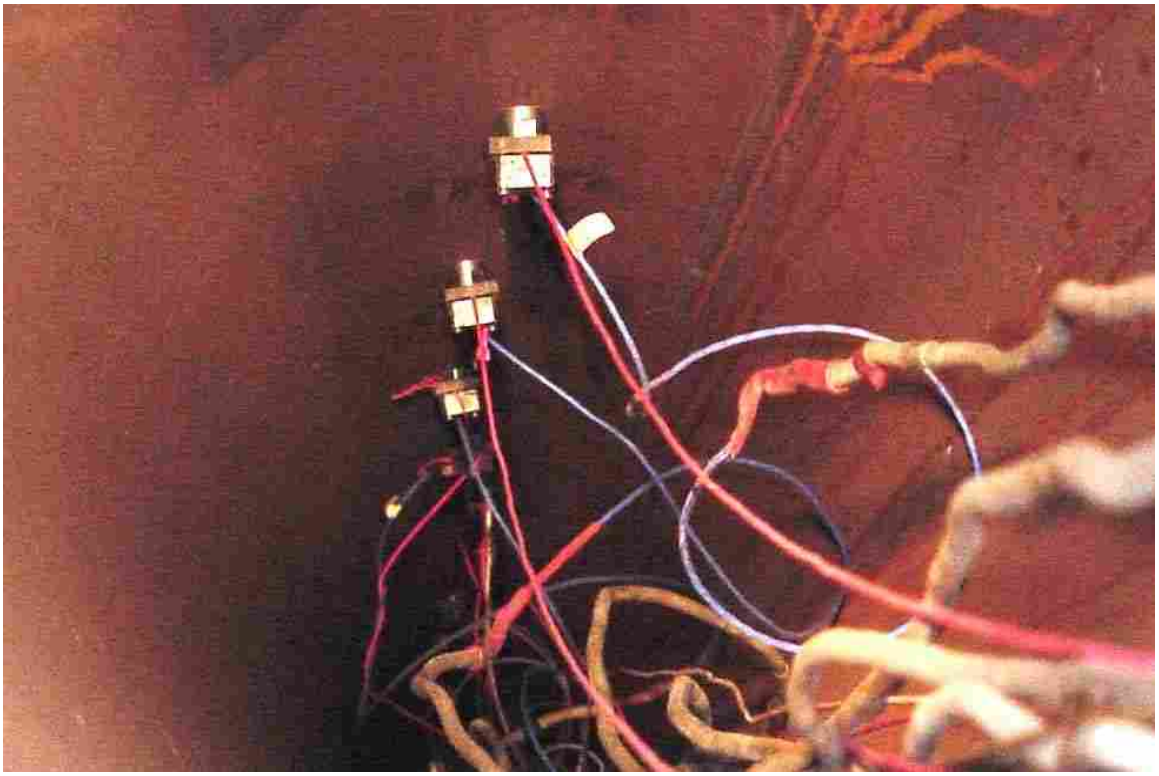

Figure 4.6: View down inside pile with accelerometers.

4.2 15-Pile Group Testing Procedures

The 15-pile group was tested on August 7th and 8th, 2002. The testing approach involved both static and statnamic load tests which were performed consecutively and produced deflection in the same direction. Fifteen cyclic static lateral load tests were performed at a target deflection followed by a statnamic load as the final 16th cyclic load. Each subsequent target defection was increased. Static load testing had seven target deflections at 6 mm, 13 mm, 25 mm, 38 mm, 51 mm, 64 mm, and 89 mm. Statnamic test firings were performed at six target deflections: 13 mm, 25 mm, 38 mm, 64 mm, and twice at 89 mm. The last two statnamic tests applied the 1st and 16th cycles of loading at the 89 mm target deflection. The first statnamic cyclic load for the 89 mm target deflection was to observe the dynamic characteristics of the group piles while loading into virgin soil.

4.3 15-Pile Group Test Results

4.3.1 Time Histories

Time histories of deflection and acceleration were obtained directly from the LVDTs and accelerometers, respectively. However, some of the accelerometer data required baseline correction as described subsequently. Velocity time histories were generally obtained by numerical integration from the acceleration time history. Figures 4.7 through 4.11 show typical acceleration, velocity and deflection time history data. The data represent one test at different elevations of the piles for test 6 (98mm target deflection). Similar plots for all the tests are provided in Appendix 1. In general, the peak deflection occurs where the velocity is zero and the peak velocity occurs where the

acceleration is zero as required by calculus. This is another indication that the test results are reasonably and accurate.

The LVDT data for each pile was averaged to obtain the motion of the pile group. By differentiating the deflection time histories from the LVDTs, velocity and acceleration time histories were also obtained in some cases for comparison purposes or when accelerometer data was not available. The initial pile head deflection for each statnamic test increased somewhat with each test, because of soil that fell into the gap behind the piles during the static load testing which prevented a complete rebound of the pile to zero deflection.

Numerical Integration was used to obtain the velocity and deflection time histories from the accelerometers. Using this process on the uncorrected acceleration time history indicated that significant baseline drift was occurring so that the velocity was not zero at the end of the record and the deflection time histories were significantly different than the measured values. Therefore, efforts were made to make baseline corrections in the acceleration time histories using the computer program Baseline (2002). Baseline is a curve-fitting program that uses the least square sums method to minimize errors and alleviate this problem.

To provide a check on the accuracy of the numerical integration procedure after baseline correction, the deflection time histories measured by the LVDTs at the pile head were compared with the time histories obtained by the accelerometers. In making these comparisons, initial deflections from LVDT data were zeroed, because accelerometers do not measure the initial position. Typically, the maximum deflections computed from the accelerometer data were within 10% of those measured by the LVDT giving confidence that the accelerometer data was reasonably accurate. Most of the down-hole

accelerometers appeared to function properly; however, the accelerometer at 3.05 m (10.0 ft) did not work for the entire period of testing on the 15-pile group.

All of the time histories obtained from the accelerometers were zeroed, because initial deflections down the pile were not known. Also notable is that the final displacement obtained from the accelerometers returns to zero, because of the baseline correction program which was used to correct the acceleration time histories. The maximum deflection of the each test was reached shortly after the maximum load. Most of the motion for all of the tests lasted about 0.6 seconds. Table 4.1 compares the maximum deflections for each test to the target deflection desired in each test. For the majority of the tests, the maximum deflection was within 10 mm of the target deflection. Tests four and six deviated slightly from the target deflections. Test four was 11 mm over the target of 64 mm. Test six was 15 mm over the target of 89 mm. Test five was the only test under the target deflection and the only test with virgin loaded soil. Because the statnamic tests were "load-controlled" tests and the load could not be controlled directly, the agreement between the actual deflection and the target deflection is reasonably good.

In addition, numerical differentiation was used on the deflection time histories where possible to obtain a second estimate of the velocity time histories and provide a check on the velocity computed using the accelerometer time histories.

Large earthquakes usually have peak ground accelerations from 0.5 to 2.0 g with velocities around 1m/s/g. The measured pile accelerations were mostly higher than earthquake accelerations; however, velocities were about the same as what would be expected from an earthquake. Comparable velocity is most important for this study, because damping effects are related to the velocity of the structure. Inertia effects which

are related to the peak accelerations can be quantified and accounted for during the analysis.

Also notable was that negative (rebound) velocities were much higher than the positive velocities. When the piles are being loaded, the pile and soil resist motion, but when rebounding, lateral soil pressure does not exist because of gaps between the piles and soil. As a result, positive velocity would be expected to be higher than negative velocity.

Table 4.1: Comparison of the Target and Actual Maximum Deflection

Test #	Target Deflection (mm)	LVDT Pile Head Deflection (mm)	Difference (mm)
1	13	15	2
2	25	30	5
3	38	47	9
4	64	75	11
5	89	87	-2
6	89	104	15

4.3.2 Profile Shape with Peak Accelerations and Velocities

Accelerometer data provided profiles in Figure 4.11 which reflect the shape of the group of piles at peak positive deflections. Peak positive and negative acceleration values were found at peak deflections. The peak positive and negative velocity values occurred when the acceleration went to zero. Peak deflections occurred also when velocities went to zero. These results are verified from the time histories which also satisfy the equations defined from integration. The results are supported by calculus, because the rules of integration are satisfied.

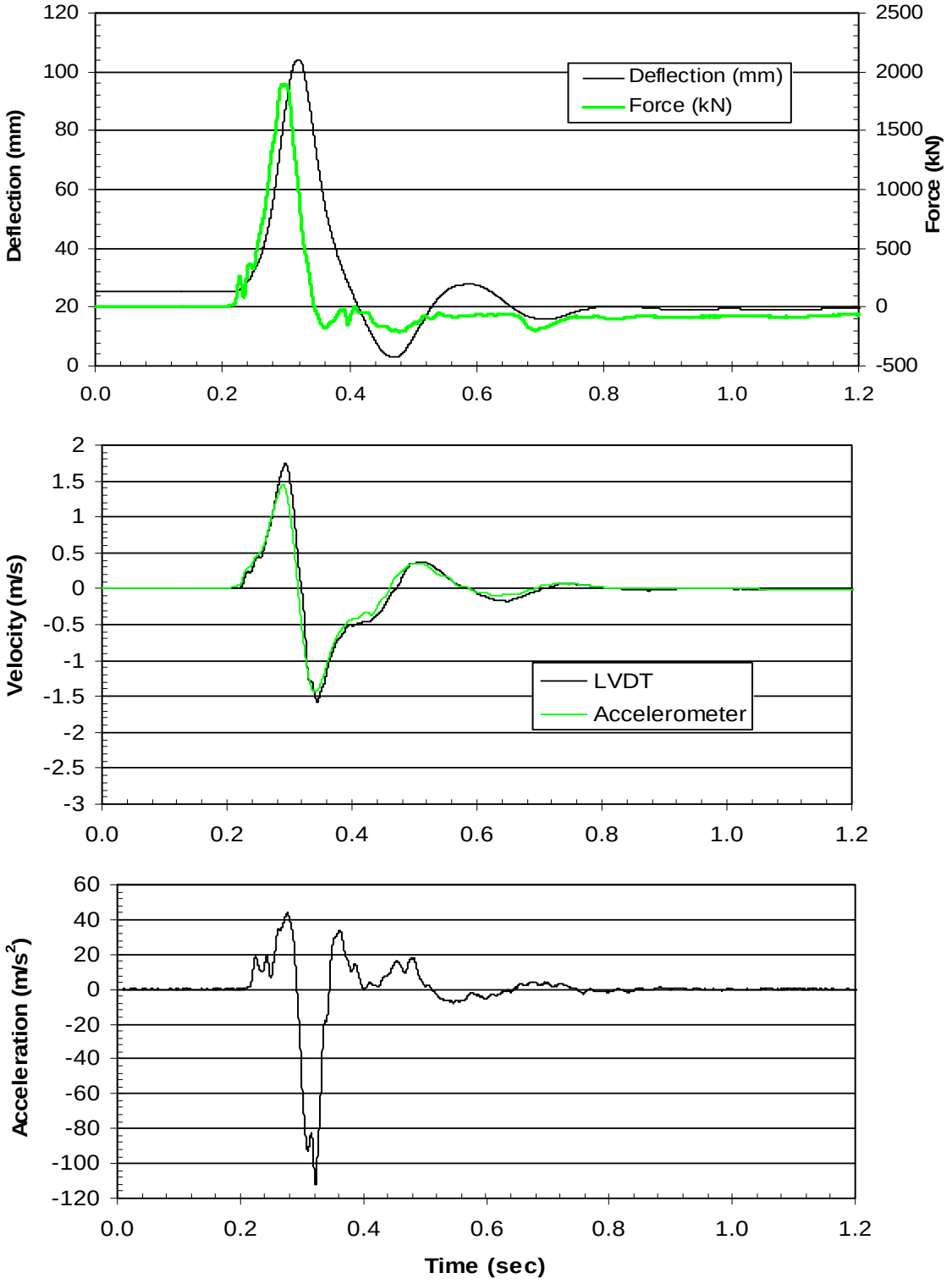

Figure 4.7: 15-pile group, test 6, 89 mm (3.5 in) target—LVDT time histories at pile head.

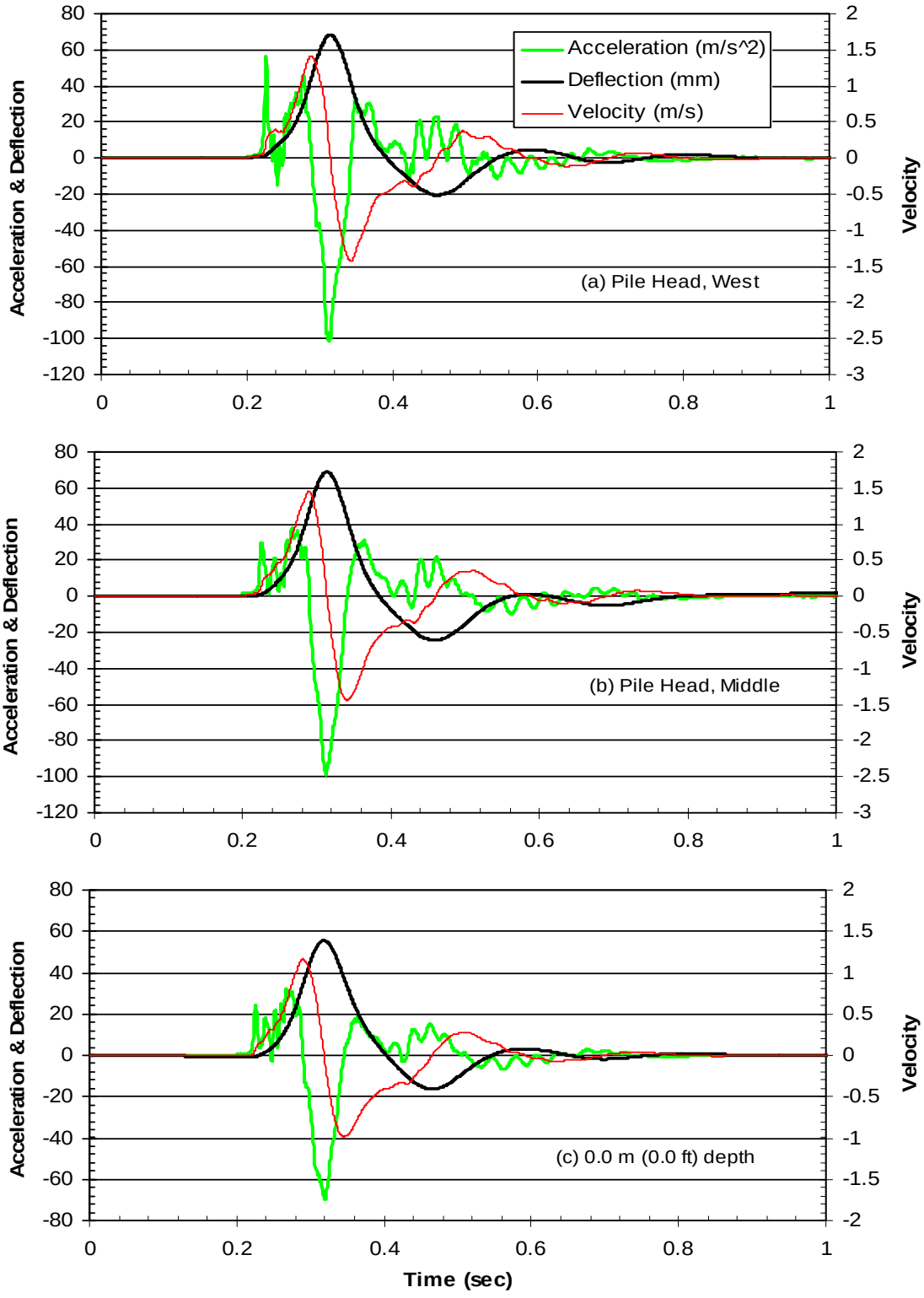

Figure 4.8: 15-pile group, test 6—accelerometer time histories at (a) pile head, west pile, (b) pile head, middle pile, and (c) 0.0 m (0.0 ft) depth.

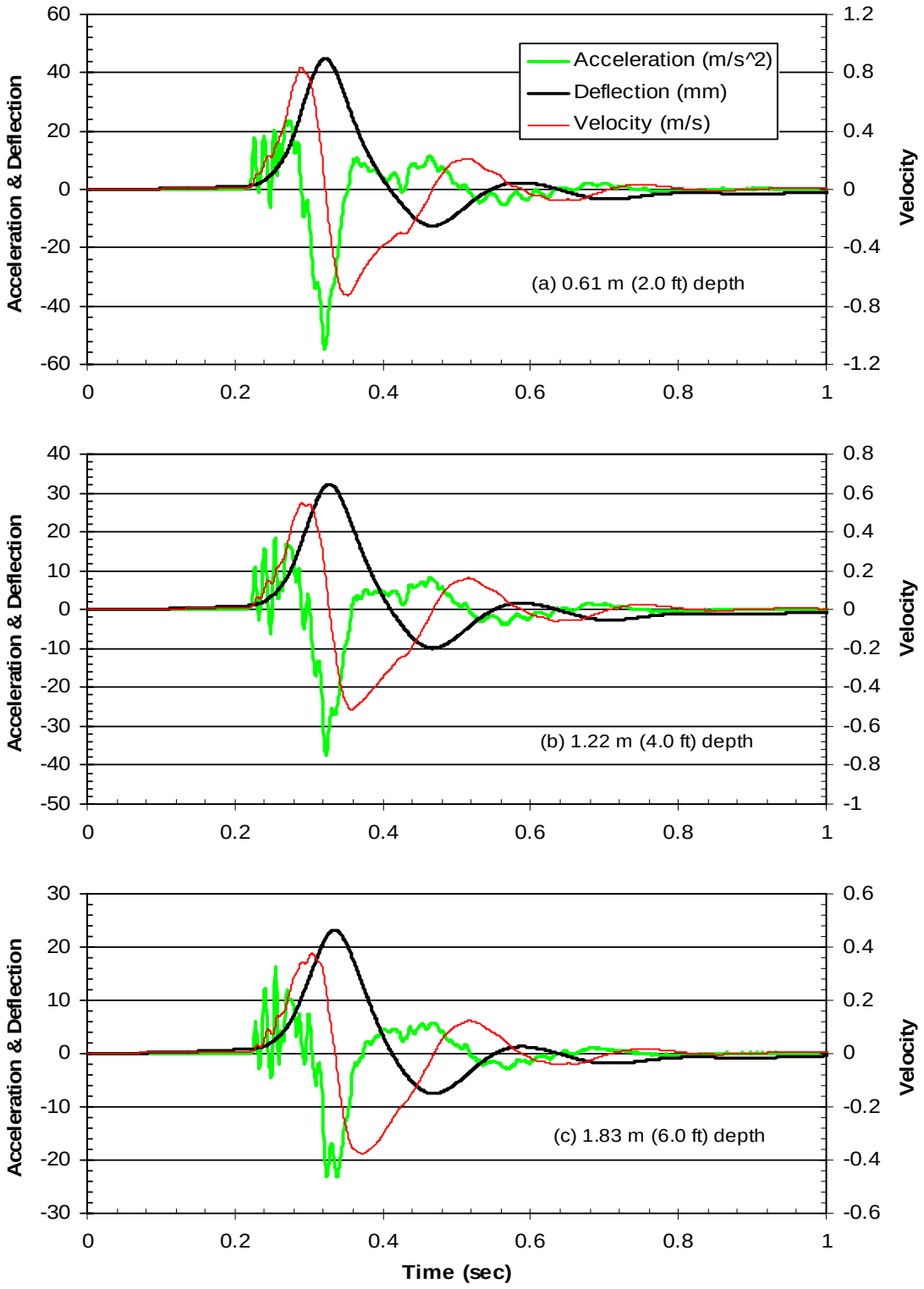

Figure 4.9: 15-pile group, test 6—accelerometer time histories at (a) 0.61 m (2.0 ft), (b) 1.22 m (4.0 ft), and (c) 1.83 m (6.0 ft) depths.

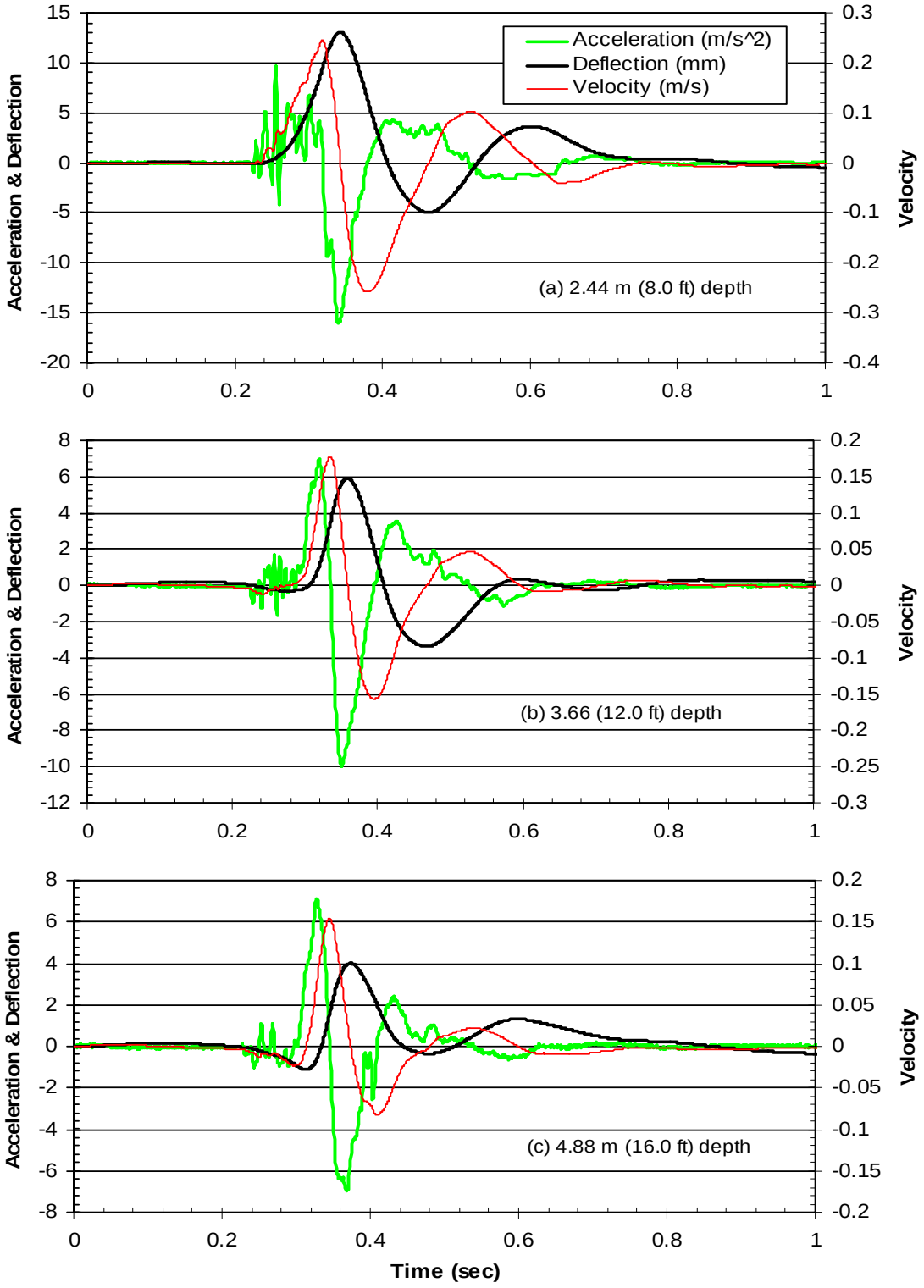

Figure 4.10: 15-pile group, test 6—accelerometer time histories at (a) 2.44 m (8.0 ft), (b) 3.66 m (12.0 ft), and (c) 4.88 m (16.0 ft) depths.

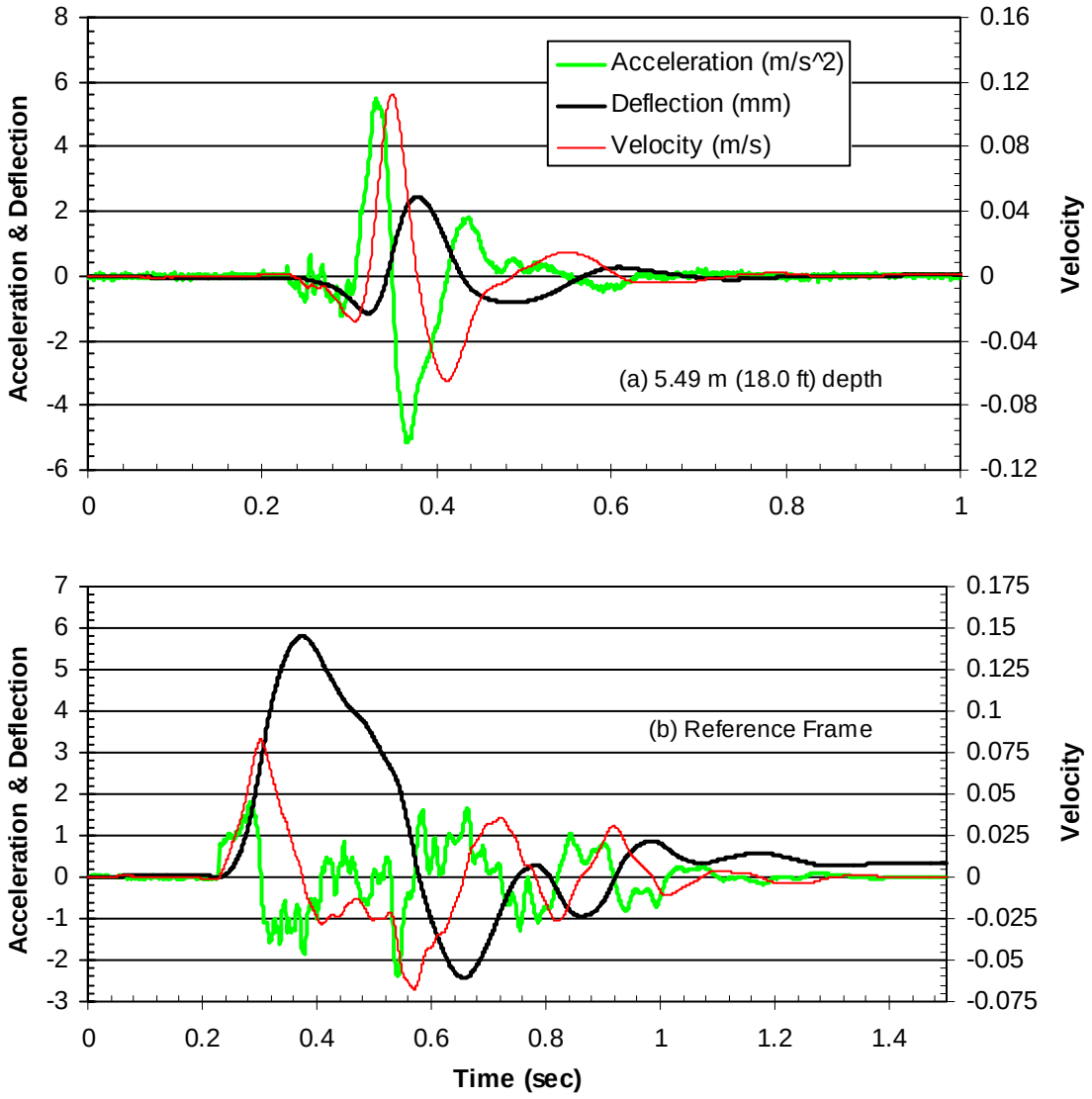

Figure 4.11: 15-pile group, test 6—accelerometer time histories at (a) 5.49 m (18.0 ft) depth and (b) reference frame.

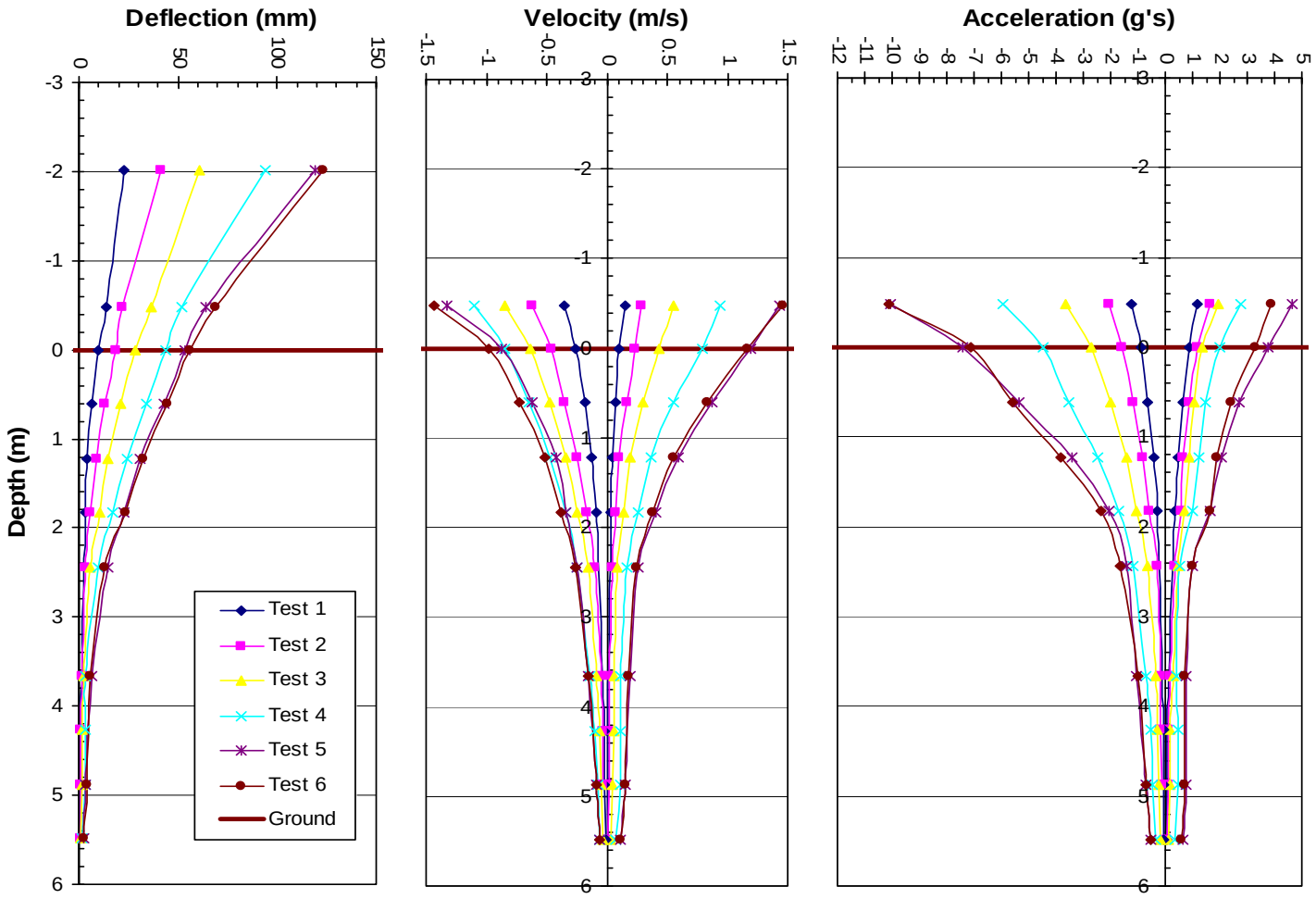

Figure 4.12: Profiles of deflection, velocity, and acceleration at the maximum pile head deflection for each statnamic test of the 15-pile group.

4.3.3 Load vs. Deflection

Figures 4.13 and 4.14 provide plots of the load vs deflection curves for the 15th static load cycle for each target deflection along with the statnamic test (16th cycle load) for each target deflection. During static loading, the hysteresis loops are relatively small; however, during the statnamic (dynamic) test the large hysteresis loops suggest that damping resistance is a significant component of the resistance. The damping produces a stiffer load-deflection curve under dynamic loading than during static loading. The initial deflection of the 15th cycle was always greater than the 16th statnamic cycle. This occurred primarily because the soil relaxed and rebounded between the static load intervals and the statnamic loading.

Figure 4.15 compares all statnamic loads versus deflection curves together. Two additional plots were added to this figure. The dashed line curve connects the points defining the deflection at the maximum load developed during each dynamic test. The solid blue curve with diamond makers connects the points defining the load at the maximum deflection for each dynamic test. Test five developed the highest load even though the maximum deflection was 17 mm less than test 6. Test five was the 1st cyclic load for the 89mm target deflection. The force is larger because the piles are loading virgin soil, whereas, test six involve reloading of the soil. The discrepancy between these two curves highlights the fact that the peak load and peak deflection occur at different times during each statnamic test. The peak deflection occurs after the peak load because the momentum of the pile carries it further after the peak load is achieved.

The load measured by the load cell mounted on the piston of the statnamic device is compared to the load obtained by summing the load cells connected to each pile in the

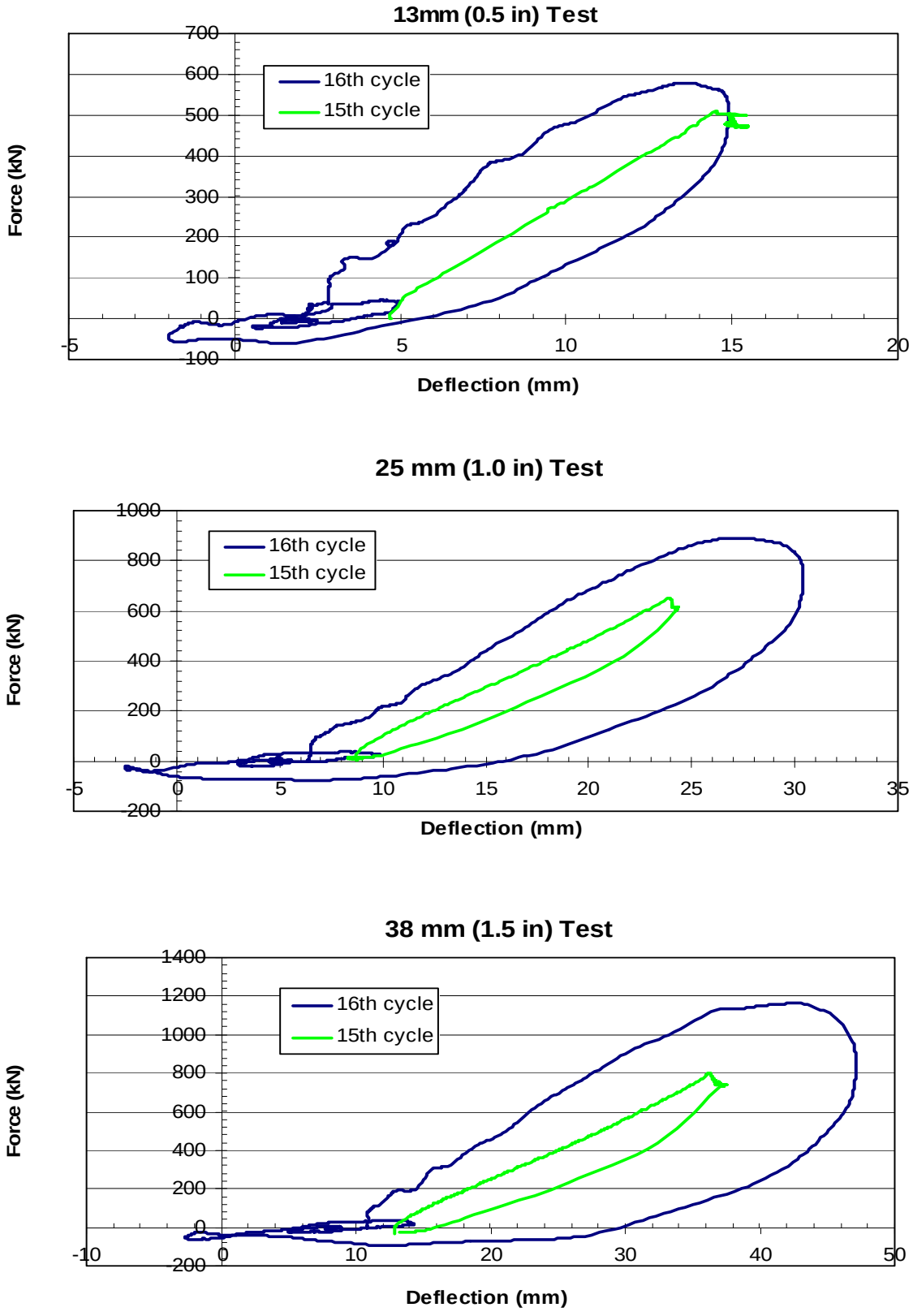

Figure 4.13: Statnamic loads compared to static loads.

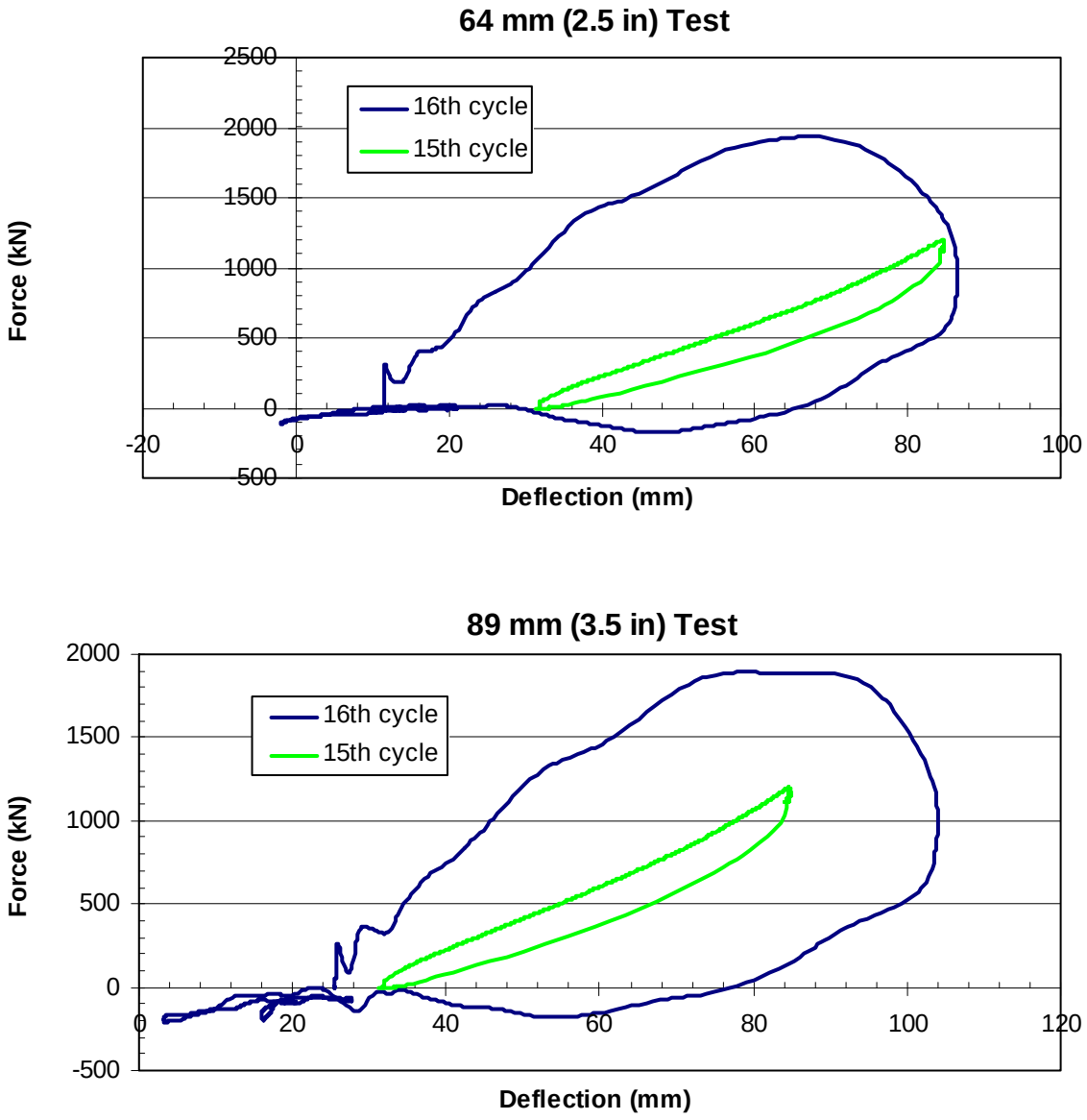

Figure 4.14: Statnamic loads compared to static loads.

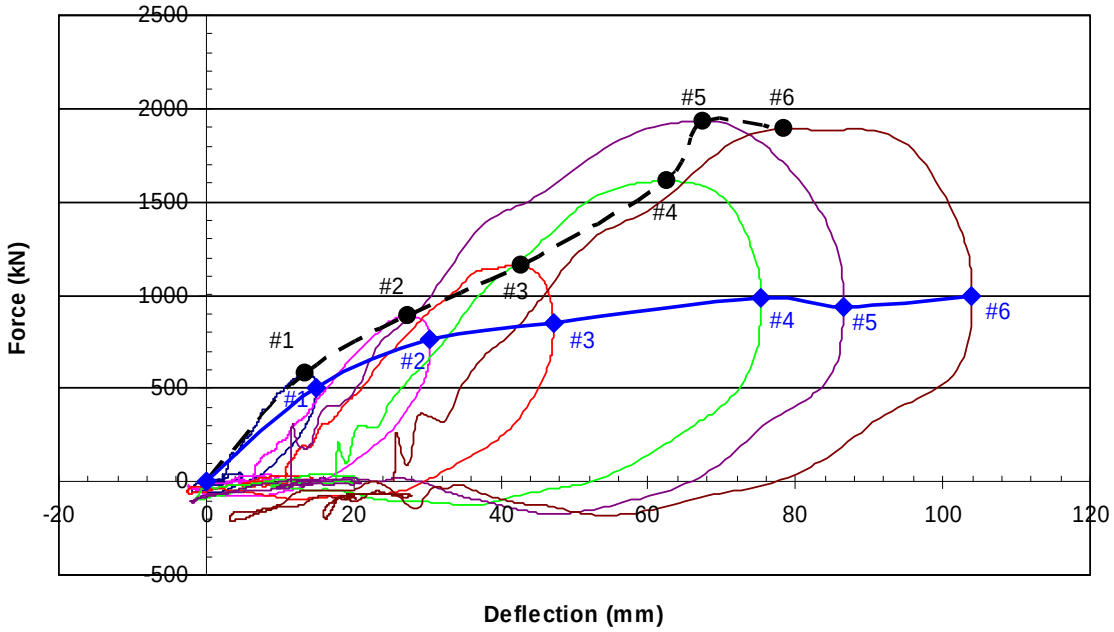

Figure 4.15: Statnamic loads and located peak loads and deflections.

plots in Figure 4.16. It is evident that there are differences between the two measured loads and these differences are more pronounced at the higher load levels. Typically, the load measured by the sum of the pile load cells is higher (15 to 20%) than that measured by the statnamic. In addition, the statnamic load cell never shows a load less than zero (tension) while the summed load cells do. These differences are caused by the inertial forces and energy loss due to friction and not from instrumentation error. Inertial forces from the mass of the load frame are particularly notable in the observed negative forces created from the summed load cells. The statnamic load cell measured only the load applied to the pile group and frame. Since the statnamic piston was not connected to the frame, no tensile force could develop. In contrast, the tie rod connected the piles to the

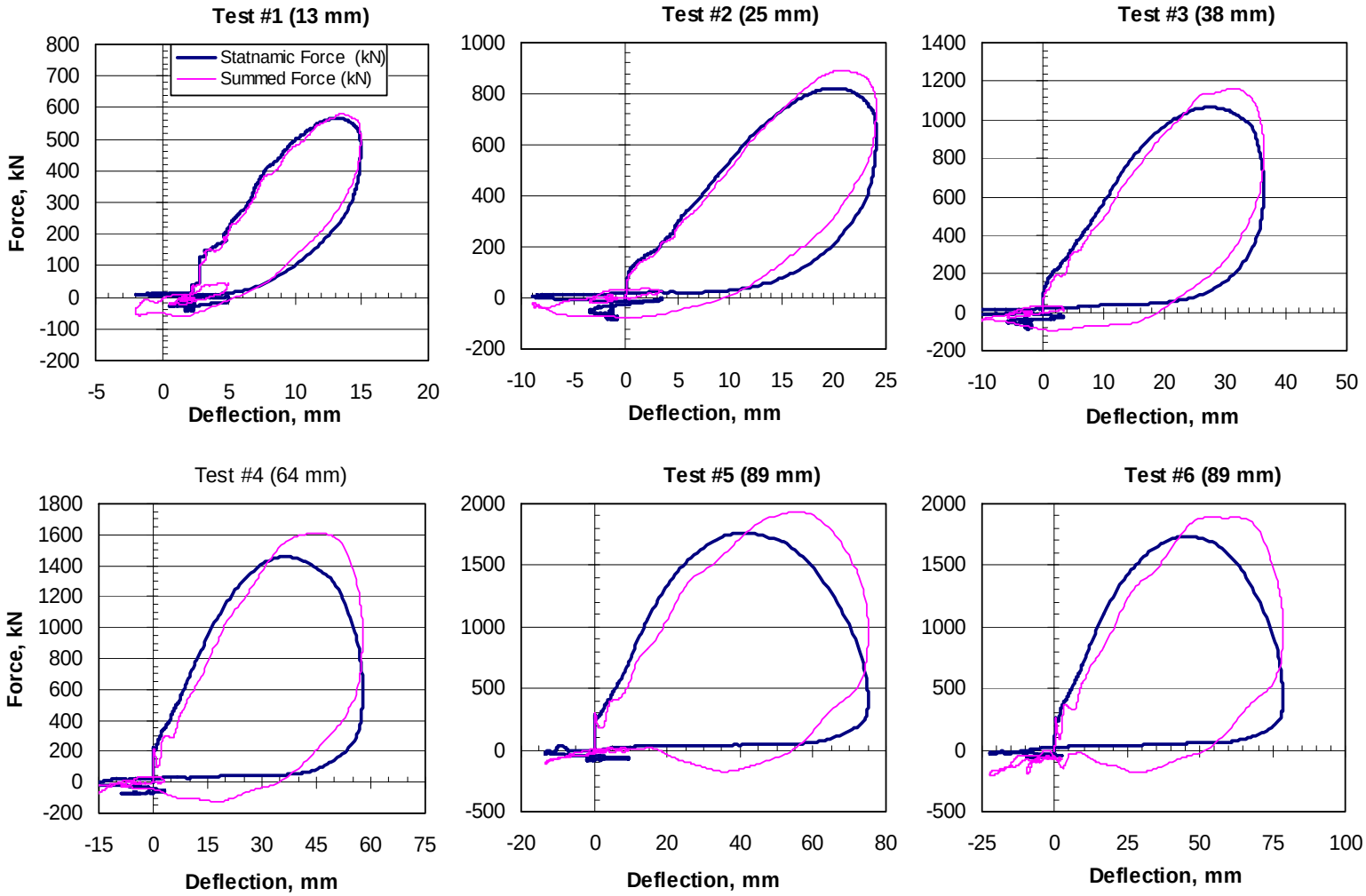

Figure 4.16: Comparison of the statnamic load cell and sum of individual pile load cells in load deflection curve.

frame so that the measured force in the tie-rod was dependent on the motion of the frame. Hence, the negative measured force is a result of inertia of the frame moving in opposition to the piles.

4.3.4 Gap Measurements

Gaps between the piles and the cohesive soil surrounding them were quite evident, particularly as the forces and deflections increased as shown in Figure 4.17. A gap formed behind the piles during loading and a gap formed in front of the pile as the load was released. The gaps in front of the west side piles were measured after each statnamic test. The measurements were made by measuring the depth to which shims of varying thickness could be inserted into the gap between the pile and the soil.

Figure 4.17: Formation of gaps.

Figures 4.18 and 4.19 plot the increasing gap width and depth adjacent to each row as the pile head loads and the deflections increased. The gap depth appeared to be greatest for row 1 and was somewhat less for row 2. The gap depths for rows 3 through 5 were about the same but less than for row 2.

4.3.5 Bending Moment Diagrams

From the stain gage data, bending moment (M) at each station was determined using the equation

$$M = \frac{EI(\varepsilon_S - \varepsilon_N)}{D_o} \tag{4.1}$$

where:

E is the Young's Modulus of Elasticity in Steel (29,000 ksi or 200×10^6 kPa)

I is the Inertia about central axis (344 in^4 or 143×10^6 mm^4)

ε_N and ε_S are the north and south strain readings

D_o is the outer diameter of the pile or the distance between the strain gages

Compression strains were defined as negative (-) values and tension was defined as positive (+) values. Some of the stain gages were damaged during pile installation, while others malfunctioned during the testing period. If only one strain gage was available at the station, an assumption was made that the strain was equal and opposite to the strain from the gage that worked.

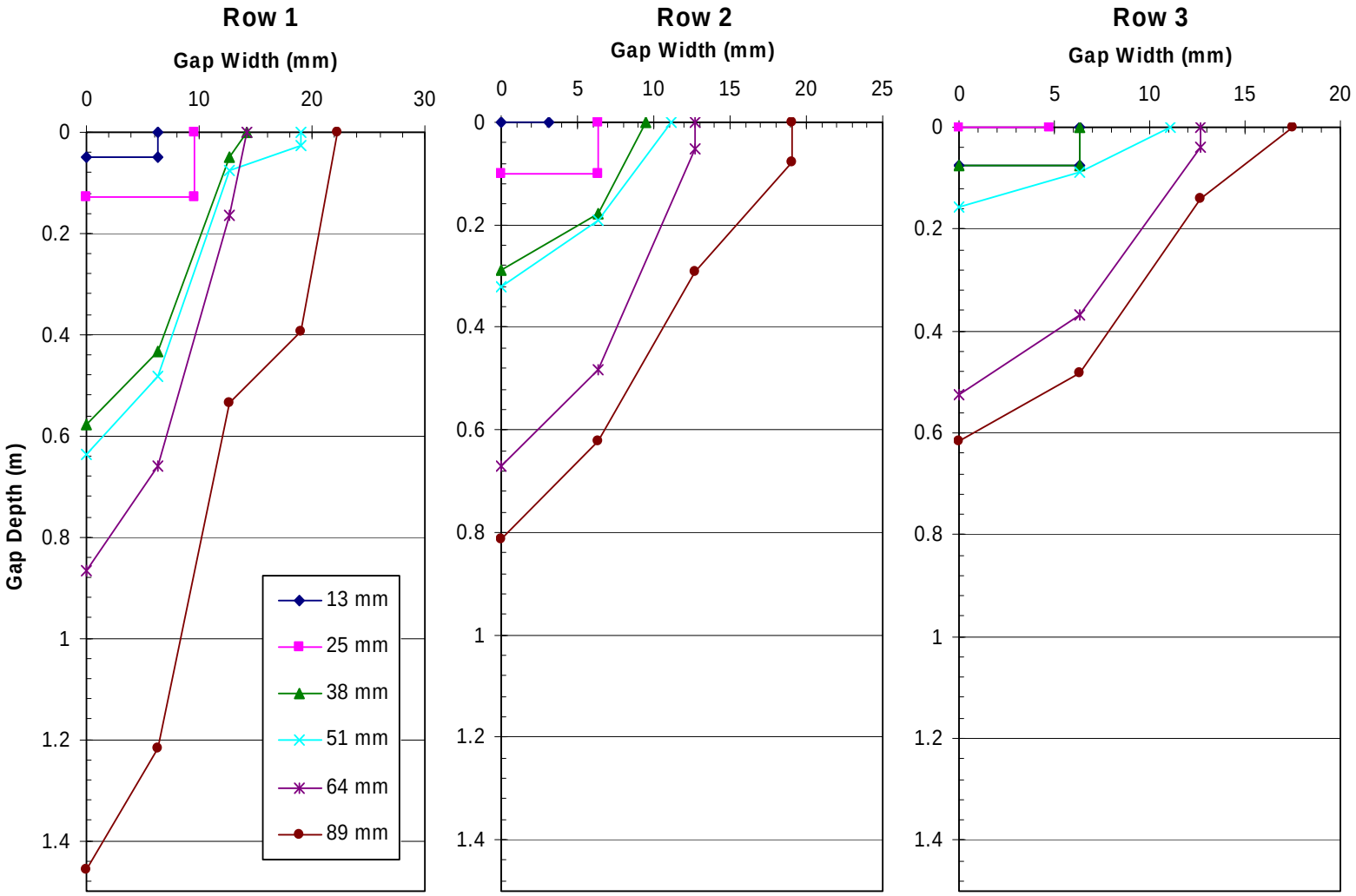

Figure 4.18: Gap widths measured from piles 3, 6, 9.

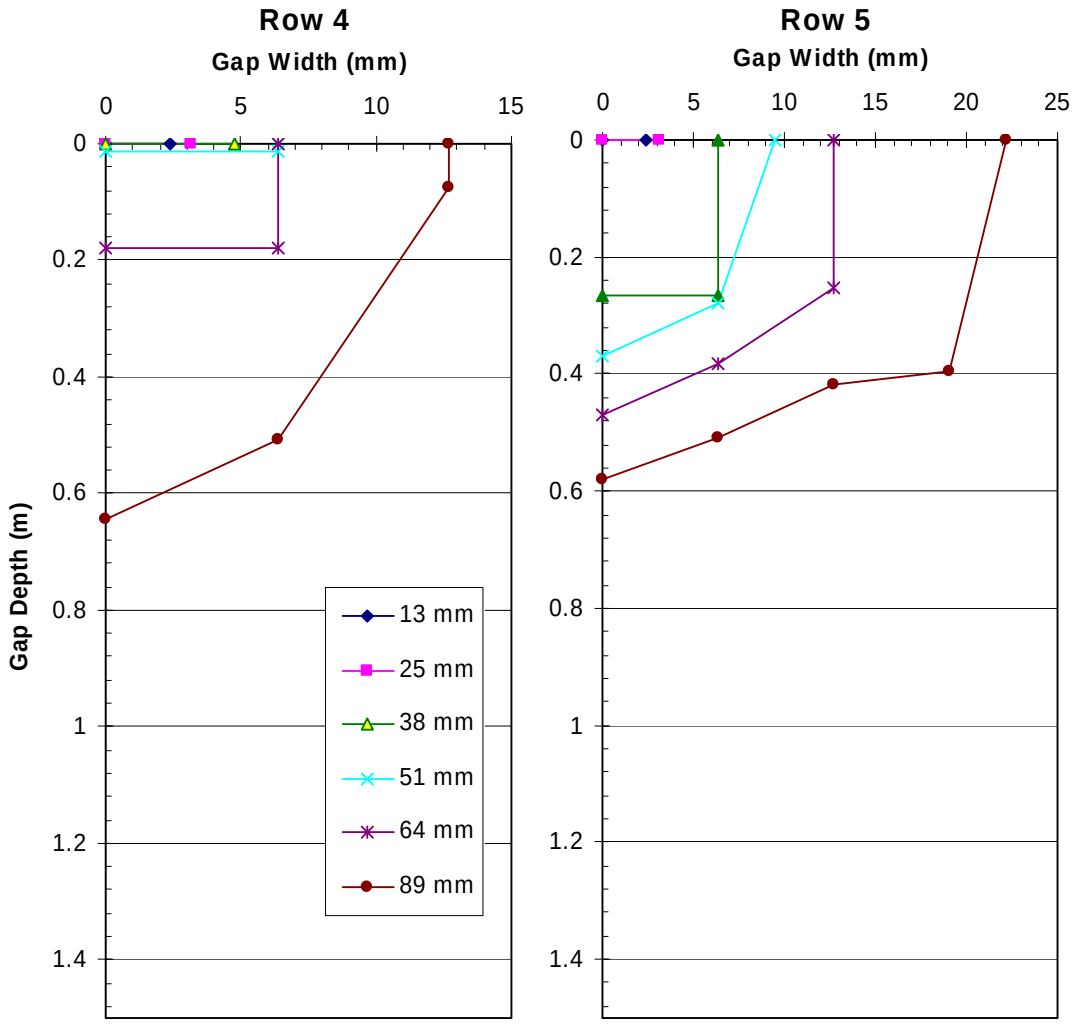

Figure 4.19: Gap widths measured from piles 12 and 15.

Figures 4.20 and 4.21 compare the bending moment versus depth diagrams of each row at the peak load. The maximum bending moments typically develop at about 1.8 m below the ground surface; however, the pile bending moment in row one develops at a more shallow depth. Rows 2, 3, and 4 consistently have smaller peak bending moments than rows 1 and 5. This can be attributed to shadowing effects of the pile-soil-pile interaction. The lead row (row 1) typically exhibited the greatest maximum bending moment of any of the rows. This can be attributed to the fact that the lead row piles carry higher loads than the piles in the other rows. The pile in row 5 sometimes exhibited relatively high bending moments despite the lower average load carried by the pile. This discrepancy is explained by the reduction in soil resistance around the pile due to group interaction effects. This reduction in soil resistance allowed greater bending moment to develop for a given load.

Figures 4.22 and 4.23 show trends of the bending moment versus depth curves for each pile separately for each dynamic test. These bending moments were also plotted at the peak load for each test. A review of these plots indicates that the depth to the peak bending moments tends to slowly increase as the lateral load and deflection increase.

The bending moment versus depth curves for the 1st cyclic load at the 89 mm target deflection (Test 5) and the 16th cyclic load at the 89 mm target deflection (Test 6) are compared to each other in Figures 4.24 and 4.25. To better compare the difference in the bending moment shapes, the moments were normalized by dividing by the maximum pile head load in each case. The normalized bending moment diagrams were very similar with no observed differences. This result suggests that apart from the reduction in load, produced by cycling, the ratio of bending moment to load is unaffected.

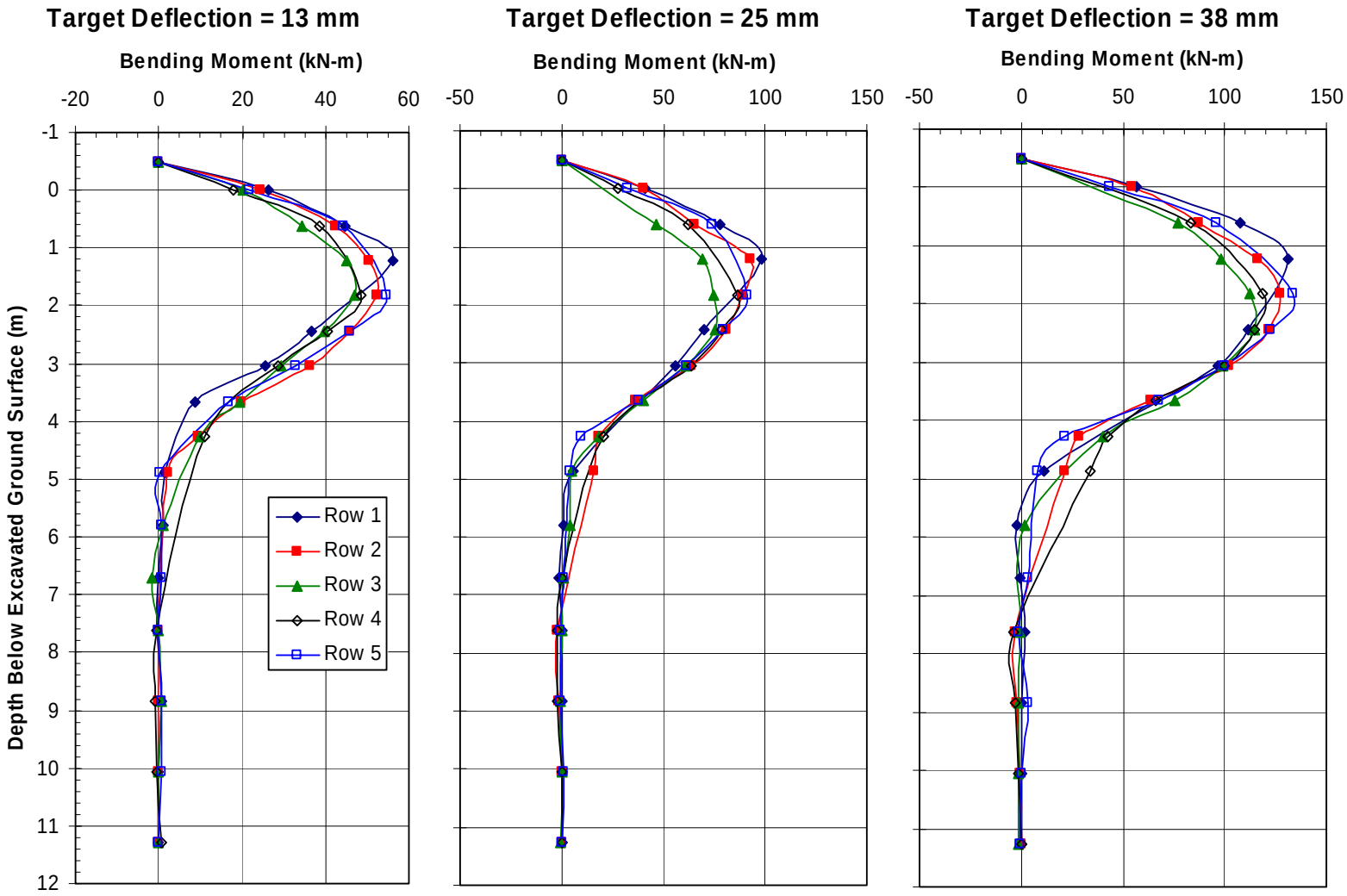

Figure 4.20: Comparing rows of bending moment diagrams for statnamic tests 1, 2, and 3.

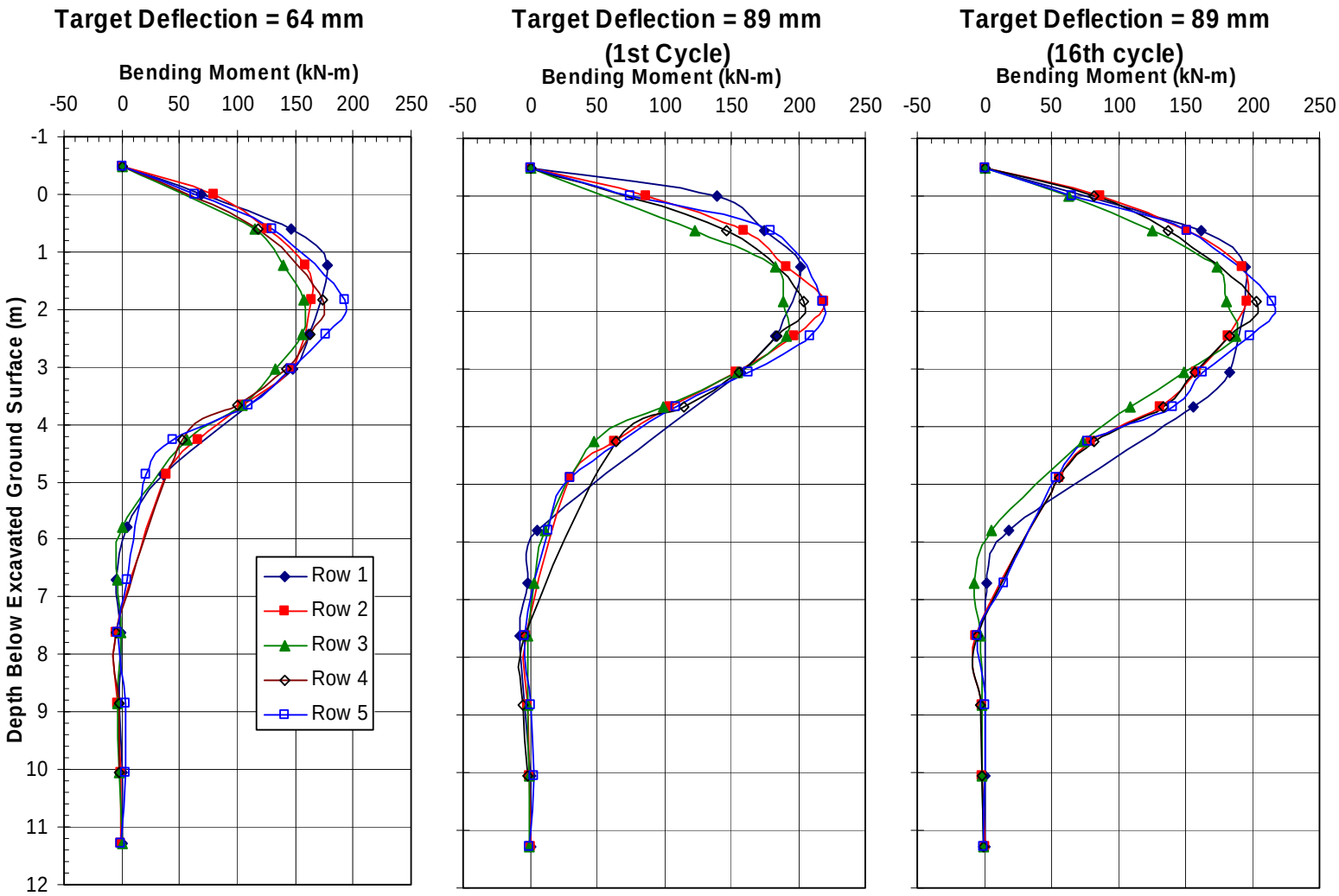

Figure 4.21: Comparing rows of bending moment diagrams for statnamic tests 4, 5, and 6.

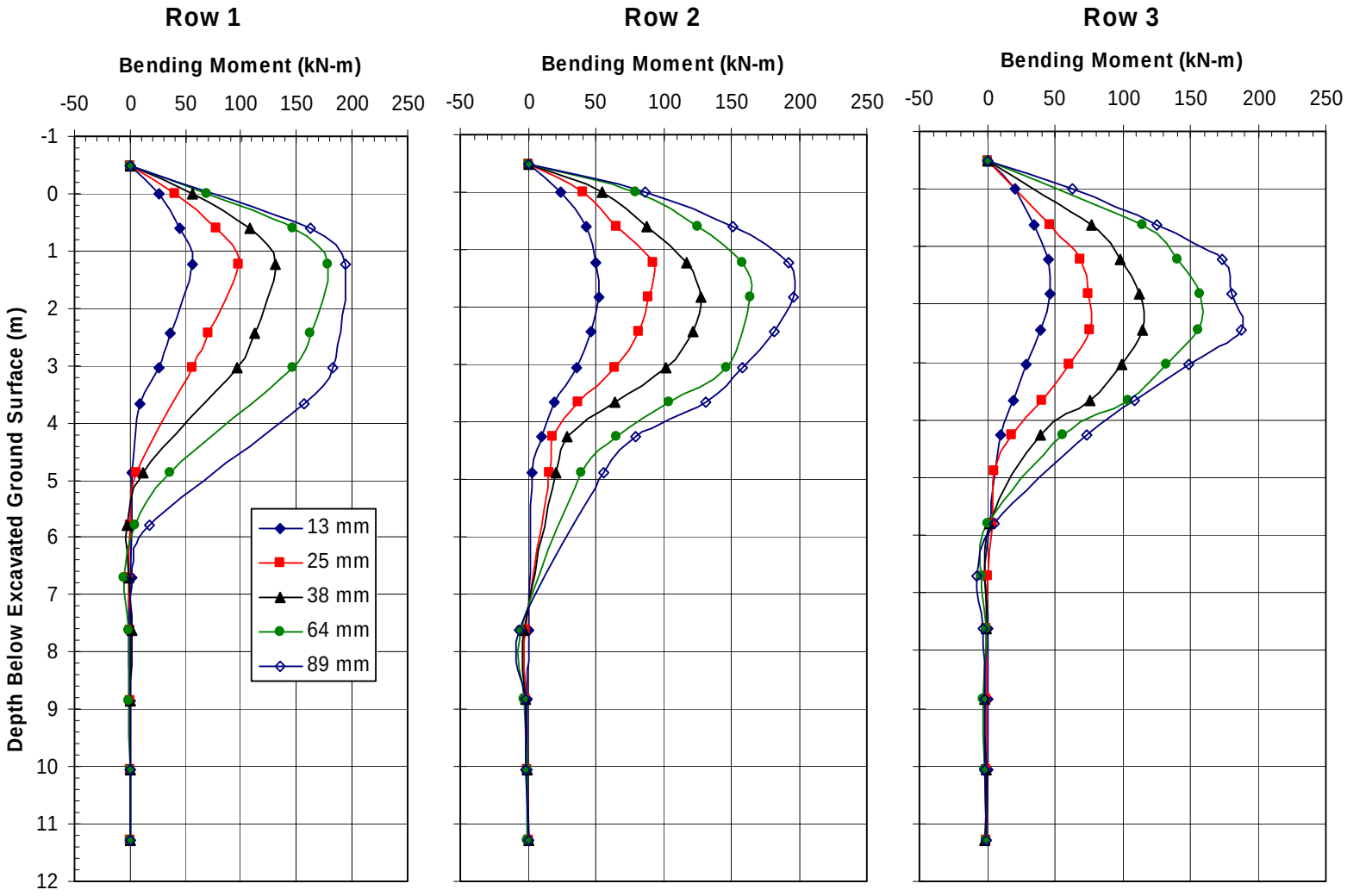

Figure 4.22: Comparing bending moment diagrams by row at peak load for each test.

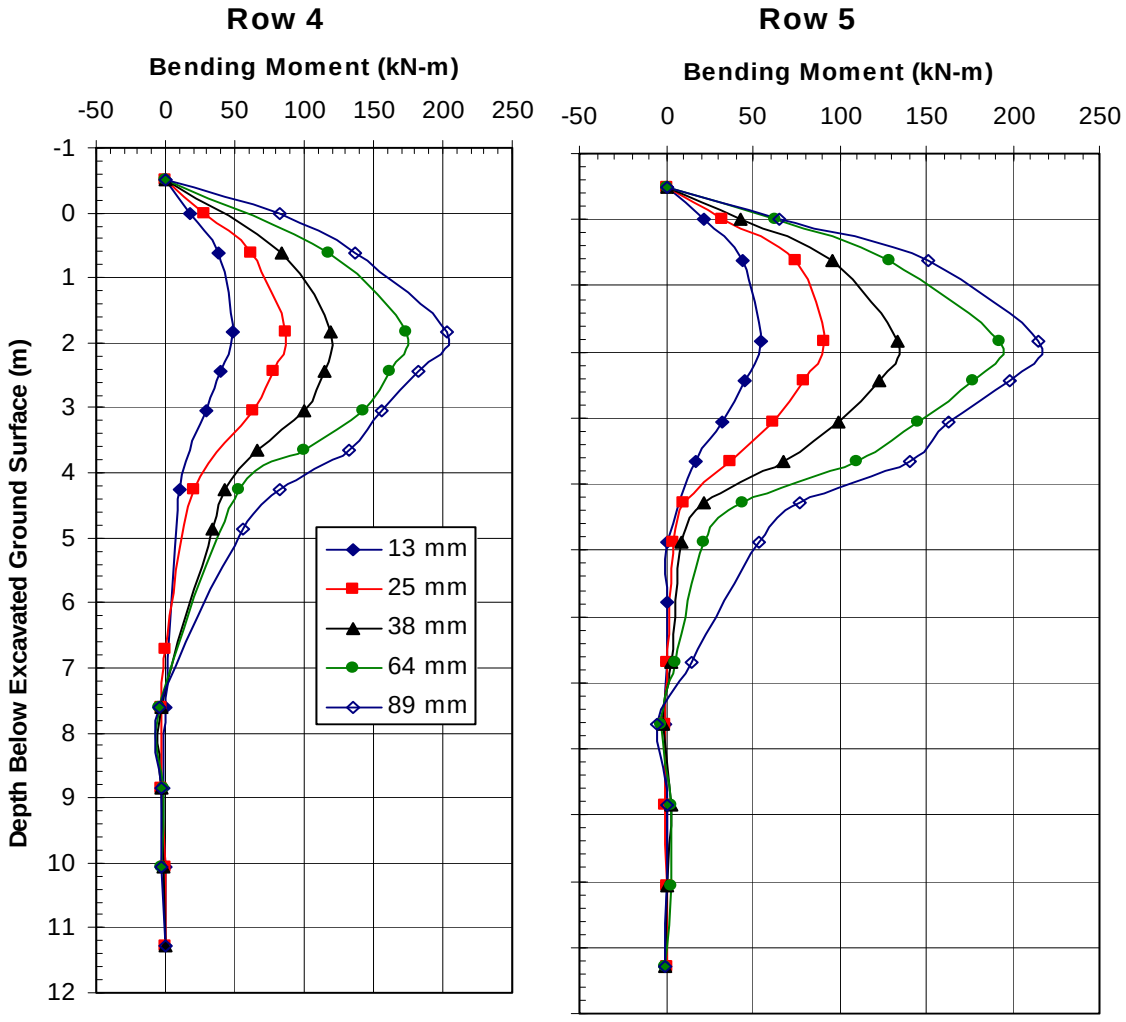

Figure 4.23: Comparing bending moment diagrams by row at peak load for each test.

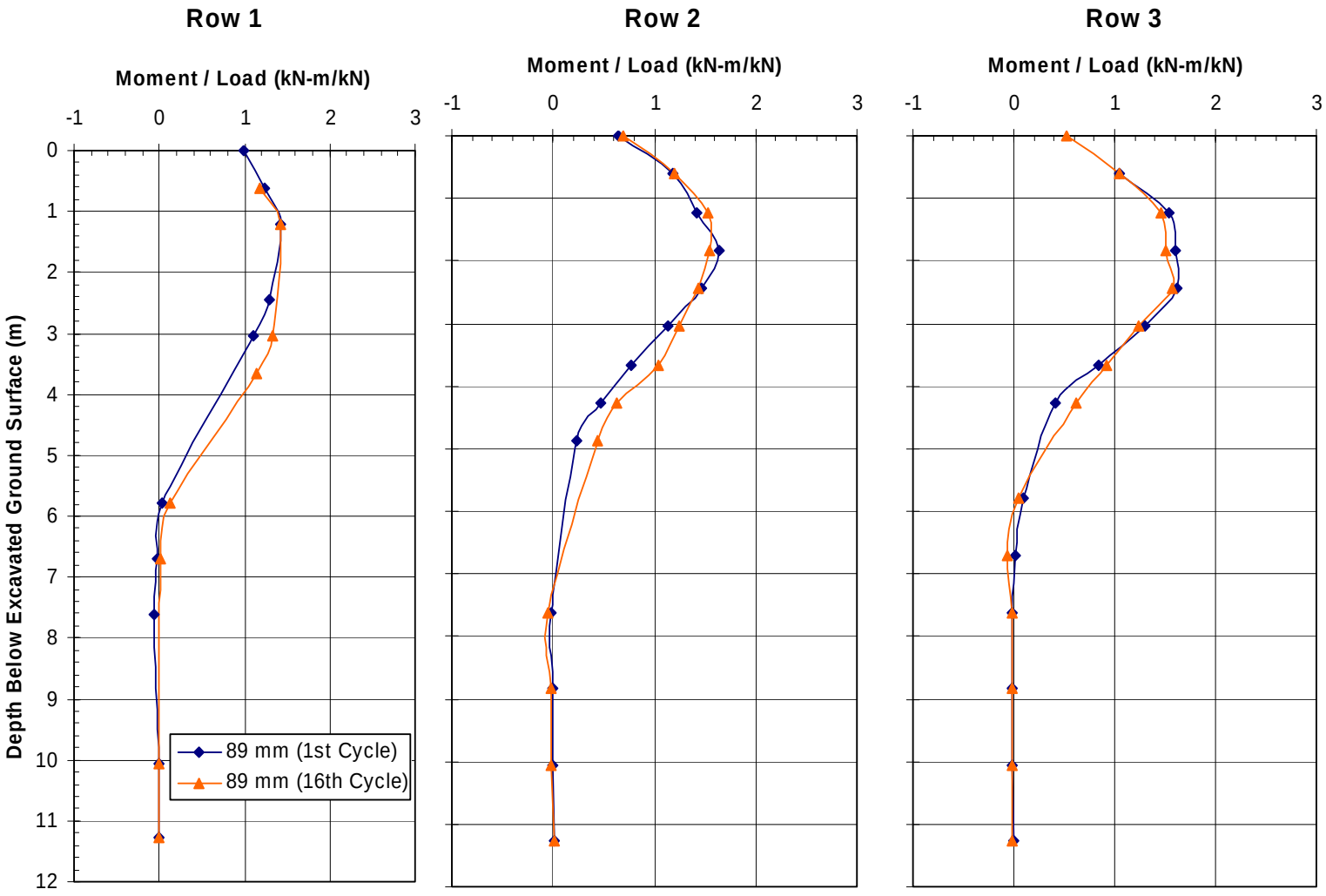

Figure 4.24: Comparing bending moment diagrams of 1st and 16th cycles of 89 mm target deflection.

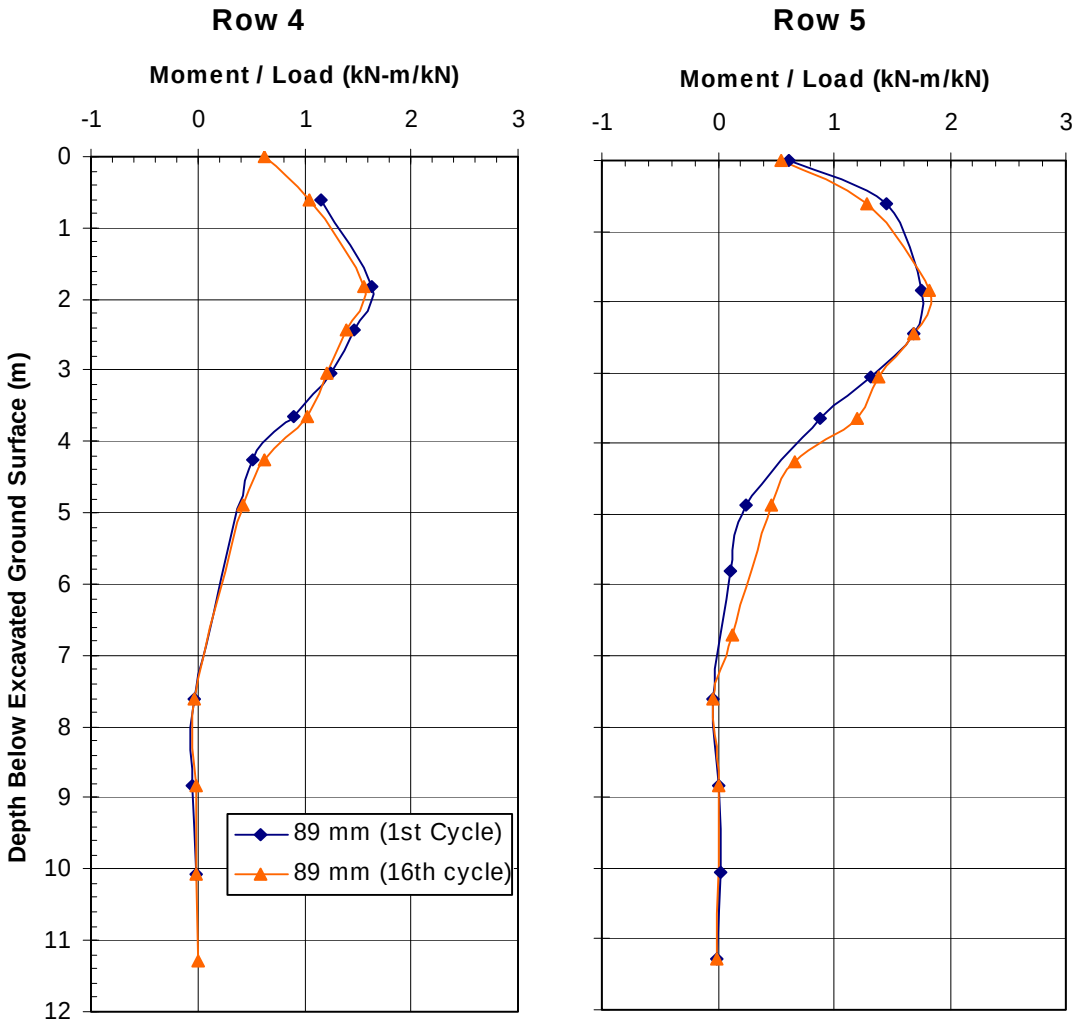

Figure 4.25: Comparing bending moment diagrams of 1st and 16th cycles of 89 mm target deflection.

CHAPTER 5 9-PILE STATNAMIC LATERAL LOAD TESTING

5.1 Test Setup

5.1.1 Layout

On June 26, 2002, the 9-pile group, consisting of 324 mm OD steel pipe piles, was driven closed-ended by a 102 kN hydraulic hammer. The energy delivered to the driven piles ranged from 7 to 27 kN-m per blow. The piles were driven with row center to center spacing (North/South) of 1.83 m or 5.65 pile diameters and a column center to center spacing (East/West) of 1.07 m or 3.29 pile diameters as shown in Figure 5.1. This column spacing was chosen, because lateral shadowing effects have no significant effects with 3 pile diameters and greater (Cox et al., 1984) when under static load testing. As shown in Figure 5.1, each pile was numbered for the convenience of identifying individual piles. The test piles conformed to ASTM A252 Grade 3 specifications with the same properties as identified for the 15-pile group in Chapter 4.

To distribute the load to each individual pile, a load frame was constructed as detailed in Figure 5.1. Each pile was pin connected to the load frame by a 51 mm (2 in) diameter tie rod shown in Figure 5.2 which was bolted to the frame. Two C250x45 (C10x30) channels were bolted to two W310x67 (W12x45) beams which ran in the direction of the load. The channels were used to anchor the tie rods to the load frame. A W760x284 beam was connected at the south end of the load fame and used for the static

load testing which pulled the pile group towards the south. The W920x313 beam at the north end of the load frame was loaded by the statnamic device which also pushed the pile group towards the south. These large I-beams were used to ensure uniform motion of the piles and to resist the large bending moments produced the by dynamic loading. To reduce friction caused by the load frame, low-friction rollers were connected to the load fame (Chapter 4, Figure 4.2). These rollers moved along steel tracks resting on the ground surface. The load reaction occurred at 483 mm (19 in) above the ground level.

A 35 ton statnamic device provided by Applied Foundation Testing, Inc. was placed in contact at the north end of the load frame. In order for the piston of the statnamic device to be level with the load frame, soil was excavated an additional 0.75 m (2.5 ft). To ensure that no excessive moments occurred in the statnamic loading, a swivel plate was used at the contact location of the load frame.

A foundation for the statnamic device was created by driving four H-piles 4.6 m (15 ft) into the ground. These four H-piles and the surrounding soft clay supported two 7.9 m (26 ft) long W920x223 (W36x150) beams lying on their weak sides which served as a "runway" for the statnamic sled. Railroad ties were placed on top of the webs of these beams to create a level surface for the runway.

5.1.2 Instrumentation

The 9-pile group was fully instrumented using load cells, linear variable differential transformer (LVDT) transducers, piezoelectric accelerometers, and electrical resistance type strain gages. With these instruments, forces, deflections, velocities, accelerations, moments, and rotations were found.

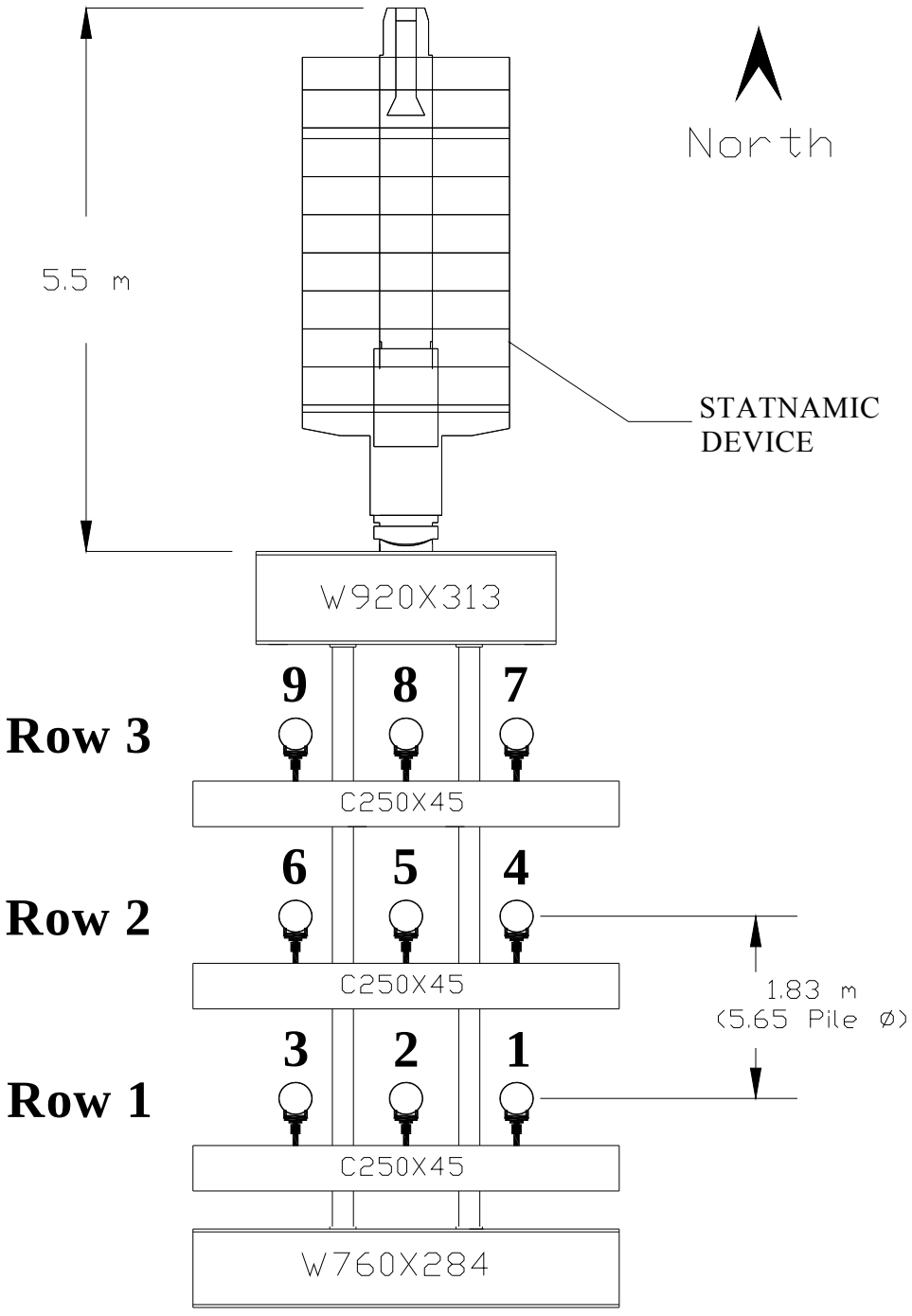

Figure 5.1: Plan view of 9-pile group layout with pile and row numbering.

Each individual tie rod connecting to the piles contained two sets of strain gages that measured the load carried by pile. Strain due to bending was canceled out using the two gage setup. The load measurements obtained from the nine load cells were typically within 2 to 5% of the load measured by two load cells in line with hydraulic jacks during the static lateral load testing (Johnson, 2003). An additional load cell was attached at the head of the piston on the statnamic device to measure the total load applied to the load frame.

Pile head deflections were measured on each pile with LVDTs as shown in Figure 5.2. These LVDTs are accurate to 0.13 mm. Two additional LVDTs were located on the center piles in the front and back rows at 1.5 m (5.0 ft) above the loading point. These LVDTs were used along with those at the load points to measure rotation. All LVDTs were connected to an independent reference frame that would not be influenced by the load on the group piles.

A total of 15 accelerometers were used for measuring the accelerations produced by the dynamic load testing. Three accelerometers (C112647, C112648, and C112650) were magnetically connected to the outside walls of piles 1, 2, and 3 on the leading row at the load point elevation. Twelve additional accelerometers were magnetically attached to the inside wall of pile 2 as shown in Figure 5.3. The accelerometers were spaced at 0.46 m (1.5 ft) increments, beginning at the ground level (0 m) and extending to a depth of 5.0 m (16.5 ft) below the ground surface. Applied Foundation Testing, Inc supplied these accelerometers.

Each center pile (piles 2, 5, and 8) was instrumented with 120 Ω quarter bridge electrical resistance type strain gages (Texas Measurements, Inc. model WFLA-6-120). These gages were located at a total of eighteen different elevations down the outside of

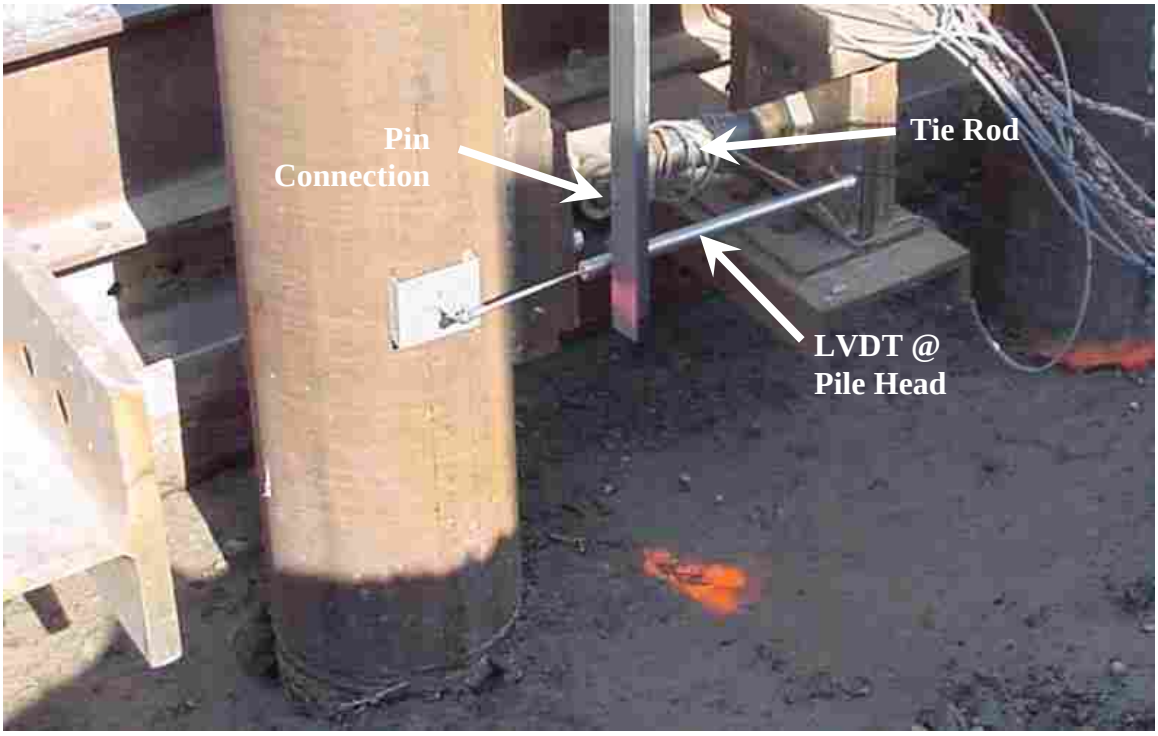

Figure 5.2: LVDT and tie rod connections to individual piles at pile head.

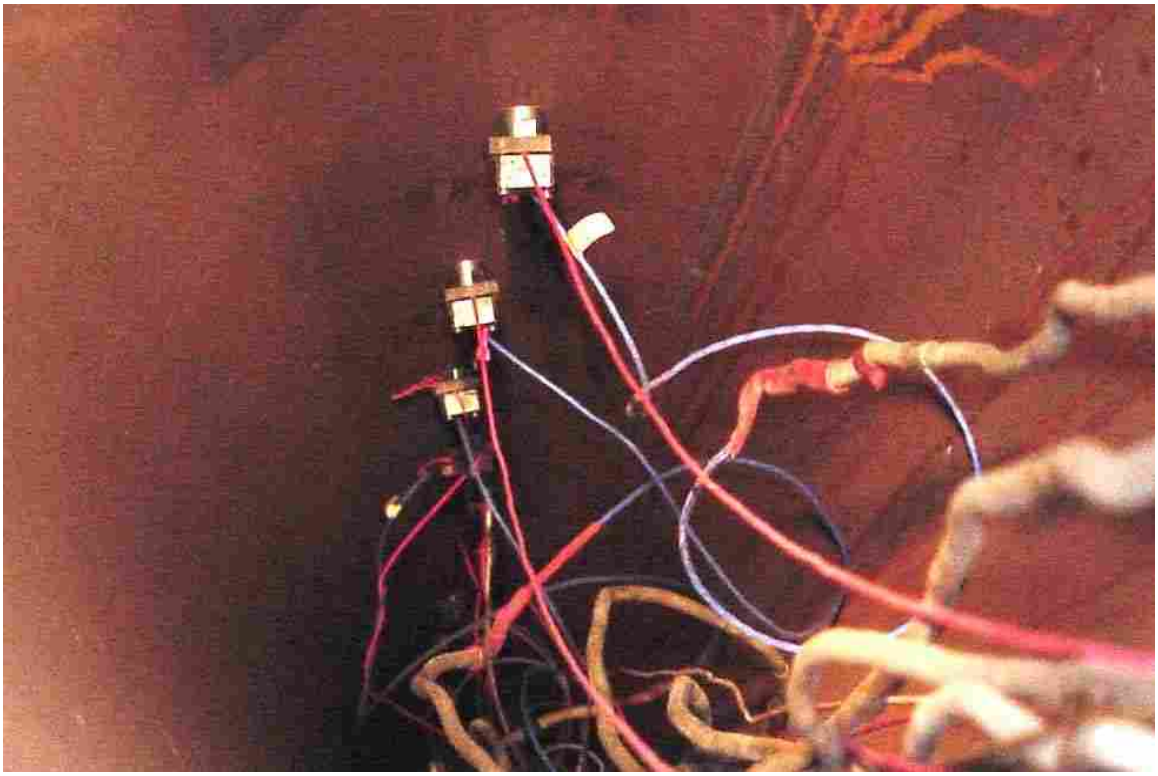

Figure 5.3: View down inside pile with accelerometers.

each pile. The first thirteen locations were at regular intervals of 0.46 m (1.5 ft) from the ground surface to a depth of 6.0 m (19.5 ft). The last five locations were spaced at 0.91 m (3.0 ft) intervals to a depth of 10.5 m (34.5 ft). Each location contained two strain gages, one on the north and the other on the south. This was done to find the maximum tensile and compressive strains that occurred during each dynamic test. The strain gages were attached to the outside of the piles by epoxy glue. To protect the strain gages from any physical damage, angle irons were welded to the piles, as previously noted in chapter 4. To further cushion the gages during pile driving and to prevent water infiltration, waterproof foam was sprayed into the void between the angle iron and pile.

Data collection from the instrumentation was obtained with an Optim Megadac data acquisition system (model 5414AC version 7.4). A total of 144 channels were used; 108 channels for strain data, 15 channels for accelerometer data, 11 channels for LVDT data, 9 channels for the tie rod load cell data, and one channel for the statnamic load cell. During statnamic testing, the data was obtained every 0.0005263 seconds (1900 Hz sampling rate). A portable electric generator powered the electrical systems.

5.2 9-Pile Group Testing Procedures

The 9-pile group was tested on August 12th and 13th, 2002. As part of the testing procedure, both static and statnamic load tests were consecutively applied in the same direction. Fifteen cyclic static lateral load tests were performed at a target deflection followed by a statnamic load as the final 16^{th} cyclic load. Subsequent target defections were progressively increased after each test. Static load testing had seven target loads at 6 mm, 13 mm, 25 mm, 38 mm, 51 mm, 64 mm, and 99 mm. Statnamic loading consisted of six target loads at 13 mm, 25 mm, 38 mm, 64 mm, and two at 99 mm. The last two

statnamic tests consisted of the 1st and 16th cyclic loading at the 99 mm target deflection. The purpose of the 1st statnamic load with a 99 mm target deflection was to observe the dynamic characteristics of group piles in virgin soil.

5.3 9-Pile Group Test Results

5.3.1 Time Histories

Time histories of deflection and acceleration were obtained directly from the LVDTs and accelerometers, respectively. Velocity data was derived by integrating the acceleration time history and differentiating the displacement time history at the pile head. Both the accelerometer data and LVDT data matched very well. Refer to Figures 5.5 through 5.9 of the time history data measured at the different stations along the depth of the piles for test 6. Similar plots for all the tests are provided in Appendix 1.

The LVDT data of each pile was averaged to obtain the motion of the pile group. By differentiating the deflection time histories from the LVDTs, velocity and acceleration time histories were obtained. The initial deflection at the start of each test progressively increased because soil fell into the gap behind the pile and the wall during loading and prevents the pile from returning to its original position.

A significant amount of drift was found from the raw data obtained from the accelerometers. Refer to Chapter 4 where the least square sums method was used to alleviate this problem.

From these time histories, the LVDT results at the pile head were compared with the results from the accelerometer at the pile head. Deflections from LVDT data were zeroed to compare the accelerometer deflections, because accelerometers do not measure the initial position. Unfortunately, all the accelerometers at the pile head malfunctioned

for the majority of the testing. To correct this problem, a factor was multiplied to the deflection time history from the accelerometer at the ground level in order to have the maximum deflections from the LVDT and accelerometer equal each other. In doing so, the compared time histories of motion at the pile head from the LVDT and accelerometer data were nearly identical, thus giving confidence that the LVDT data and accelerometer data are accurate. Figure 5.4 compares the LVDT deflection time history with the deflection time history obtained from the accelerometer in test 4. Most of the down-hole accelerometers worked; however, the accelerometers at elevations 3.2 m (10.5 ft) and 4.1 m (13.5 ft) did not work for the last three tests on the 9-pile group.

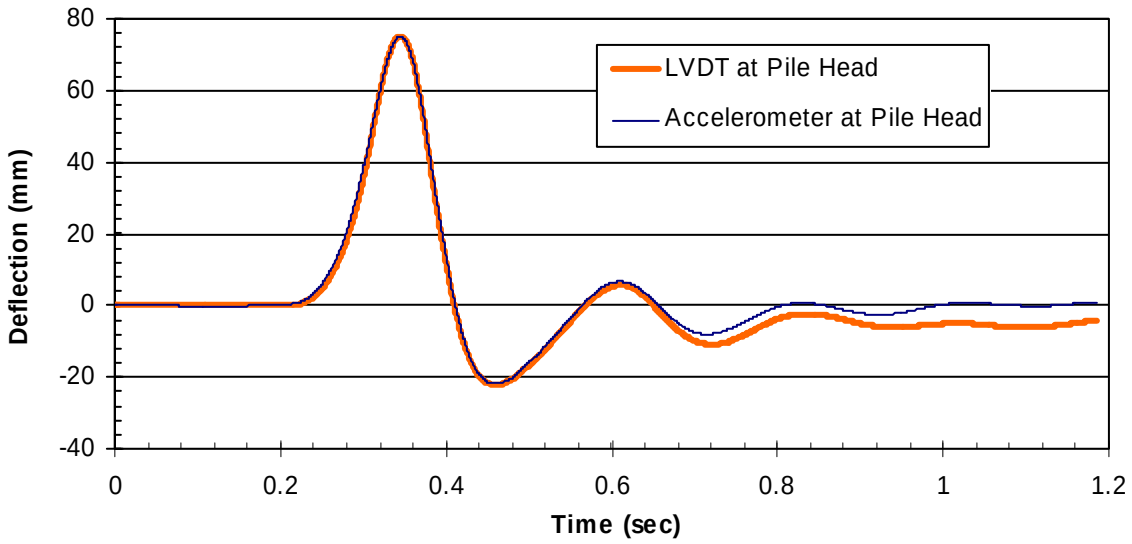

Figure 5.4: Comparing LVDT and accelerometer for accuracy (test 4).

All of the time histories obtained from the accelerometers were zeroed, because initial deflections down the pile were not known. Also notable is that the final displacement obtained from the accelerometers returns to zero, because of the least squares method used to remove noise. The maximum deflection of the each test was

reached after the maximum load. Most of the motion for all of the tests lasted about 0.8 seconds. Table 5.1 shows the maximum deflections reached and compared to the target deflection desired in each test. For the majority of the test, the maximum deflection was within 10 mm from the target deflection; however, tests three and four were significantly different from their target deflections. Test three was 20 mm over the target of 38 mm. Test four was 32 mm over the target of 64 mm. Although the first test was only 10 mm over the target of 13 mm, the target deflection was almost doubled.

Table 5.1: Comparison of the Target and Actual Maximum Deflection

Test #	Target Deflection (mm)	LVDT Pile Head Deflection (mm)	Difference (mm)
1	13	23	10
2	25	26	1
3	38	58	20
4	64	96	32
5	99	93	-6
6	99	102	3

5.3.2 Profile Shape with Maximum Accelerations and Velocities

Accelerometer data provided profiles in Figure 5.10 which reflect the shape of the group of piles at peak positive deflections. Peak positive and negative acceleration and velocity values were also obtained. The shape showed a good representation of the shape of the piles at peak deflections. Acceleration zeroed when velocity reached peak values. Velocity zeroed at peak deflections and accelerations. Thus, the principals of integration were followed.

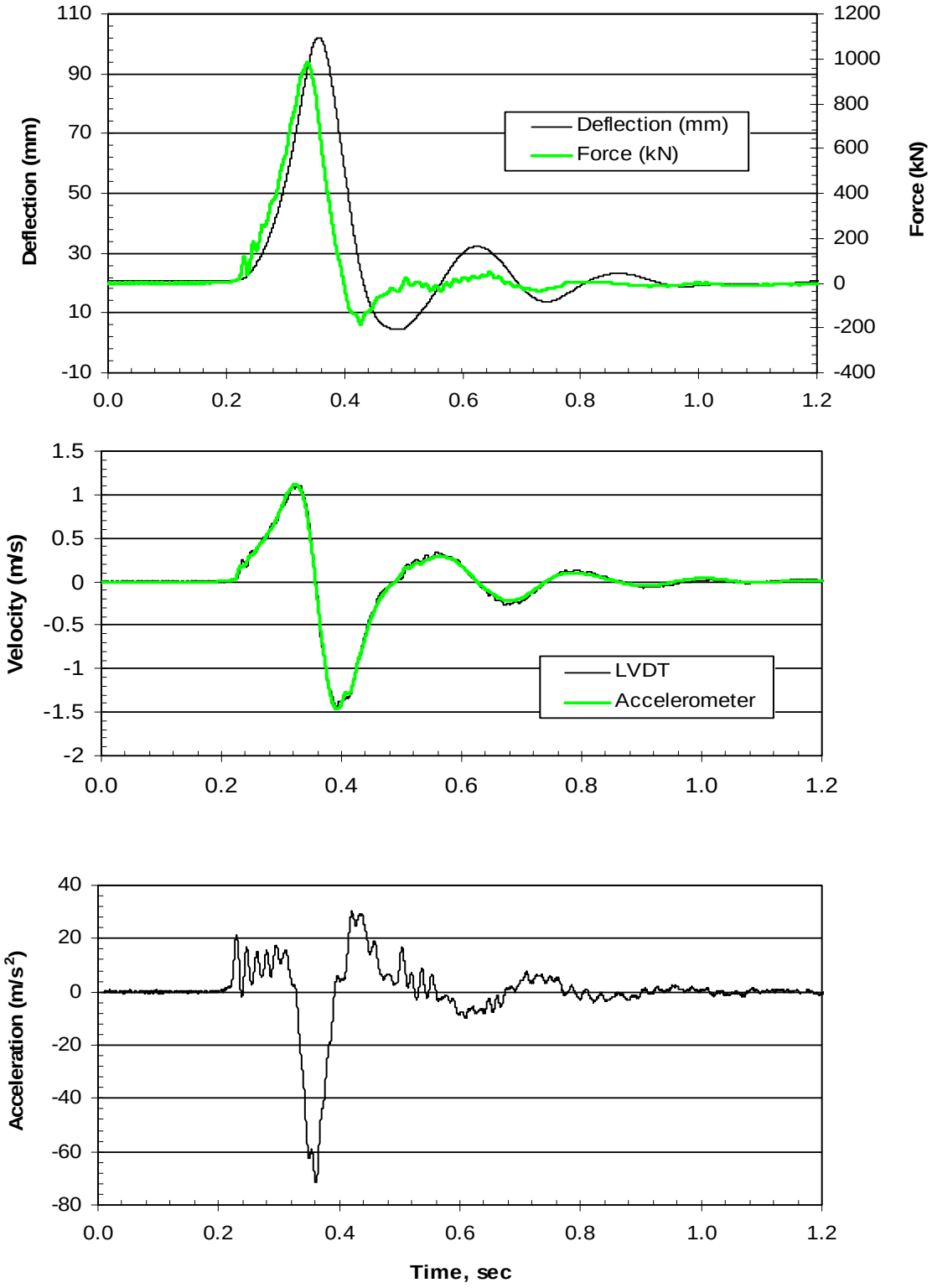

Figure 5.5: 9-pile group, test 6, 99 mm (3.75 in) target—LVDT time histories at pile head.

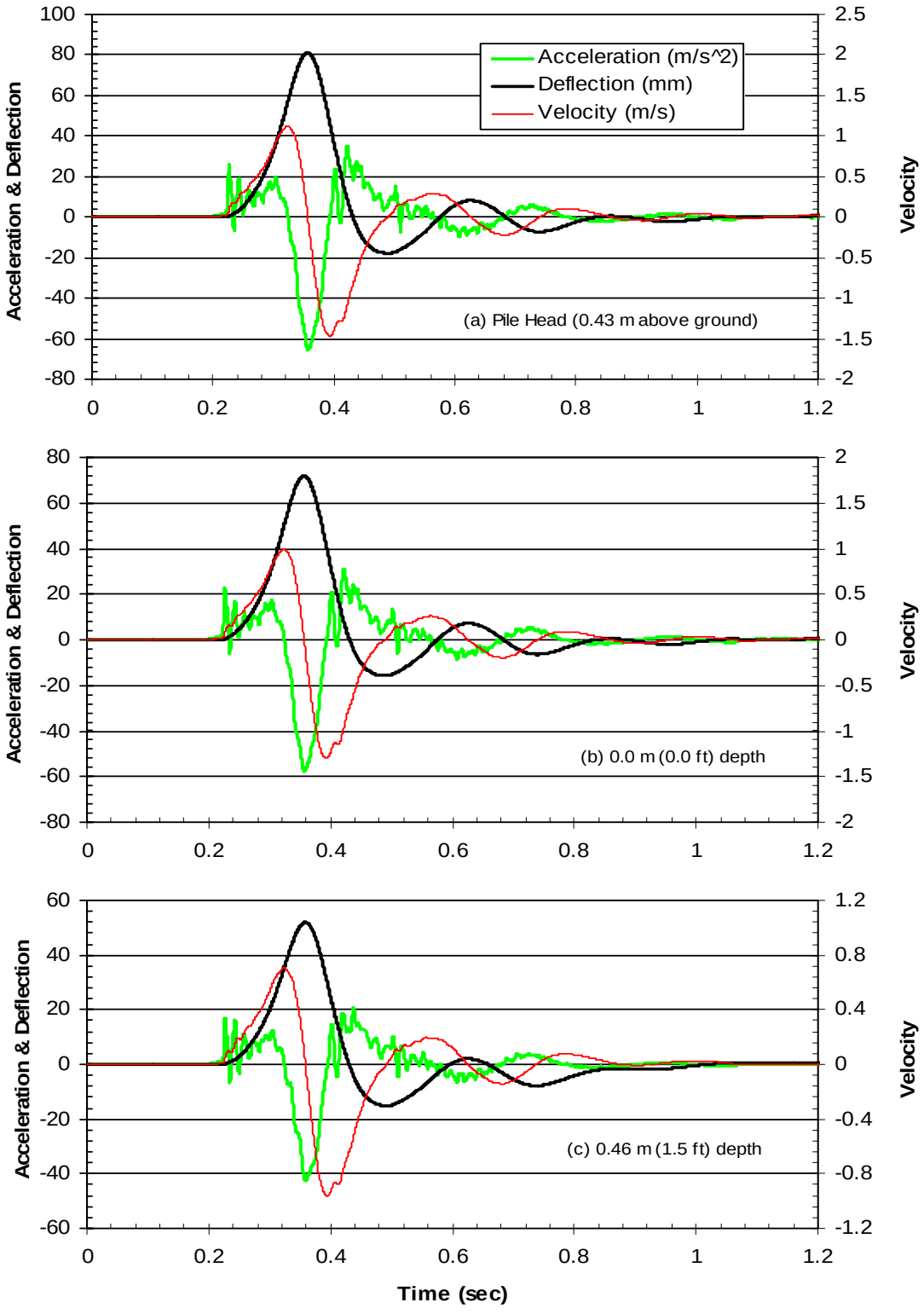

Figure 5.6: 9-pile group, test 6—accelerometer time histories at (a) pile head, (b)0.0m (0ft), and (c) 0.45m (1.5ft) depths.

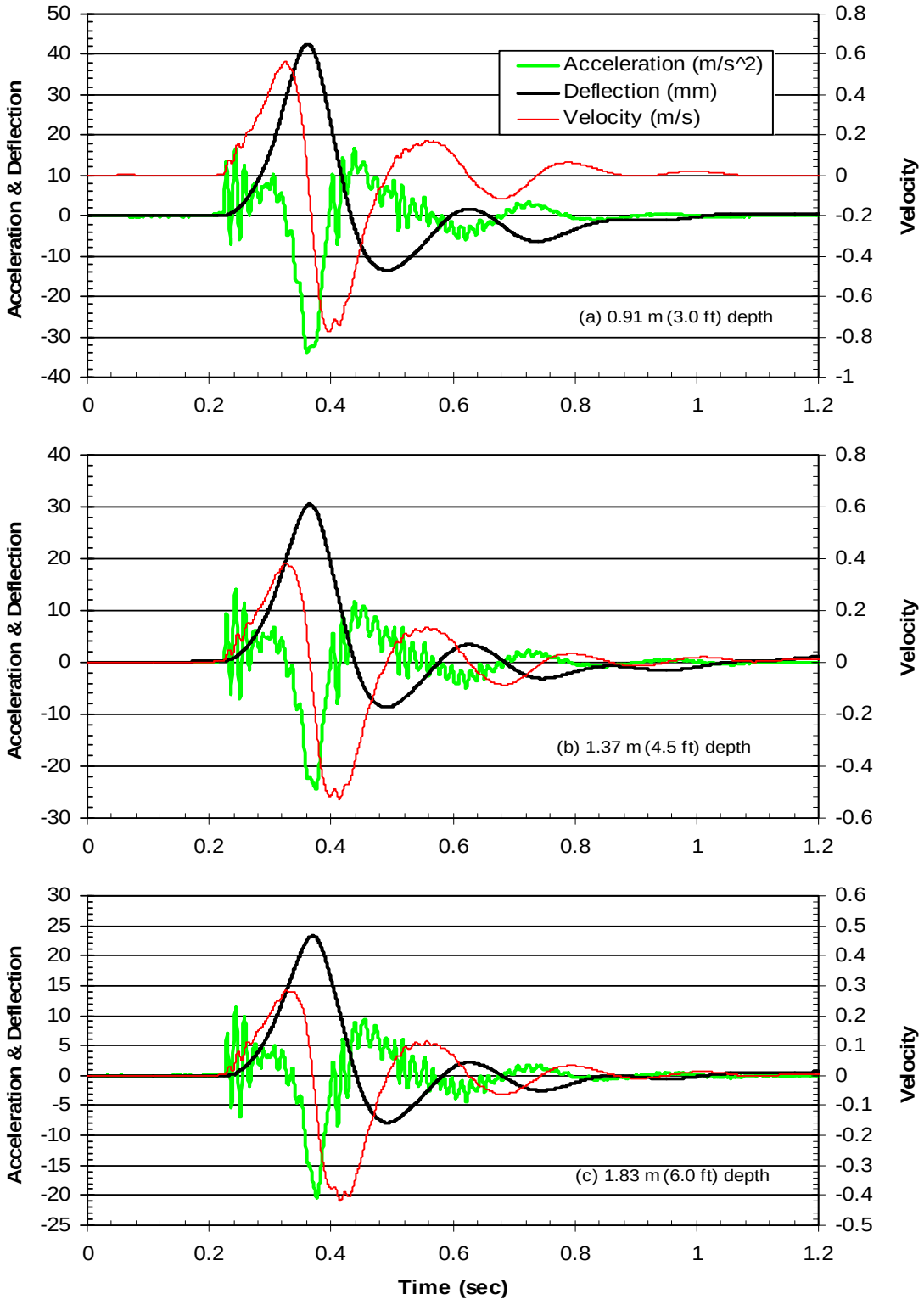

Figure 5.7: 9-pile group, test 6—accelerometer time histories at (a) 0.91m (3.0ft), (b)1.37m (4.5ft), and (c) 1.83m (6.0ft) depths.

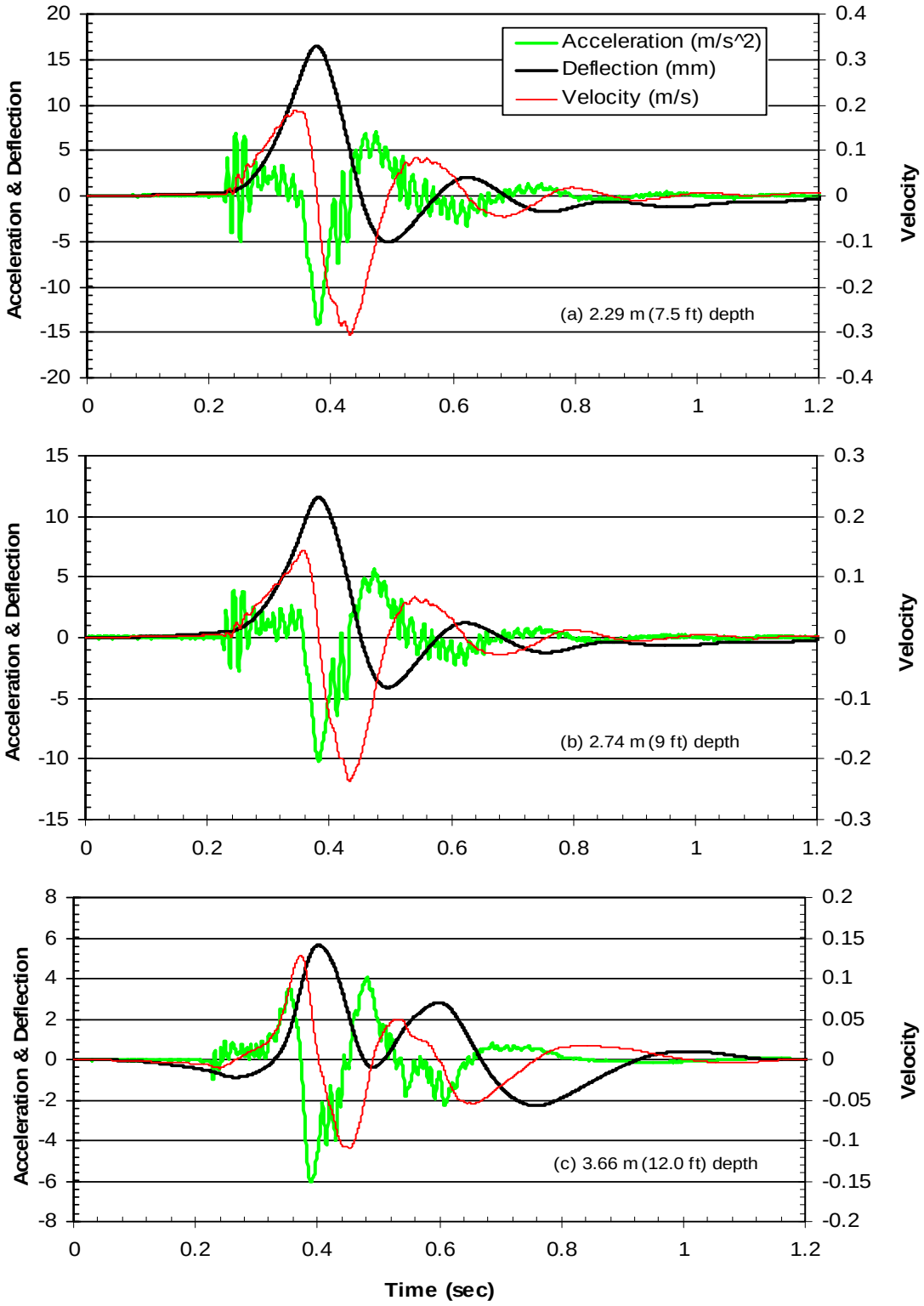

Figure 5.8: 9-pile group, test 6—accelerometer time histories at (a) 2.29m (7.5ft), (b) 2.74m (9.0ft), and (c) 3.66m (12.0ft) depths.

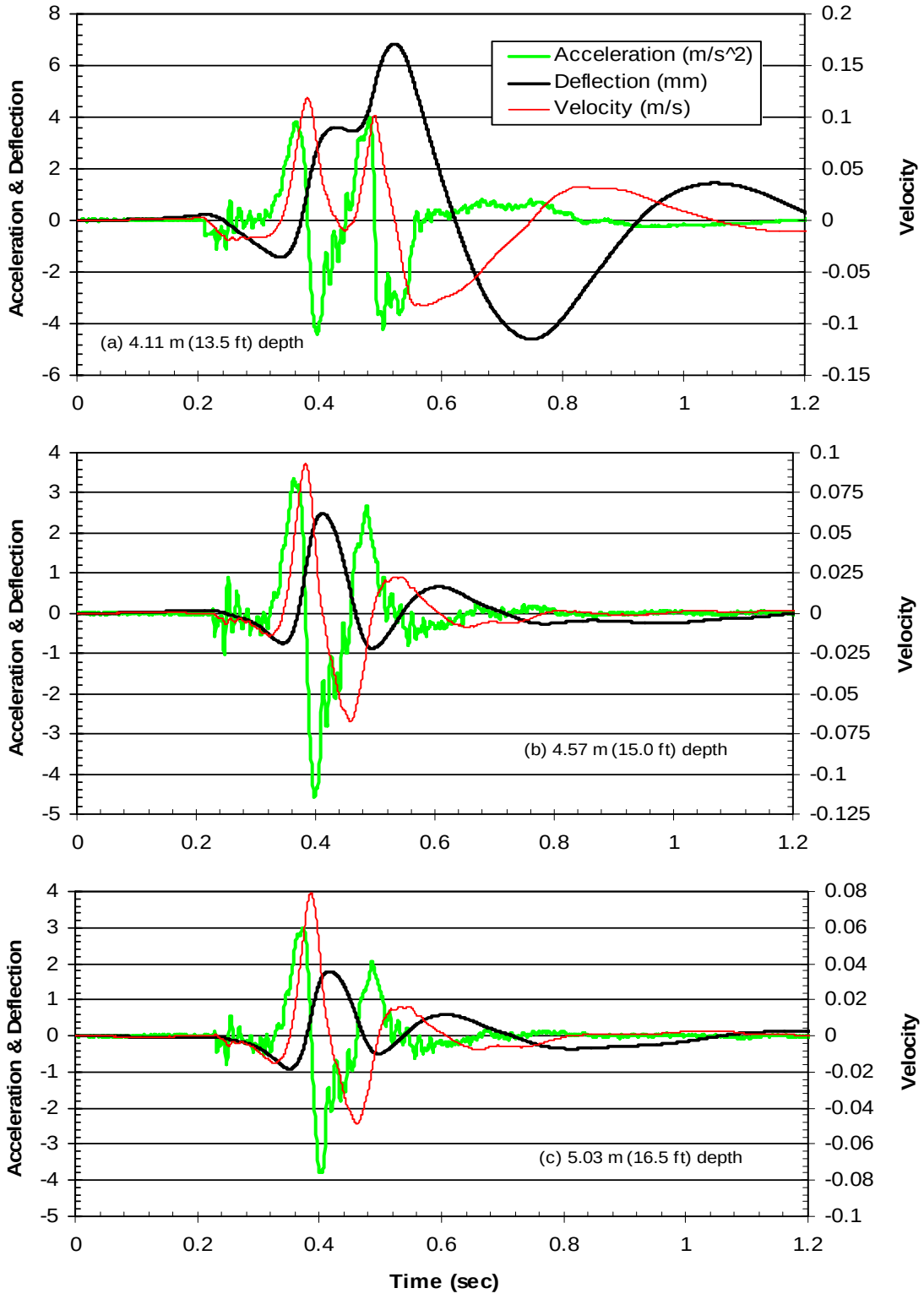

Figure 5.9: 9-pile group, test 6—accelerometer time histories at (a) 4.11m (13.5ft), (b) 4.57m (15.0ft), and (c) 5.03m (16.5ft) depths.

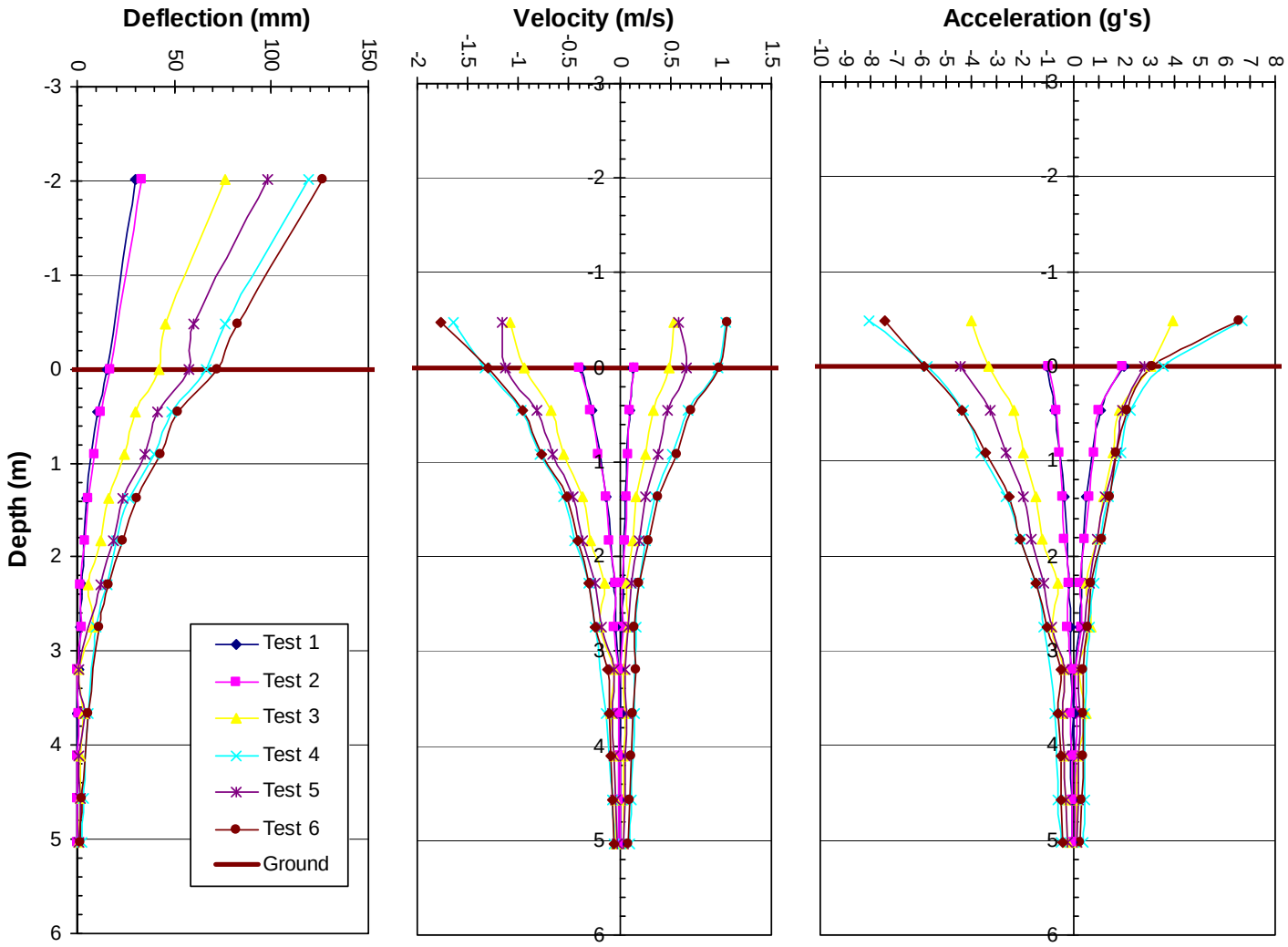

Figure 5.10: Profile of 9-pile group layout under statnamic testing.

5.3.3 Load vs. Deflection

Figures 5.11 and 5.12 provide plots of load versus deflection for the 15th cycle of static loading at each target deflection along with the load versus deflection curve for the statnamic test at that deflection level which represents the 16th cycle of loading.

Figure 5.13 shows the continuous load versus deflection curves for all six statnamic lateral load tests. Significant increases in the peak lateral loads were observed between tests 1, 3, and 4. Test four was significantly far from the target deflection, which possibly caused the results for tests five and six to not have a gradually increasing maximum load for each test. Because tests three and four deflected significantly over the target deflections, virgin soil loadings were observed.

The load cell located at the statnamic device was compared to the summed load cells on each pile (Figure 5.14). It is evident that there are differences between these comparisons. Generally, the agreement is reasonably good during the loading stage until the peak load is approached. At this point the load from the piles starts to exceed the measure load at the statnamic load cell where it is not physically connected to the load frame. This is most likely caused from the inertial forces and energy loss due to friction and not from instrumentation error. Inertial forces from the mass of the load frame are observed from negative forces created from the summed load cells.

5.3.4 Gap Measurements

Gaps between the piles and the soil occurred similar to the 15-pile group. Gaps were measured on the west side of the 9-pile group after each statnamic test. The measurements were made using the same procedure described previously in chapter 4.

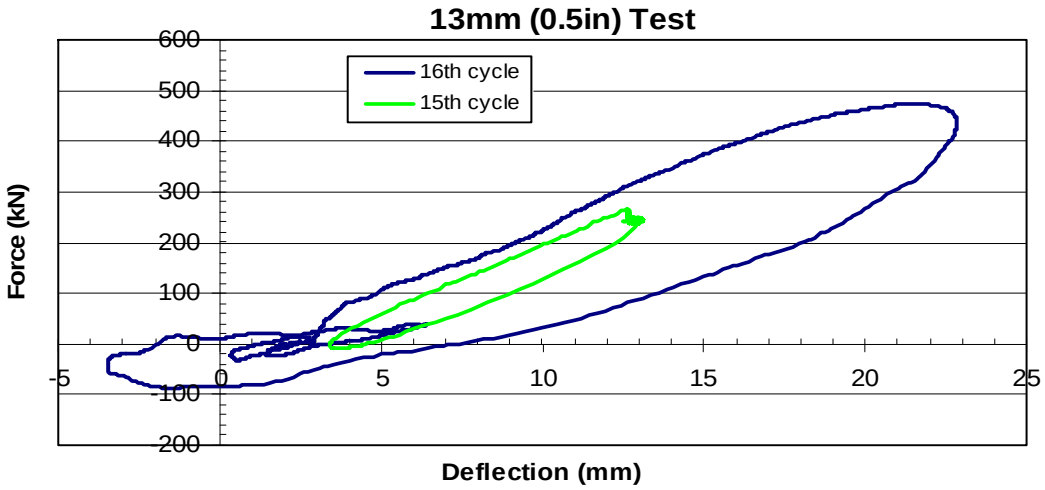

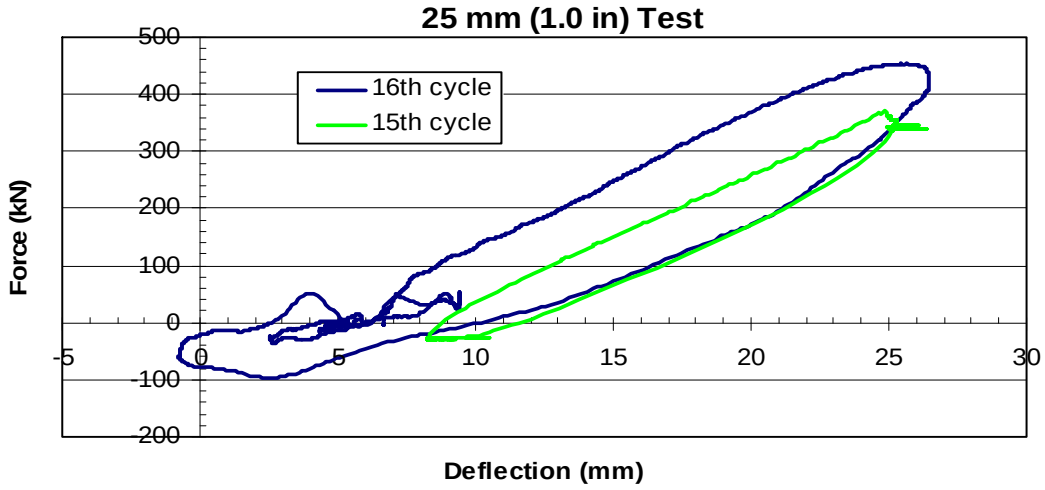

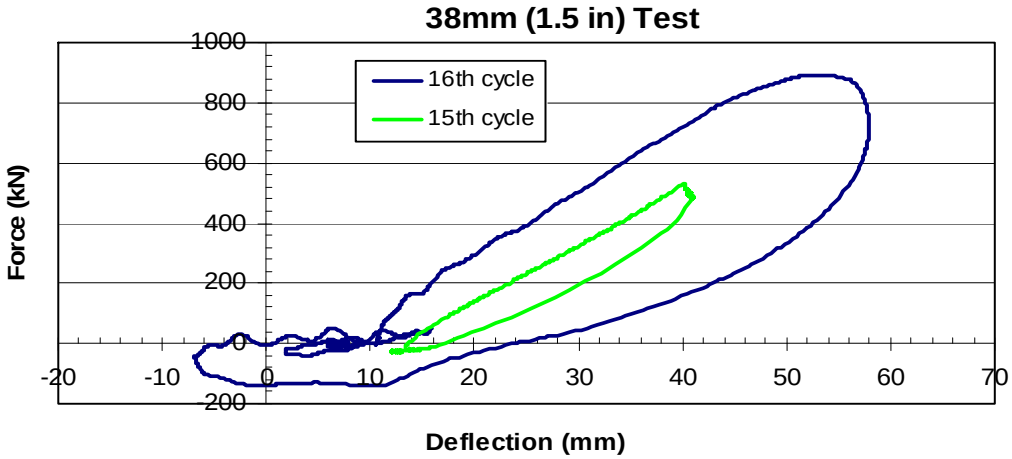

Figure 5.11: Statnamic loads compared to static loads.

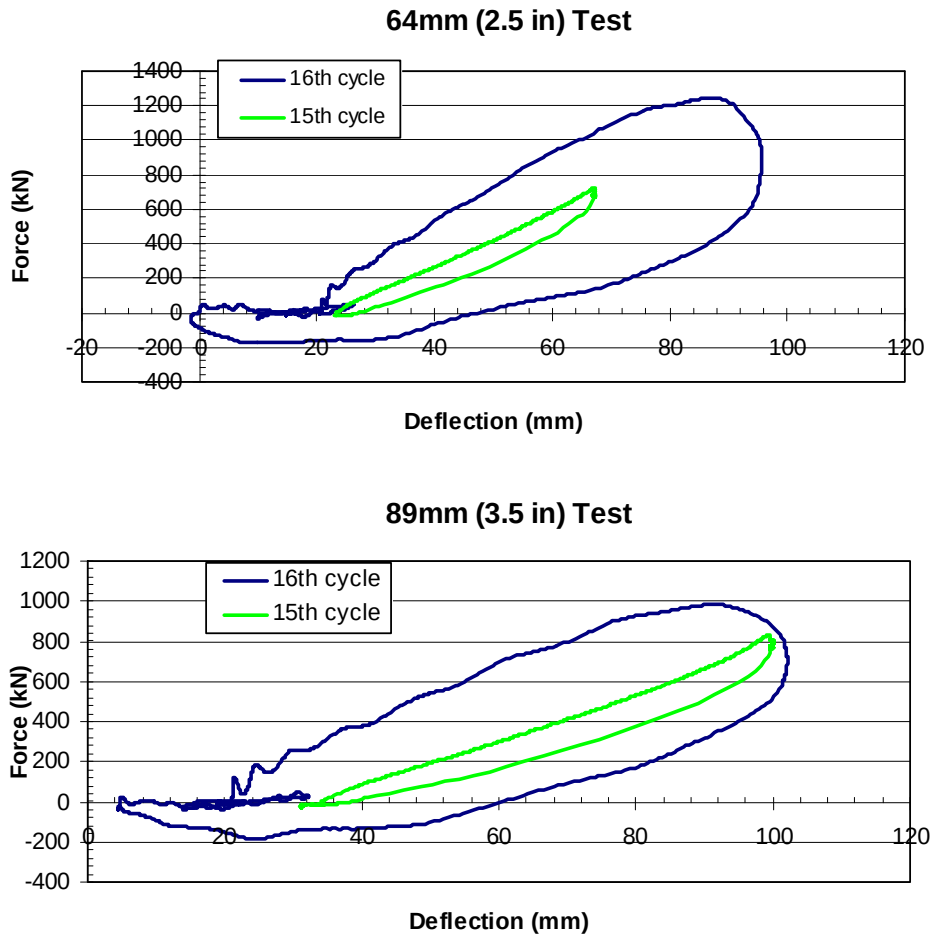

Figure 5.12: Statnamic loads compared to static loads.

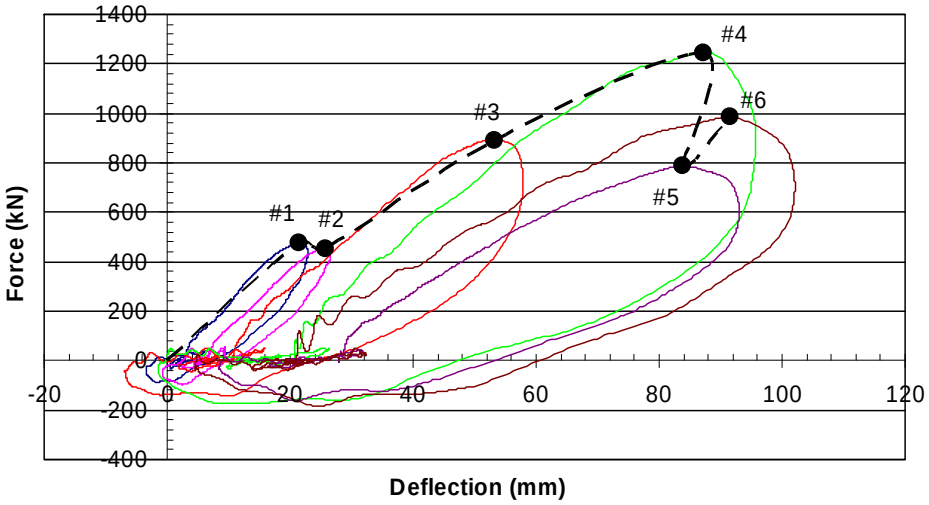

Figure 5.13: Statnamic loads and order locating peak loads.

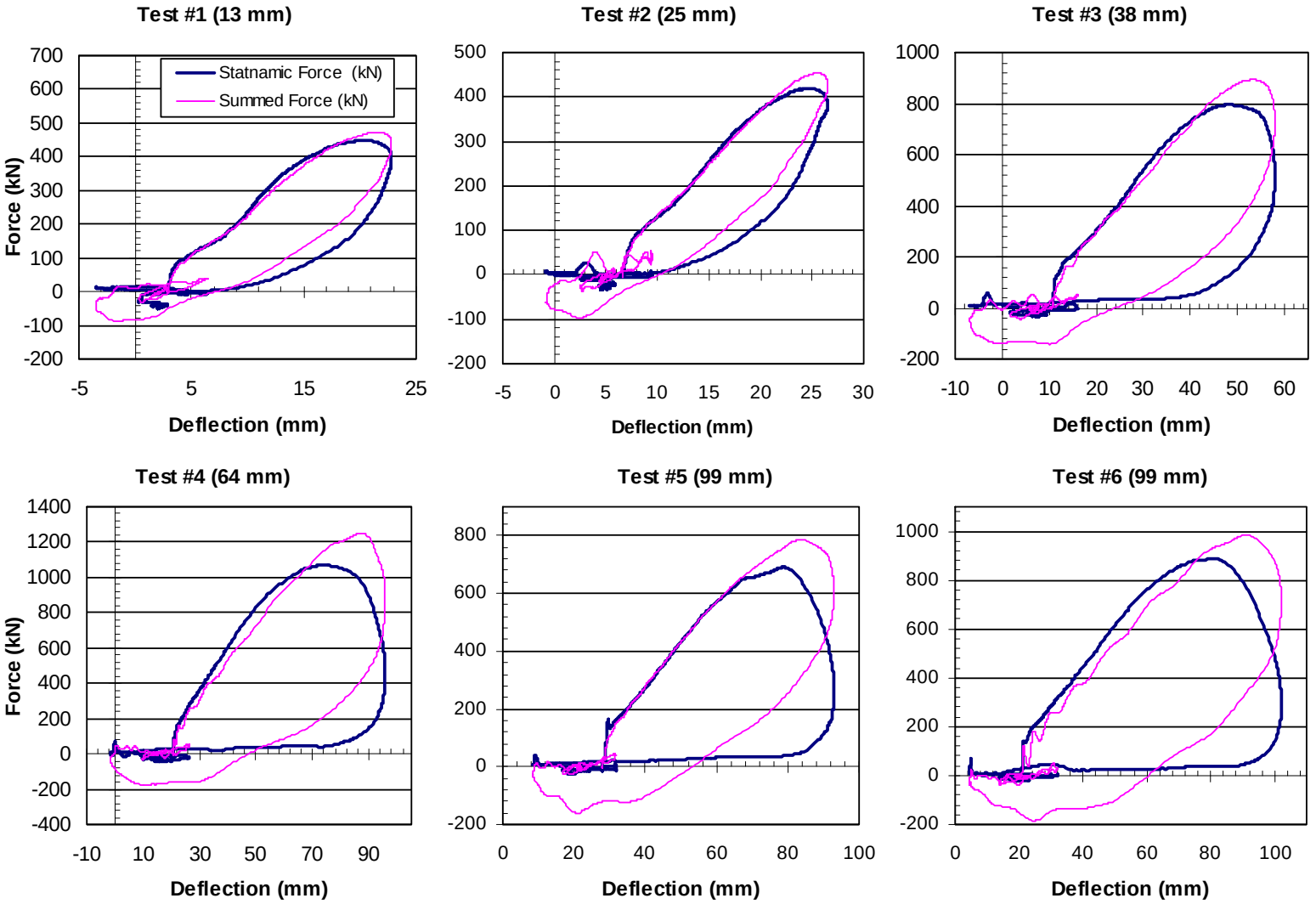

Figure 5.14: Comparison of the statnamic load cell and sum of individual pile load cells in load deflection curve.

Figure 5.15 shows the increasing gap width and depth in each row as the loads and the deflections increased. In contrast to the gap measurements for the 15-pile group, the gap measurements are relatively similar for each row. This may be a consequence of the large spacing of the piles which produced more consistent loads in each row in the group. The largest gaps reached 26 mm and to a depth exceeding 1.2 m below the surface.

5.3.5 Bending Moment Diagrams

Bending moment versus depth profiles were obtained from each pile using the measured strain gage data and equation 4.4. Figures 5.16 and 5.17 compare the bending moment versus depth curve for each row at the peak deflection for each of the statnamic tests. The bending moments versus depth curves are somewhat more erratic than was the case for the 15-pile group test. In contrast to the 15-pile group test in which the front row pile typically exhibited the highest maximum moment, the maximum moments for each row in the 9-pile group are very similar. This again may be a result to the large pile spacing for the 9-pile group which would reduce group interaction effects allowing each pile to behave more similarly.

By taking the average of the rows, the bending moments were compared with each test. Figure 5.18 identifies this comparison and also compares the moment diagrams at the peak load and at the peak deflection. As mentioned earlier, the peak deflections occurred after the peak load. Test 4 had the largest bending moments overall (223 kN-m—at peak load and 234 kN-m—at peak deflection). This can be attributed to the extra 32 mm of virgin soil loaded.

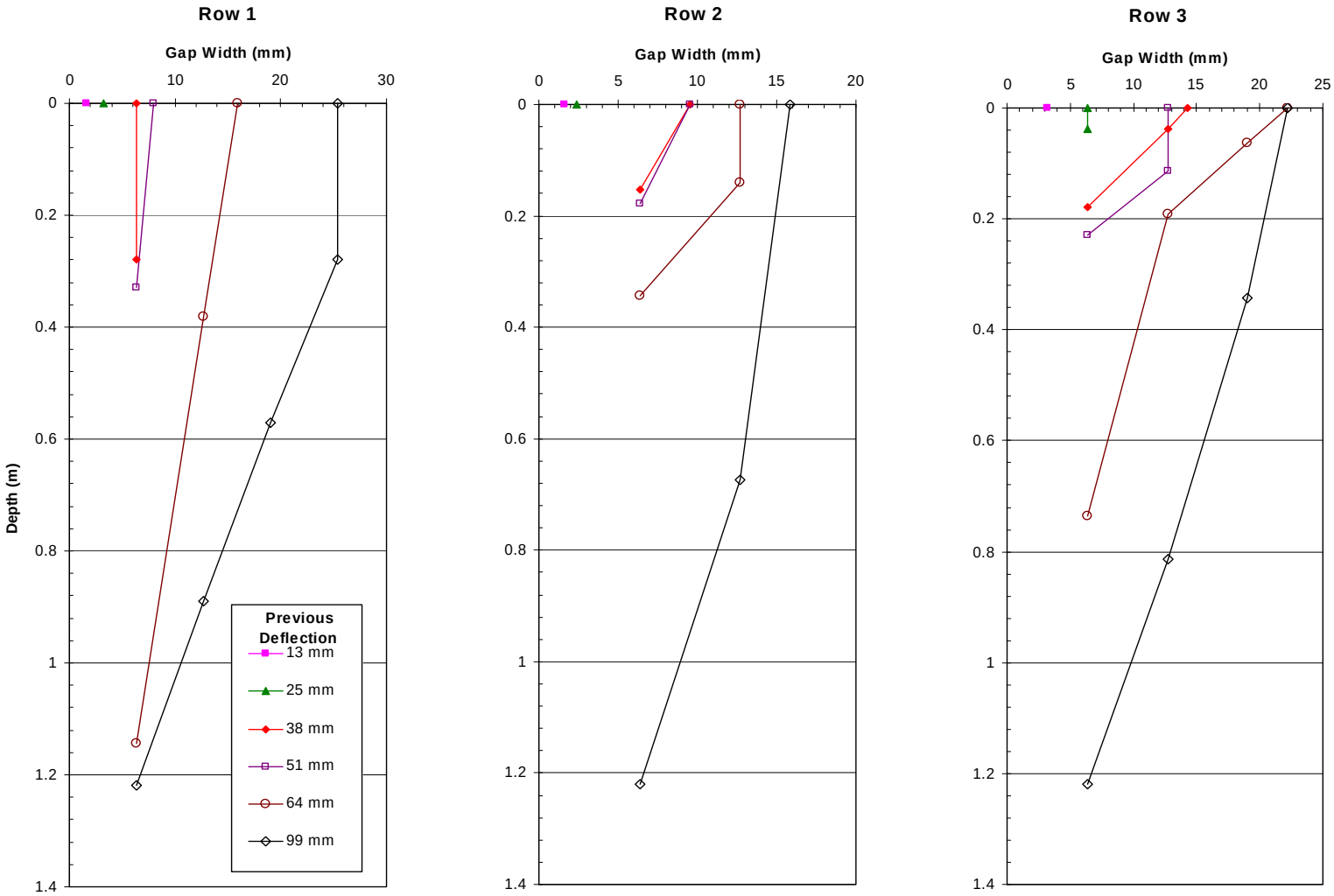

Figure 5.15: Gap widths measured from piles 3, 6, and 9.

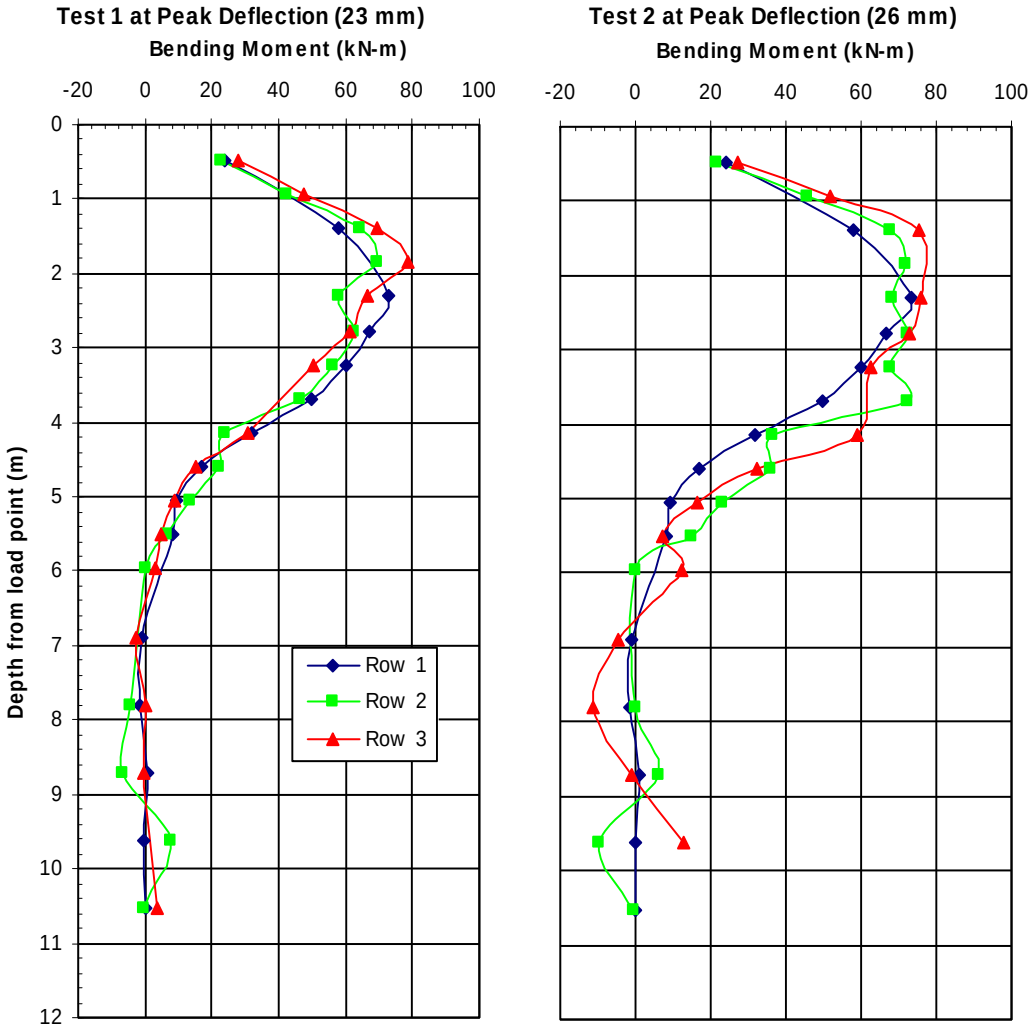

Figure 5.16: Comparing bending moment diagrams (by row) for tests 1 & 2.

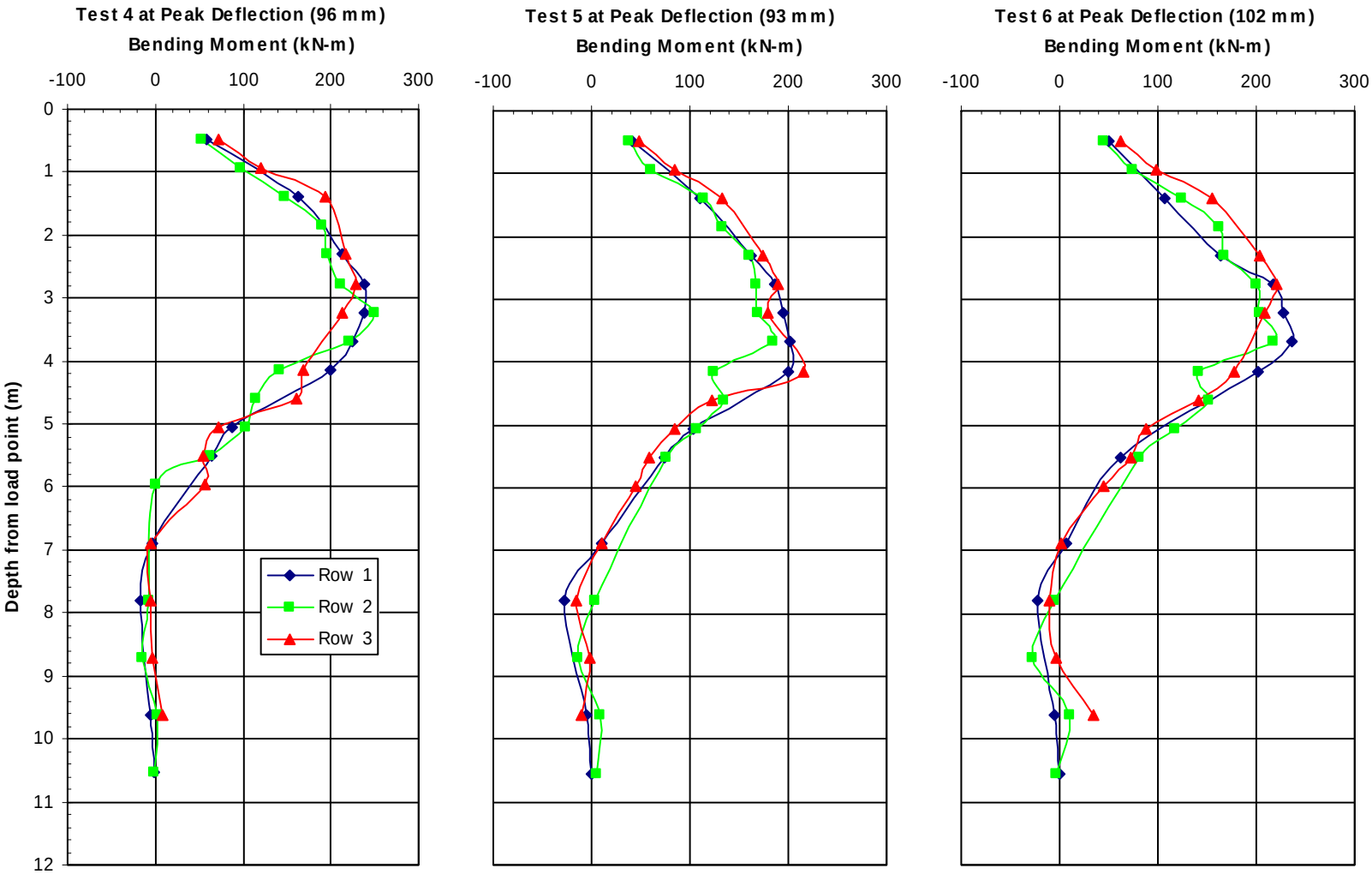

Figure 5.17: Comparing bending moment diagrams (by row) for tests 4, 5, and 6.

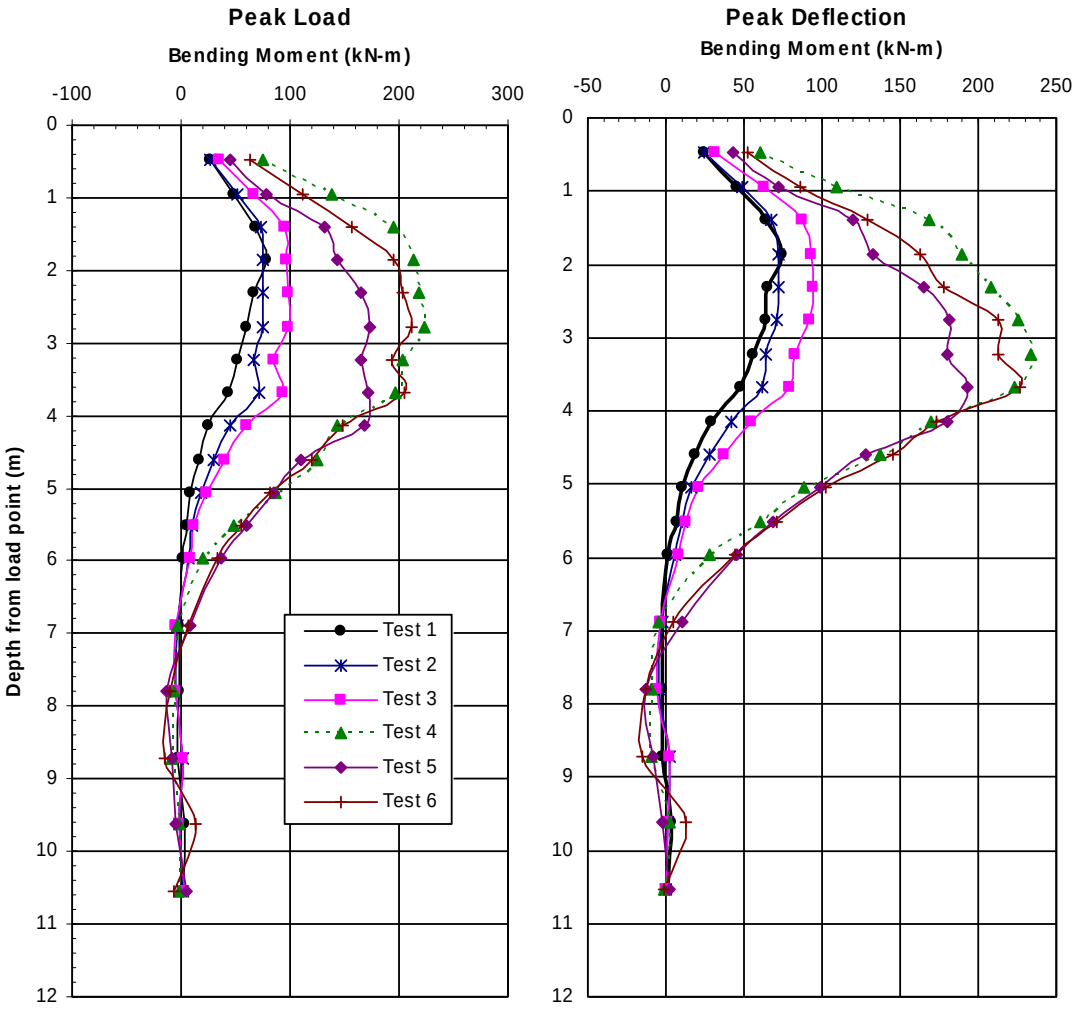

Figure 5.18: Bending moment diagrams at peak load and peak deflection.

By observation, the bending moment diagram changes within each test. The maximum moments at peak deflection occurred up to 0.9 m (3 ft) down the pile after the peak loading occurred. Test 1 has a 6 percent decrease from the maximum moment; while test 5 has a 10 percent increase in the maximum moment (Table 5.2).

Table 5.2: Peak Bending Moments and Percentage Differences.

Test #	Max Moment @ Peak Load (kN-m)	Depth (m)	Max Moment @ Peak Deflection (kN-m)	Depth (m)	Moment Percentage difference (%)
1	78	1.9	74	1.9	-5.6
2	76	2.3	72	2.3	-4.6
3	98	2.3	94	2.3	-4.6
4	223	2.8	234	3.2	4.8
5	173	2.8	193	3.7	10.3
6	212	2.8	227	3.7	6.6

Changes in the bending moments were also noticed in the overall testing. As the cycles of the increasing deflections continued, the maximum moment occurred further down the pile group. From test 1 to test 6, maximum bending moments changed 0.91 m (3 ft) at the peak load. Maximum bending moments changed 1.8 m (6 ft) at the peak deflections.

CHAPTER 6 MODELING IDEALIZED SYSTEM IN DYNAMIC LOADING

Chapters four and five investigated the testing process and the results of the lateral statnamic tests for the 15- and 9-pile groups. Using optimization techniques, the test results will be used to help find idealized systems that can match the measured motion of each pile group. As a result of this study, it will be possible to determine stiffness and damping ratios for the two pile groups. To create an idealized system in motion that accurately predicts the measured response, the method outlined by the flow chart in Figure 6.1 was developed. Chapter 6 provides background regarding two essential components of this study. First, this chapter will go into depth on how a pile-soil interaction model was developed. Second, the chapter will review numerical methods that were studied for computing the response of the pile-soil model. Chapter 7 will evaluate the ability of the chosen idealized model and numerical method to compute the response of the physical system.

6.1 Modeling of Cyclic Loading

Several models were studied in the process of developing an idealized pile-soil interaction model. Of these, three models will be discussed in this thesis. These models include a single degree of freedom (SDOF) system, a two degree of freedom (2DOF) system, and finally a SDOF system with variable parameters for mass (m), damping coefficient (c), and stiffness (k) for different parts of the time history.

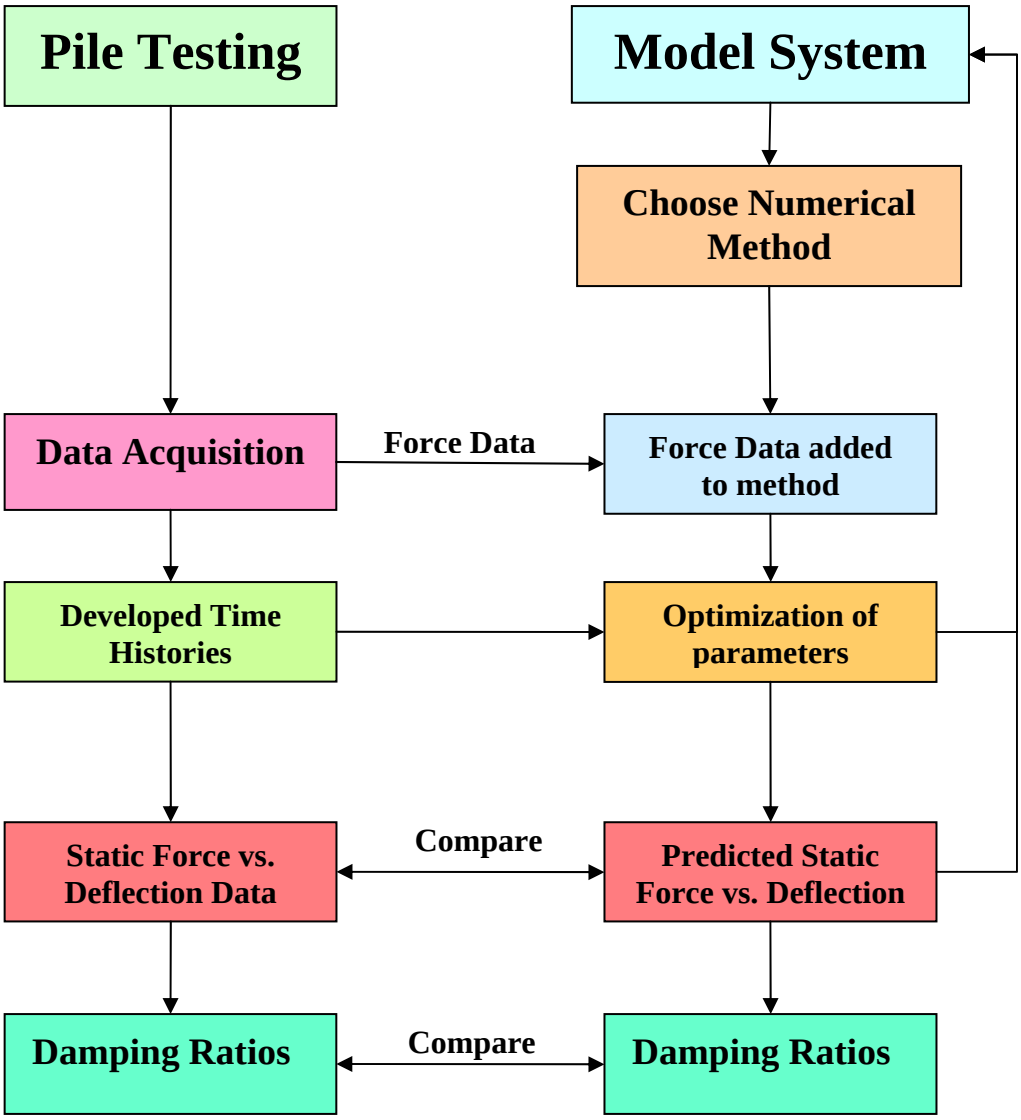

Figure 6.1: Flow chart of creating ideal dynamic model and obtaining results of stiffness and damping ratios.

6.1.1 SDOF—One Mass, Damping Coefficient, and Stiffness

Several researchers (Rollins 1998; Brown 1998; Gazetas and Dobry, 1984) have modeled a pile or a group of piles with a single degree of freedom system to evaluate lateral motion produced by a statnamic loading.

The dynamic equation of motion for a single degree of freedom model is given by the equation:

$$F_i = ma_i + cv_i + kx_i \tag{6.1}$$

where:

F_i = total force applied to the group of piles

m = total mass of the system

a_i = average acceleration of the pile group

c = total damping coefficient

v_i = average velocity of the pile group ($v_i = a_i \Delta t + v_{i-1}$)

k = total stiffness constant

x_i = average deflection of pile group ($x_i = v_i \Delta t + x_{i-1}$)

Middendorp (1992) first employed a single degree of freedom model in analyzing the response of deep foundations during axial statnamic load tests. The SDOF method Middendorp designed is most commonly known as the Unloading Point Method (UPM). The model of the Unloading Point Method is fairly simple and as shown in Figure 6.2. An additional sliding feature could be added to the model to account for the separating of the soil and pile which was quite evident as the deflections and cycles increased (see Figure 4.15).

According to Middendorp (1992) there are five major regions within the typical statnamic load versus deflection curve as shown in Figure 6.3. A summary description for each region is provided below.

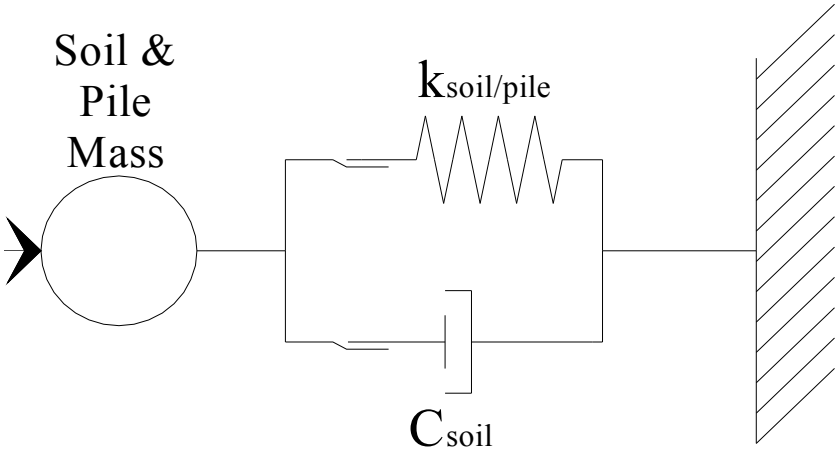

Figure 6.2: SDOF model.

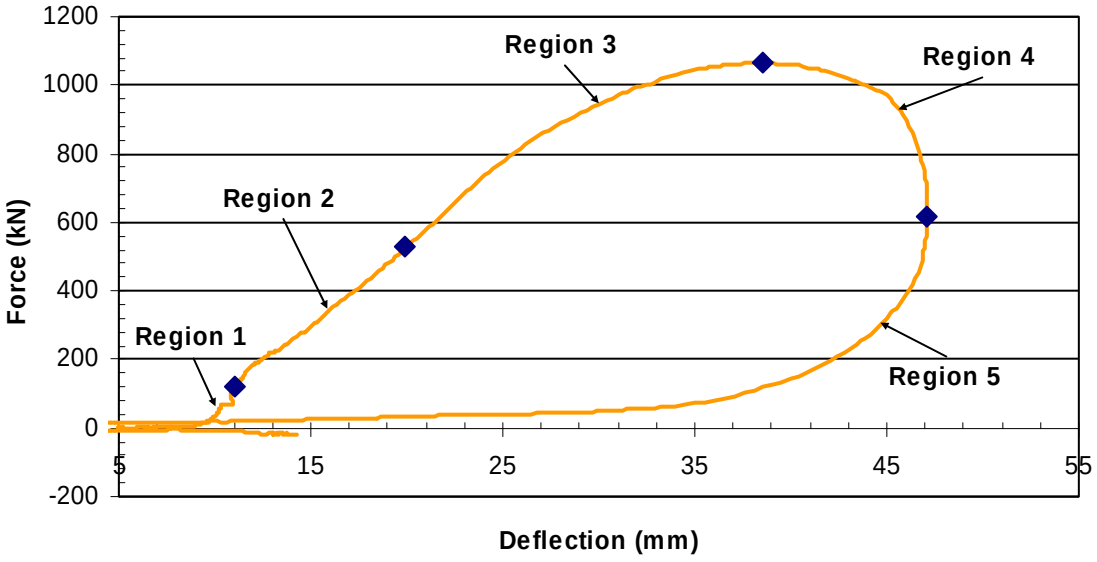

Figure 6.3: Five regions of Unloading Point Method.

1. Static Loading—This region is the initial deflection caused by the load frame, statnamic device, and etc. that causes initial stress to the system. At this stage an initial stiffness in the pile and soil may be found (Equation 6.2).

$$k_1 = \frac{F_{static}}{u_{static}} \tag{6.2}$$

where:

k_1 = initial stiffness of the soil

F_{static} = initial force

u_{static} = initial deflection

2. Initial statnamic launching stage—This region is the beginning of the launching stage. At this point the soil resistance is elastic. The damping coefficient could be found by Equation 6.3:

$$c_2 = \frac{F_{stn}(t) - k_{static}u(t) - ma(t)}{v(t)} \tag{6.3}$$

where:

c_2 = Damping coefficient in region 2

$F_{stn}(t)$ = Statnamic Force at time t

m = mass of the system

$u(t)$ = displacement at time t

$v(t)$ = velocity at time t

$a(t)$ = acceleration at time t

3. The third region reaches the peak statnamic load. Also the static soil resistance is considered to reach a maximum at this peak loading. The velocity and acceleration are increasing causing both the inertia and damping of the system to increase in this region.

4. Within this stage the statnamic load is decreasing, however, the displacement is still increasing. Although the acceleration is now negative and the velocity is decreasing, the momentum of the mass keeps the pile moving forward. At the end of this region, the maximum deflection is reached (x_{max}). At the maximum deflection, the velocity is zero which means that the damping resistance ($F_v = C \cdot v = 0$) becomes zero. At this point, the damping coefficient maybe found using the equation

$$c = \frac{F_{stn}(t) - F_{u\max} - ma(t)}{v(t)} \tag{6.4}$$

where:

$$F_{u\max} = F_{stn\max}(t) - ma(t) \tag{6.5}$$

$F_{stn\ max}$ = maximum statnamic force

5. The last region is the unloading region of the statnamic testing. This is where the final deflection develops as the pile rebounds, causing the velocity to become negative and the displacement to decrease.

The unloading point method includes a number of assumptions which may not be entirely valid. For example, the method assumes that the spring force and damping coefficient are constant values throughout the majority of the loading. In addition, the method when applied to a pile group, assumes that the load frame and the piles move together as one mass, which may not be completely true.

6.1.2 Two Degree of Freedom (2DOF) System—Load Frame and Pile/Soil

The physical system could also be analyzed using a two degree of freedom system. In this model, the mass, stiffness and damping coefficient of the pile group and

soil were associated with one of the degrees of freedom and the mass, stiffness and damping coefficient of the load frame was taken as an additional degree of freedom as shown schematically in Figure 6.4. The basic equations defining the motion of the 2DOF system are given by

$$\mathbf{F}(t) = \begin{bmatrix} m_1 \\ m_2 \end{bmatrix} a(t) + \begin{bmatrix} c_1 \\ c_2 \end{bmatrix} v(t) + \begin{bmatrix} k_1 \\ k_2 \end{bmatrix} x(t) \tag{6.6}$$

where:

m_1, c_1, k_1 = mass, damping and stiffness properties of the load frame

m_2, c_2, k_2 = mass, damping and stiffness properties of the pile group and soil

$\boldsymbol{F(t)}$ = F1 and F2 where F1 is the force from the statnamic device and F2 is the force applied to the piles from the load frame.

The force time history from the statnamic load cell was used as the applied force in place of the summed tie rod load cells time history.

The mass of the load frame was found to be 4800 kg by summing up the mass of the various components. The damping of the load frame was assumed to be very small with a damping ratio of 2 percent which is common for steel structures. The stiffness of the load frame would be the smaller stiffness constant of either the tie rods or the two channels.

To find the axial stiffness of a tie rod, equation 6.7 was used

$$K_{rod} = \frac{AE}{L} \tag{6.7}$$

where:

K_{rod} = single tie rod stiffness

Two Degree of Freedom System

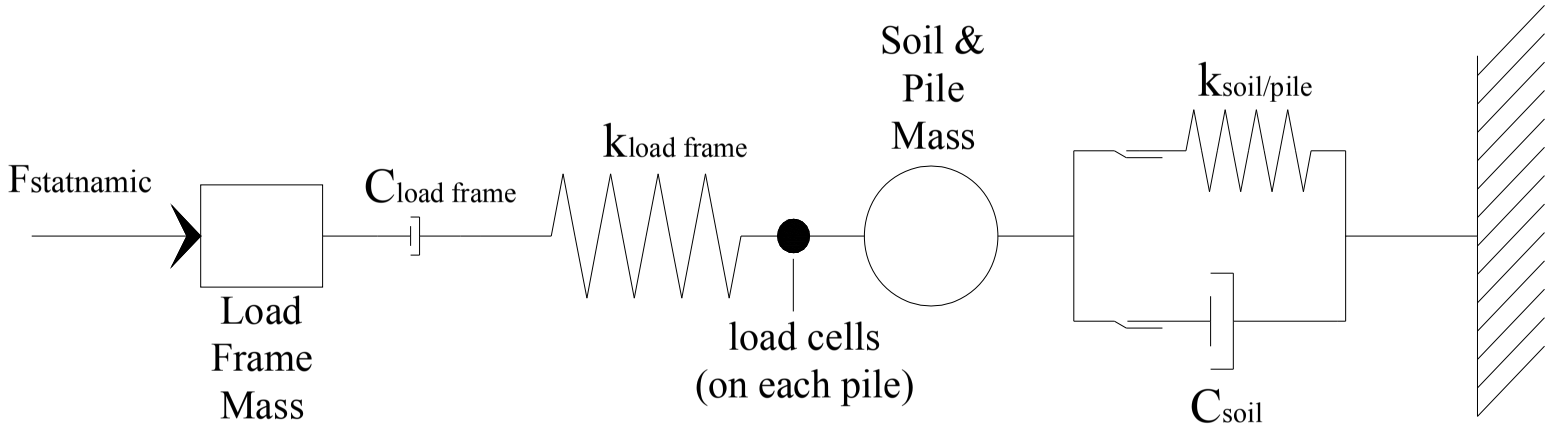

Figure 6.4: Two degree of freedom system model.

A = area of tie rods (A = 0.002027m^2)

E = Young's modulus of elasticity (200 MN/m^2)

L = length of tie rod (L = 0.368 m)

Equation 6.8 was used to determine the bending stiffness of the two channels per row

$$K_C = 66.667 \frac{EI}{L^3} \tag{6.8}$$

where:

K_c = bending stiffness of 2 channels per row

E = Young's modulus of elasticity (200 MN/m^2)

I = inertia on strong axis for 2 channels (I = 8.57x10^{-5} m^4)

L = length between supports (L = 1.07 m)

The stiffness of a single tie rod is 1.10x10^6 kN/m (6.28x10^6 lb/in). The stiffness for a row of channels is 0.941x10^6 kN/m (5.38x10^6 lb/in). Because the channels had a smaller stiffness, this stiffness was used as the stiffness of the load frame in the two DOF system. Based on the load test results discussed that will be discussed in Chapter 7, the pile group stiffness is on the order of 50 to 21kN/m for the 15-pile group and 28 to 12 kN/m for the 9-pile group. The load frame stiffness is extremely large relative to the pile group stiffness, which suggests that the entire system may simply move as one unit when subjected to an applied force.

By using numerical methods that will be described later in this chapter, the motion of the pile group computed with the 2 DOF system was found to be only marginally different than that computed by the SDOF approach using estimated stiffness

and damping coefficients. Therefore, it was determined that it would not be beneficial to model the motion any further with the 2DOF, particularly because accurate load time histories were taken by the load cell attached to each pile. The load cells at the piles would measure all additional forces caused by the load frame that would not be able to be accounted for with a single DOF model.

6.1.3 Single Degree of Freedom (SDOF) —Variable Mass, Damping, and Stiffness

A final model was developed to consider variable mass, stiffness, and damping coefficients during several time intervals. This approach was used to account for variations in these properties due to the presence of gaps around the test piles. Values for these three parameters were averaged throughout each region they represented. The changing parameters were originally separated into four regions as illustrated in Figure 6.5 for analysis purposes.

1. The first region is defined by deflections ranging from zero to the gap width that was measured after each test at a given target deflection as described in Chapters 4 and 5. Within this region, the mass of system would be the mass of the piles in motion or the active pile length. The calculation of the mass of the active pile length will be discussed later in this chapter. The stiffness would be about the stiffness of the pile group to the active length. The damping would be relatively small because there is little interaction between the soil and the pile until the pile moves through the gap and contacts the soil.
2. Region two ends at a deflection equal to the previous maximum deflection. This distance is typically greater than the gap width because the soil tends to rebound somewhat after loading. Because the soil resistance was mobilized by 15 static

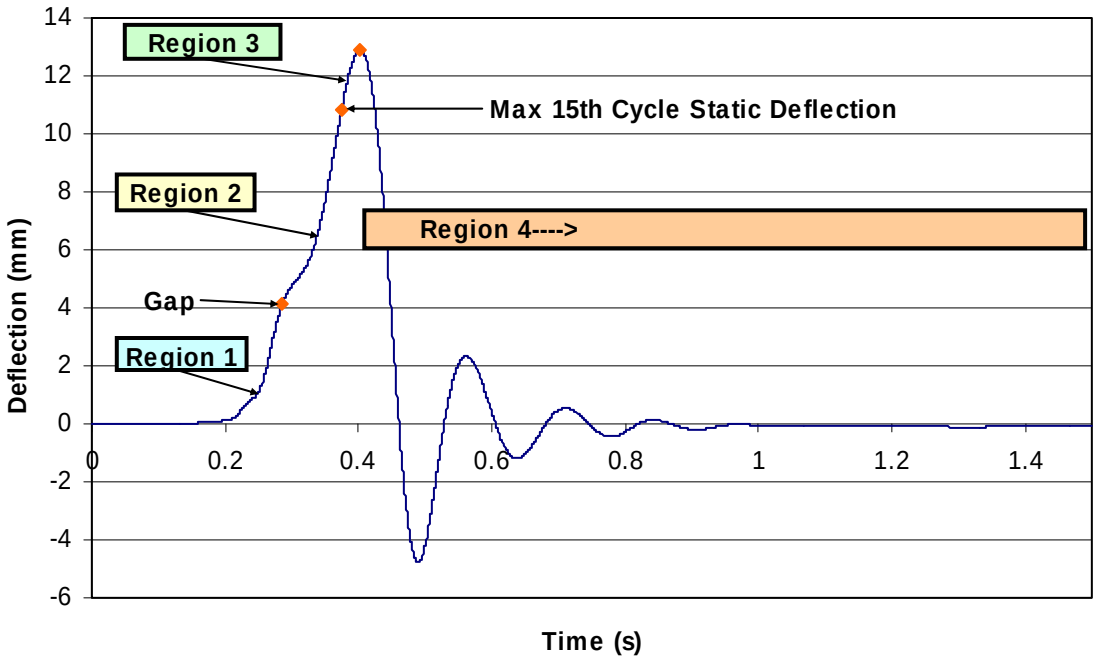

Figure 6.5: Model parameters separated by four regions.

cyclic loads prior to the 16th cycle statnamic test, the soil showed relatively constant stiffness properties as illustrated in Figure 6.6. Within this region, the mass includes the pile mass down to the active lateral length and the mobilized soil mass. The mobilized soil mass is the soil that moves with the pile group. This mass of the soil could potentially increases as the deflections increased. The mobilized soil mass is unknown, but could be estimated or obtained using optimization techniques. The damping would significantly increase within this region because the pile is now in contact with the soil.

3. The third region ranges between the maximum loading and maximum deflection (Figure 6.5). This region is the loading within virgin soil. The stiffness, damping, and mass of the system slightly increase from region two, because the virgin soil is now mobilized.

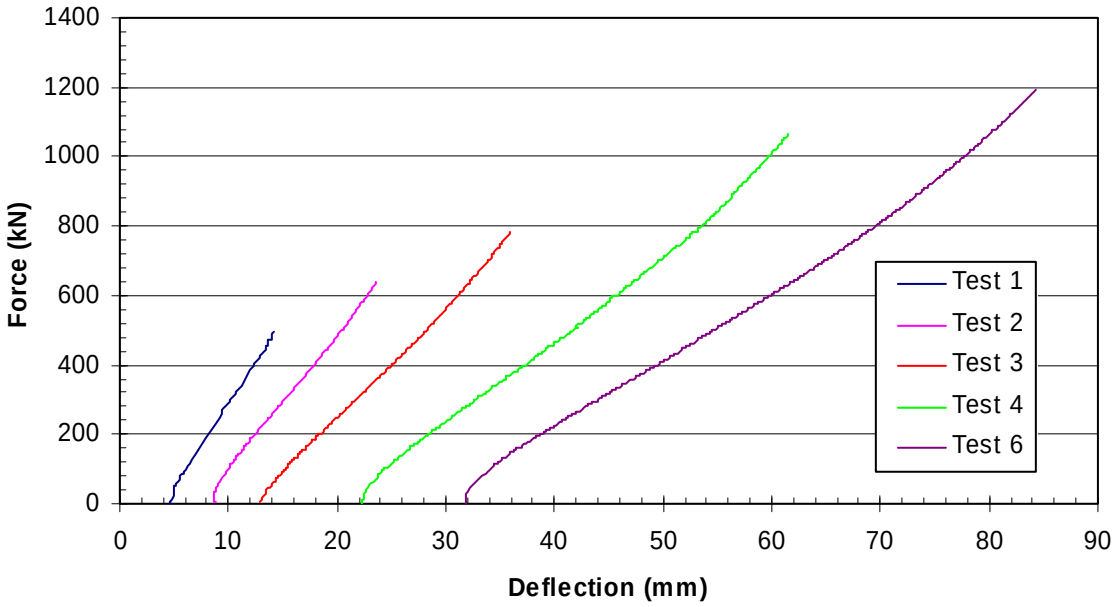

Figure 6.6: Continuous load-deflection cures for the 15th static loadings immediately prior to the specified statnamic load test.

4. The last region consists of the motion of the system after the maximum deflection. For the soil mass of the system, the maximum amount of soil is assumed to be fully mobilized. The damping and stiffness are assumed to be the same as region 3.

Of the various models investigated, this variable property SDOF model followed the measured motion most accurately. This SDOF system may be modeled as shown in Figure 6.7. $C_{soil\ 1}$ and k_{pile} represent region 1. Damping and stiffness in this region account for the gapping with a sliding plate. To simplify the model, the same damping coefficient ($C_{soil\ 2}$) and stiffness ($k_{soil/pile\ 2}$) were used to represent regions 2, 3, and 4. The outer regions are more elastic and thus do not need to account for the soil/pile separation (El Naggar, 1998). An additional spring and dashpot is shown at the left of the pile in Figure 6.7 to visualize the motion in negative displacements while in region 4.

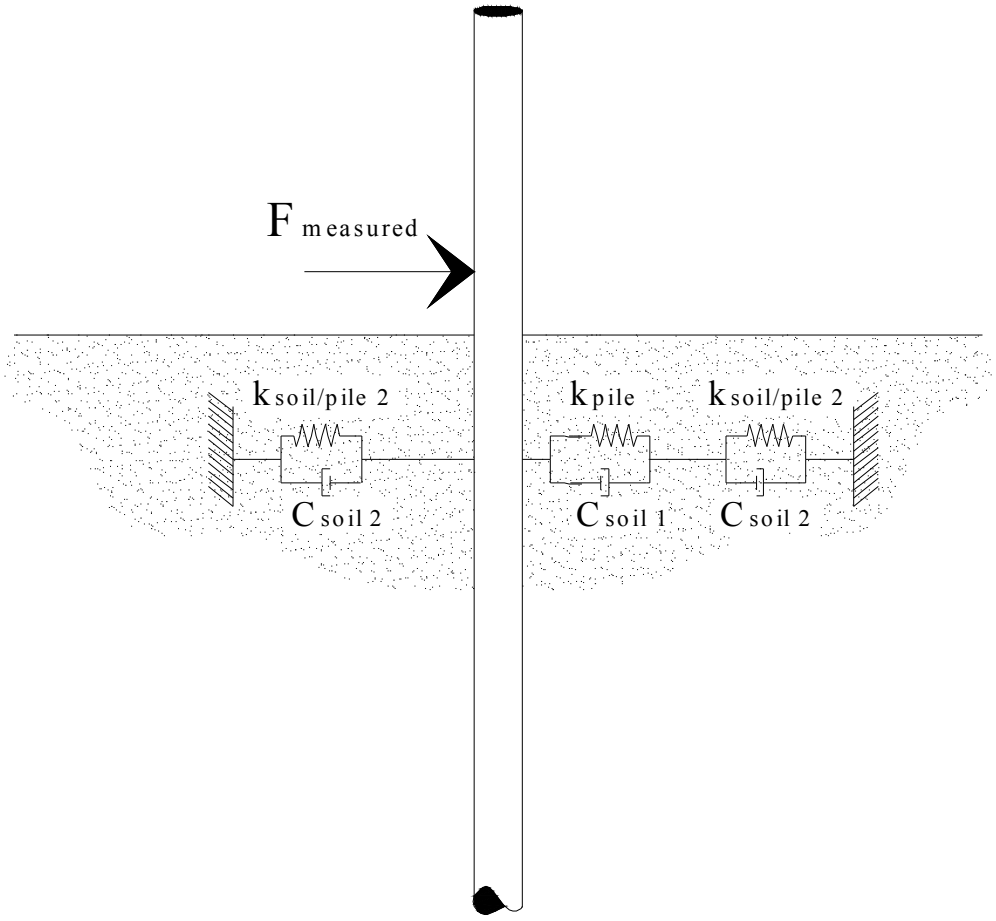

Figure 6.7: Model of changing mass, stiffness, and damping.

Calculating the Active Pile Length

The active pile length could be determined by using the accelerometers that were installed down the piles to determine where significant motion was occurring. However in most cases, this information would not be available to an analyst. Gazetas and Dobry (1984) developed an equation to calculate this length for small horizontal vibrations. According to Gazetas and Dobry (1984) the active length (l_a) for pipe piles in inhomogeneous soil is given by the equation

$$l_a = 3.2b(E_p S / E_s)^{1/6} \tag{6.9}$$

where:

b = outside diameter of pile

E_p = Young's modulus of pile

E_s = inhomogeneous soil modulus (linearly increasing)

S = pile cross section dimensionless shape factor

[for hollow pipes $S = 1-(b_i/b)^4$]

b_i = inside diameter of pile

Based on equation 6.8 an active length of 4.91 m (16.1 ft) was found for the pipe piles in this investigation. Adding an additional length of the pile above the ground of 2.13 m (7.0 ft), gave a full length of 7.0 m (23 ft). The active length obtained with the Dobry and Gazetas equation agreed well with the limit of significant deflection in the pile based on the time histories derived from the accelerometers. The mass of the 15-pile group came to 7760 kg (8.5 tons) and the mass of the 9-pile group came to 4660 kg (5.1 tons). The mass in regions 2, 3, and 4 includes the soil that is mobilized and added to the mass of the piles is optimized and discussed in more detail in Chapter 7.

6.2 Numerical Method Analysis

6.2.1 Introduction

Computing the motion of a SDOF model using a digitized force time history (excitation function) is not an exact procedure. Several numerical methods are used to predict approximate motions. The best analytical methods follow three requirements (Chopra, 2001): (1) convergence—as the time step decreases, the solution should be closer to the actual motion, (2) stability—the method should be stable in the presence of

round off errors, and (3) accuracy—the numerical procedure should be close to the actual motion.

The various numerical methods may be separated into three categories: (1) methods based on interpolation of the excitation function, (2) methods based on finite difference expressions of acceleration, velocity, and displacement, and (3) methods based on assumed variation of acceleration. One method from each of these three categories was used to determine the best method to use and the variation that might result in the computed motion. The selected analysis procedures were:

1. A force equilibrium method that is dependant on the excitation function.
2. A Central Difference Method that is based on a finite difference equation for the displacement, velocity, and acceleration.
3. The Linear Acceleration Method which is based on the assumed linear variation of acceleration.

All three of these methods are conditionally stable. This means that selection of the time step is vital for the stable calculation of the motion of the system. The Central Difference Method requires the minimum time step Δt given by the equation (Chopra, 2001)

$$\Delta t \leq \frac{T_N}{\pi} \tag{6.10}$$

where:

T_N is the natural period

The Linear Acceleration Method requires the following minimum time step

$$\Delta t \leq \frac{T_N}{0.551} \tag{6.11}$$

As a rule of thumb, all the conditionally stable methods should have the following minimum time step (Tedesco et. al., 1999):

$$\Delta t \leq \frac{T_N}{10} \tag{6.12}$$

The shortest natural period for both the 15-pile and the 9-pile group was test 6. The natural period for the 15-pile group was 0.14 s, thus the time step according to equation 6.11 must be less than 0.014 seconds. The natural period for the 9-pile group was 0.15 s, thus the minimum time step recommended should be under 0.015 seconds. Both time steps are much smaller than the recommended time steps (Δt_{15} = 0.000667 s; Δt_9 = 0.000526 s), thus the force data will work well for the all the conditionally stable methods.

After determining that the physical model could be best represented using a SDOF model, these three methods were compared to see if any significant differences in the computed motion would occur using optimized values for the stiffness and damping coefficient. This investigation found that the three methods produced nearly identical motions as shown in Figure 6.8. Because of the accuracy of the three analysis procedures any of the three could be chosen with little difference in the result. Ultimately, the force equilibrium method was chosen because of the simplicity of the method. Therefore, the force equilibrium method will be discussed in further detail in the following section of this chapter.

6.2.2 Force Equilibrium Method

For many applications the mass, stiffness and damping coefficient for a system are known and the acceleration, velocity and displacement are computed for a given force

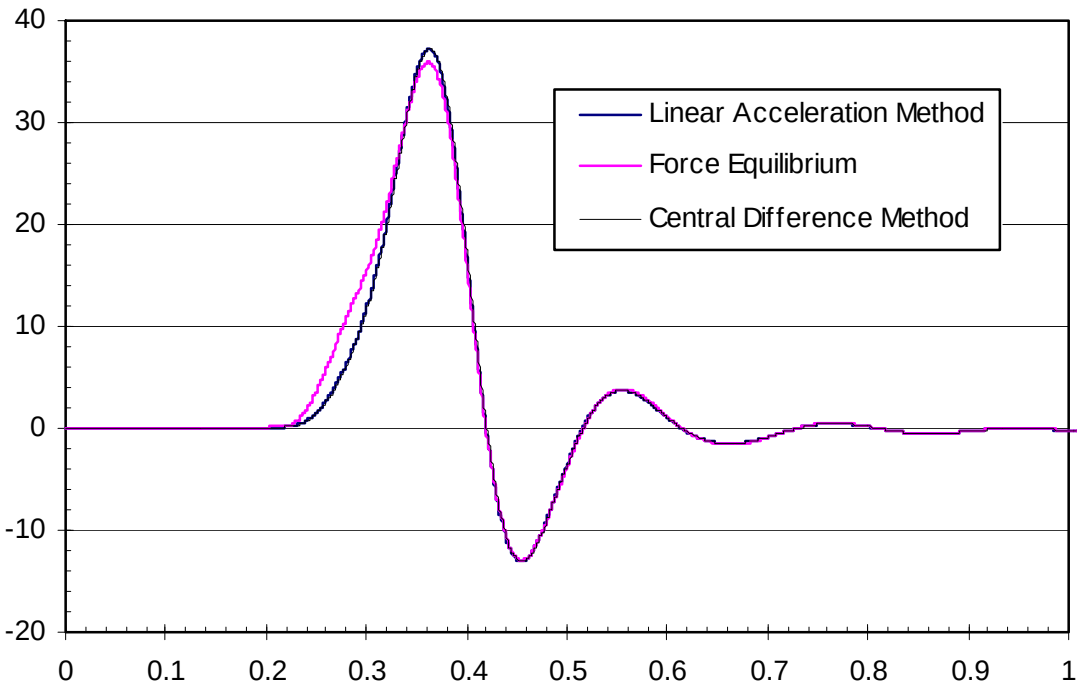

Figure 6.8: Comparison of SDOF motion computed by the force equilibrium, central difference, and linear acceleration methods (test 3 for 15-pile group).

time history. However, as discussed in Chapters 4 and 5, force, acceleration, velocity, and deflection were measured for both Salt Lake City Airport pile test groups. With these variables measured and the use of computer optimization, the mass, damping coefficient, and static stiffness constants were back-calculated using the fundamental equation of force equilibrium given by equation 6.1 as discussed at the beginning of the chapter.

For this study, a response analysis of the motion was performed using only the measured force time history in the force equilibrium equation. Acceleration may be calculated with equation 6.13:

$$a_i = \frac{F_i - cv_{i-1} - kx_{i-1}}{m} \tag{6.13}$$

where:

v_{i-1} = Velocity from the previous time step

x_{i-1} = Displacement from the previous time step

Velocity and displacement may then be calculated through integration with the equations

$$v_i = a_i \Delta t + v_{i-1} \tag{6.14}$$

$$x_i = v_i \Delta t + x_{i-1} \tag{6.15}$$

where:

Δt = constant time step.

Mass, damping coefficient, and static stiffness are the unknown model parameters for the analysis which must be iteratively adjusted to produce agreement between the measured and computed acceleration, velocity and displacement. Dr. Dan A. Brown in the Civil and Engineering Department at Auburn University followed a similar procedure (Brown, 2000).

Optimization or matching is achieved by minimizing the sum of the differences of the calculated motion to the measured time history motion. The sum of the squares error may be minimized with respect to the deflection, velocity, acceleration, or force time histories. For this research, the analyses were optimized to the measured deflection and acceleration. It is noteworthy that when optimizing with several parameters, it is possible to reach only a local minimum and not the ultimate minimum. A good robust optimization program should be used or several manual trials should be performed to ensure that a viable solution has been acquired.

As mentioned earlier in the chapter, the model that will be used has four different regions throughout the motion of the piles. Each region is dependant on averaged parameters of mass, damping coefficient, and stiffness. This simplified approach allows engineers to more easily understand the motion of the complex behavior and reaction of group foundation piles. Chapter 7 will show the optimization results using this model (SDOF with variable values for m, c, k) with the Force Equilibrium Method.

CHAPTER 7 MOTION ANALYSIS RESULTS

Now that the Single degree of freedom (SDOF) model and Force Equilibrium numerical method have been defined, optimization of the computed motion is ready to be performed. Stiffness values and damping ratios will be the product of optimizing the computed motion to match the measured motion. (See Flow Chart, Figure 6.1). Before performing these analyses for the 15- and 9-pile groups, analysis of the measured motion will help find reasonable results of the stiffness values and damping ratios.

7.1 Analysis of Natural and Forcing Frequencies and Damping Ratios From Measured Data

To ensure that accurate results were obtained, the measured motion data was analyzed to determine values of forcing frequencies, natural frequencies, and damping ratios.

7.1.1 Forcing Frequency

The forcing frequency was approximated using the following procedure. The statnamic device applied only one load pulse to the system for each test. The force period was found by taking the rise time (the time from initial force application to the peak force) and multiplying this time by four. The forcing frequency is defined as the inverse of the force period. This procedure is illustrated in Figure 7.1. The measured force period and frequency for each test are tabulated in Tables 7.1 and 7.2. The forcing

frequency increased as the applied force and pile head deflections increased. The 9-pile group generally had a smaller forcing frequency (longer period) than the 15-pile group.

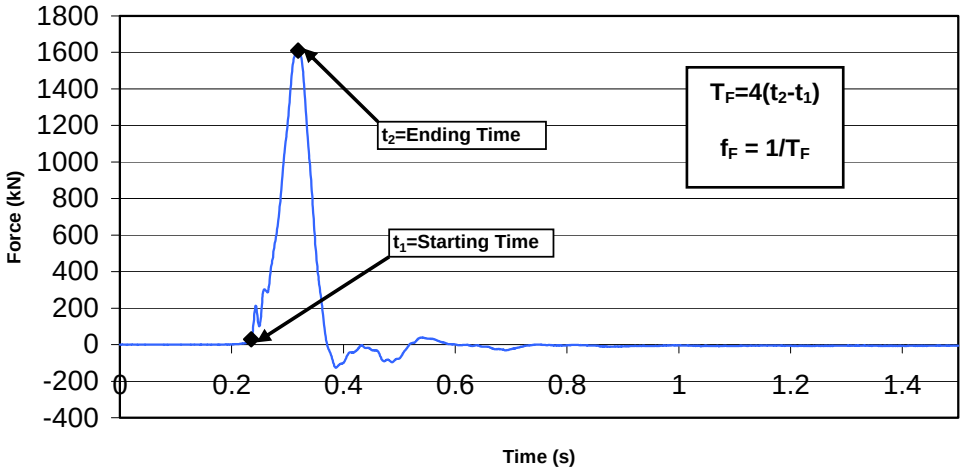

Figure 7.1: Illustration of procedure for finding the forcing frequency (test 4 of 15-pile group).

7.1.2 Natural Period and Frequency of the Pile Groups

The natural period of vibration for each pile group during each statnamic test was measured as the time from peak to peak in the amplitudes of motion. This could be done using the deflection, velocity, or acceleration time histories after the force from the statnamic device was applied. The first amplitudes are best for evaluating the natural period of the motion because the gaps that affect the motion are less influential when the piles are near their peak motion. The tests with smaller lateral deflections tended to have relatively longer load pulses from the statnamic device, thus the time interval from the first peak amplitude to the second peak amplitude was influenced by the load application and was not completely in a free vibration condition.

Of course, the natural frequency is the inverse of the natural period. The natural frequencies obtained from the displacement and acceleration time histories are also listed in Tables 7.1 and 7.2. The natural frequencies obtained from the displacement and acceleration time histories are very similar. While the frequency of the statnamic force time history increased with deflection, the natural frequency of the pile group decreased as the lateral deflections increased. Also, the natural frequencies of the 15- and 9-pile groups seemed to be about the same for comparable displacement levels. This observation suggests that the natural frequencies are not as much dependant on the number of piles in a group as they are on the lateral displacement. Figure 7.2 provides plots of the measured natural frequencies versus the maximum displacements for both the 15-pile and the 9-pile groups. The darker points locate the 15-pile group and the lighter points mark the 9-pile group. A best-fit equation defining the relationship between natural frequency and displacement was found to be

$$f = 15.115\, d^{-0.2949} \tag{7.1}$$

This would be valuable when observing pile reactions under earthquake loads.

Table 7.1: Natural and Force Frequencies and Periods for the 15-Pile Group

Test #	Target Deflection (in)	Force		Displacement		Acceleration	
		Period (sec)	Frequency (Hz)	Period (sec)	Frequency (Hz)	Period (sec)	Frequency (Hz)
1	**0.5**	0.59	1.70	0.14	6.94	0.12	8.47
2	**1.0**	0.47	2.14	0.18	5.66	0.18	5.60
3	**1.5**	0.42	2.40	0.19	5.17	0.17	5.79
4	**2.5**	0.33	3.02	0.25	4.01	0.20	4.89
5	**3.5**	0.30	3.32	0.23	4.40	0.21	4.79
6	**3.5**	0.30	3.32	0.24	4.13	0.24	4.18

Table7.2: Natural and Force Frequencies and Periods for the 9-Pile Group

Test #	Target Deflection (in)	Force		Displacement		Acceleration	
		Period (sec)	Frequency (Hz)	Period (sec)	Frequency (Hz)	Period (sec)	Frequency (Hz)
1	**0.5**	0.71	1.41	0.15	6.71	0.13	7.60
2	**1.0**	0.77	1.30	0.16	6.35	0.15	6.57
3	**1.5**	0.84	1.18	0.19	5.16	0.19	5.19
4	**2.5**	0.43	2.33	0.23	4.39	0.21	4.85
5	**3.5**	0.61	1.65	0.23	4.41	0.21	4.68
6	**3.5**	0.47	2.15	0.24	4.14	0.22	4.57

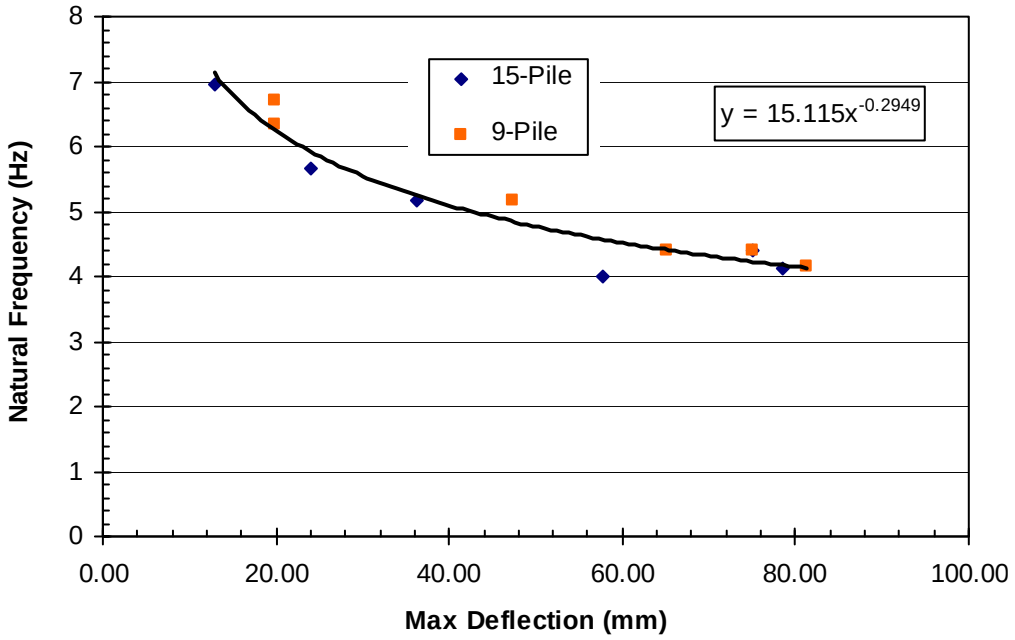

Figure 7.2: Trend of natural frequency vs peak deflection for the tests on the 15- and 9-pile groups.

7.1.3 Damping Ratios by Logarithmic Decrement

It is relatively difficult to estimate the damping coefficient accurately using optimization techniques and numerical methods alone; therefore, the measured data from full-scale pile experiment is extremely valuable in finding correct coefficients (Chopra, 2001; Tedesco et. al., p.86). If the system is underdamped, the logarithmic decrement (δ)

may be used to find the damping ratio (ζ) of the system. The logarithmic decrement is given by the equation

$$\delta = \ln\left(\frac{X_1}{X_2}\right) \tag{7.2}$$

where:

X_1 = the first peak amplitude of displacement

X_2 = the second amplitude of displacement

The damping ratio is then found using the equation

$$\zeta = \frac{\delta}{\sqrt{(2\pi)^2 + \delta^2}} \tag{7.3}$$

If the damping ratio is 20 percent or less, an accurate damping ratio may be found by using the simpler equation

$$\zeta = \frac{\delta}{2\pi} \tag{7.4}$$

The plots of logarithmic decrement (δ) versus the damping factor (ζ) in Figure 7.3 show the variance of Equations 7.3 and 7.4.

For most structural systems the damping ratio is under twenty percent; however, when piles react with soil the damping ratios have been reported to be 40 to 60 percent(Rollins, et. al., 2004). Because of potentially high damping ratios, the exact equation (Equation 7.3) is typically better to use for systems in soil and was used in this study.

The logarithmic decrement method should not be considered to provide the exact damping ratio for these tests; rather, it provides an estimate of the damping ratio. For one, the gaps in the soil around the pile can cause different damping ratios during a

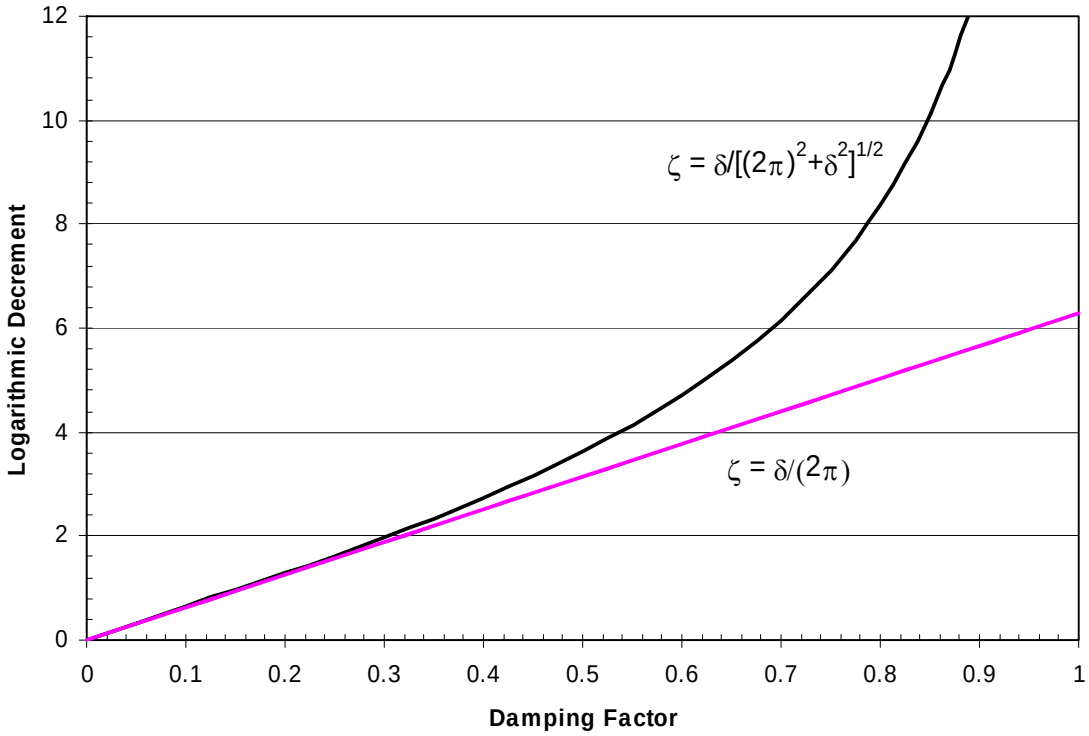

Figure 7.3: Comparison of damping ratio calculations using equations 7.3 and 7.4.

complete period of motion depending on whether or not the pile is in contact with the soil. Secondly, the method is based on the assumption of free-vibration; however, the applied force is not always zero at the time of the first peak amplitudes that are used for the calculations. These are similar issues to the problems described in calculating the natural frequency of the pile group. Observing the force data, the motion is affected on the first amplitude; however, in each test, the forces are small and will not likely affect the calculated damping ratios significantly. Table 7.3 provides a tabulation of the computed damping ratios for each test using the logarithmic decrement. These ratios,

obtained from the measured response, will be valuable when determining if the values obtained from the numerical analyses are reasonable estimates of the damping ratios for the pile groups.

Table 7.3: Calculated Damping Ratios by Logarithmic Decrement Method

Test #	Defl. Target (in)	15-pile group Damping ratio, ζ (%)	9-pile group Damping ratio, ζ (%)
1	**0.5**	23.2	26.6
2	**1.0**	29.2	29.7
3	**1.5**	34.8	32.6
4	**2.5**	42.0	38.1
5	**3.5**	31.2	41.0
6	**3.5**	48.9	29.9

Dynamic Magnification Factor (DMF)

Now that the frequency of the forcing function and natural frequency of the pile groups have been estimated along with the damping ratios, the Dynamic Magnification Factors (DMF) may be found. This factor is dimensionless and defines the ratio between the dynamic and static displacement amplitude. The damping ratio and frequency ratio (r) are the two variables required to determine the dynamic magnification factor. The frequency ratio is found by using the equation

$$r = \frac{\Omega}{\omega} \tag{7.5}$$

where:

Ω = the forcing frequency (rad/s)

ω = the natural frequency (rad/s)

The dynamic magnification factor is then found using the equation

$$R_d = \frac{1}{\sqrt{(1 - r^2)^2 + (2\zeta r)^2}} \tag{7.6}$$

Table 7.4 summarizes the displacement response factors with the accompanying frequency ratio and damping ratio for each test.

Table 7.4: Dynamic Magnification Factors (DMF) for 15- and 9-Pile Group Tests

Test #	15-Pile Group			9-Pile Group		
	Frequency ratio, r =(Ω/ω)	DMF	15-pile group Damping ratio, ζ (%)	Frequency ratio, r =(Ω/ω)	DMF	9-pile group Damping ratio, ζ (%)
1	0.25	1.06	23.2	0.21	1.04	26.6
2	0.38	1.13	29.2	0.20	1.04	29.7
3	0.46	1.18	34.8	0.23	1.04	32.6
4	0.75	1.31	42.0	0.53	1.21	38.1
5	0.75	1.57	31.2	0.37	1.10	41.0
6	0.80	1.16	48.9	0.52	1.26	29.9

Figures 7.4 and 7.5 compare these computed magnification factors and show how they relate to each other and the maximum magnification factors (at resonance, r≈1) obtainable for various damping ratios. Because most of the frequency ratios for the various tests are relatively low, the DMF is not highly sensitive to the damping ratio. In addition, as the displacement amplitude for each test increases leading to an increase in the frequency ratio, the DMF also tends to increase. The tests that had the largest DMF were those that loaded virgin soil.

7.2 15-Pile Group Motion Analysis Results

Based on the studies performed in Chapter 6, the model that was determined to be the most accurate for the pile groups was the SDOF Model with variable mass, stiffness, and damping values. As noted in Chapter 6, separate parameters were used for deflection less than and greater than the pre-existing gap width. For a further review of this model please refer to Chapter 6.

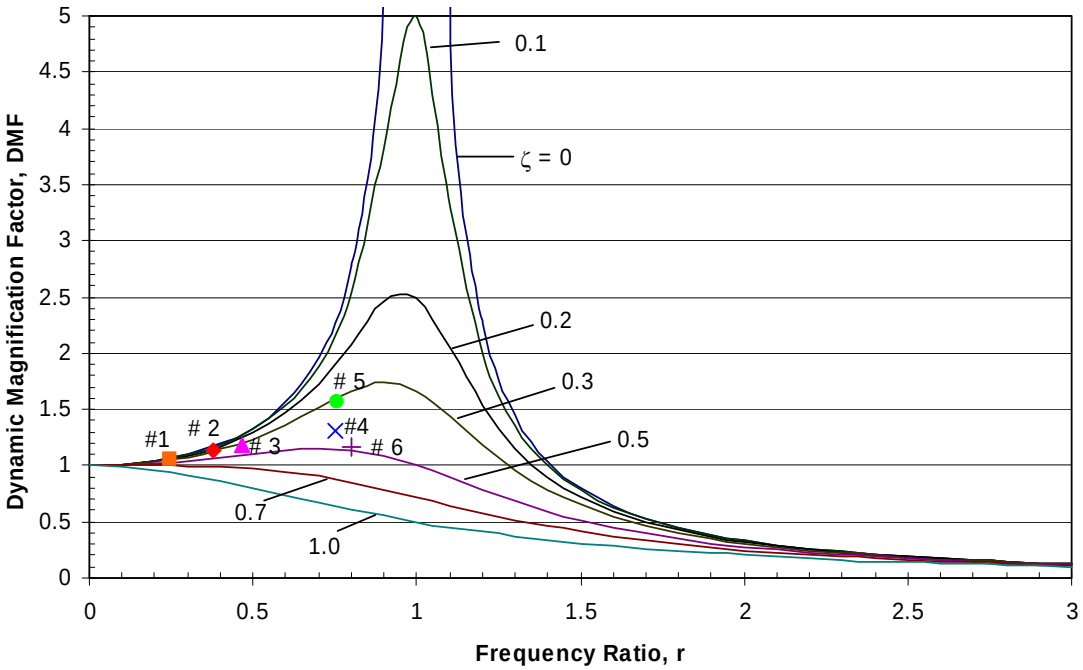

Figure 7.4: Dynamic magnification factor (DMF) as a function of frequency and damping ratios along with results from 15-pile group tests.

The Force Equilibrium Method was used with the measured force to optimizing the motion of the piles. This was also discussed in depth in Chapter 6. Optimizing the calculated motion was achieved by minimizing the sum of the differences to the measured time history of motion. This least sum of the squares fit may be minimized

using deflection, velocity, acceleration, or force. For this research, the analyses were optimized to both the measured deflection and acceleration. All unknown parameters were optimized at the same time with no additional weighing factors.

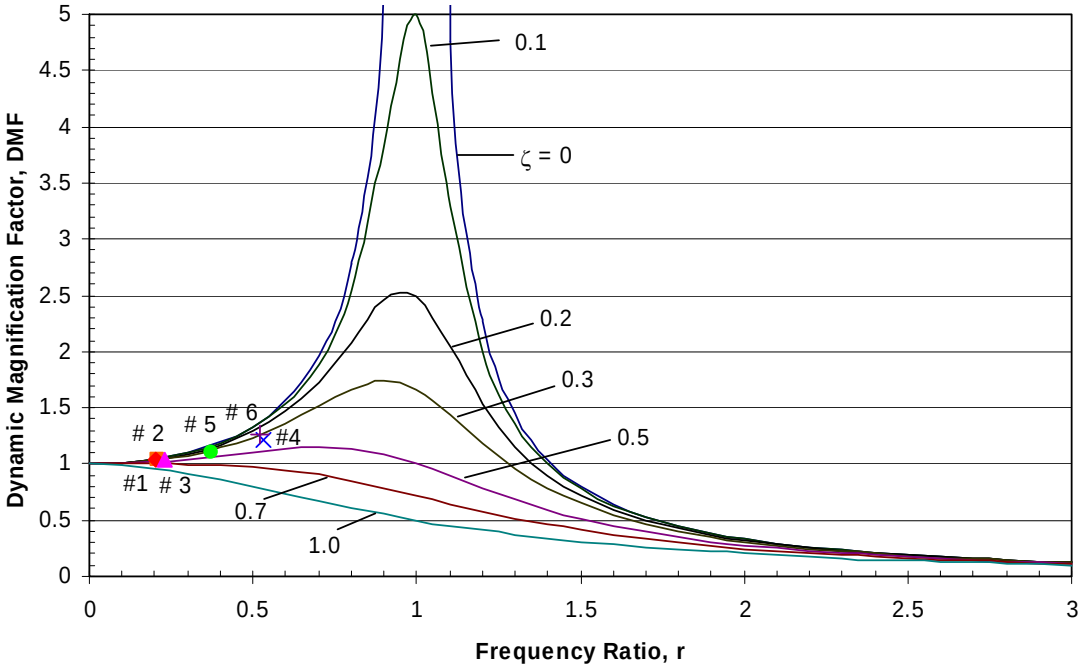

Figure 7.5: Dynamic magnification factor (DMF) as a function of frequency and damping ratios along with results from 9-pile group tests.

Once an ultimate minimum of differences were achieved, the calculated stiffness and damping ratios were obtained. Refer to Tables 7.5 and 7.6 for the calculated values of the stiffness and damping ratios compared with estimated measured values. As discussed in Chapter 6, the mass of the system in regions 2, 3, and 4 included the mass of the load frame, piles, and mobilized soil. Refer to Table 7.7 for the optimized mass obtained for each test.

In all cases, the calculated stiffness was in excellent agreement with the stiffness of the structure measured for the 15th cycle of static loading. In addition, the back-

Table 7.5: Comparison of Measured and Computed Stiffness with Equivalent Single Degree of Freedom Model for 15-Pile Group

Test #	Stiffness (kN / mm)		
	Measured	Calculated	% Error
1	50.0	49.5	-1.0
2	40.0	39.7	-0.7
3	33.0	32.6	-1.2
4	25.0	25.2	0.8
5	23.0	23.0	0.0
6	21.0	21.0	0.0

Table 7.6: Comparison of Measured and Calculated Damping Ratio with Equivalent Single Degree of Freedom Model for 15-Pile Group

Test #	Damping Ratio (%)		
	Measured	Calculated	% Error
1	23.2	28.5	22.8
2	29.2	31.9	9.2
3	34.8	34.8	0.0
4	42.0	42.6	1.4
5	31.2	43.4	39.1
6	48.9	45.3	-7.4

Table 7.7: Optimized Mass for 15-Pile Group

Test #	Mass at Region 1 (kg)	Mass at Regions 2-4 (kg)
1	7800	19000
2	7800	23000
3	7800	23000
4	7800	20000
5	7800	21000
6	7800	22000

calculated damping ratios values were generally within 10 percent of the ratio obtained with the log-decrement method. However, for tests 1 and 5 the differences were much higher. This can be for a couple reasons: 1) the log decrement assumes free-vibration while some force was still being applied to the actual pile group, 2) Averaging values in

the system may cause inaccuracies in a dynamic system that has mass, damping, and friction constantly changing.

Comparisons between the measured and computed time histories as well as the measured and computed load-deflection curves for each of the six tests on the 15-pile group are presented in Figures 7.6 through 7.11. In part (a) of each figure the computed and measured deflection time histories are plotted along with the measured force time history. The average force time history from the load cells is added here to show the interaction which the statnamic device and load frame had on the system. Generally, the computed deflection is quite close to the measured deflection although the agreement is better for the first cycle of motion than for subsequent cycles. In addition, the agreement appears to be somewhat better for positive deflections than for negative deflections.

In part (b) of Figures 7.6 through 7.11, the pile head acceleration time histories measured by the accelerometer are compared with time histories computed with the numerical model. The agreement is relatively good for tests 1 through 4; however the calculated acceleration is smoother than the measured acceleration which appears to contain some higher frequency oscillations which are not captured by the model. These oscillations could be vibrations associated with each pile itself or perhaps components of the frame. Greater discrepancies between the measured and computed accelerations are apparent for Tests 5 and 6. The discrepancies are particularly pronounced with respect to the peak negative accelerations. This can be attributed to the presence of gaps behind the piles which would not inhibit negative acceleration as would otherwise occur if the soil remained in contact with the pile.

In part (c) of Figures 7.6 through 7.11 the measured static and dynamic load-deflection curves are plotted along with the static load-deflection curve calculated by the

numerical model. In nearly all cases the computed static load-deflection curve has a slope that is very close to the measured curve during loading; however, in some cases the computed and measured curves appear to be offset by some initial value. These offsets can be explained by (1) relaxation of the pile following static loading or (2) rebounding of the soil wall into the gap during the 30 to 40 minute time interval between the static and dynamic load tests. Because the model stiffness is a constant, the computed static unload curve is a straight line while the measured stiffness decreases when the pile group is unloaded as shown in Figures 7.6-11(c). Therefore, during unloading the stiffness is overestimated which may also partially account for the underestimate of the measured peak negative acceleration.

The error between the computed and measured maximum and minimum deflection and accelerations for each statnamic test on the 15-pile group are summarized in Tables 7.8 and 7.9. Generally, deflection errors were the smallest with a maximum difference for positive deflection of 5 mm or less. Maximum deflections obtained using the optimization approach was found to be on average 2.6 mm greater than the measured maximum deflections. Visually notable from the graphs, positive accelerations had a greater error difference than deflection. Most tests had a difference of about 0.2 g's difference; however, tests 5 and 6 had an error of about 1 g. Typically, the error in estimating the minimum deflection and acceleration is substantially greater than that for the maximum values. This increasing error is likely a result of the reduced stiffness behind the pile during rebound resulting from the presence of gaps behind the piles.

The calculated and measured damping ratios for the statnamic tests on the 15-pile group are plotted as a function of the maximum deflection in Figure 7.12. As the deflections increased, the damping ratios also increased. Best-fit lines have also been

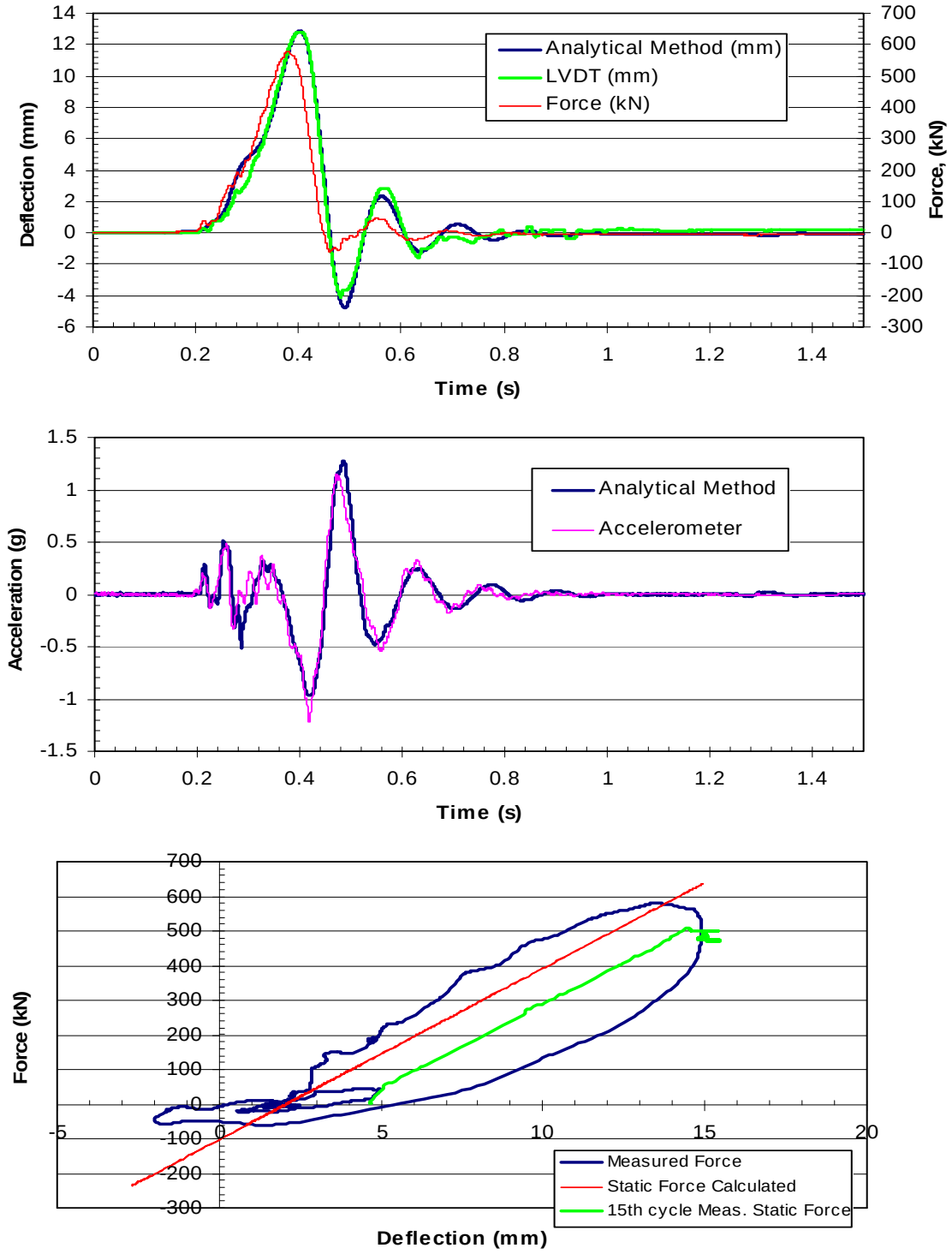

Figure 7.6: Comparison of (a) measured and computed deflection time histories (b) measured and computed acceleration time histories and (c) measured and computed static force-deflection curves –test 1 on the 15-pile group.

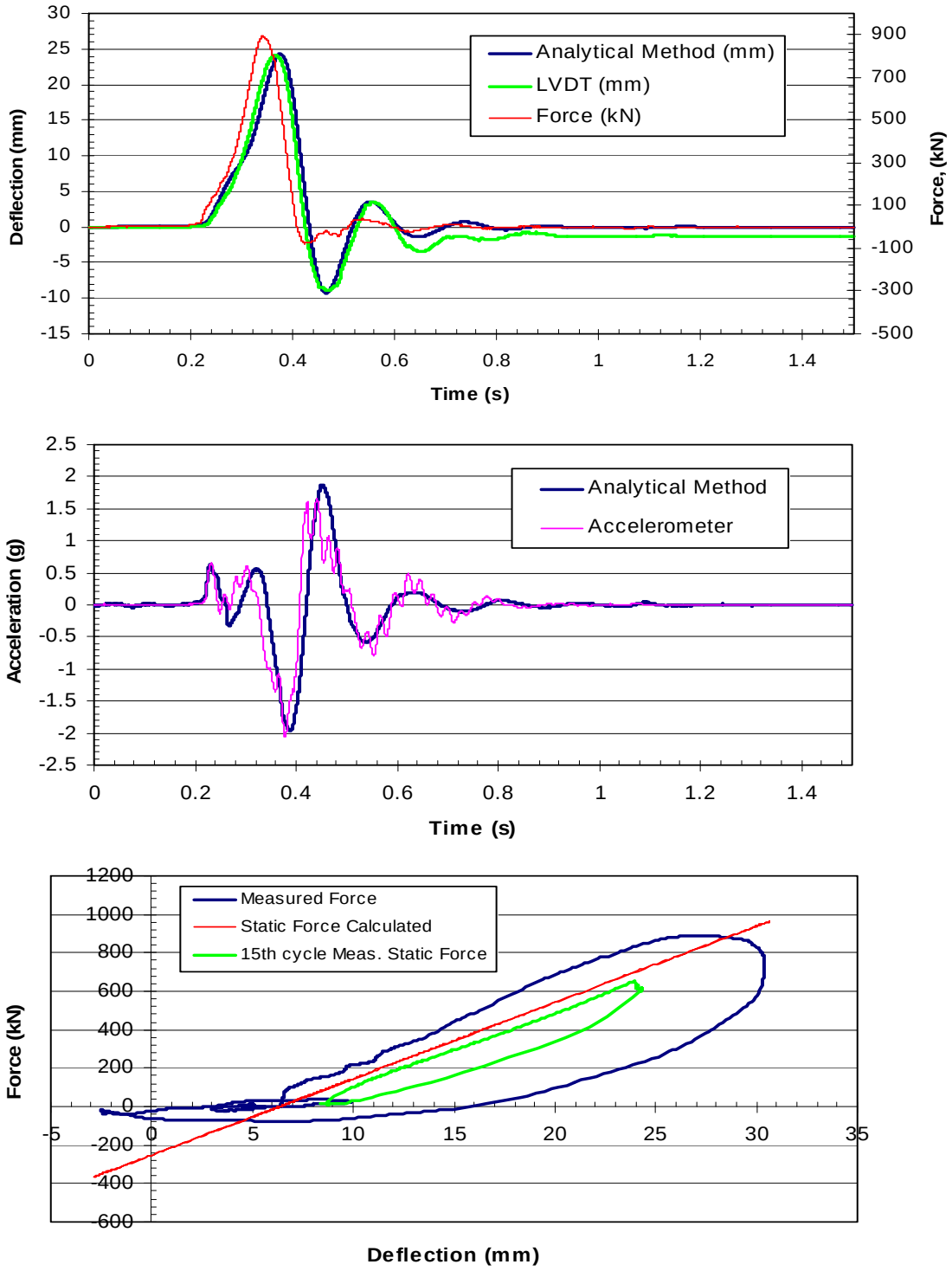

Figure 7.7: Comparison of (a) measured and computed deflection time histories (b) measured and computed acceleration time histories and (c) measured and computed static force-deflection curves –test 2 on the 15-pile group.

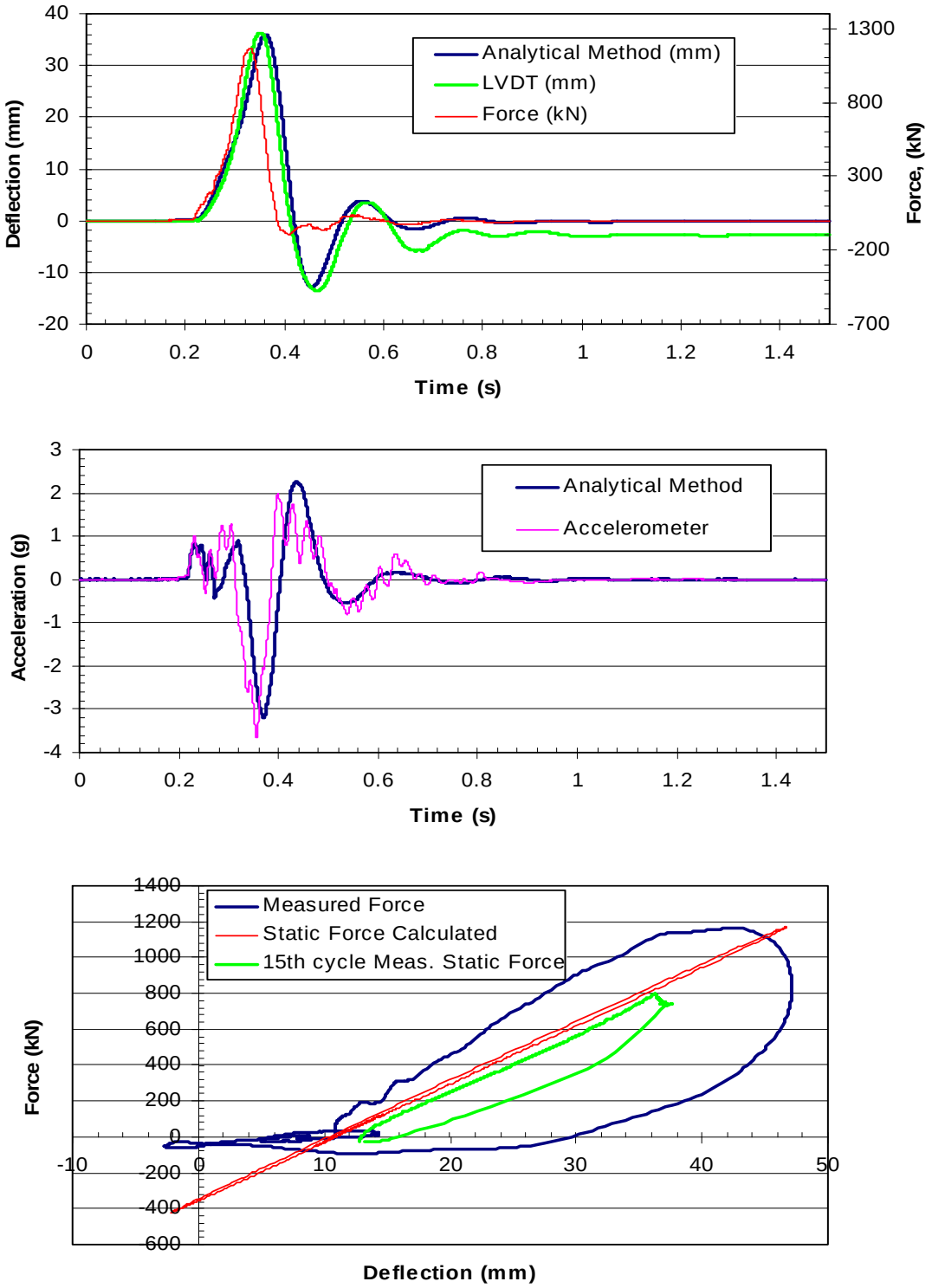

Figure 7.8: Comparison of (a) measured and computed deflection time histories (b) measured and computed acceleration time histories and (c) measured and computed static force-deflection curves –test 3 on the 15-pile group.

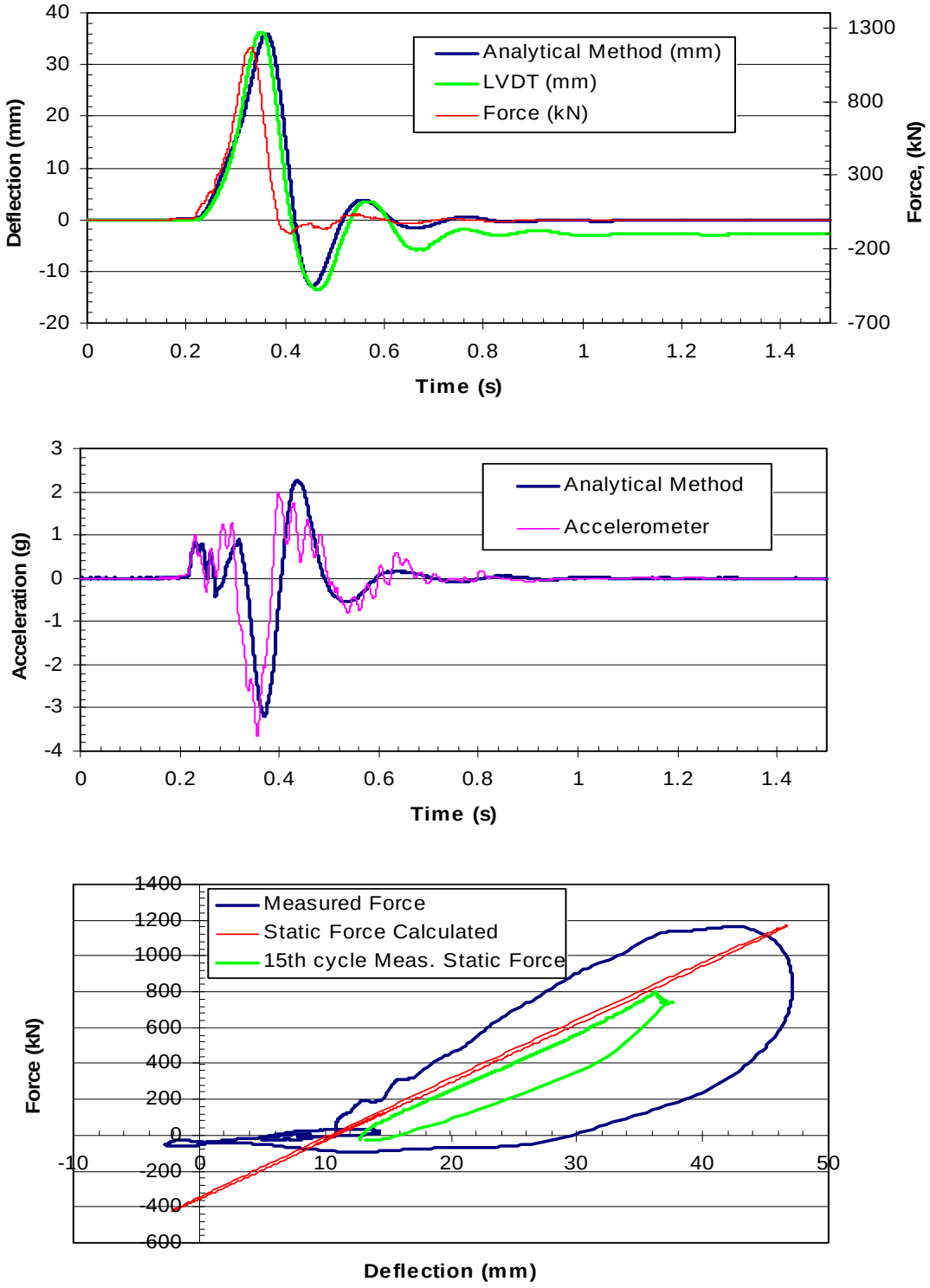

Figure 7.9: Comparison of (a) measured and computed deflection time histories (b) measured and computed acceleration time histories and (c) measured and computed static force-deflection curves –test 4 on the 15-pile group.

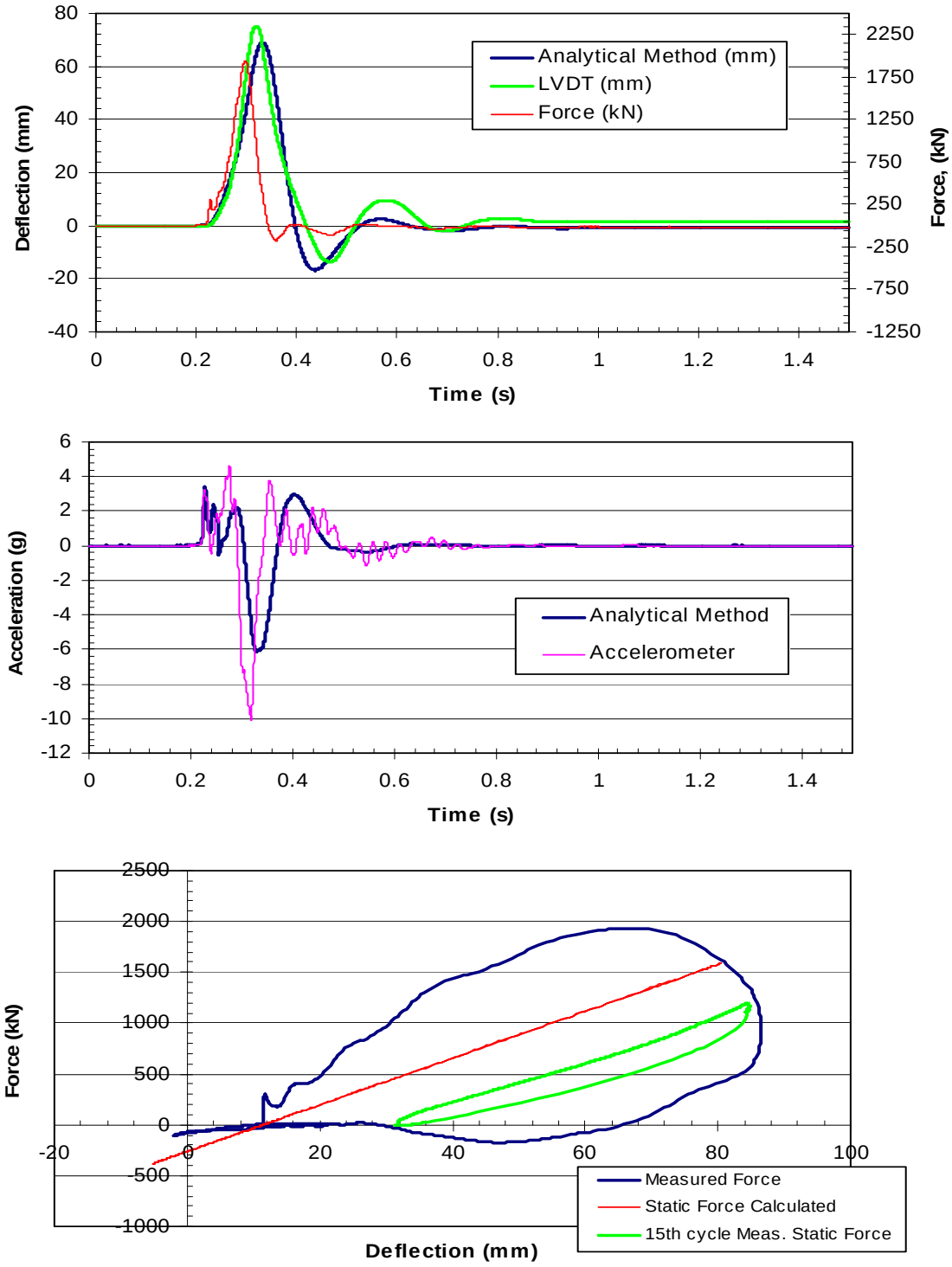

Figure 7.10: Comparison of (a) measured and computed deflection time histories (b) measured and computed acceleration time histories and (c) measured and computed static force-deflection curves –test 5 on the 15-pile group.

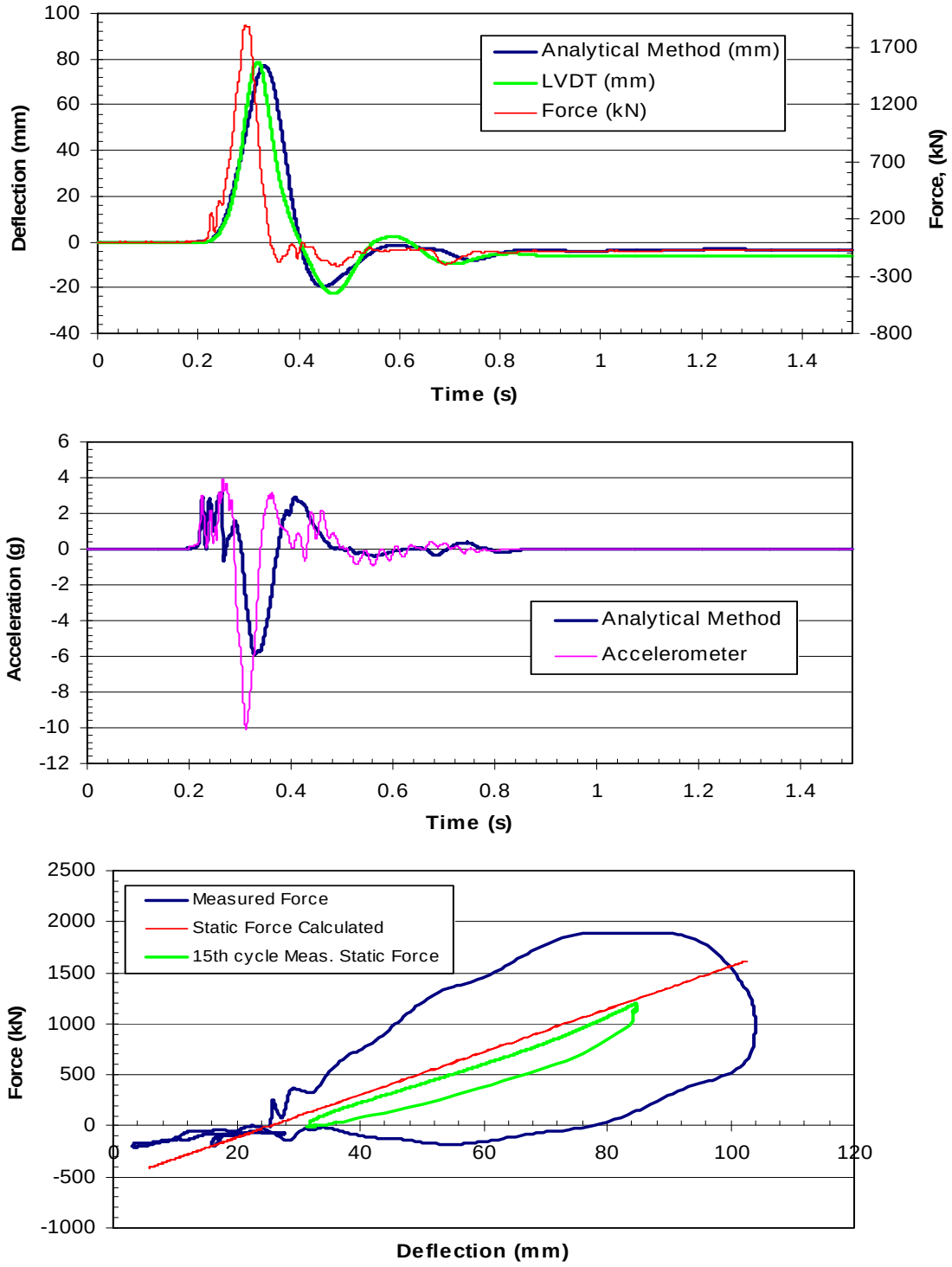

Figure 7.11: Comparison of (a) measured and computed deflection time histories (b) measured and computed acceleration time histories and (c) measured and computed static force-deflection curves –test 6 on the 15-pile group.

Table7.8: Error Between Computed and Measured Peak Deflections for the Statnamic Tests on the 15-Pile Group

Test #	Max Deflection (mm)			Min Deflection (mm)		
	calc.	meas.	Error (mm)	calc.	meas.	Error (mm)
1	12.9	12.7	-0.2	-4.8	-3.7	1.1
2	24.3	24.0	-0.3	-9.3	-8.7	0.6
3	35.9	36.2	0.3	-12.9	-13.4	-0.5
4	58.6	57.4	-1.2	-15.5	-18.8	-3.3
5	68.9	74.6	5.7	-16.7	-13.4	3.3
6	77.1	78.0	0.9	-19.6	-22.3	-2.7

Table 7.9: Error Between Computed and Measured Peak Accelerations for the Statnamic Tests on the 15-Pile Group

Test #	Max Acceleration (g's)			Min Acceleration (g's)		
	calc.	meas.	Error (g's)	calc.	meas.	Error (-g's)
1	1.28	1.15	-0.13	-0.97	-1.21	-0.24
2	1.87	1.65	-0.22	-1.97	-2.06	-0.09
3	2.26	1.97	-0.29	-3.18	-3.66	-0.48
4	2.92	2.74	-0.18	-5.24	-5.94	-0.70
5	3.46	4.64	1.18	-6.12	-10.07	-3.95
6	3.16	3.90	0.74	-5.89	-10.12	-4.23

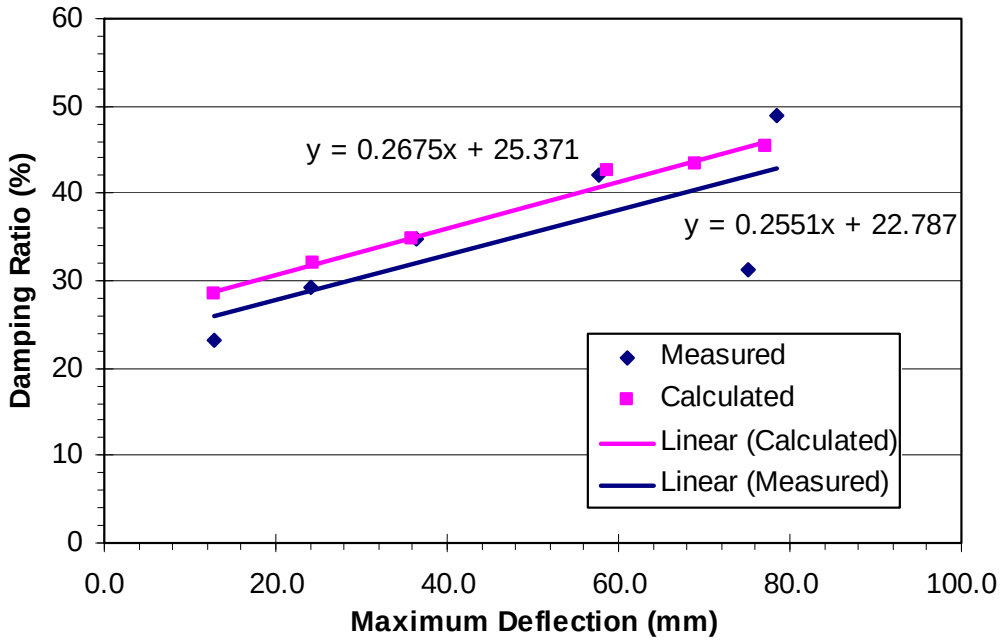

Figure 7.12: Measured and calculated damping ratios as a function of maximum displacement of 15-pile group.

defined for the measured and calculated damping ratios and are also shown in Figure 7.12. This relationship appears to be linearly increasing. The rate of change from the measure and calculated damping ratios are very consistent. The results from Figure 7.12 suggest that the optimization was accurate to finding the damping of the 15-pile group.

7.3 9-pile Group Analysis Results

The modeling of the 9-pile group was performed using the same method as the 15-pile group. The SDOF Model with variable mass, stiffness, and damping values was used to find an optimized calculated motion compared to the measured motion. In the process of optimization, more unknown forces in the motion caused the optimization of the 9-pile group to be more difficult and ultimate minimization was not as well defined as the 15-pile group. To compensate, optimization of the mass and damping values were the only values optimized. The stiffness values from the preceding static test were used. From the comparisons of Table 7.5 on the 15-pile group, this appears to be a reasonable approach for estimating the dynamic stiffness. Table 7.10 provides the stiffness values that were used in the analysis of the dynamic tests.

Table 7.11 provides a summary of the damping ratios obtained by the optimization procedure compared with damping ratios measured with the log decrement procedure while Table 7.12 summarizes the optimized mass obtained for each test. The damping ratios obtained by optimization were usually about 10 percent greater than the damping ratios obtained from the logarithmic decrement approach. However, the damping ratio obtained from logarithmic decrement method for test 6 was significantly lower (the second oscillation had a larger deflection) than expected. A possible reason why this value was significantly lower could be that gapping around the piles allowed the

piles to rebound more then normal on the second oscillation. The mass of the model obtained from the optimization approach was around 12000 kg for most of the tests. The equipment and frame weighed 4300 kg. The mass of the group piles is estimated to be

Table 7.10: Comparison of Measured and Computed Stiffness with Equivalent Single Degree of Freedom Model for 9-Pile Group

Test #	Stiffness (kN / mm)		
	Measured	Calculated	% Error
1	27.9	27.9	0.0
2	23.9	23.9	0.0
3	20.8	20.8	0.0
4	17.0	17.0	0.0
5	12.3	12.3	0.0
6	12.3	12.3	0.0

Table 7.11: Comparison of Measured and Calculated Damping Ratio with Equivalent Single Degree of Freedom Model for 9-Pile Group

Test #	Damping Ratio (%)		
	Measured	Calculated	% Error
1	26.6	28.5	7.1
2	29.7	35.2	18.5
3	32.6	36.0	10.4
4	38.1	41.7	9.4
5	41	45.3	10.5
6	29.9	49.0	63.9

Table 7.12: Optimized Mass for 9-Pile Group

Test #	Mass at Region 1 (kg)	Mass at Regions 2-4 (kg)
1	4677	11910
2	4677	11960
3	4677	14560
4	4677	11960
5	4677	11960
6	4677	11960

about 2300kg, which assumes an average of 3.5m length of pile mass in motion. This would leave an estimate of 0.5m of soil (p = 130 lb/ft3) mass in motion.

Comparisons between the measured and computed time histories as well as the measured and computed load-deflection curves for each of the tests on the 9-pile group are presented in Figures 7.13 through 7.18. As noted for the 15-pile group, part (a) of each figure compares measured and calculated deflection time histories. The averaged load cells force time history is also added here to show the interaction that both the statnamic device and load frame had on the system. Part (b) of each figure compares the plots of the measured and calculated acceleration time histories.

As the statnamic loads increased, the calculated deflections and accelerations have greater error. This is likely from giving average values of mass and damping to a dynamic system that undergoes significant changes with these parameters.

Part (c) represents the measured static and dynamic load-deflection curves plotted along with the static load-deflection curve calculated by the numerical model. As observed from the 15-pile group, the slope of the computed static load-deflection curve is close to the measured curve during loading; however, as the tests continued to increase, the computed and measured curves are offset by an initial value. These offsets can be explained by (1) relaxation of the piles following static loading and (2) rebounding of the soil walls into the gaps between testing intervals of the static and dynamic load tests. Because the model stiffness is a constant, the computed static unload curve is a straight line while the measured stiffness from the preceding static test decreases when the pile group is unloaded as shown in Figure 7.13-18(c). The reduced stiffness at the unloading of the static load gives evidence that the stiffness of the system possibly reduces when rebounding.

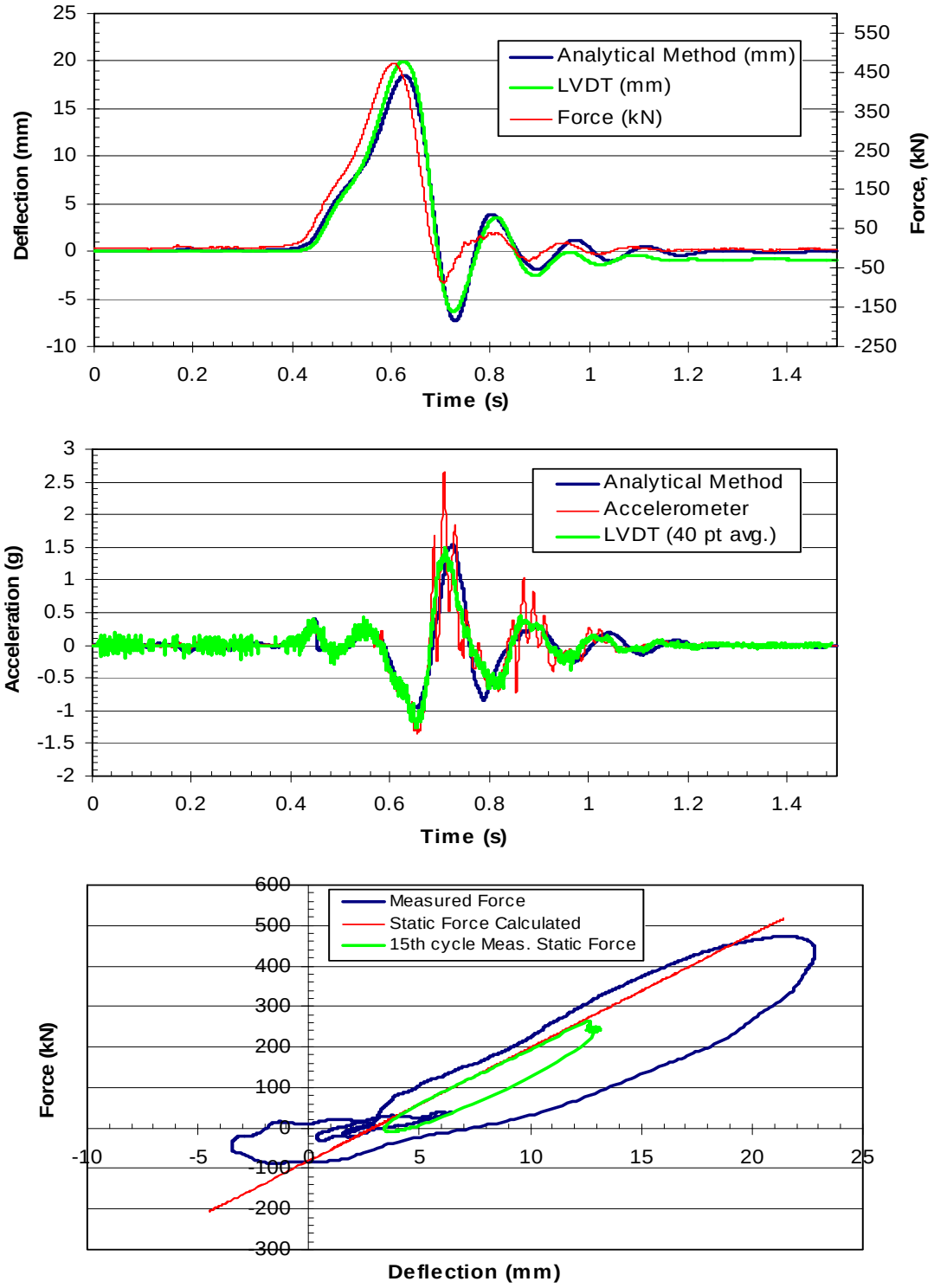

Figure 7.13: Comparison of (a) measured and computed deflection time histories (b) measured and computed acceleration time histories and (c) measured and computed static force-deflection curves –test 1 on the 9-pile group.

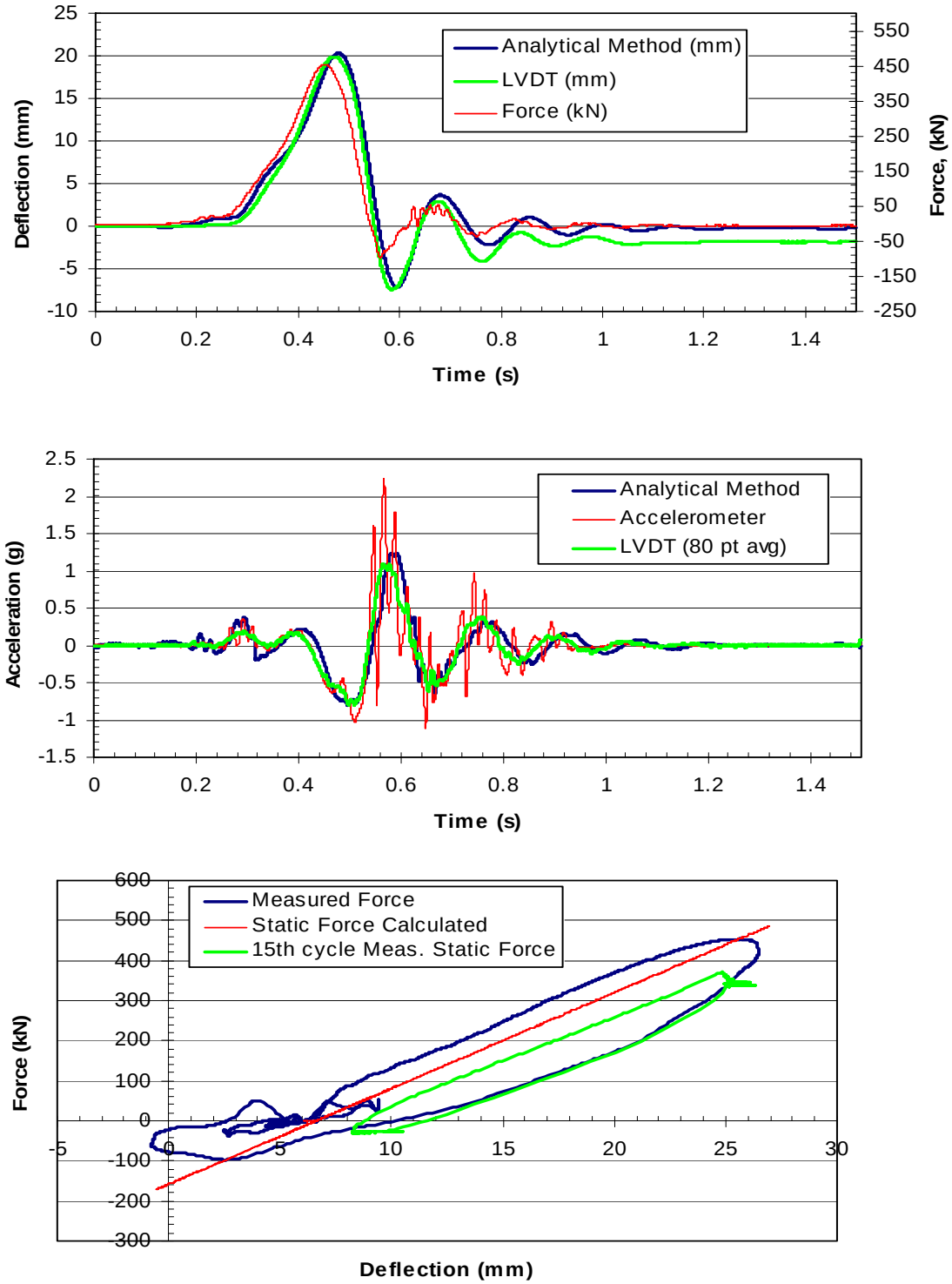

Figure 7.14: Comparison of (a) measured and computed deflection time histories (b) measured and computed acceleration time histories and (c) measured and computed static force-deflection curves –test 2 on the 9-pile group.

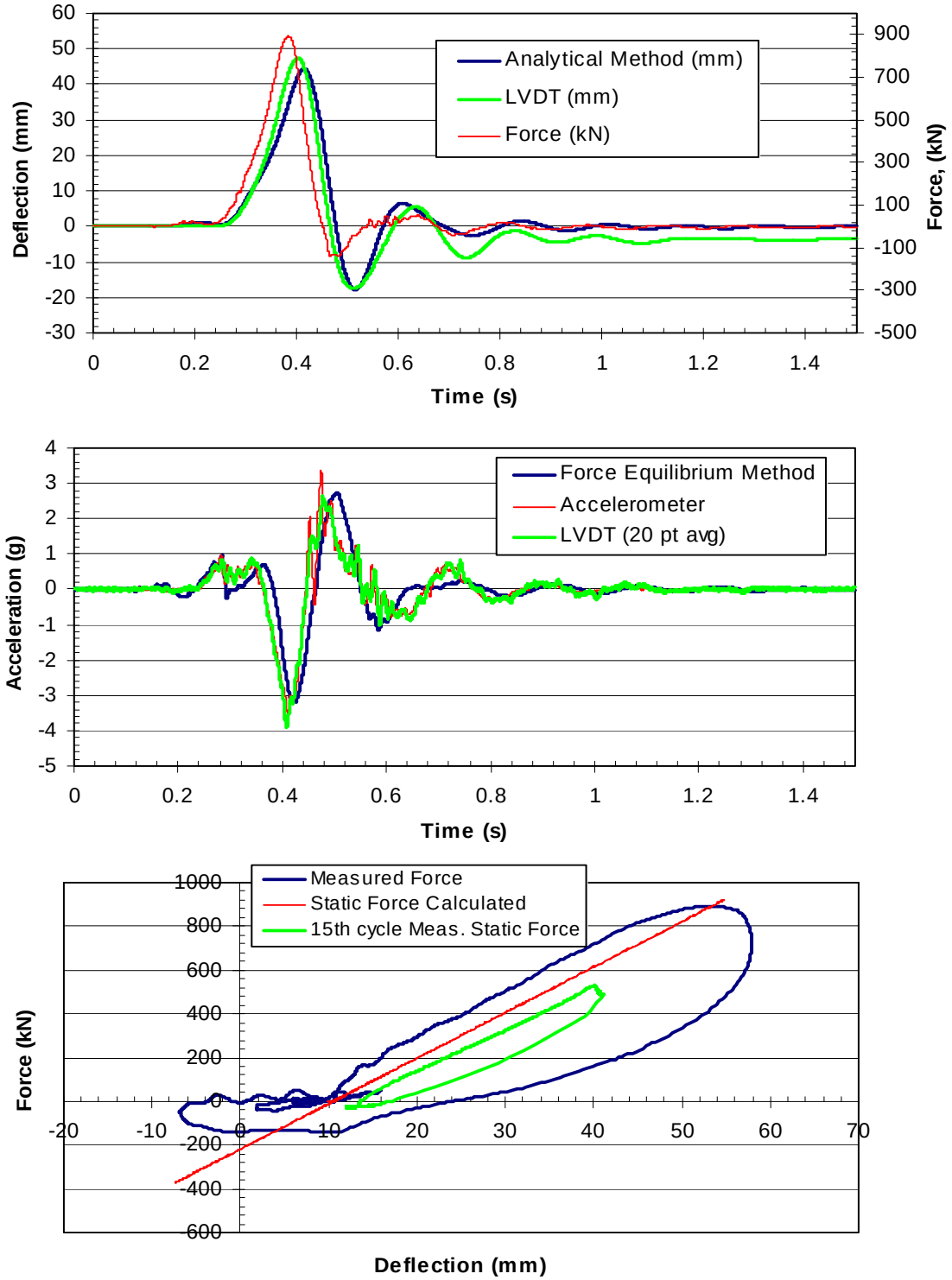

Figure 7.15: Comparison of (a) measured and computed deflection time histories (b) measured and computed acceleration time histories and (c) measured and computed static force-deflection curves –test 3 on the 9-pile group.

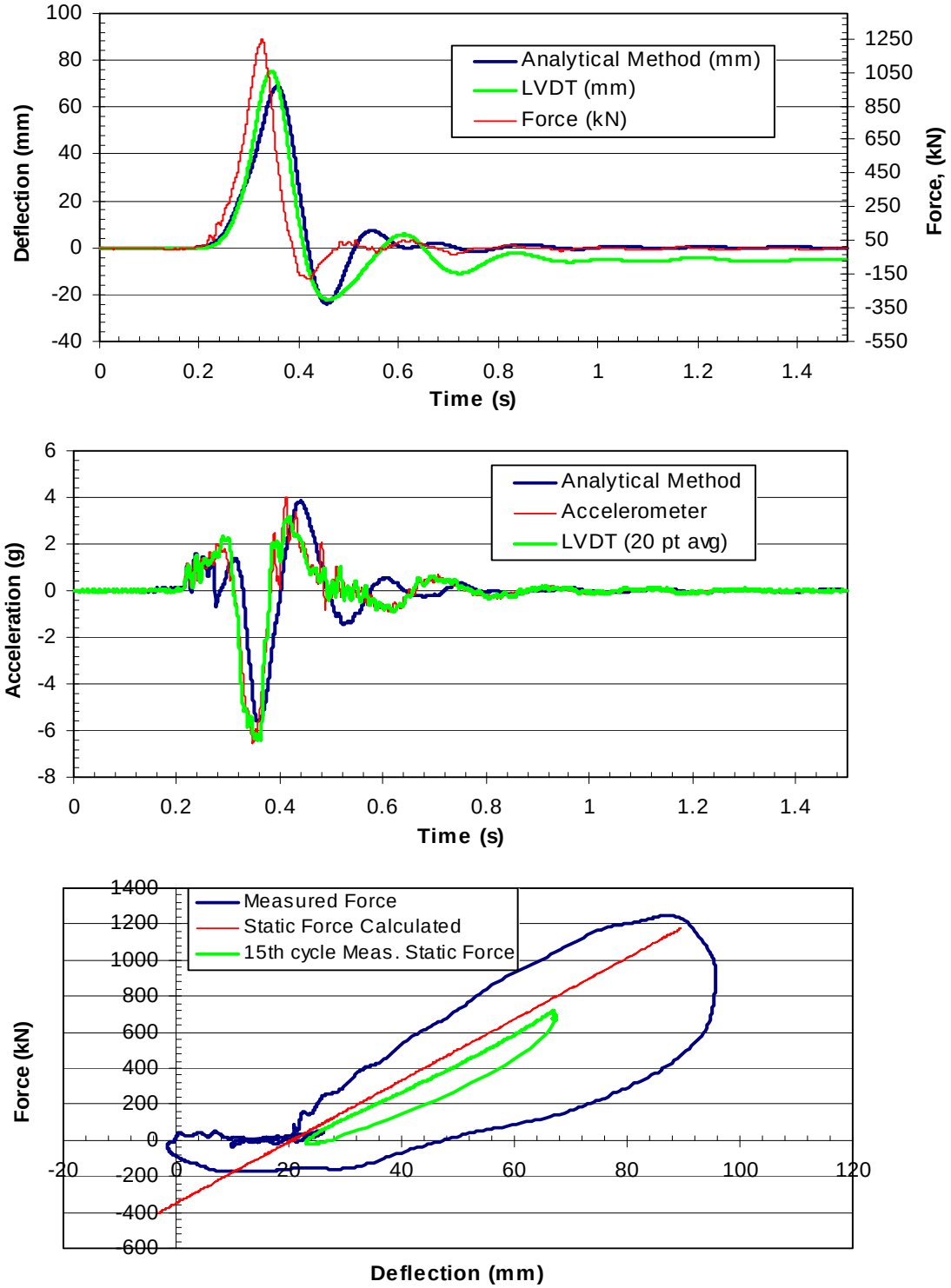

Figure 7.16: Comparison of (a) measured and computed deflection time histories (b) measured and computed acceleration time histories and (c) measured and computed static force-deflection curves –test 4 on the 9-pile group.

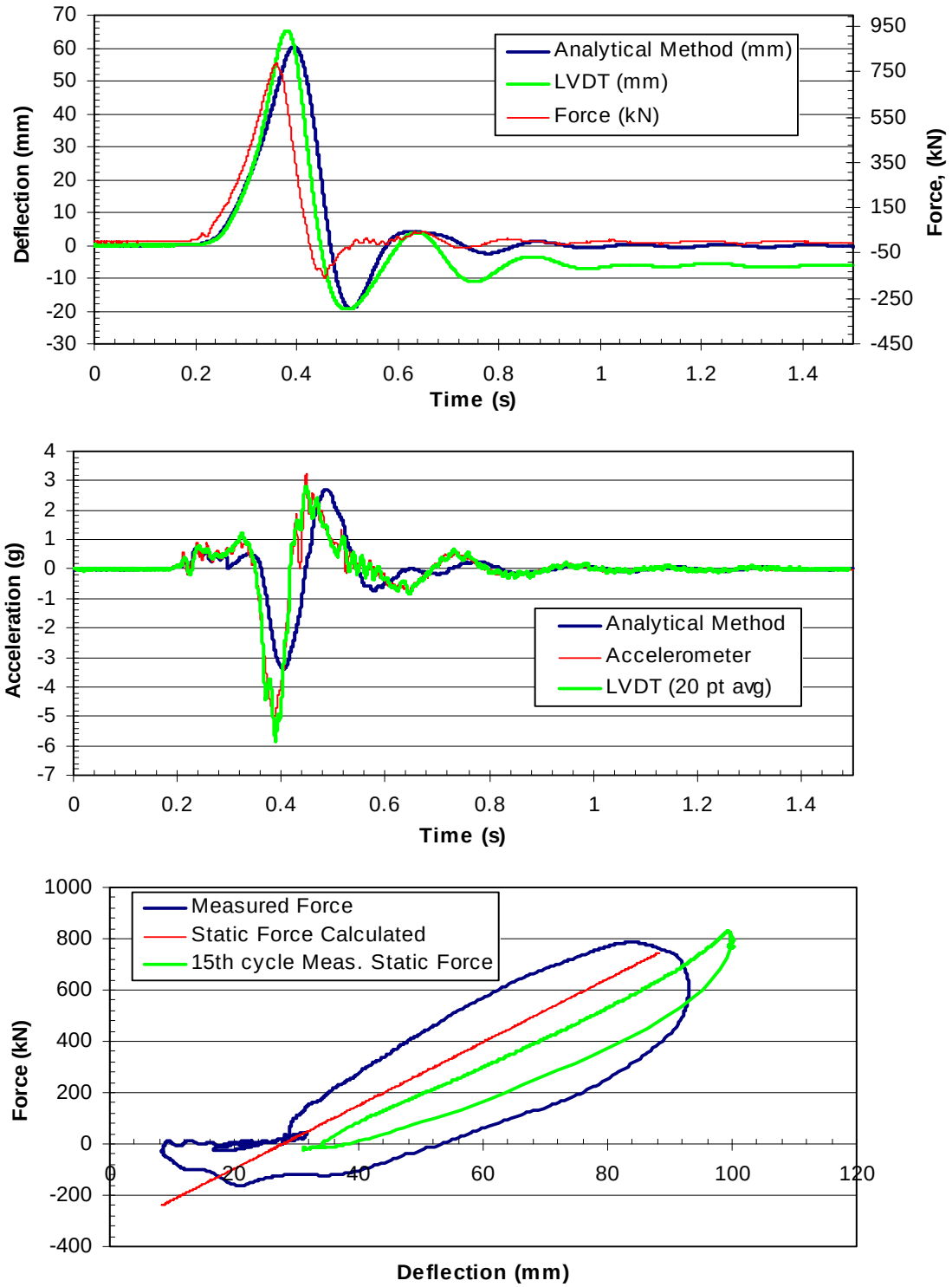

Figure 7.17: Comparison of (a) measured and computed deflection time histories (b) measured and computed acceleration time histories and (c) measured and computed static force-deflection curves –test 5 on the 9-pile group

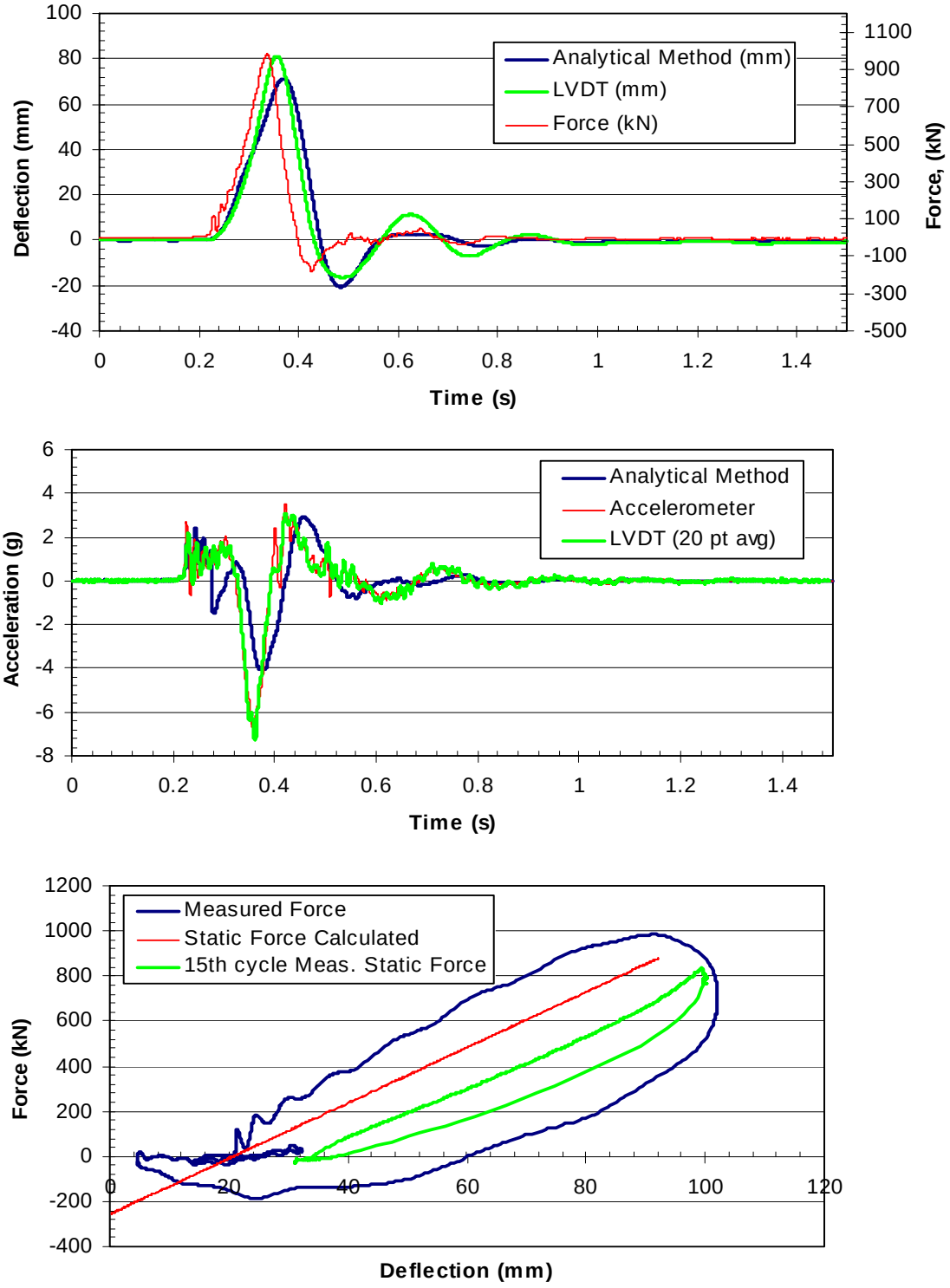

Figure 7.18: Comparison of (a) measured and computed deflection time histories (b) measured and computed acceleration time histories and (c) measured and computed static force-deflection curves –test 6 on the 9-pile group.

Table 7.13: Error Between Computed and Measured Peak Deflections for the Statnamic Tests on the 9-Pile Group

	Max Deflection (mm)			Min Deflection (mm)		
Test #	calc.	meas.	Error (mm)	calc.	meas.	Error (mm)
1	18.3	19.9	1.6	-7.3	-6.4	0.9
2	19.5	19.8	0.3	-7.0	-7.4	-0.4
3	48.5	47.4	-1.1	-18.4	-17.4	1.0
4	78.1	75.1	-3.0	-25.4	-22.1	3.3
5	69.7	65.2	-4.5	-21.1	-19.5	1.6
6	90.7	81.2	-9.5	-23.6	-16.4	7.2

Table 7.14: Error Between Computed and Measured Peak Accelerations for the Statnamic Tests on the 9-Pile Group

	Max Acceleration (g's)			Min Acceleration (g's)		
Test #	calc.	meas.	Error (g's)	calc.	meas.	Error (-g's)
1	1.52	1.49	-0.03	-0.92	-1.26	-0.34
2	1.22	2.24	1.02	-0.77	-1.11	-0.34
3	2.74	2.63	-0.11	-3.15	-3.93	-0.78
4	4.01	4.02	0.01	-5.97	-6.55	-0.58
5	2.78	3.22	0.44	-5.54	-5.04	0.50
6	3.40	3.54	0.14	-4.88	-6.68	-1.80

The error between the computed and measured maximum and minimum deflection and accelerations for each statnamic test on the 9-pile group are summarized in Tables 7.13 and 7.14. Deflection errors increased as the deflections increased. Optimization of maximum deflections was found to be on average 3.0 mm greater than the measured maximum deflections. The calculated maximum and minimum deflections were typically greater than the measured deflections. Similar to the 15-pile group, accelerations had a greater error than deflections. The acceleration is possibly not as accurate because (1) optimization of the model more heavily weights deflections differences and (2) acceleration is affected more greatly from changing variables within the model rather than averages of mass, damping and stiffness.

The calculated and measured damping ratios for the statnamic tests on the 9-pile group are plotted as a function of the maximum deflection in Figure 7.19. As the deflections increased, the damping ratios also increased. Best-fit lines have also been defined for the measured and calculated damping ratios and are also shown in Figure 7.19. This relationship appears to be linearly increasing. The rate of change from the measured and calculated damping ratios is very consistent. Optimization of maximum deflections were found to be on average 3.0 mm greater than the measured maximum deflections. The results from Figure 7.19 suggest that the optimization was accurate in finding the damping for the 9-pile group statnamic tests.

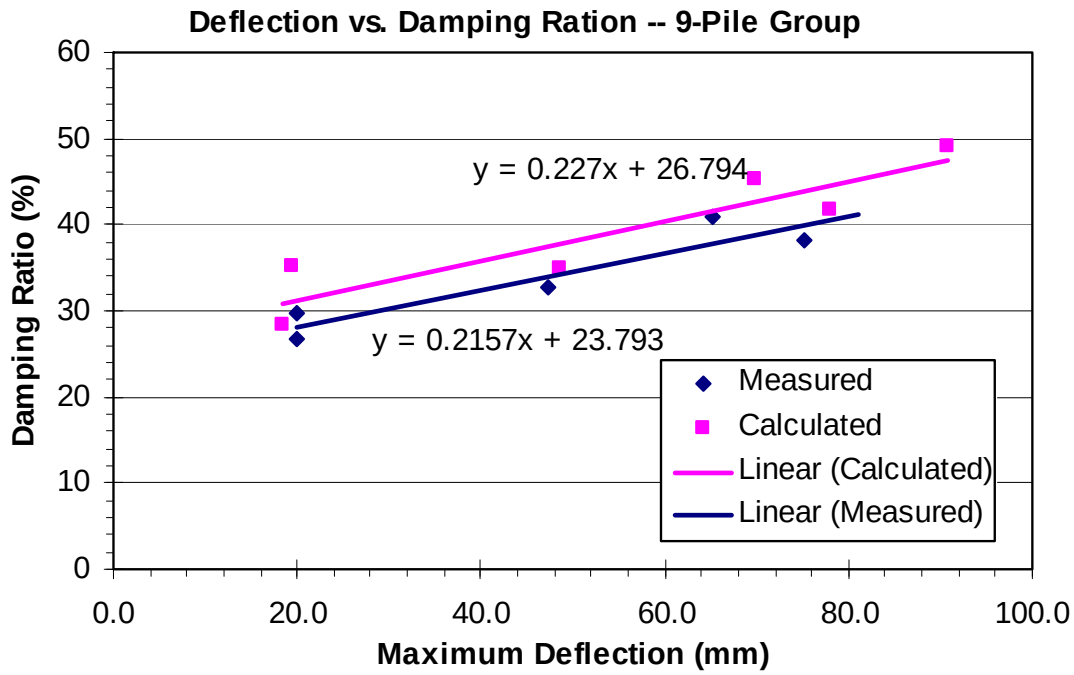

Figure 7.19: Measured and calculated damping ratios as a function of maximum displacement of 9-pile group

CHAPTER 8 CONCLUSIONS

8.1 Concluding Results

1. Analyses conducted in this study indicated that the response (acceleration, velocity and deflection) of both the 9- and 15-pile groups during statnamic loading of the pile and load frame system could be reasonably modeled using a simple one-degree-of-freedom model.

2. The numerical model (Force Equilibrium Method) of the single-degree-of-freedom system was successfully used to optimally determine the effective mass, stiffness, and damping ratio for each pile group. The optimization was accomplished using built-in routines with the excel spreadsheet program. Using this approach, the majority of the computed peak deflections were within about 7 percent of the measured peak deflection and the computed peak acceleration was typically within 9 percent of the measured peak acceleration.

3. The effective mass was found be 21,000kg for the 15-pile group and 14,000 kg for the 9-pile group for most of the statnamic load tests. These mass values correspond to the mass of the piles in motion plus the mass of the soil to a depth

of less than 1m. This depth was optimized to the mass of the soil with significant movement with the pile group.

4. The back-calculated (optimized) stiffness values for 15-pile group during statnamic loading were typically within 1.5 percent of the stiffness measured for the static load test performed immediately prior to the statnamic tests. Optimization for the 9-pile group found best results by not optimizing the stiffness values of the system. Instead, the stiffness values of the static load tests performed immediately prior to the statnamic tests were used to minimize the number of optimized values. Based on the accuracy of the 15-pile group, this assumption for the 9-pile group optimization is accurate.

5. For both the 9- and 15-pile groups, the stiffness decreased as the deflection level increased. However, the stiffness per pile was higher for the 9-pile group than that for the 15-pile group. This is likely due to the fact that rows in the 15-pile group were spaced at 1.27 m on centers whereas the rows in 9-pile group were spaced at 1.83 m on centers. As a result, greater group interaction occurred for the 15-pile group than for the 9-pile group leading to a lower stiffness.

6. The damping ratio difference between the log decrement (measured) verses the optimization approach for statnamic tests differed on average 4.5 and 9.4 percent for the 15-pile and 9-pile groups respectively.

7. The damping ratios for both pile groups increased approximately linearly as the applied force and deflection level increased. Damping ratio values were approximately 24% for a deflection of 12 mm and increased to about 50% at a deflection of about 80 mm. The back-calculated damping ratios for both groups were very similar although the ratio for the 15-pile group was slightly higher.

8.2 Recommendations for Future Tests

This research focused on the basic system of foundation piles in motion. The test results should prove valuable for future research and studies on dynamic loads on pile foundations. The following are some recommendations for future testing:

- As discovered in the analysis results, several nonlinear variables exist. It was found that stiffness of the system reacted in a linear manner; however, mass and damping values changed while the piles were in motion. To help understand these properties, it would be preferable to reduce as much as possible variables in the system.

- A statnamic lateral load on only one foundation pile at the same site would be advantages to help explain group reactions. This would allow a more solid analytical proof to the resulting damping affects directly related from the soil.

- The tests performed in this study had several cyclic loads which caused reduction of the stiffness and damping of the soil with time. I would recommend having studies with only statnamic loading. The statnamic load time interval would have

significantly less affect on the soil than static loads, thus virgin soil load conditions may be observed.

- Additional studies may be performed with the data acquired for the field results. Moment and accelerometer data down the depth of the piles can prove to be valuable information for understanding stresses, motion and soil properties and different depth of the piles.

8.3 Concluding Remarks

With these results and future studies similar to this, stiffness and damping properties will become more readily available to understanding motion of piles in soil. Structures will more likely not exceed their strength and at the same time use less material. Predicting the reaction of structures before natural and other impact events not only saves value to the structure, it also protects life from potentially unsafe conditions. Thus, the cost of predicting the future motion of structures becomes invaluable.

REFERENCES

Bermingham, P. and White, J. (1995). "Pyrotechnics and the Accurate Prediction of Statnamic Peak Loading and Fuel Charge Size." *First International STATNAMIC Seminar,* September 27-30, 1995, Vancouver, British Columbia, Canada: pp. 1-12.

Bielefeld, M. and Middendorp, P. "Statnamic Simulation." *First International STATNAMIC Seminar*, September 27-30, 1995, Vancouver, British Columbia, Canada: pp. 207-222.

Brown, D.A. 1998. "STATNAMIC Lateral Load Response of Two Deep Foundations." *STATNAMIC Loading Test*. Kusakabe, O., et. al. 2000. pp. 418-422.

Brown, D. A. (1999). "An Experiment with Statnamic Lateral Loading of a Drilled Shaft." *Journal of Geotechnical Engineering*, ASCE, No.88, pp. 309-318.

Burr, J.P., Pender, et al. (1997). "Dynamic Response of Laterally Excited Pile Groups." *Journal of Geotechnical Engineering*, ASCE, 1997.

Chopra, A.K. (2001). Dynamics of Structures: Theory and Applications to Earthquake Engineering, Second Edition. Prentice Hall, New Jersey.

Cox, et al. (1984). "Lateral Load Tests on 25.4mm (1in.) Diameter Piles in Very Soft Clay in Side-by-Side and In-Line Groups." *Laterally Loaded Deep Foundations: Analysis and Performance*, ASCE STP 835, pp. 112-139.

Egbert, J.J. (2001). "Static and Dynamic Testing of a Laterally Loaded Group of 15 Steel Pipe Piles," MS Thesis. Civil and Environmental Engineering Dept., Brigham Young University. Provo, UT.

El Naggar, M.H. (1998). "Interpretation of Lateral Statnamic Load Test Results." *Journal of Geotechnical Engineering*, ASCE, Vol. 21, No. 3, 1998, pp. 169-179.

El Naggar, M.H. (2002). "Dynamic Analysis of Laterally Loaded Pile Groups in Sand and Clay." *First International STATNAMIC Seminar.*

Gerber, T. (2002). Created Spreadsheet Program: Base Line. Used for removing "noise" from test data for piles in motion. Brigham Young University, Civil Engineering Department.

Gazetas, G. (1984). "Seismic Response of End-Bearing Single Piles," International Journal of Soil Dynamics and Earthquake Engineering. pp. 82-93.

Gazetas, G. & Dobry, R, (1983). "Horizontal Response of Piles in Layered Soils." *Journal of Geotechnical Engineering*, ASCE. Vol. 110, No. 1, 1984, pp. 20-40.

Johnson, S.R. (2003a). Photos and Site Map. (http://www.et.byu.edu/groups/Airport/Photos/airport_photos.htm). Civil and Environmental Engineering Dept., Brigham Young University. Site Map Image courtesy of USGS (http://terraserver-usa.com/).

Johnson, S.R. (2003b). "Static Lateral Load Testing a Full-Scale Pile Group Spaced at 5.65 Pile Diameters." MS Thesis. Civil and Environmental Engineering Dept. Brigham Young University, Provo, UT.

Middendorp, P., Bermingham, P., and Kuiper B. "Statnamic Load Testing of Foundation Piles." 4th International Conference on Stress Waves, September 21-24, 1992, pp. 581-588.

Olsen, R. (2001). "Full-scale Static and Dynamic Lateral Load Behavior of a Three-Row Pile Group," MS Thesis. Civil and Environmental Engineering Dept., Brigham Young University. Provo, UT.

Peterson, (1996). "Static and Dynamic Lateral Load Testing a Full-Scale Pile Group in Clay." MS Thesis. Civil and Environmental Engineering Dept. Brigham Young University. Provo, UT.

Poulos, H.G. (2000). "Pile Testing—From the Designer's Viewpoint." Edited by Kusakabe, O., Kuwabara, F. & Matsumoto, T. (2000). "STATNAMIC Loading Test." pp 3-21.

Rollins, K , Peterson, K., and Weaver, T. (1998). "Lateral Load Behavior of Full-Scale Pile Group in Clay." *Journal of Geotechnical Engineering*, ASCE, Vol. 124, no.6, pp 468-478.

Rollins, K and Sparks, A. (2002). "Lateral Statnamic Load Testing & Analysis of a Pile Group." *Journal of Geotechnical Engineering*, ASCE, Vol. 128, no.9, pp 711-723.

Snyder, Jeff (2004). "Full-Scale Lateral Load Tests of a 3x5 Pile Group in Soft Clays and Silts." MS Thesis. Civil and Environmental Engineering Dept. Brigham Young University, Provo, UT.

Tedesco et. al. (1999). Structural Dynamics—Theory and Applications. Addison Wesley Longman, Inc. California. p 86

Terzaghi, K. and Peck, R. (1948). Soils Mechanics in Engineering Practice. Wiley, New York.

Tsubakihara, Y., et al. (1995). "An Analytical Study on Statnamic Lateral Pile Testing." *1st International STATNAMIC Seminar.* pp 235-242.

Wells, D. and Coppersmith, K. "New Empirical Relationships among Magnitude, Rupture Length, Rupture Width, Rupture Area, and Surface Displacement." *Bulletin of Seismological Society of America*, 1994, pp. 974-1002.

APPENDIX

Calculation for Mean Magnitude Earthquake at Salt Lake City Segment of the Wasatch Fault (Wells D. & Copersmith, 1999):

$$M = a + b*\log(RLD) \qquad (A.1)$$

where:

M = Magnitude

a = Coefficient (Tbl—All) = 4.38

b = Coefficient (Tbl—All) = 1.49

RLD = Subsurface rupture lenth (km)

Solving for M:

M = 4.38 + 1.49 Log (65)

M = 7.1 (with standard deviation of 0.26) ← Answer

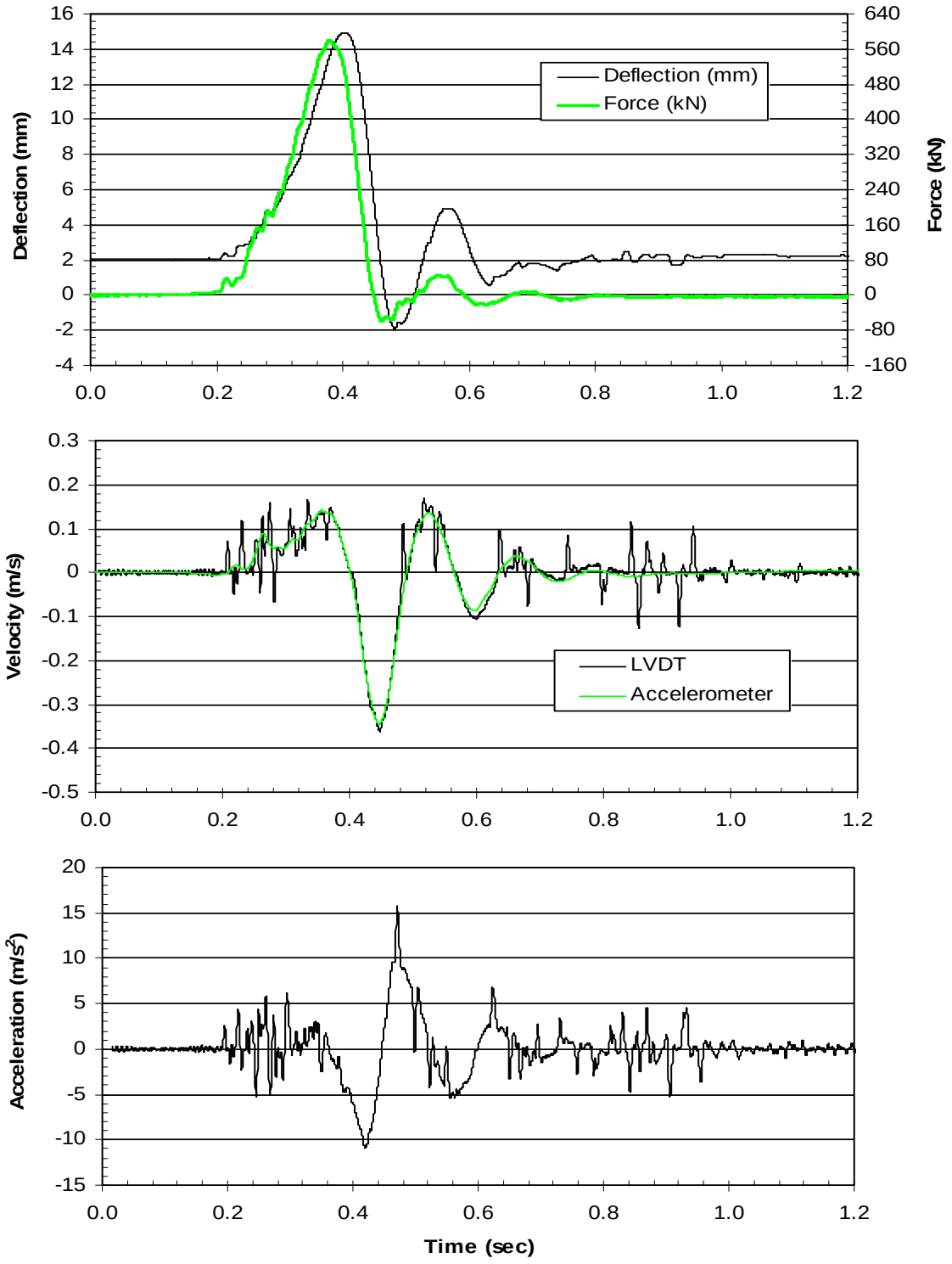

Figure A.1: 15-pile group, test 1, 13 mm (0.5 in) target—LVDT time histories at pile head.

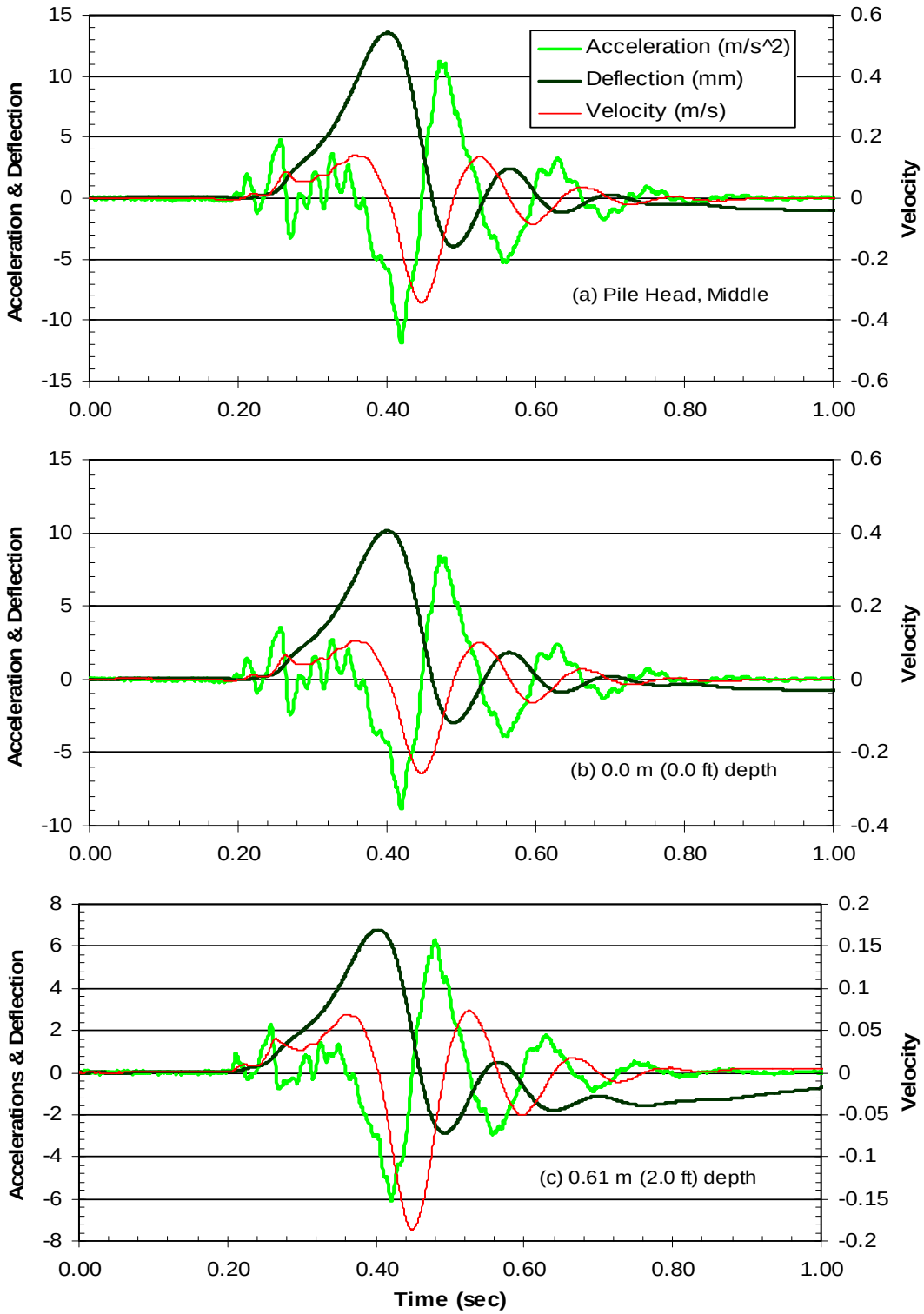

Figure A.2: 15-pile group, test 1—accelerometer time histories at (a) pile head, middle pile, (b) 0.0 m, and (c) 0.61 m (2.0 ft) depths.

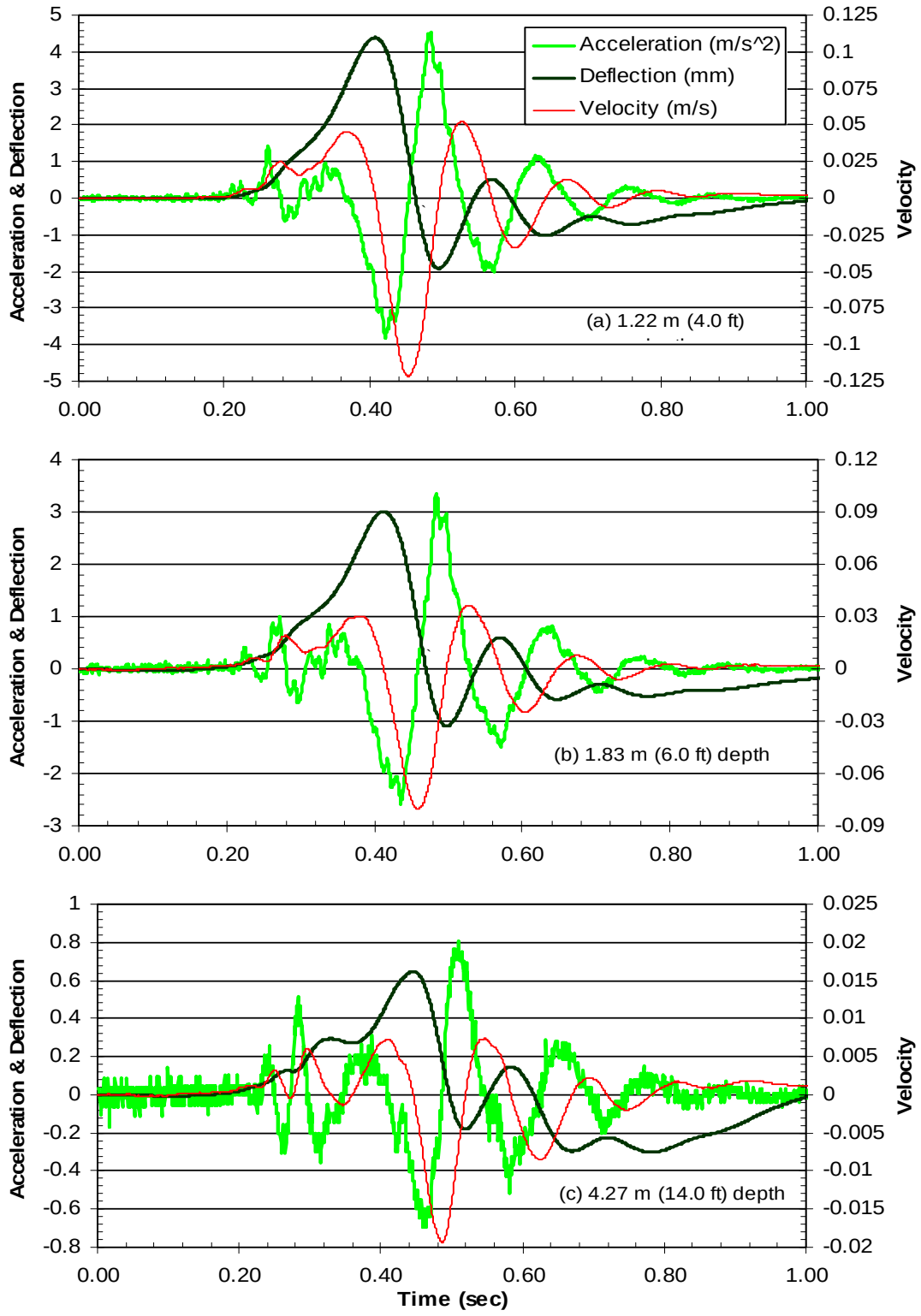

Figure A.3: 15-pile group, test 1—accelerometer time histories at (a) 1.22 m (4.0 ft), (b) 1.83 m (6.0 ft), and (c) 4.27 m (14.0 ft) depths.

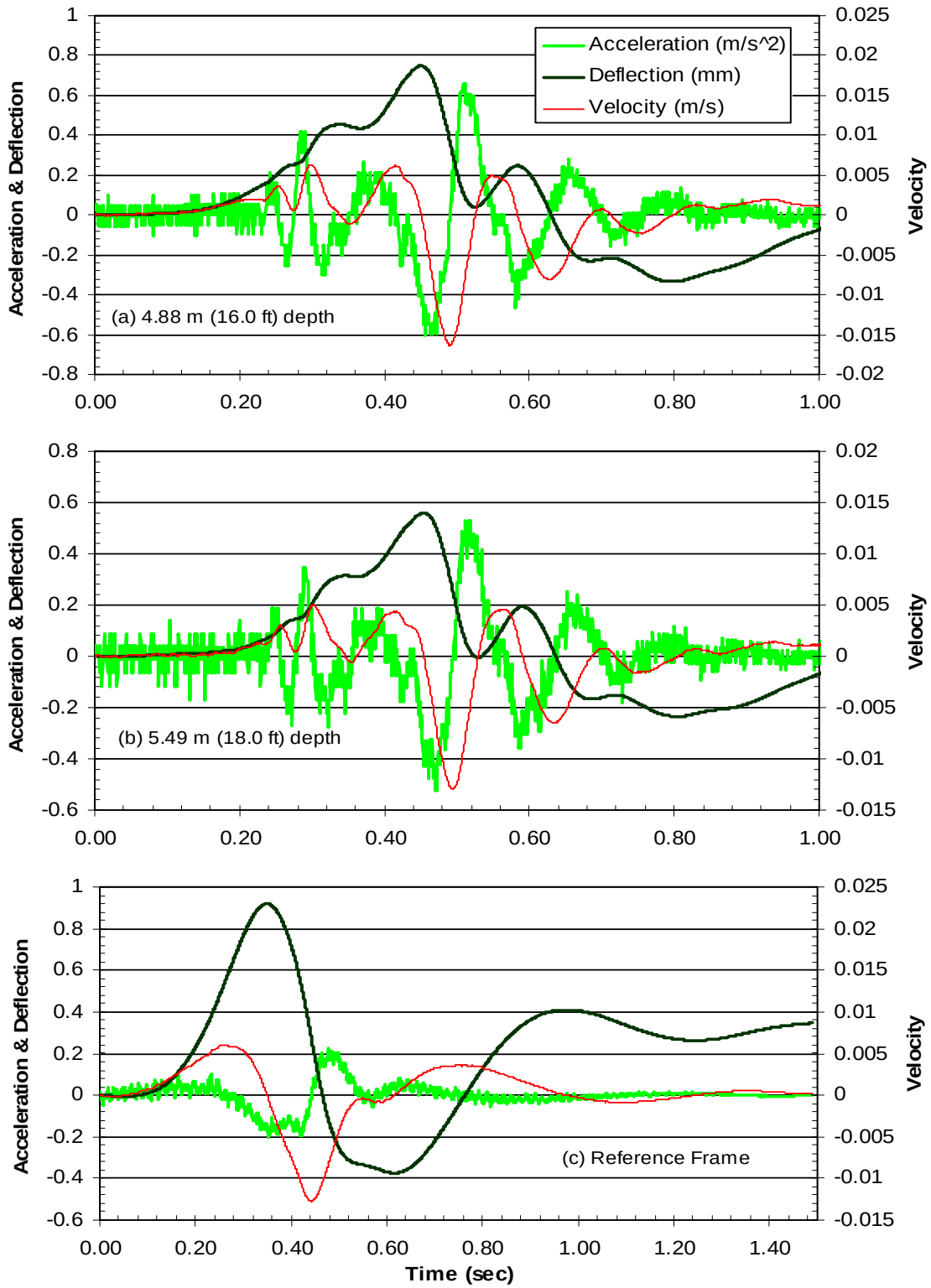

Figure A.4: 9-pile group, test 1—accelerometer time histories at (a) 4.88 m (16.0 ft) and (b) 5.49 m (18.0 ft) depths and (c) reference frame.

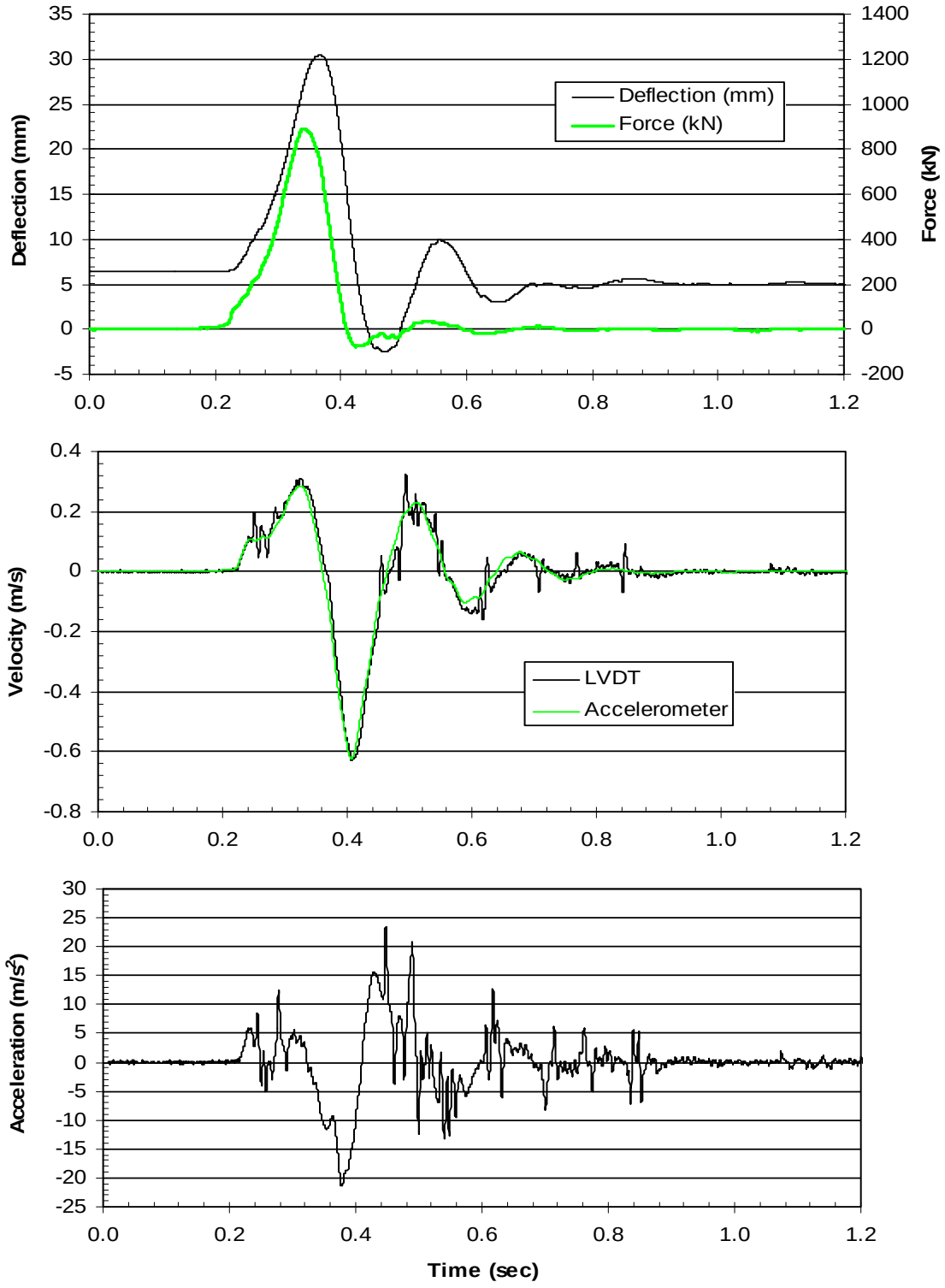

Figure A.5: 15-pile group, test 2, 25 mm (1.0 in) target—LVDT time histories at pile head.

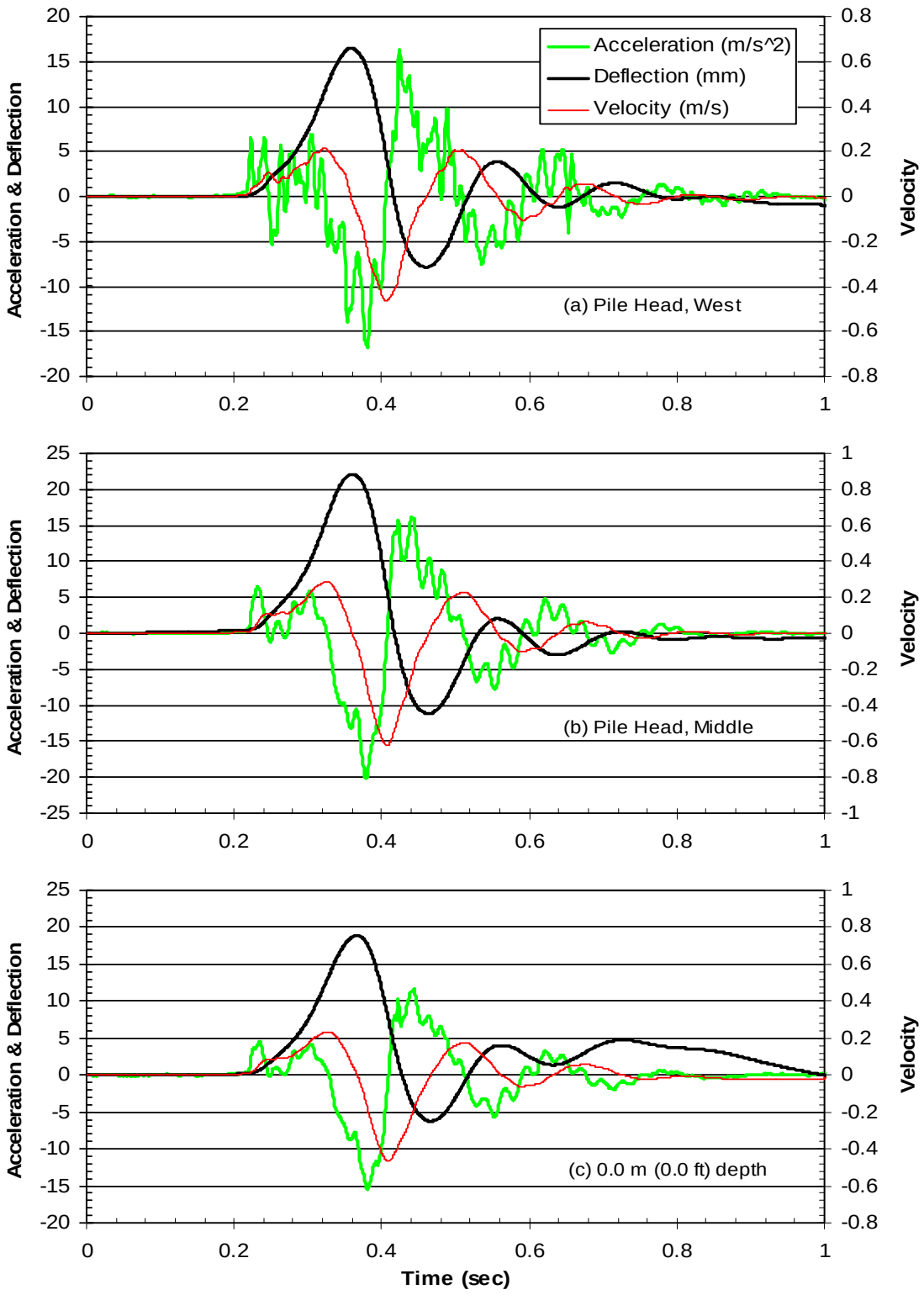

Figure A.6: 15-pile group, test 2—accelerometer time histories at (a) pile head, west pile, (b) pile head, middle pile, and (c) 0.0 m (0.0 ft) depths.

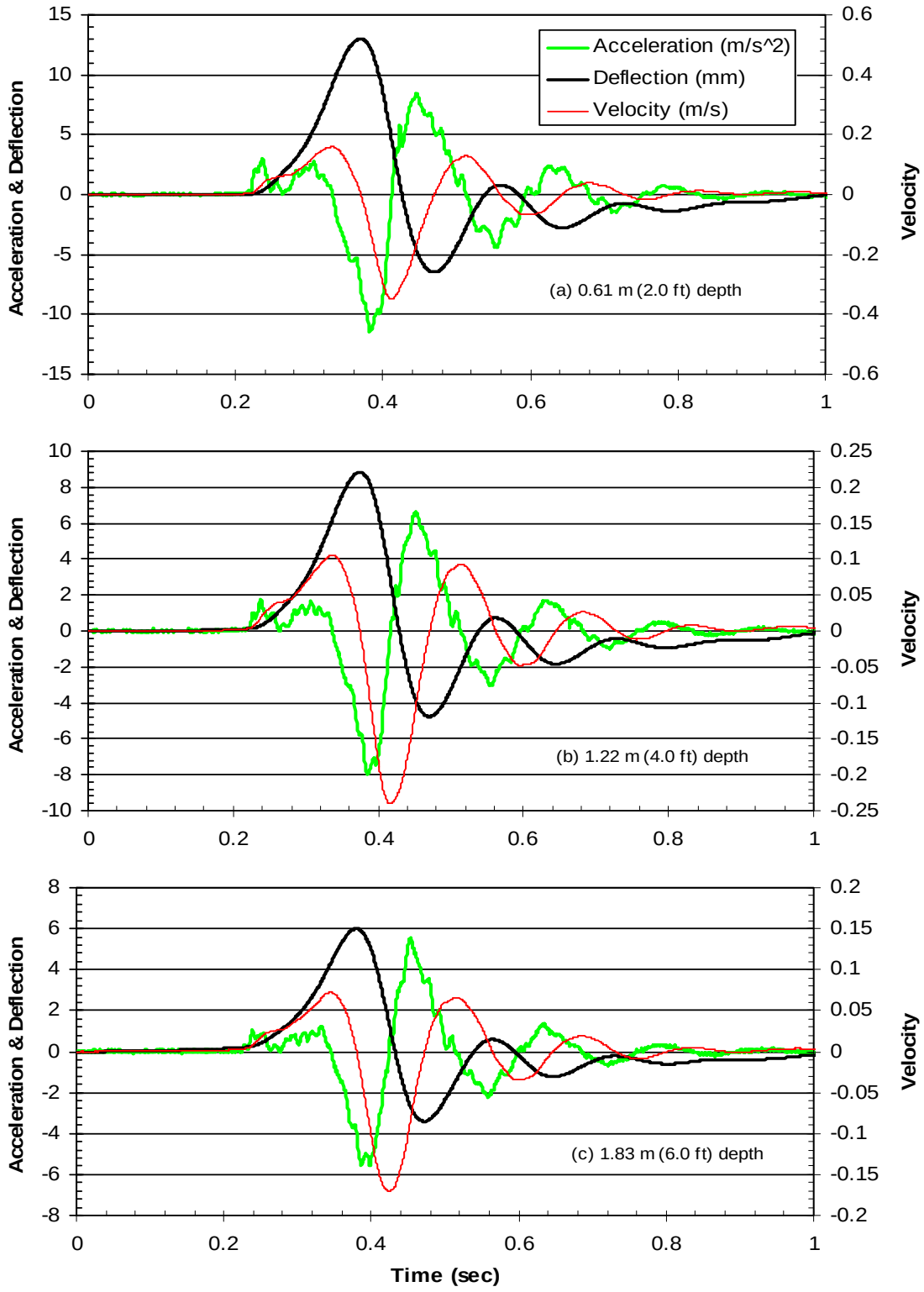

Figure A.7: 15-pile group, test 2—accelerometer time histories at (a) 0.61 m (2.0 ft), (b) 1.22 m (4.0 ft), and (c) 1.83 m (6.0 ft) depths.

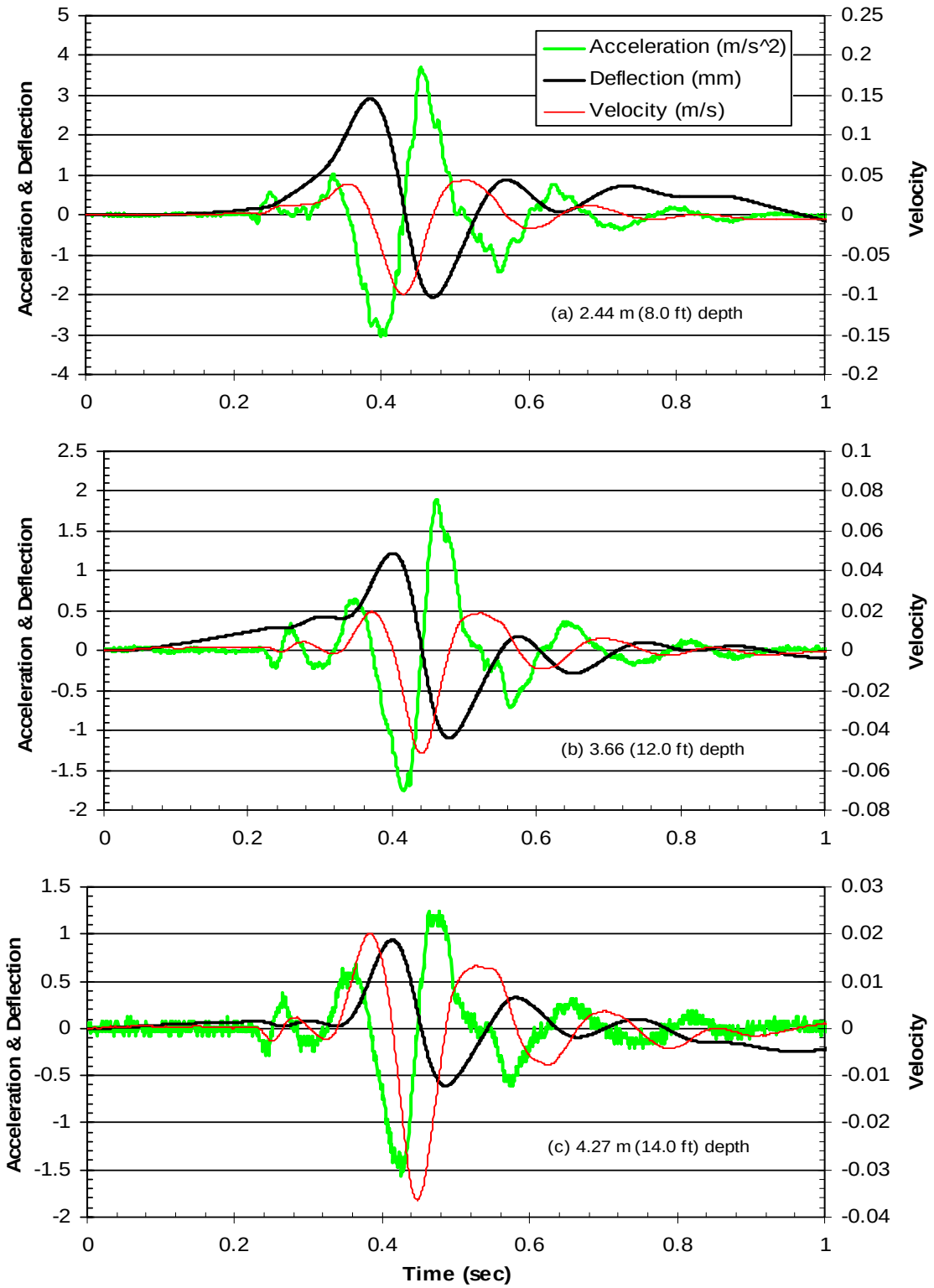

Figure A.8: 15-pile group, test 2—accelerometer time histories at (a) 2.44 m (8.0 ft), (b) 3.66 m (12.0 ft), and (c) 4.27 m (14.0 ft) depths.

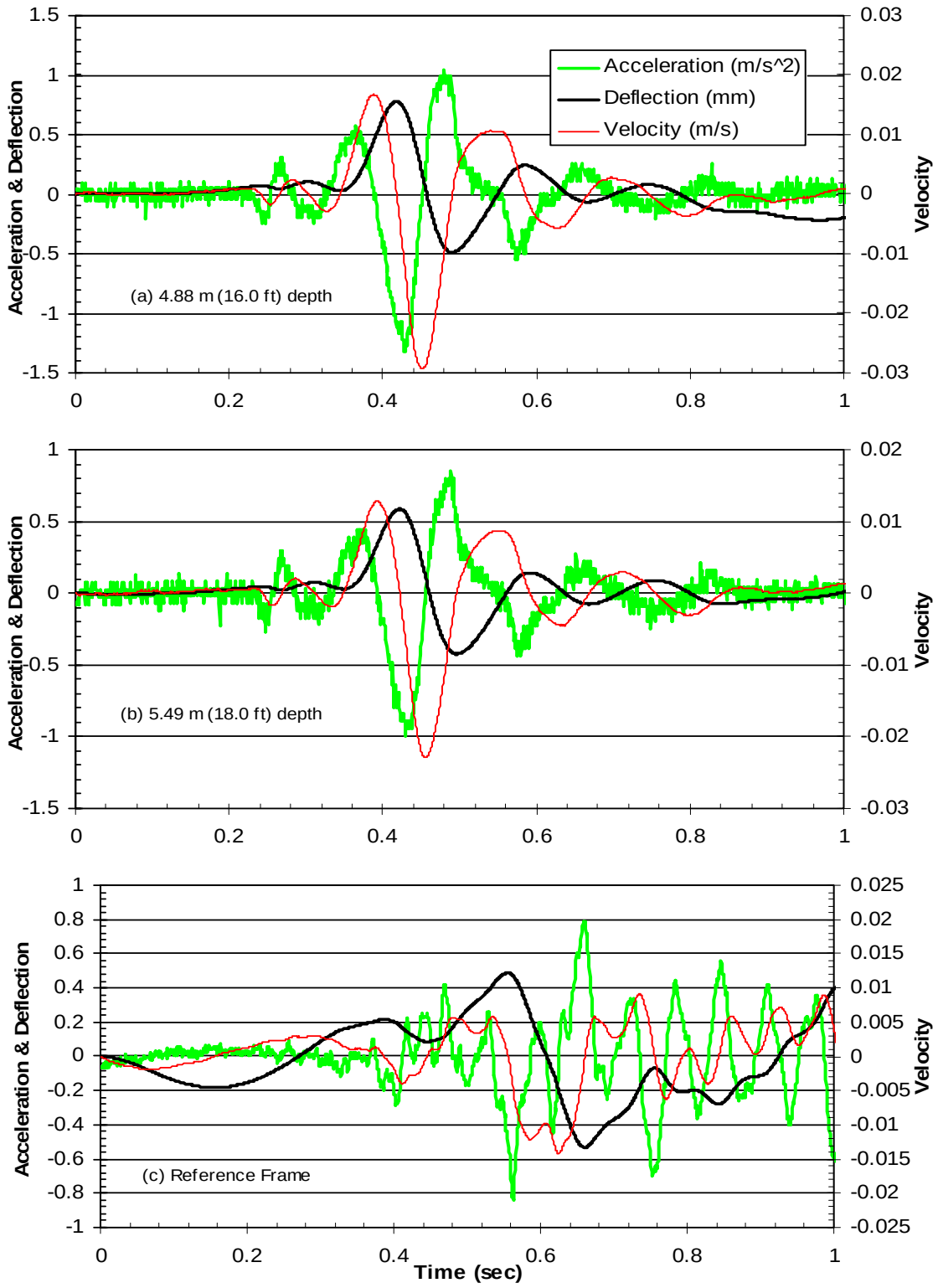

Figure A.9: 15-pile group, test 2—accelerometer time histories at (a) 4.88 m (16.0 ft) and (b) 5.49 m (18.0 ft) depths and (c) reference frame.

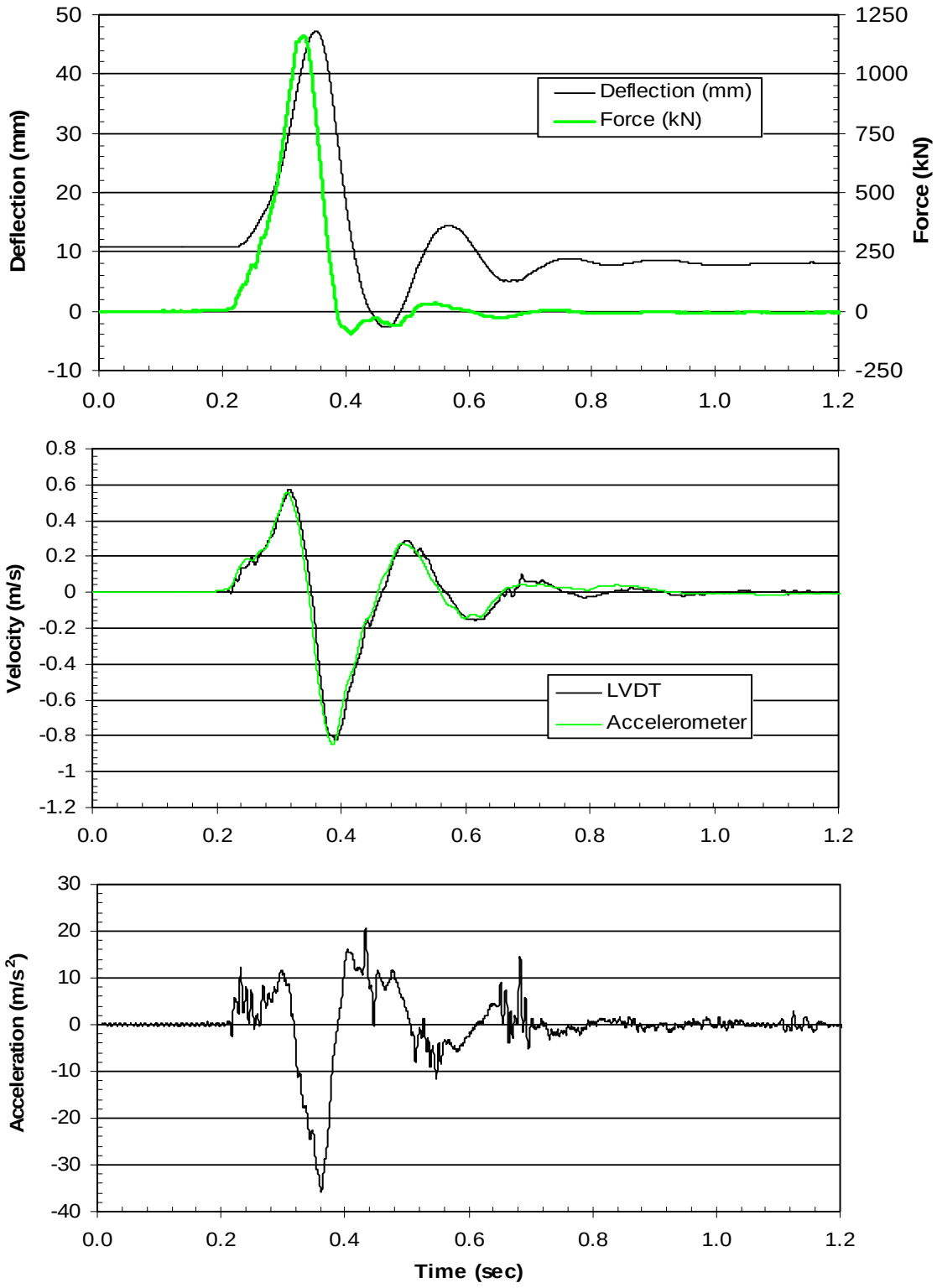

Figure A.10: 15-pile group, test 3, 38 mm (1.5 in) target—LVDT time histories at pile head.

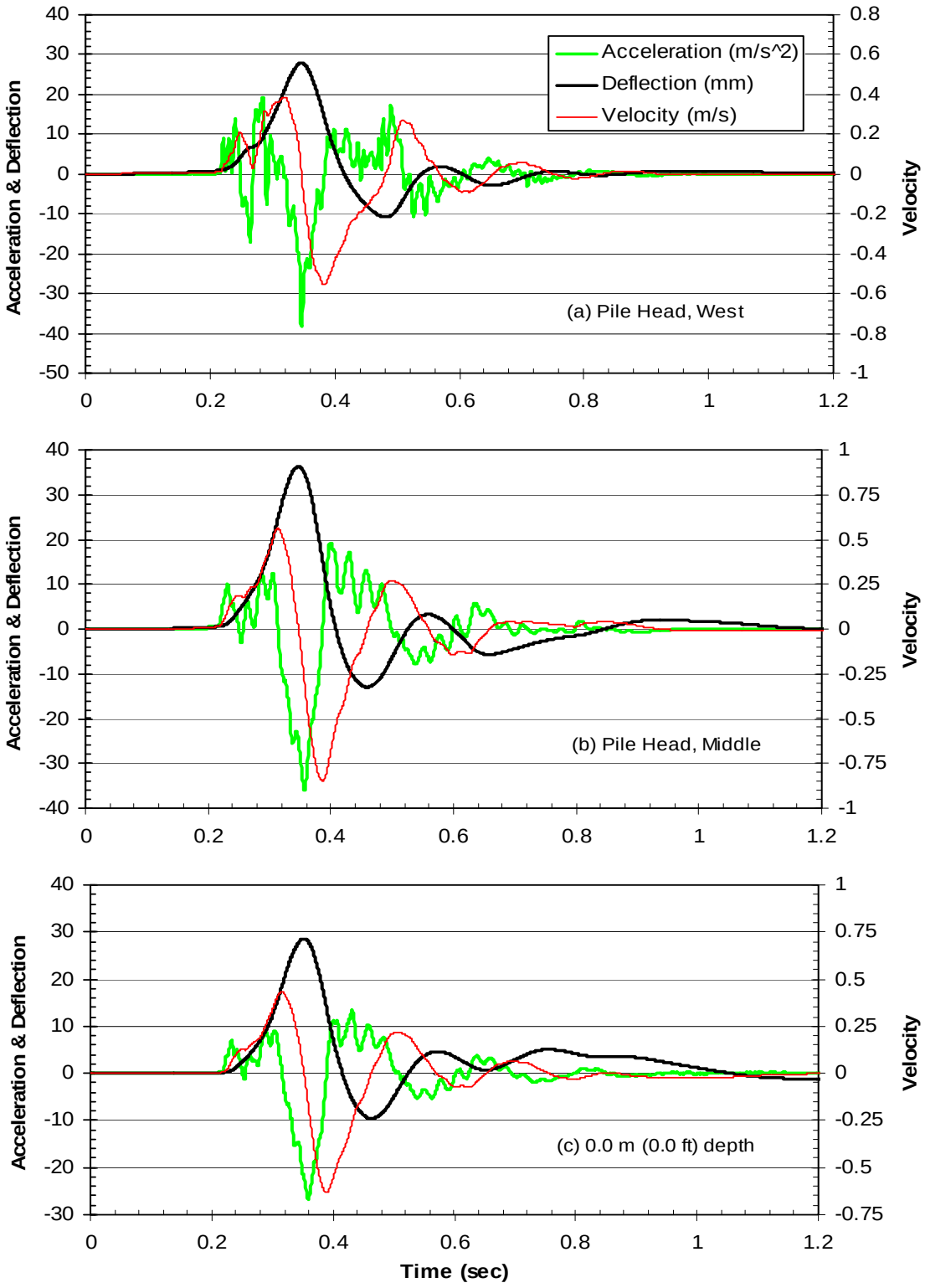

Figure A.11: 15-pile group, test 3—accelerometer time histories at (a) pile head, west pile and (b) pile head, middle pile and (c) 0.0 m (0.0 ft) depth.

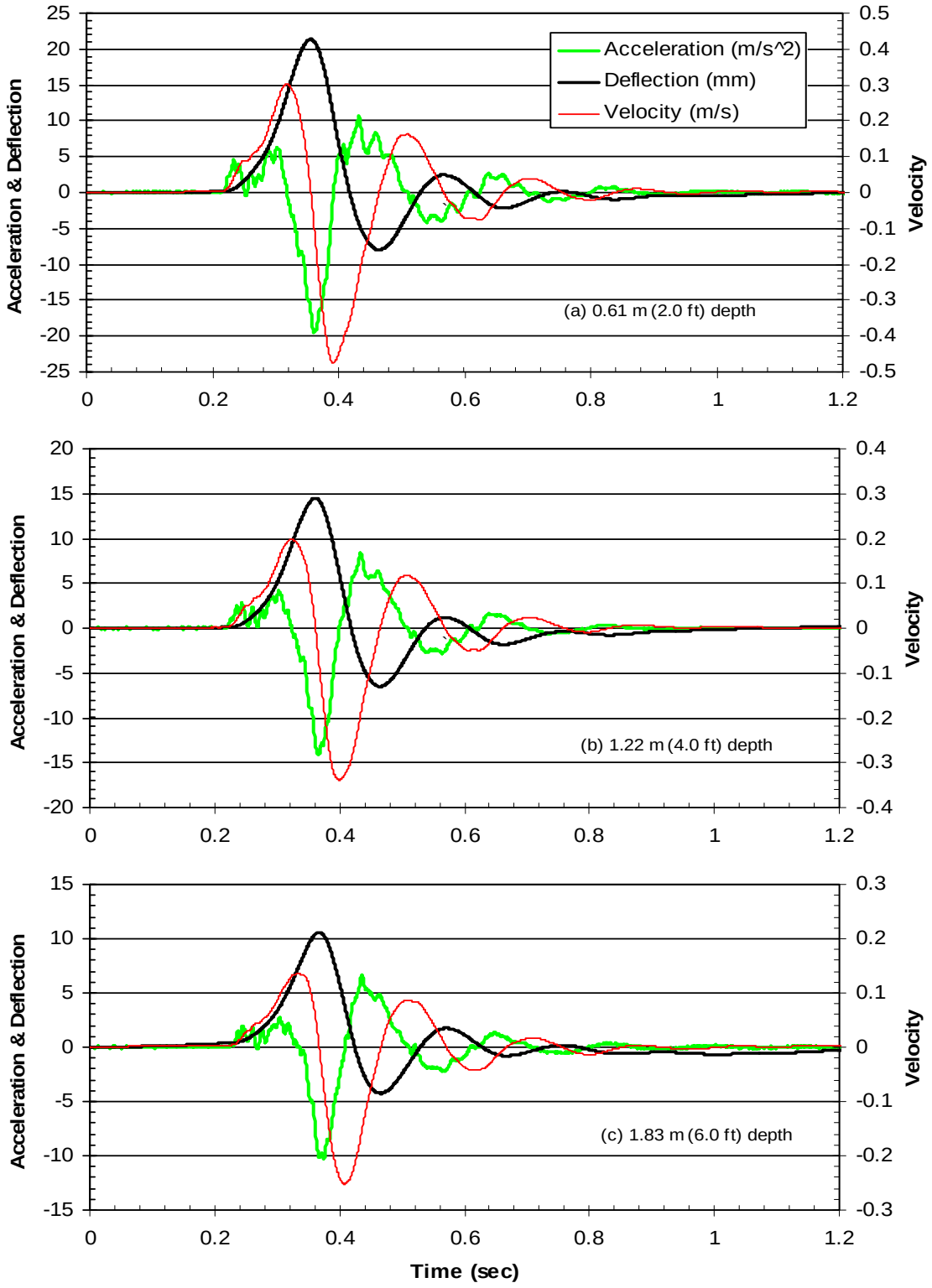

Figure A.12: 15-pile group, Test 3--accelerometer time histories at (a) 0.61 m (2.0 ft), (b) 1.22 m (4.0 ft), and (c) 1.83 m (6.0 ft) depths.

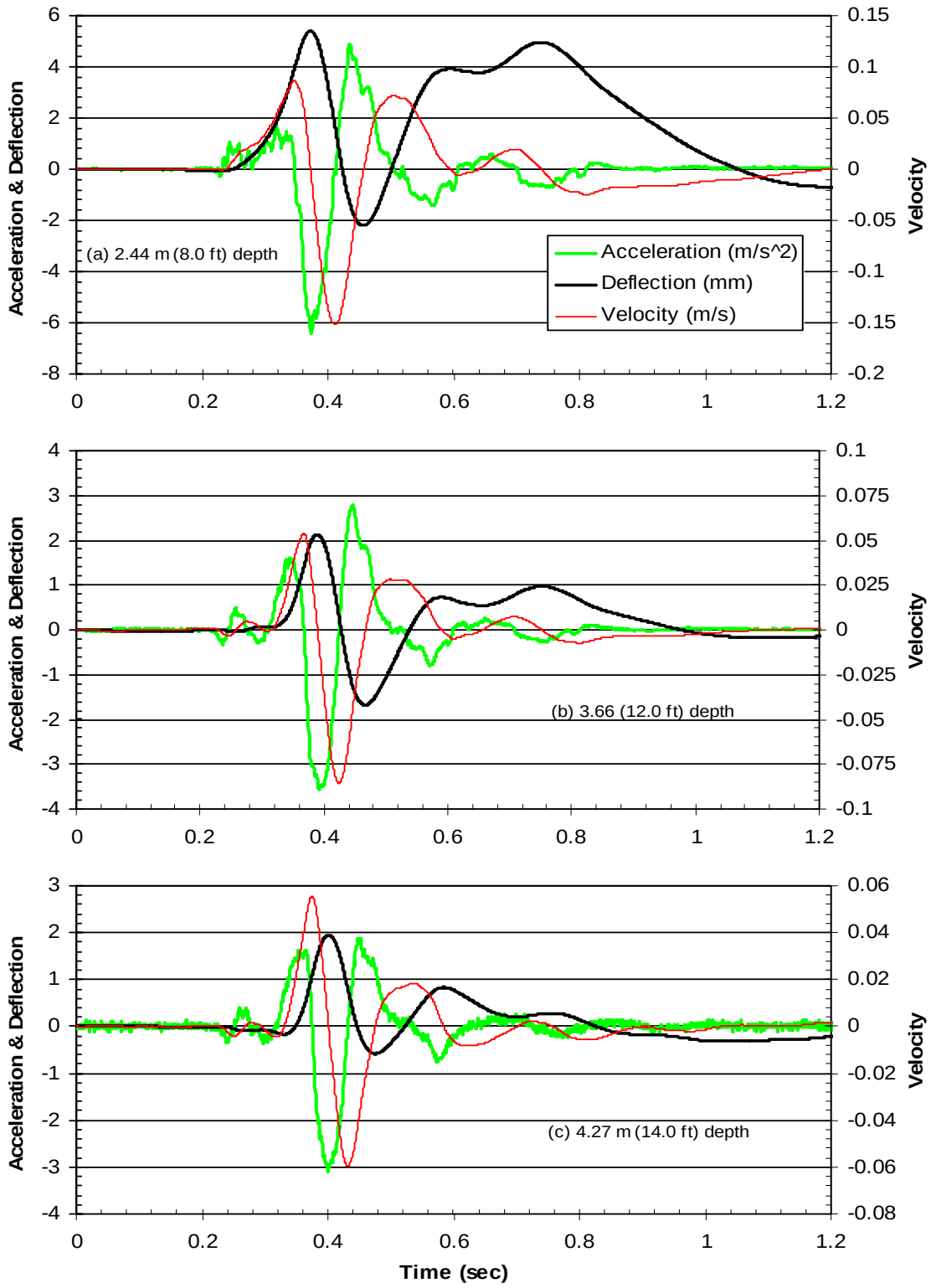

Figure A.13: 15-pile group, test 3—accelerometer time histories at (a) 2.44 m (8.0 ft), (b) 3.66 m (12.0 ft), and (c) 4.27 m (14.0 ft) depths.

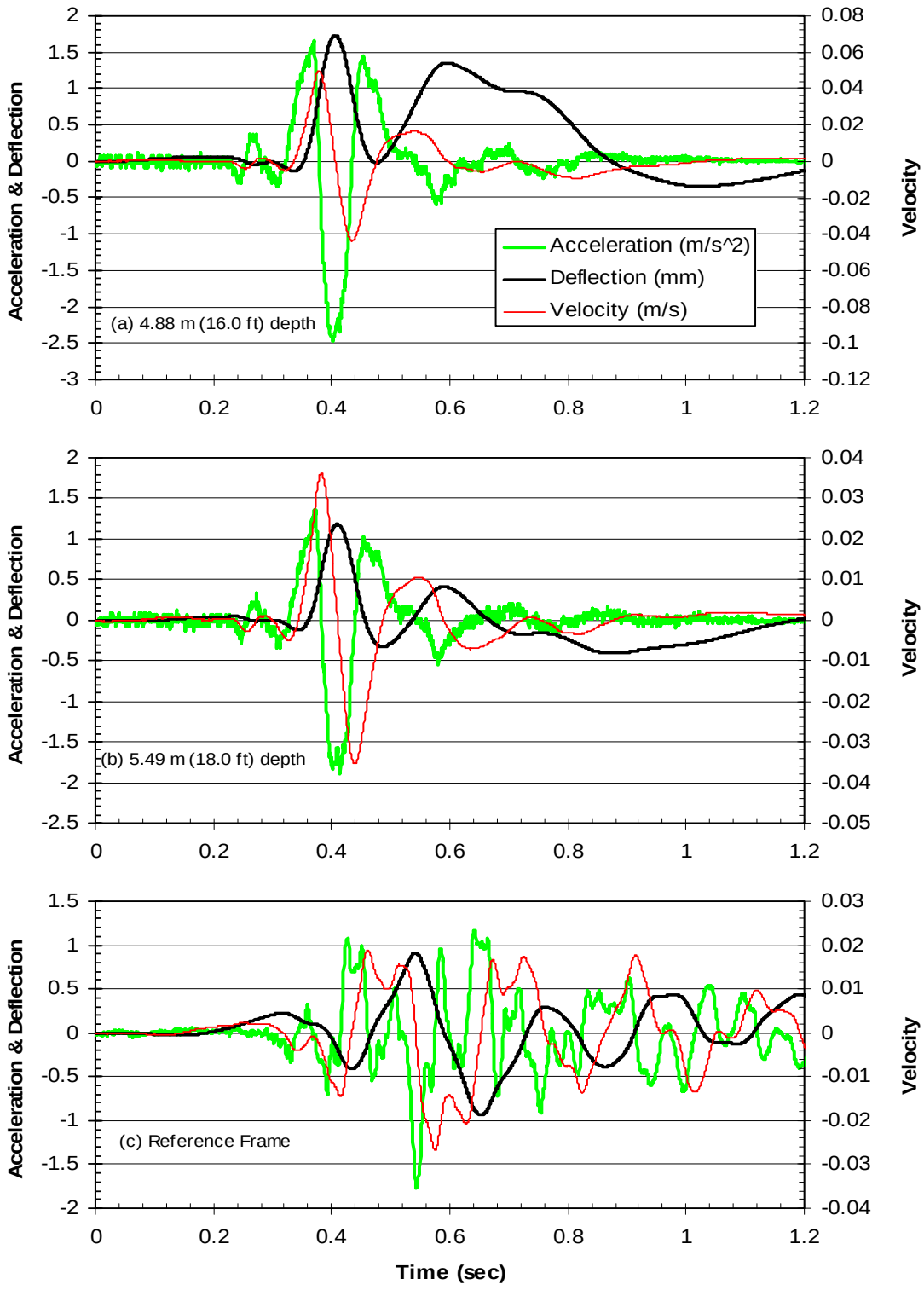

Figure A.14: 15-pile group, test 3—accelerometer time histories at (a) 4.88 m (16.0 ft) and (b) 5.49 m (18.0 ft) depths and (c) reference frame.

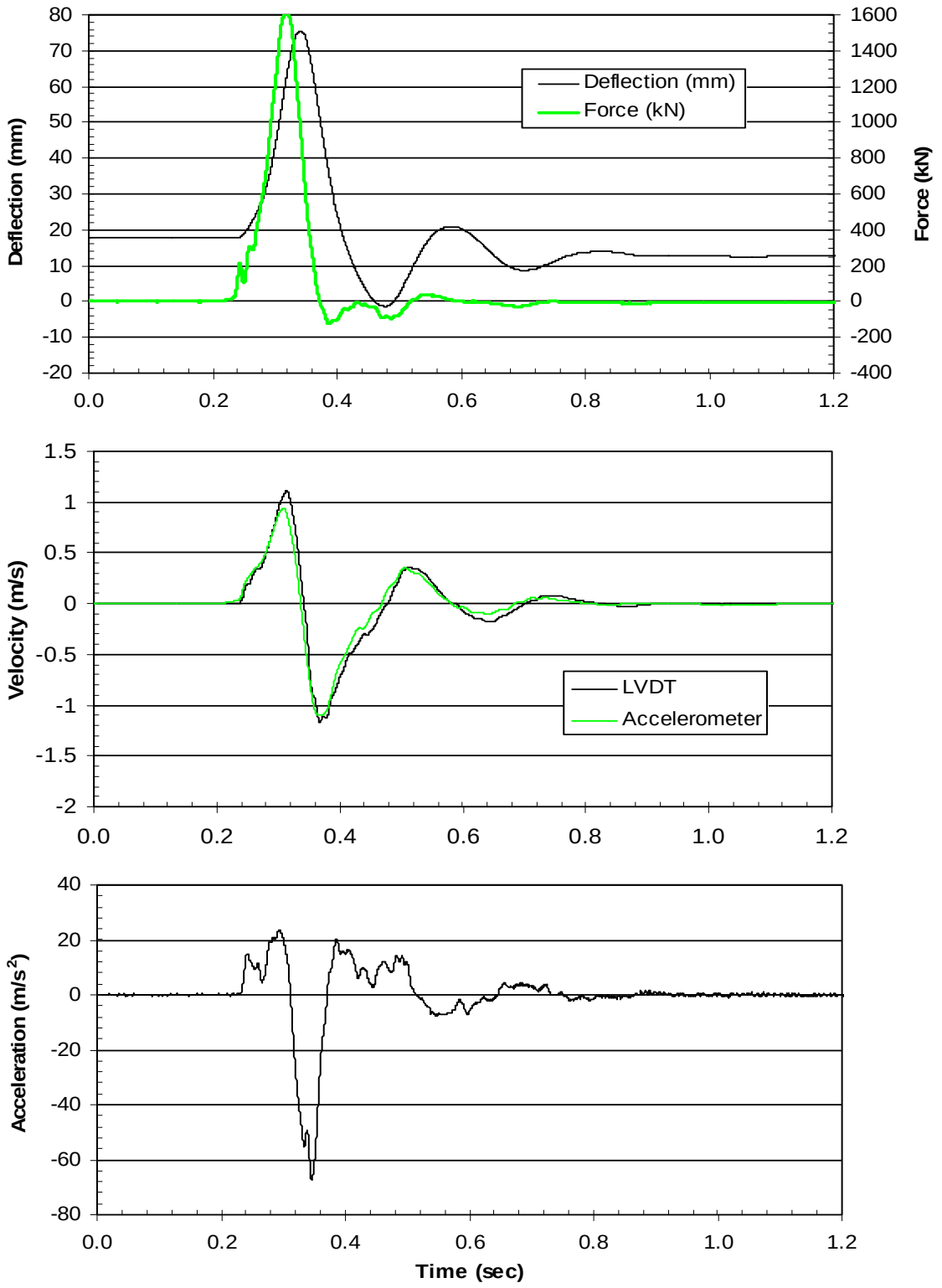

Figure A.15: 15-pile group, test 4, 64 mm (2.5 in) target—LVDT time histories at pile head.

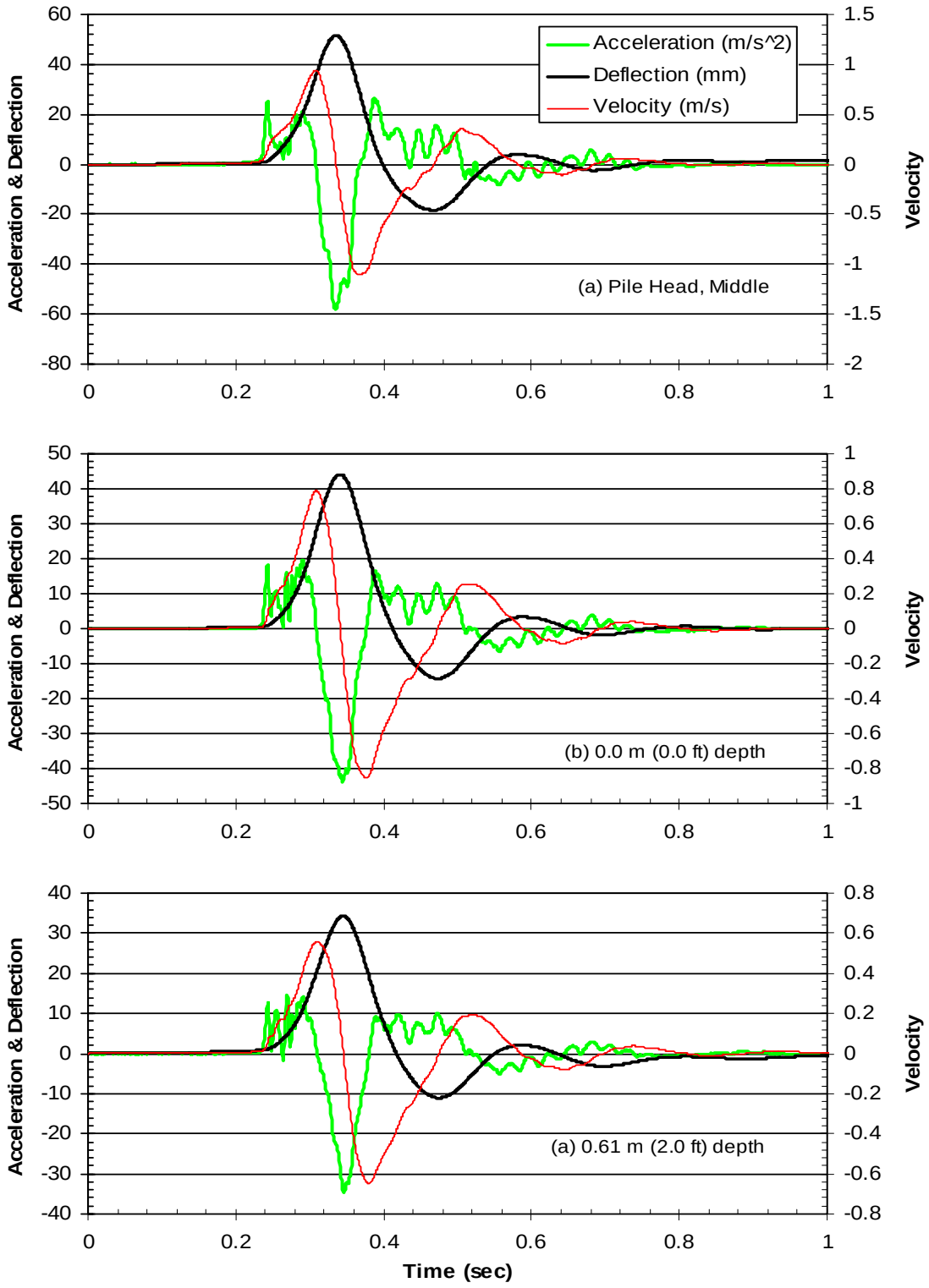

Figure A.16: 15-pile group, test 4—accelerometer time histories at (a) pile head, middle pile, (b) 0.0 m (0.0 ft), and (c) 0.61 (2.0 ft) depths.

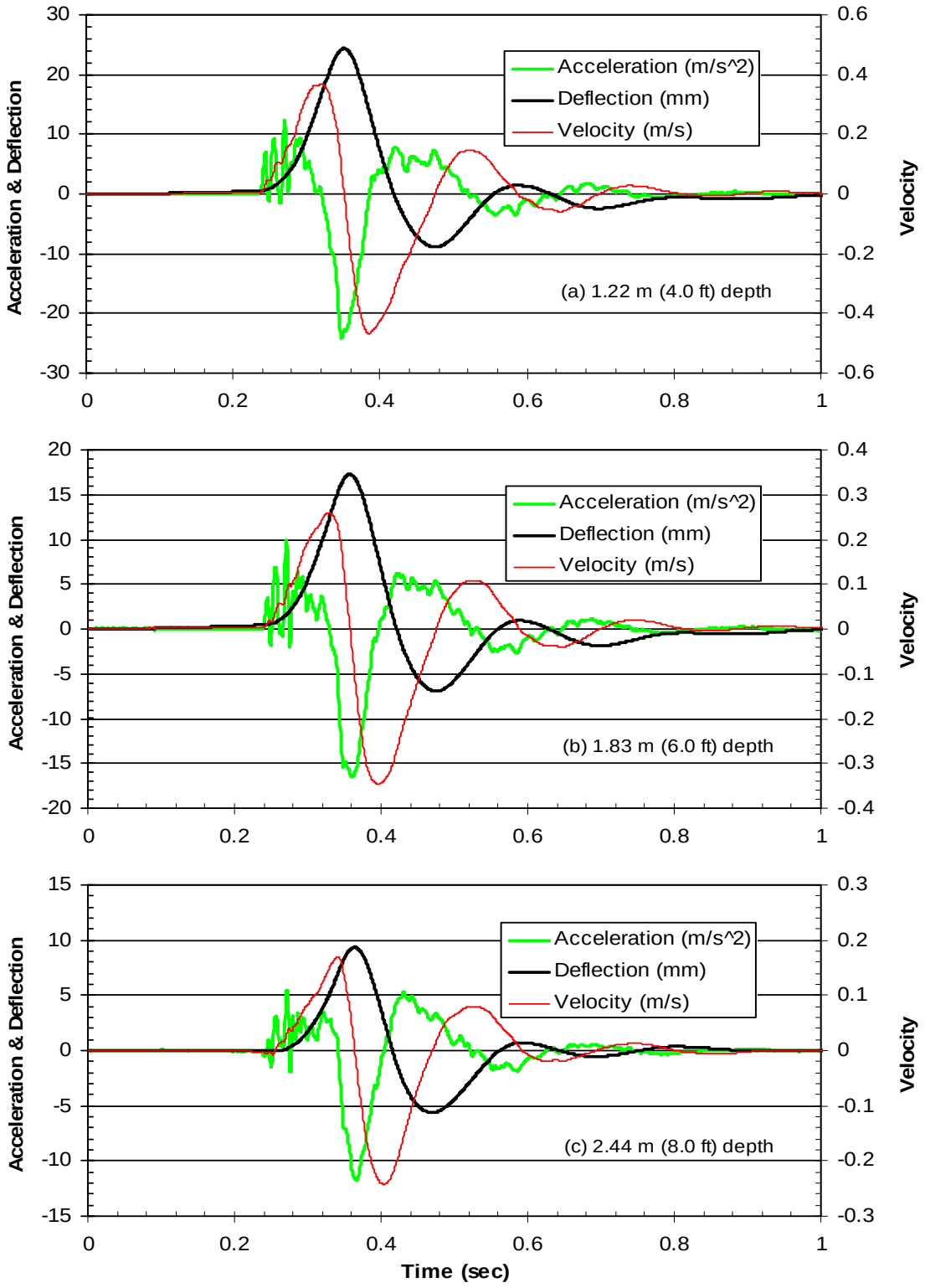

Figure A.17: 15-pile group, test 4—accelerometer time histories at (a) 1.22 m (4.0 ft), (b) 1.83 m (6.0 ft), and (c) 2.44 m (8.0 ft) depths.

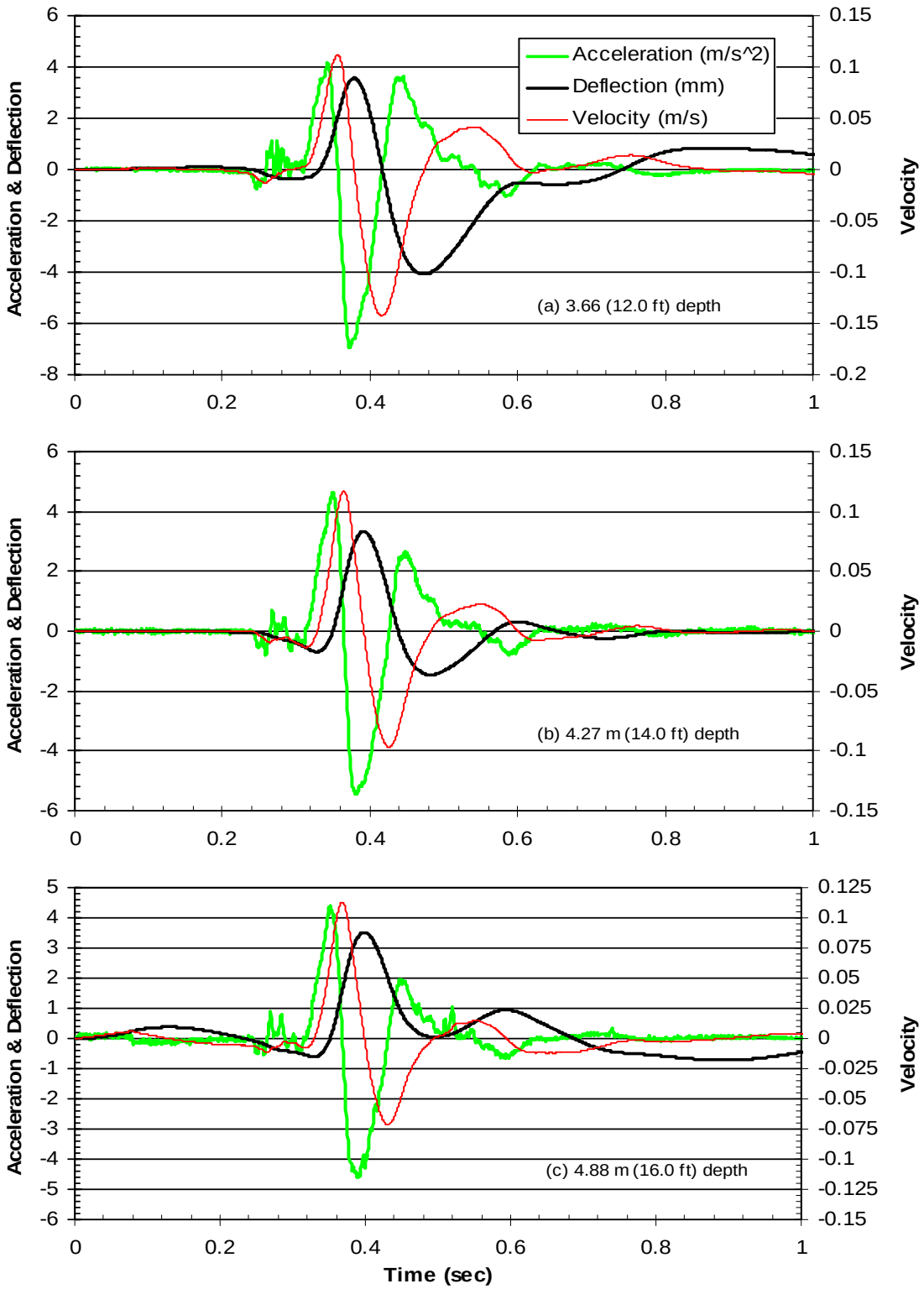

Figure A.18: 15-pile group, test 4—accelerometer time histories at (a) 3.66 m (12.0 ft), (b) 4.27 m (14.0 ft), and (c) 4.88 m (16.0 ft) depths.

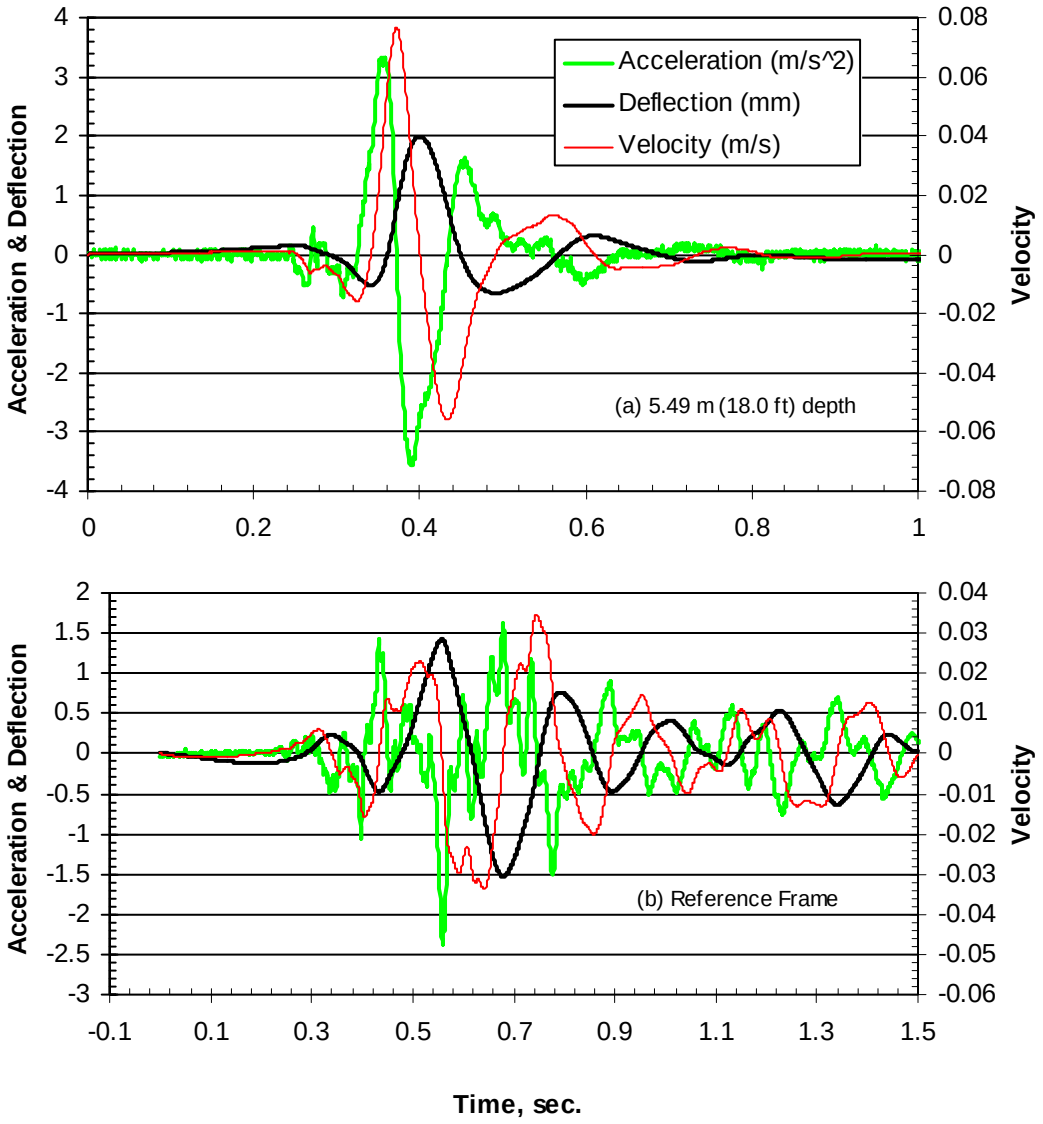

Figure A.19: 15-pile group, test 4—accelerometer time histories at (a) 5.49 m (18.0 ft) depths and (b) reference frame.

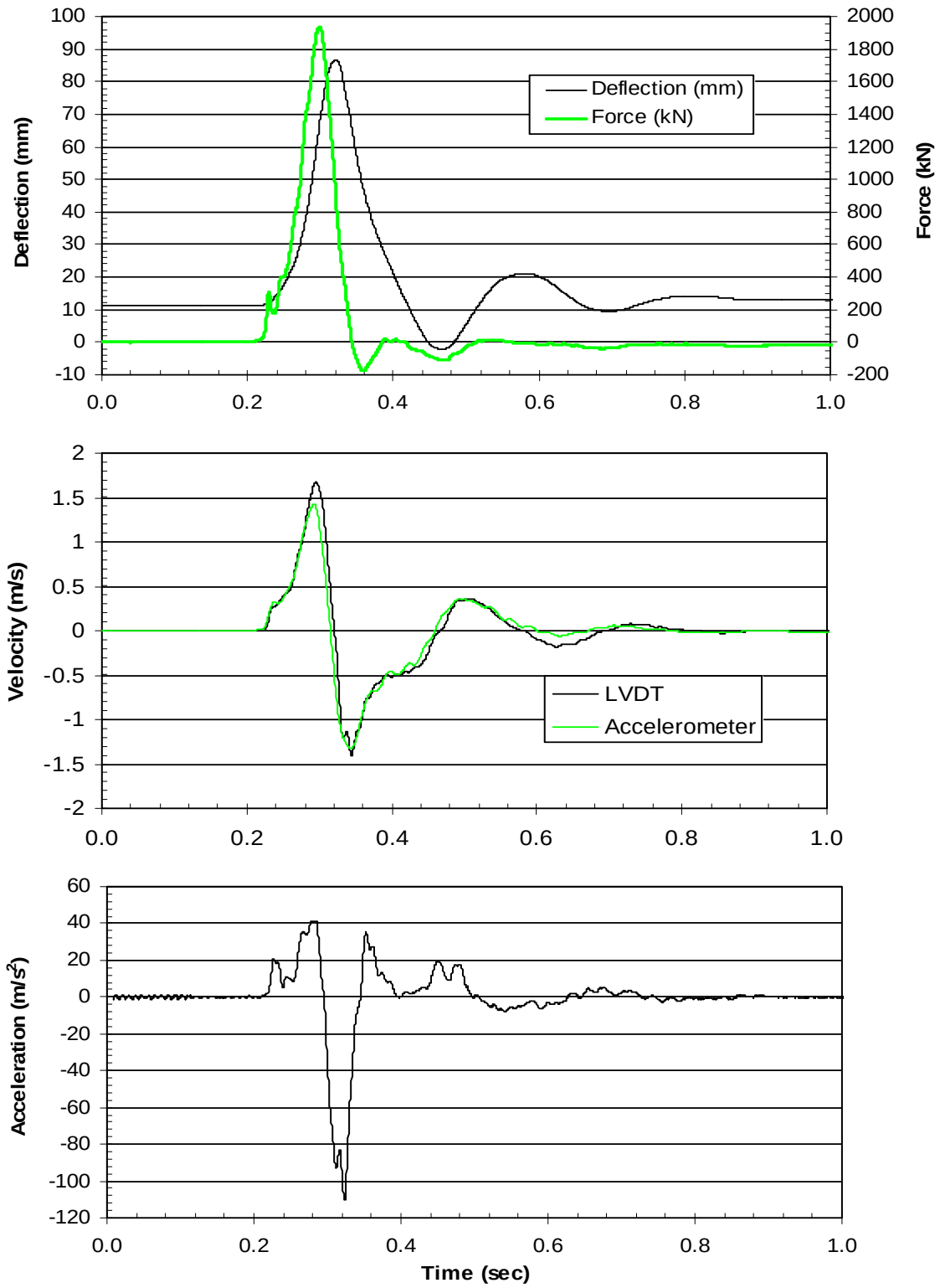

Figure A.20: 15-pile group, test 5, 89 mm (3.5 in) target—LVDT time histories at pile head.

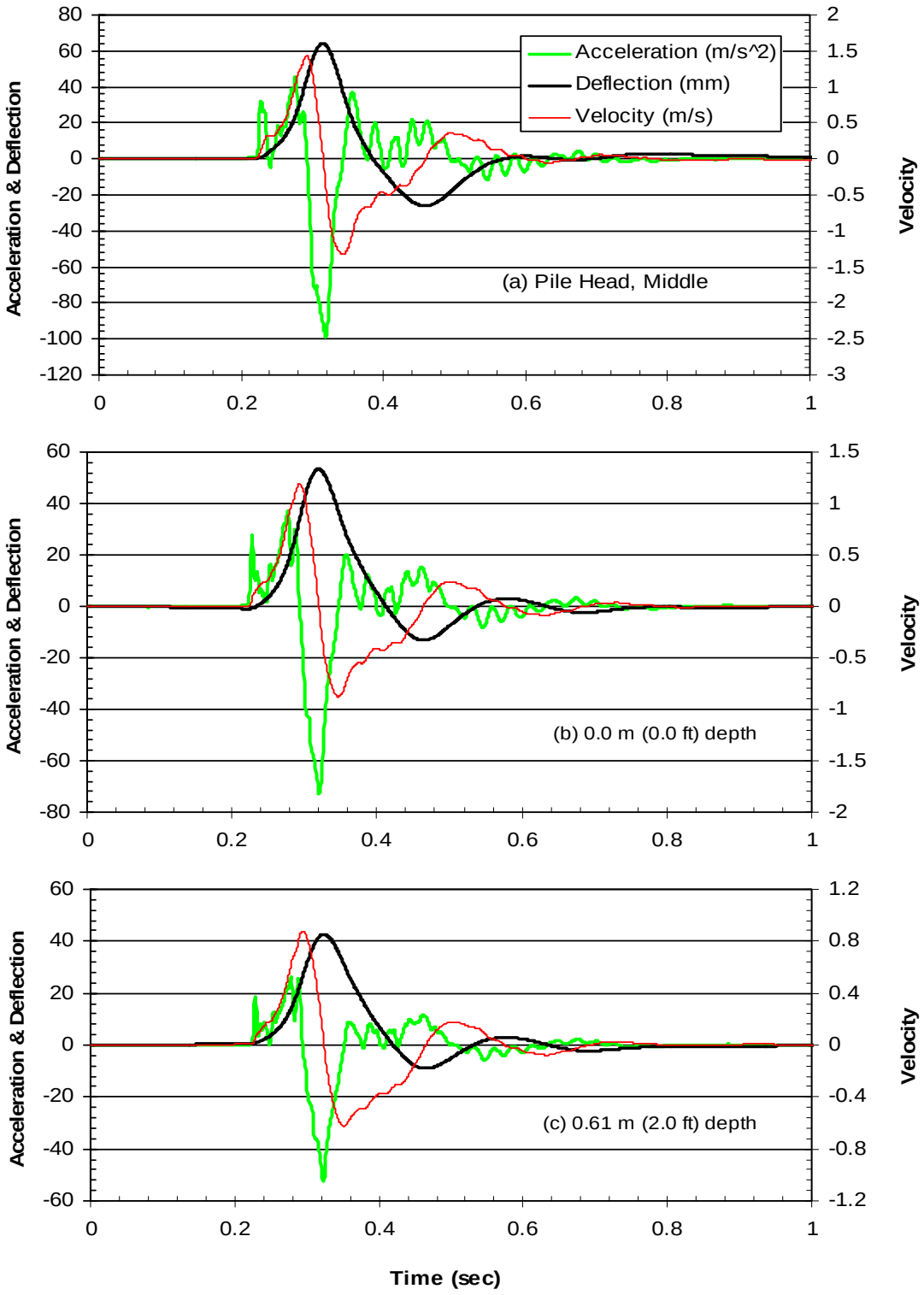

Figure A.21: 15-pile group, test 5—accelerometer time histories at (a) pile head, middle pile, (b) 0.0 m (0.0 ft), and (c) 0.61 (2.0 ft) depths.

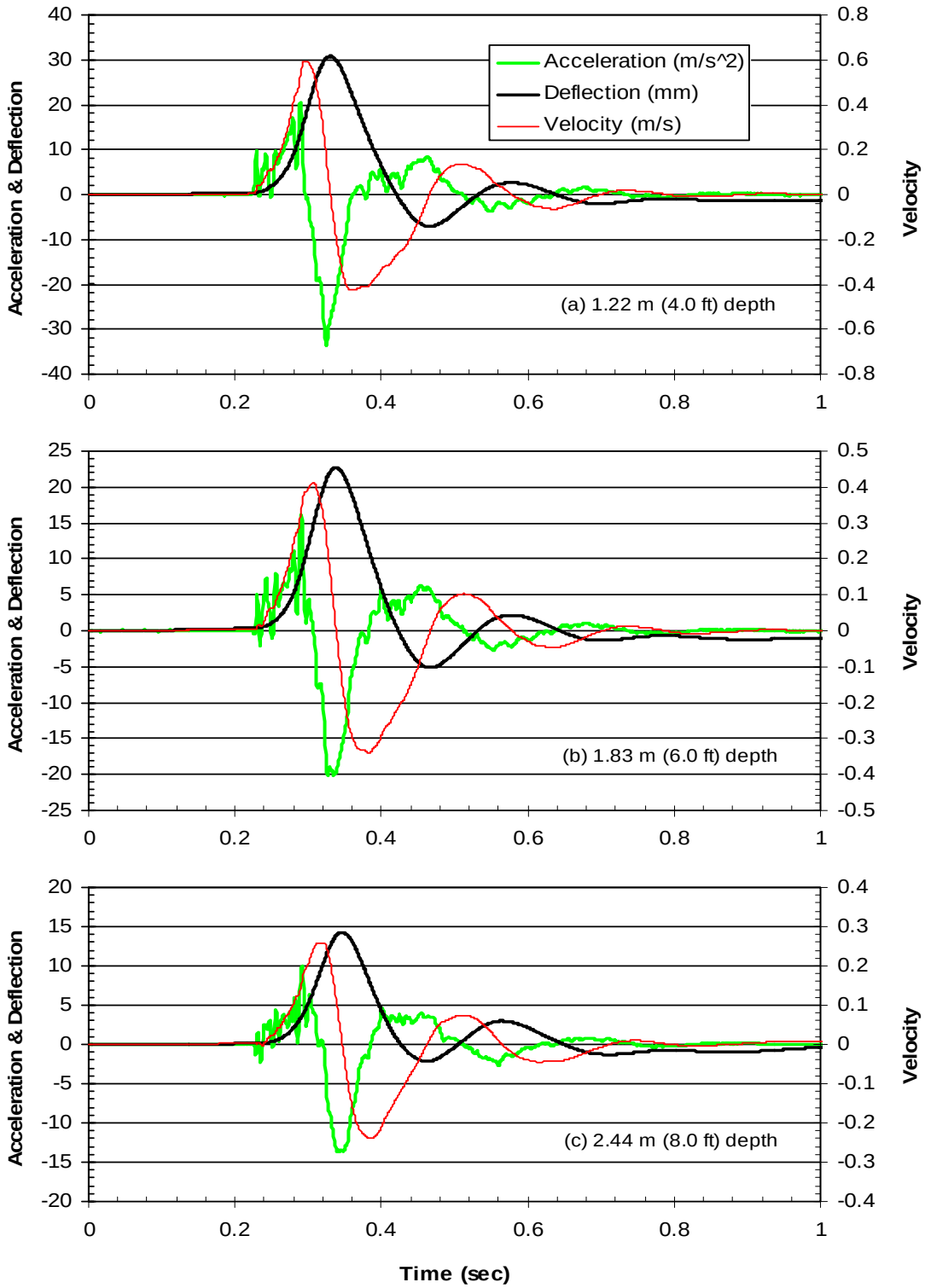

Figure A.22: 15-pile group, test 5—accelerometer time histories at (a) 1.22 m (4.0 ft), (b) 1.83 m (6.0 ft), and (c) 2.44 m (8.0 ft) depths.

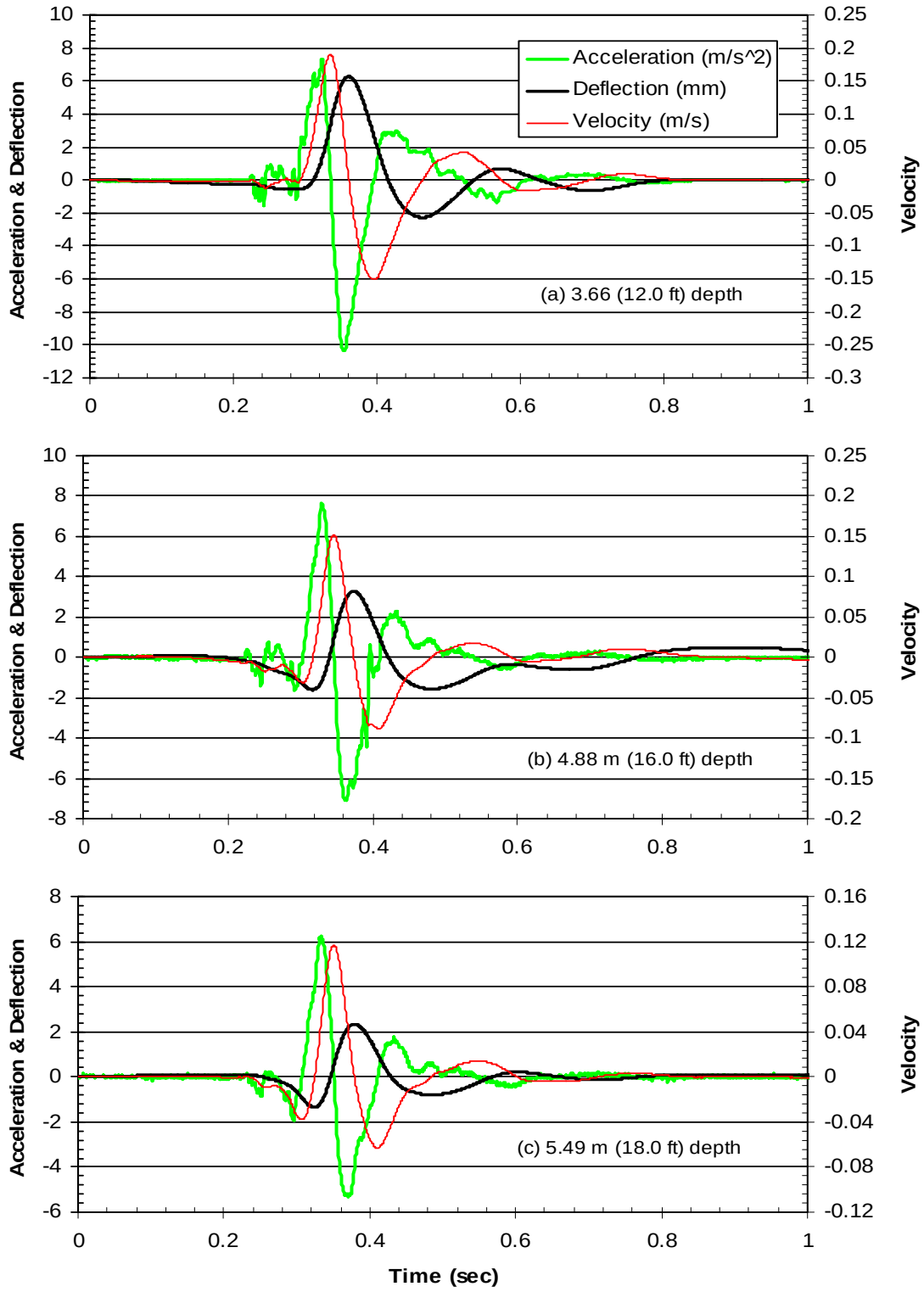

Figure A.23: 15-pile group, test 5—accelerometer time histories at (a) 3.66 m (12.0 ft), (b) 4.88 m (16.0 ft), and (c) 5.49 (18.0 ft) depths.

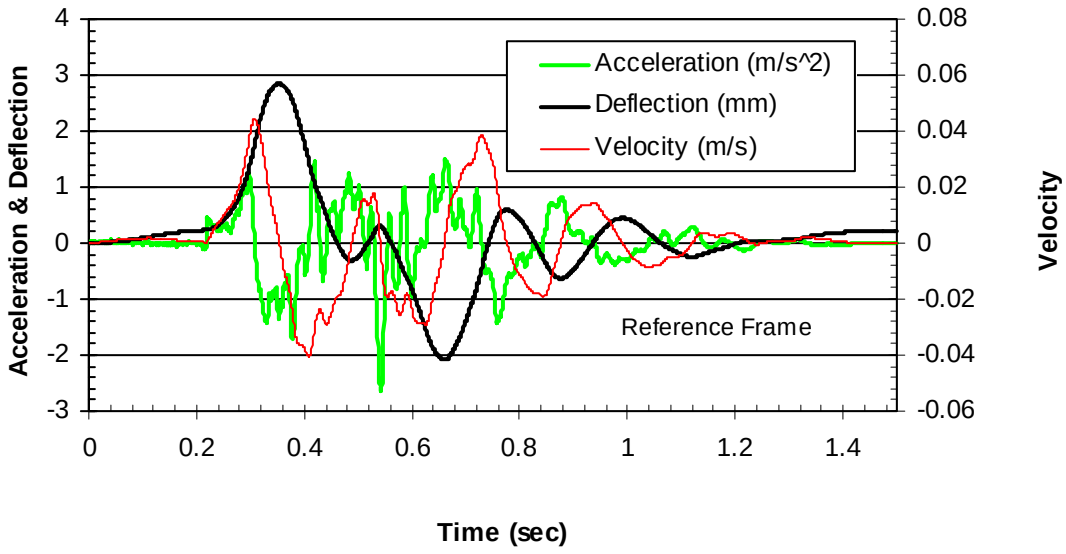

Figure A.24: 15-pile group, test 5—accelerometer time histories at reference frame.

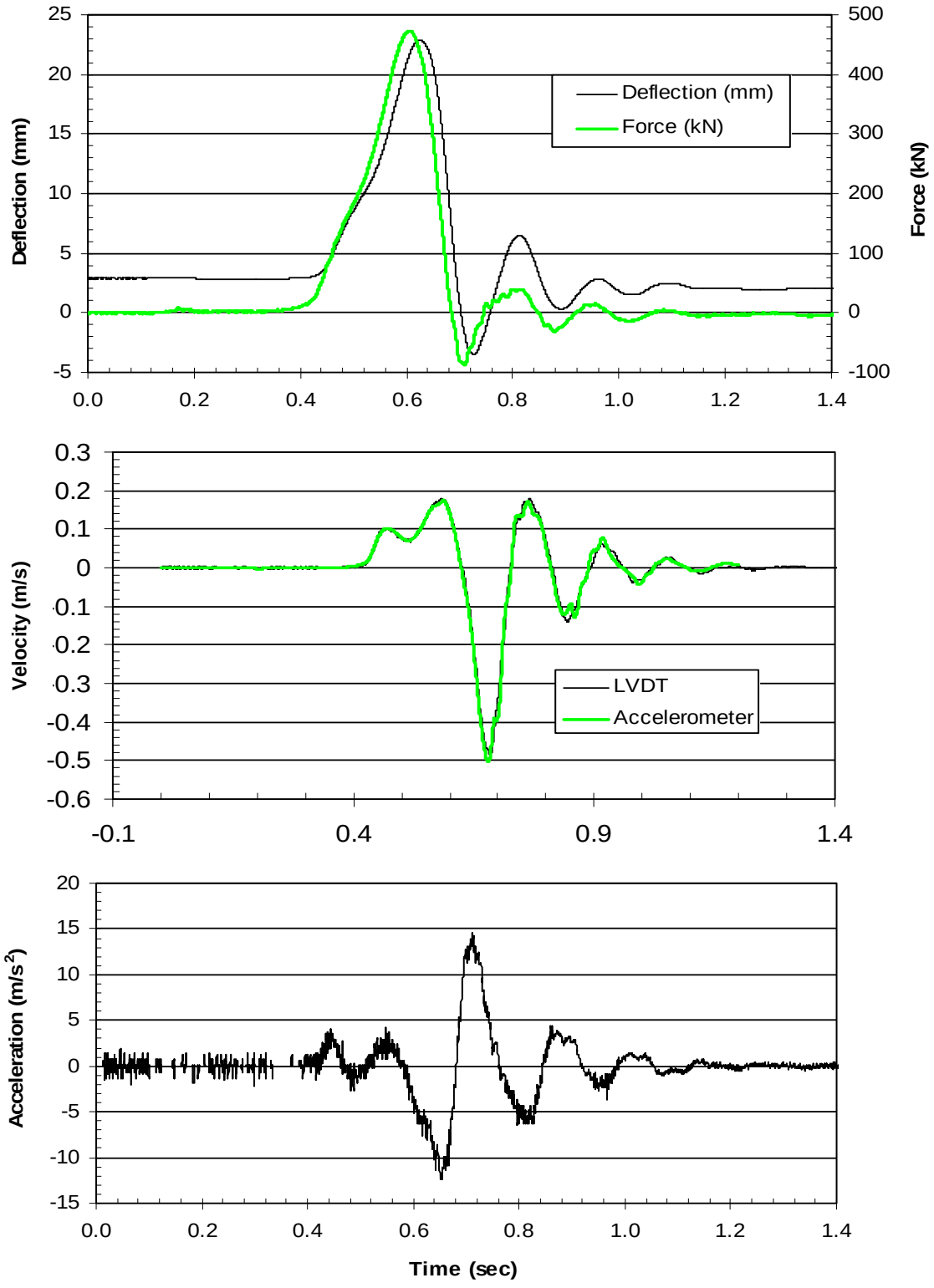

Figure A.25: 9-pile group, test 1, 13 mm (0.5 in) target—LVDT time histories at pile head.

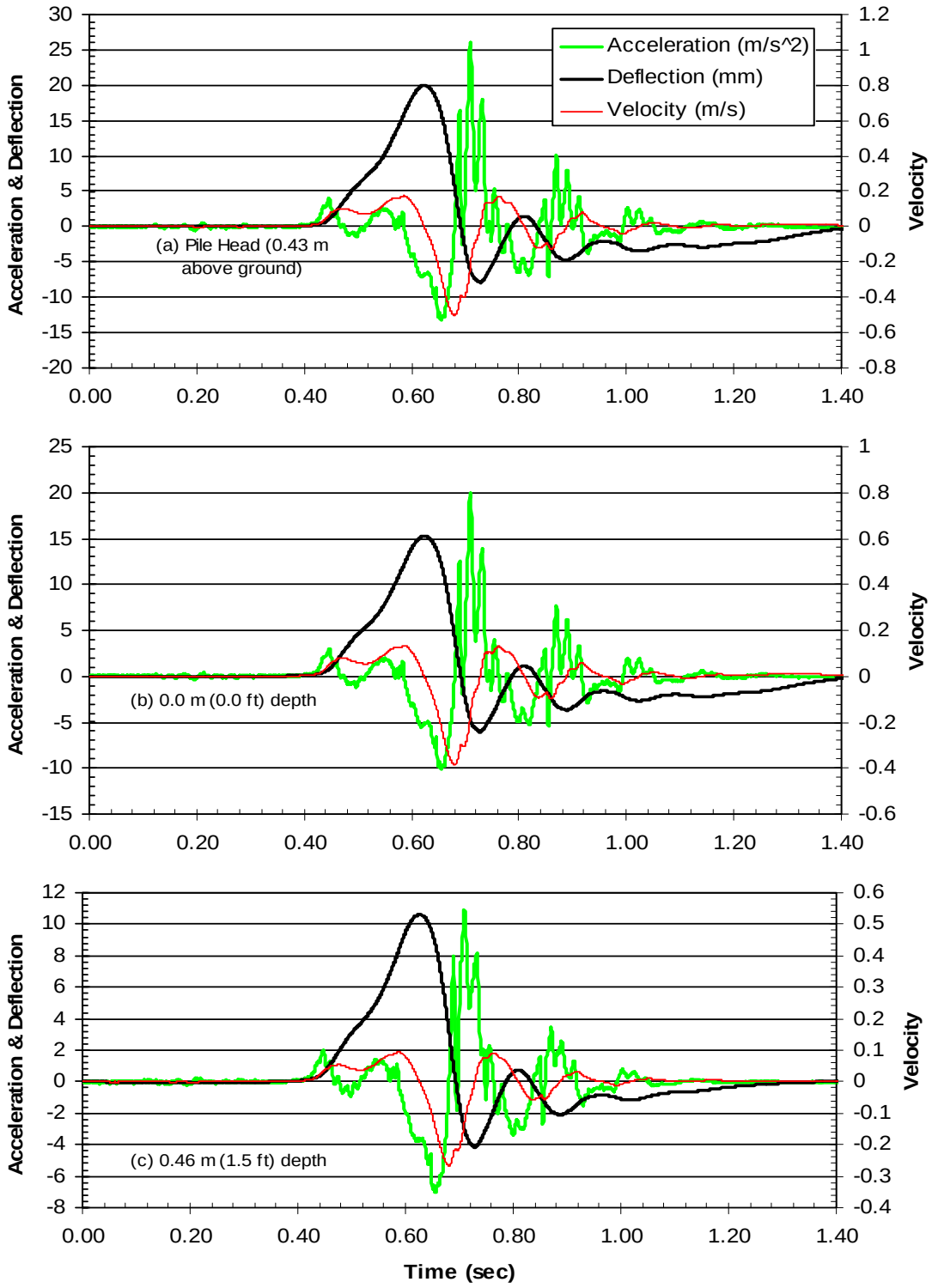

Figure A.26: 9-pile group, test 1—accelerometer time histories at (a) pile head, (b) 0.0m, and (c) 0.46 m (1.5 ft) depths.

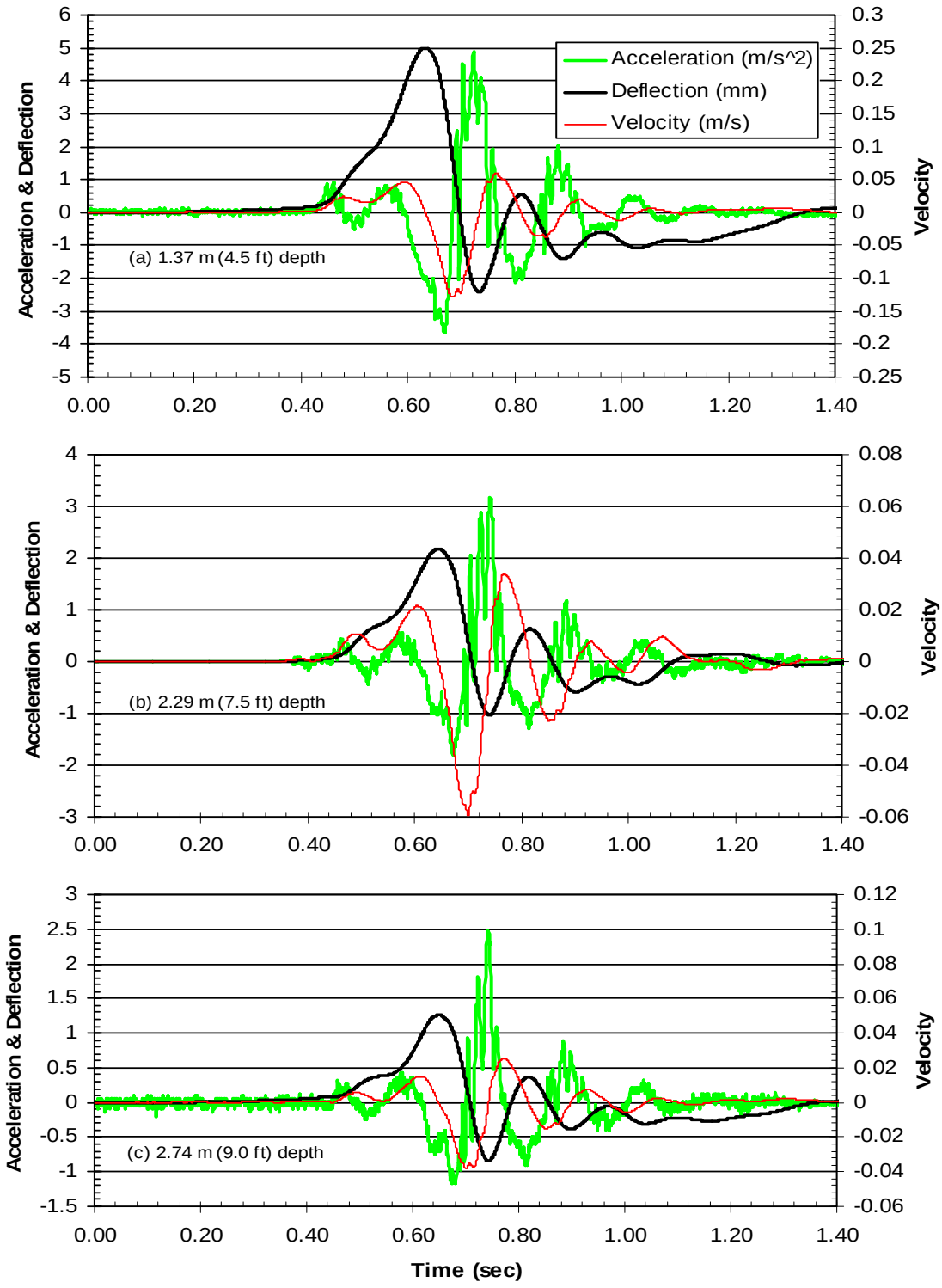

Figure A.27: 9-pile group, test 1—accelerometer time histories at (a) 1.35m (4.5ft), (b)2.29 (7.5ft), and (c) 2.74m (9.0ft) depths.

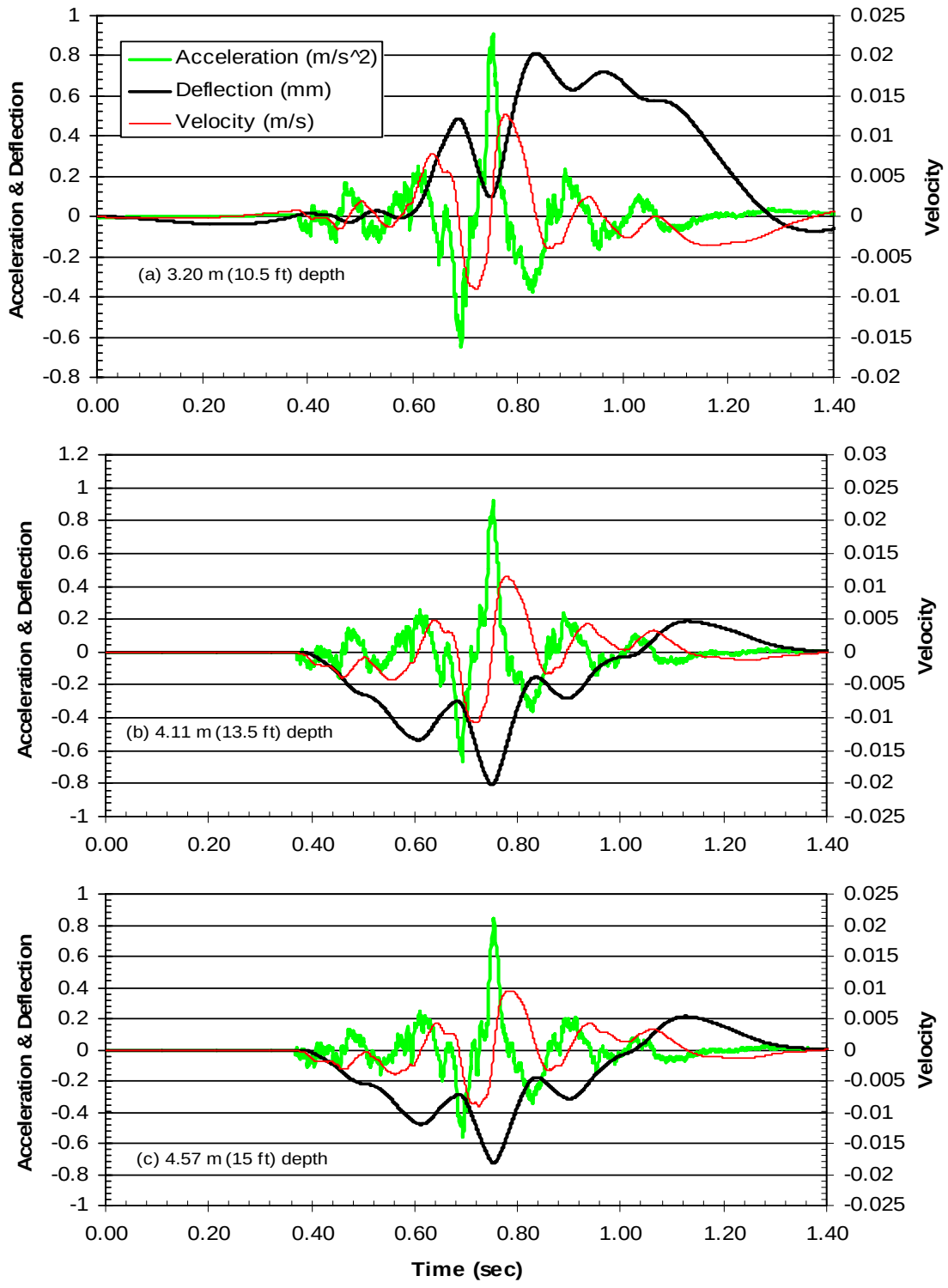

Figure A.28: 9-pile group, test 1—accelerometer time histories at (a) 3.20m (10.5ft), (b) 4.11 m (13.5ft), and (c) 4.57m (15.0ft) depths.

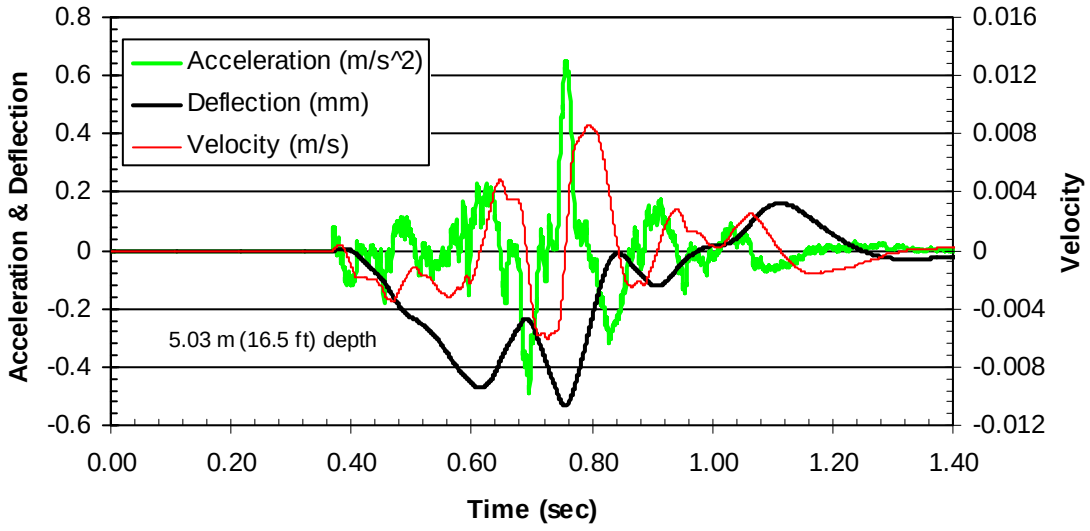

Figure A.29: 9-pile group, test 1—accelerometer time history at 5.03m (16.5ft) depth.

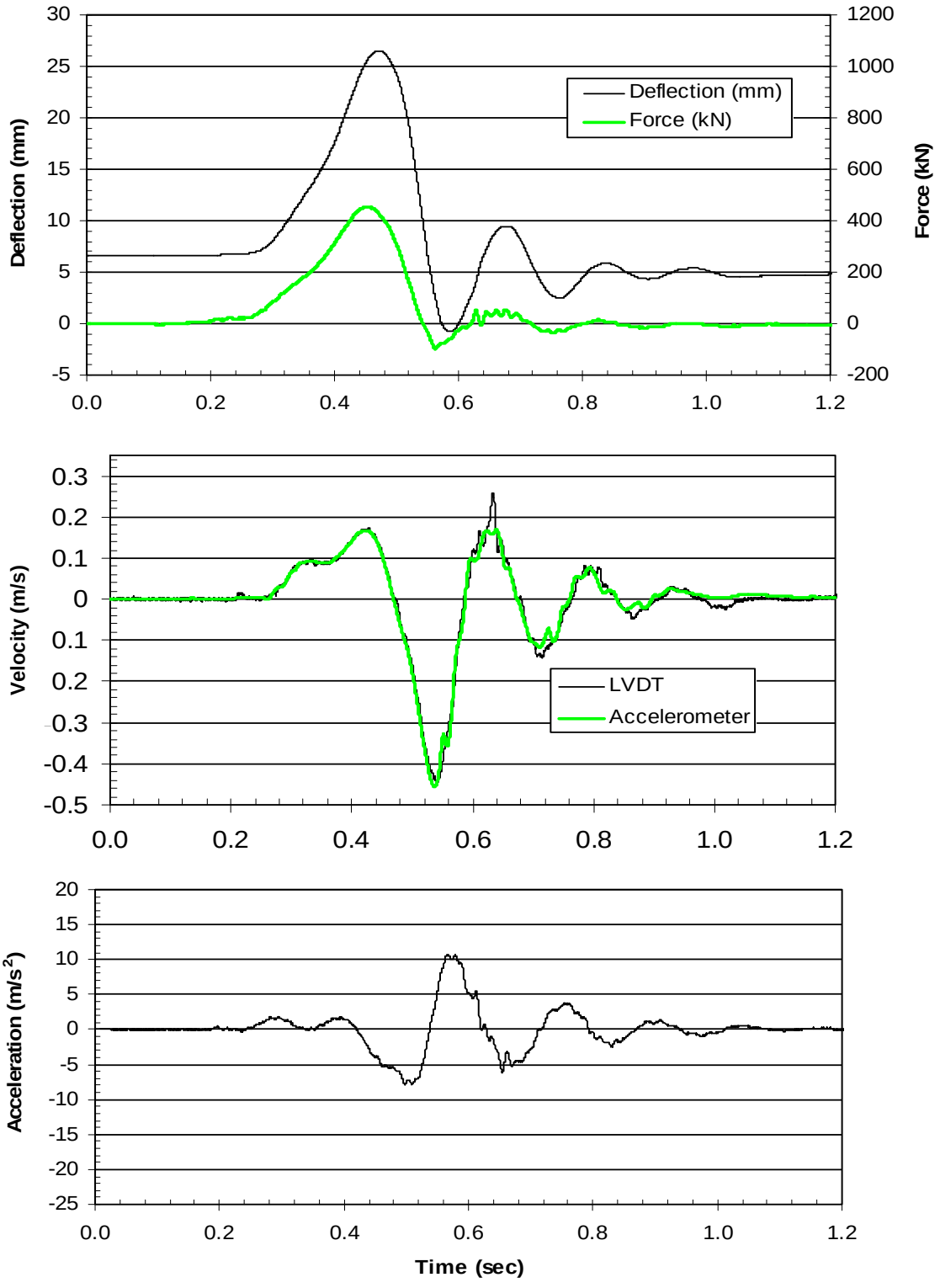

Figure A.30: 9-pile group, test 2, 25 mm (1.0 in) target—LVDT time histories at pile head.

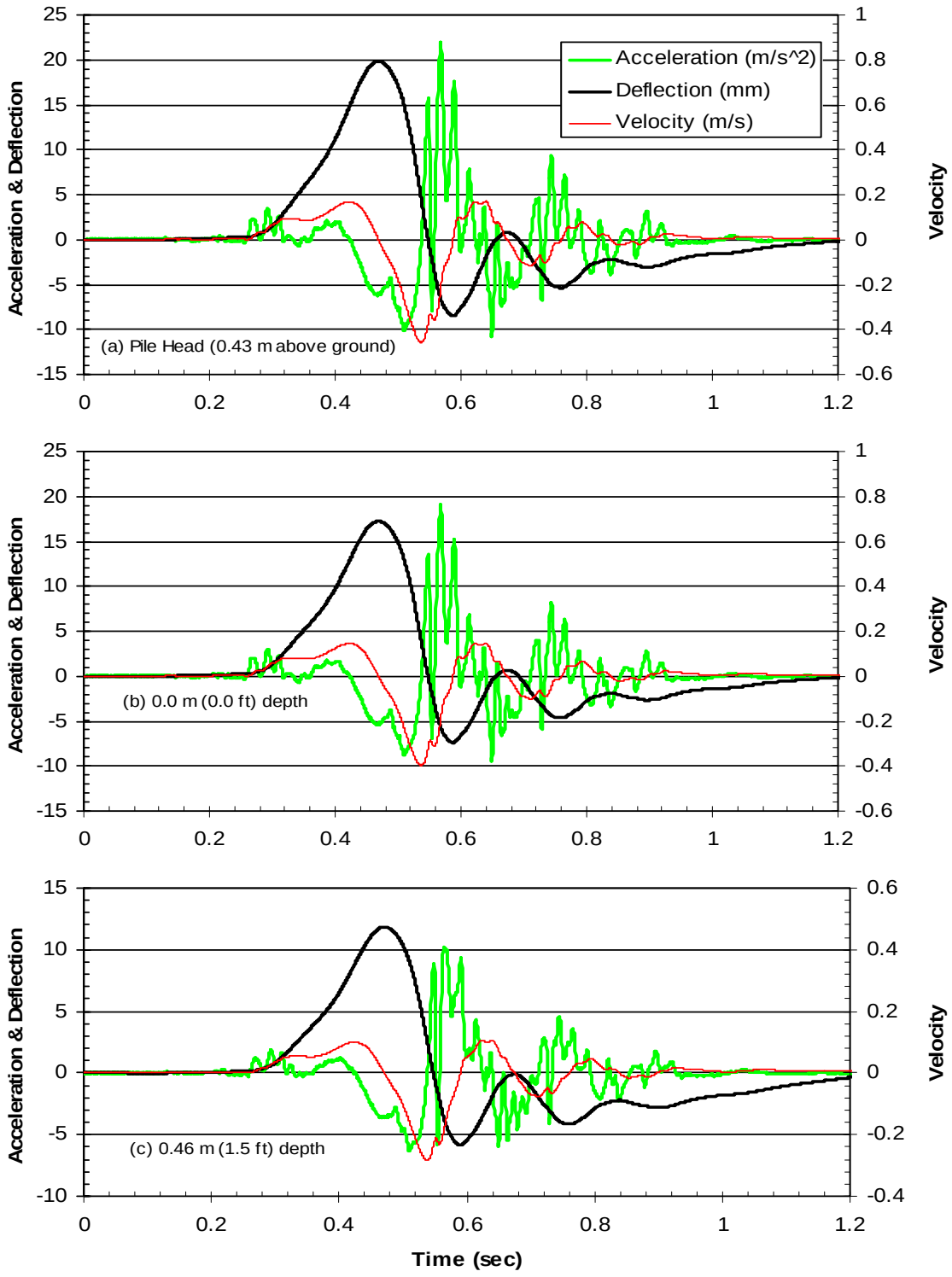

Figure A.31: 9-pile group, test 2—accelerometer time histories at (a) pile head, (b)0.0m (0ft), and (c) 0.46m (1.5ft) depths.

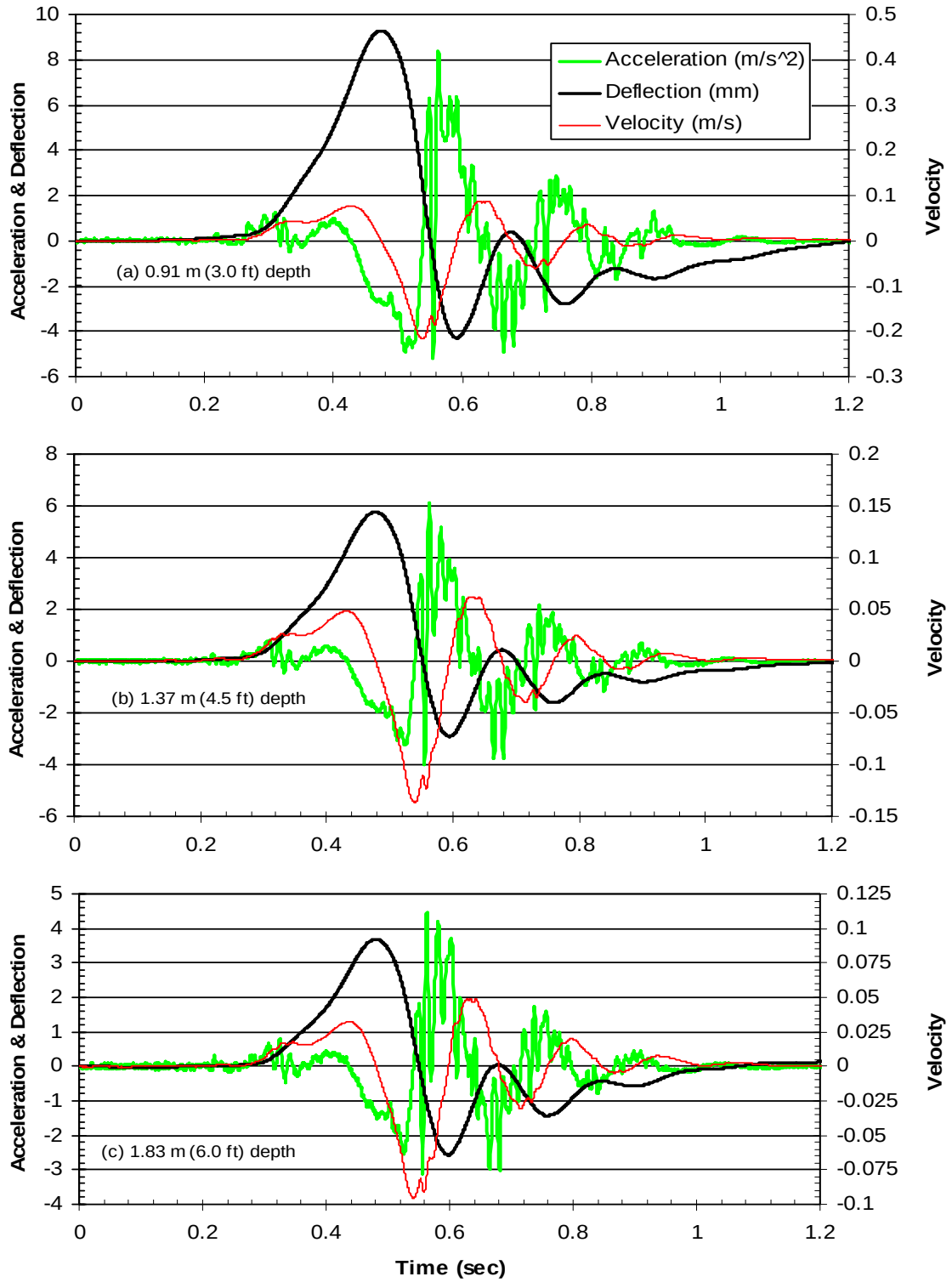

Figure A.32: 9-pile group, test 2—accelerometer time histories at (a) 0.91m (3.0ft), (b)1.37m (4.5ft), and (c) 1.83m (6.0ft) depths.

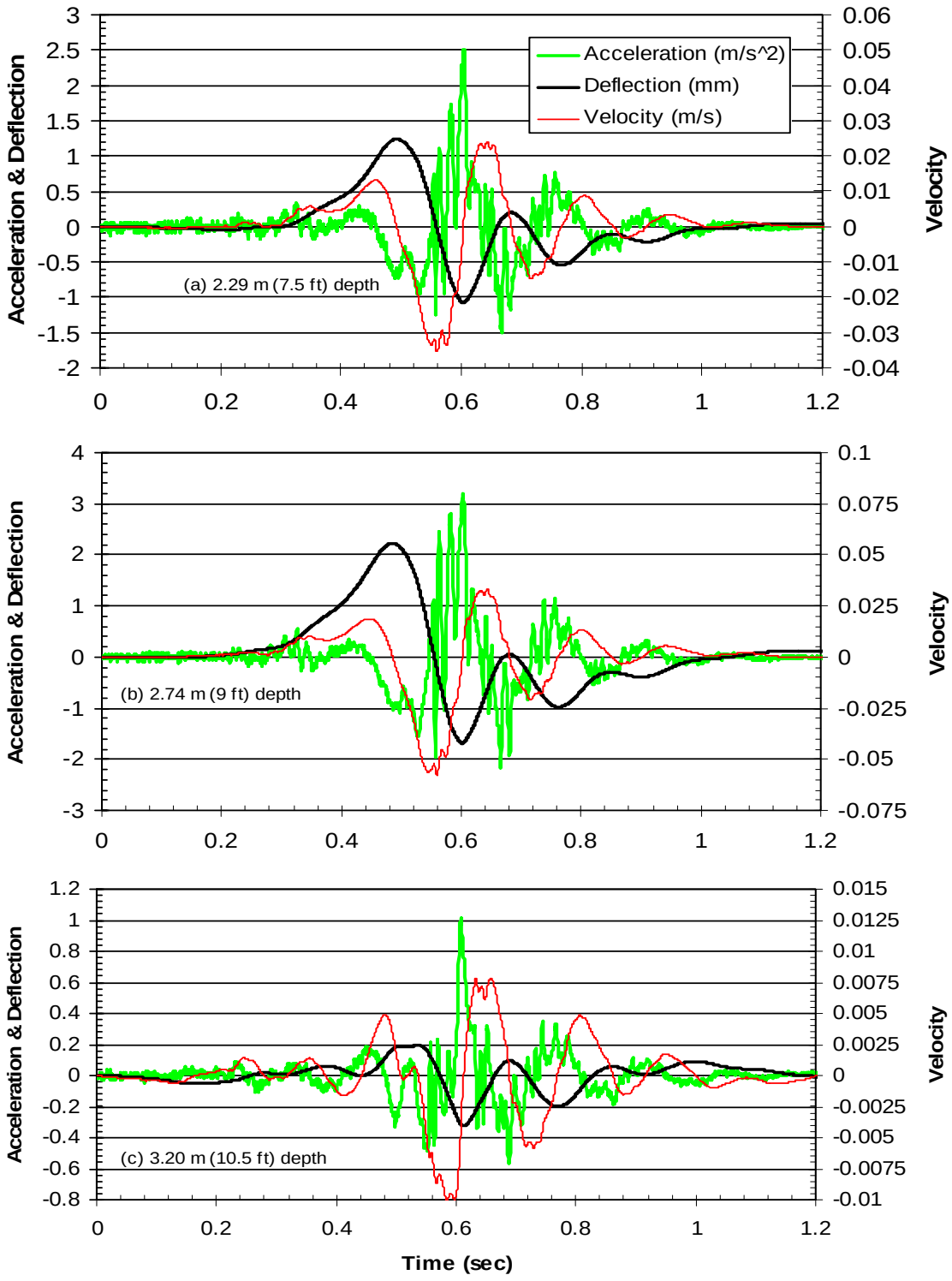

Figure A.33: 9-pile group, test 2—accelerometer time histories at (a) 2.29m (7.0ft), (b)2.74m (9.0ft), and (c) 3.20m (10.5ft) depths.

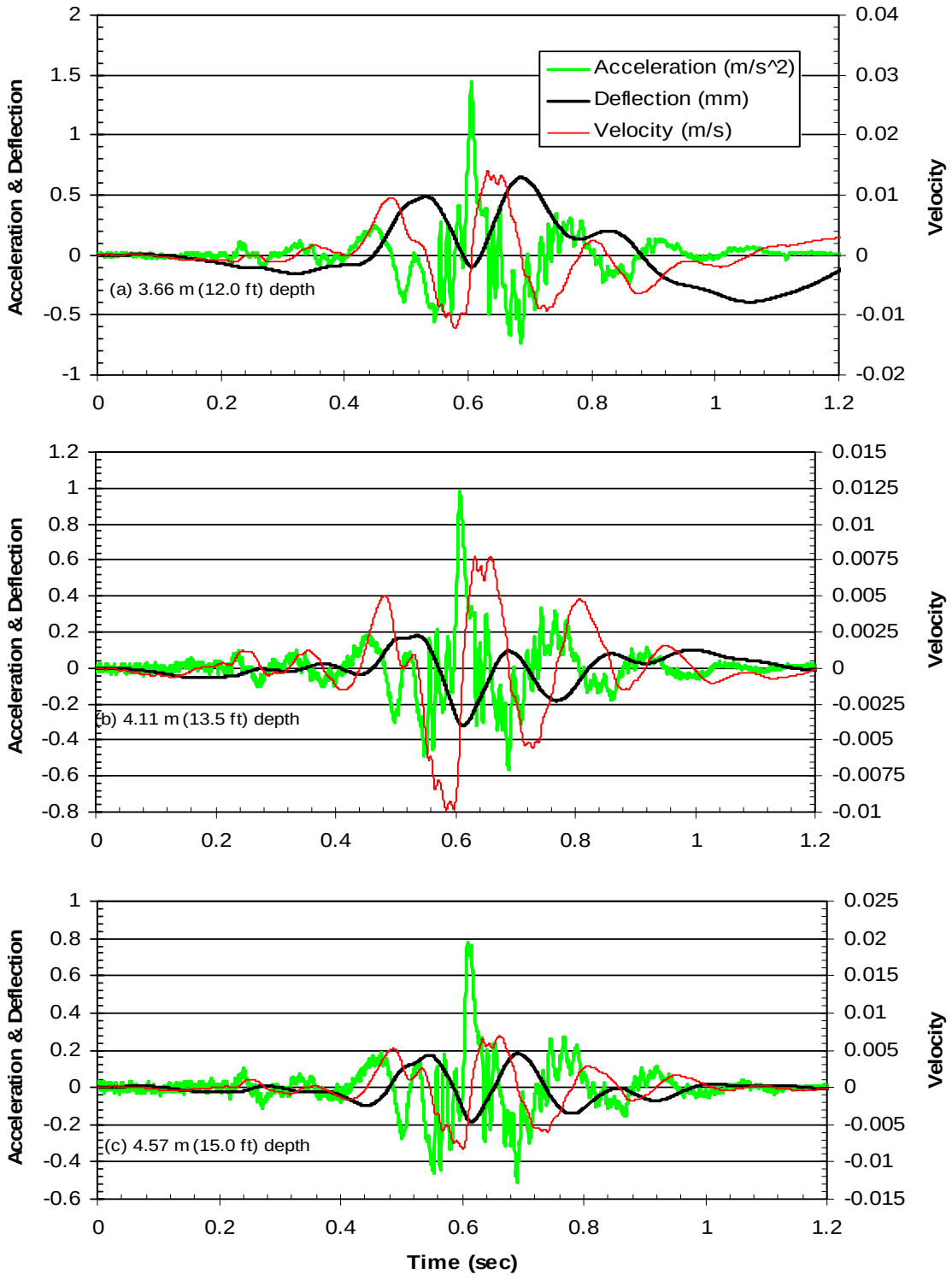

Figure A.34: 9-pile group, test 2—accelerometer time histories at (a) 3.66m (12.0ft), (b) 4.11m (13.5ft), and (c) 4.57m (15.0ft) depths.

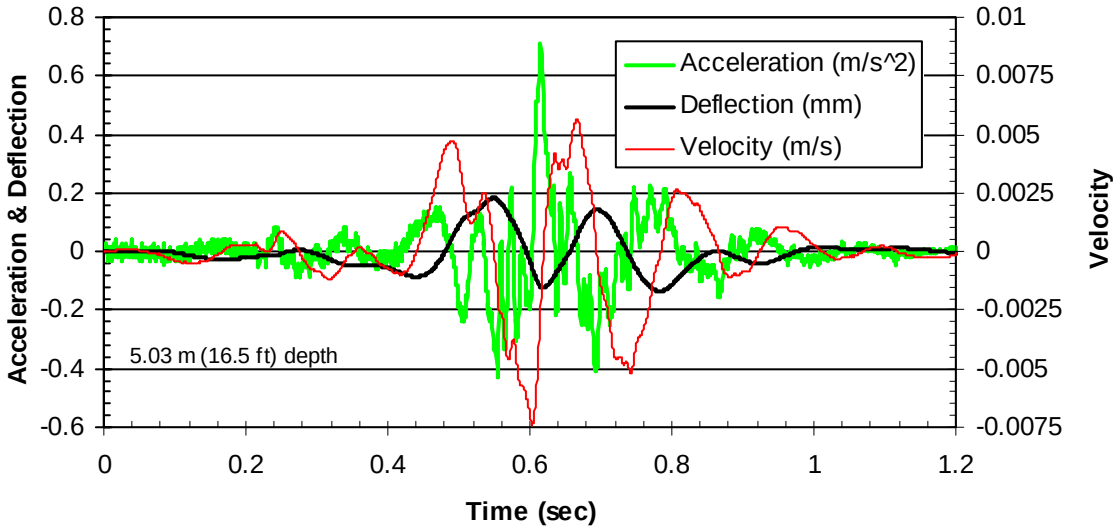

Figure A.35: 9-pile group, test 2—accelerometer time history at 5.03m (16.5ft) depth.

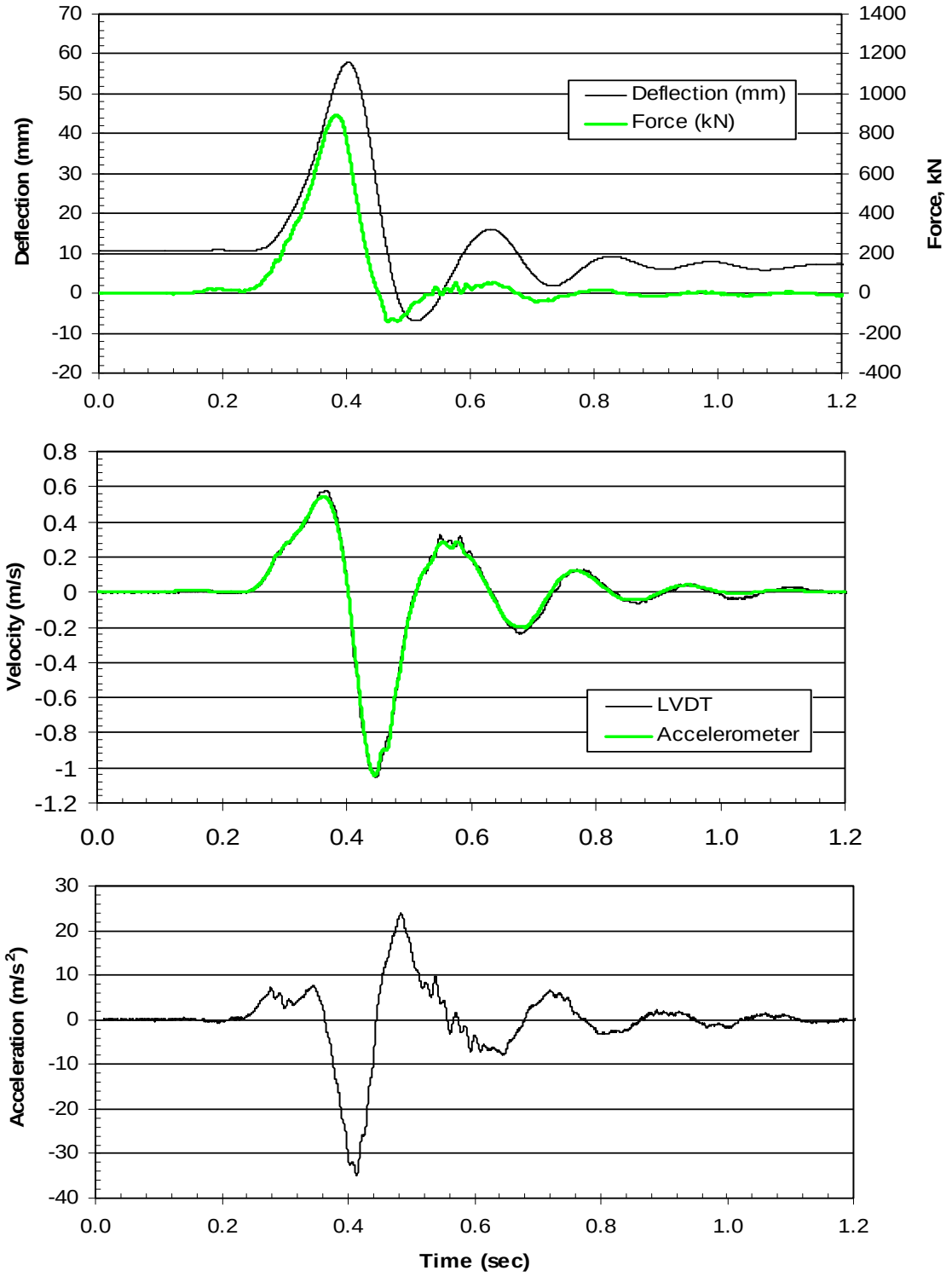

Figure A.36: 9-pile group, test 3, 38 mm (1.5 in) target—LVDT time histories at pile head.

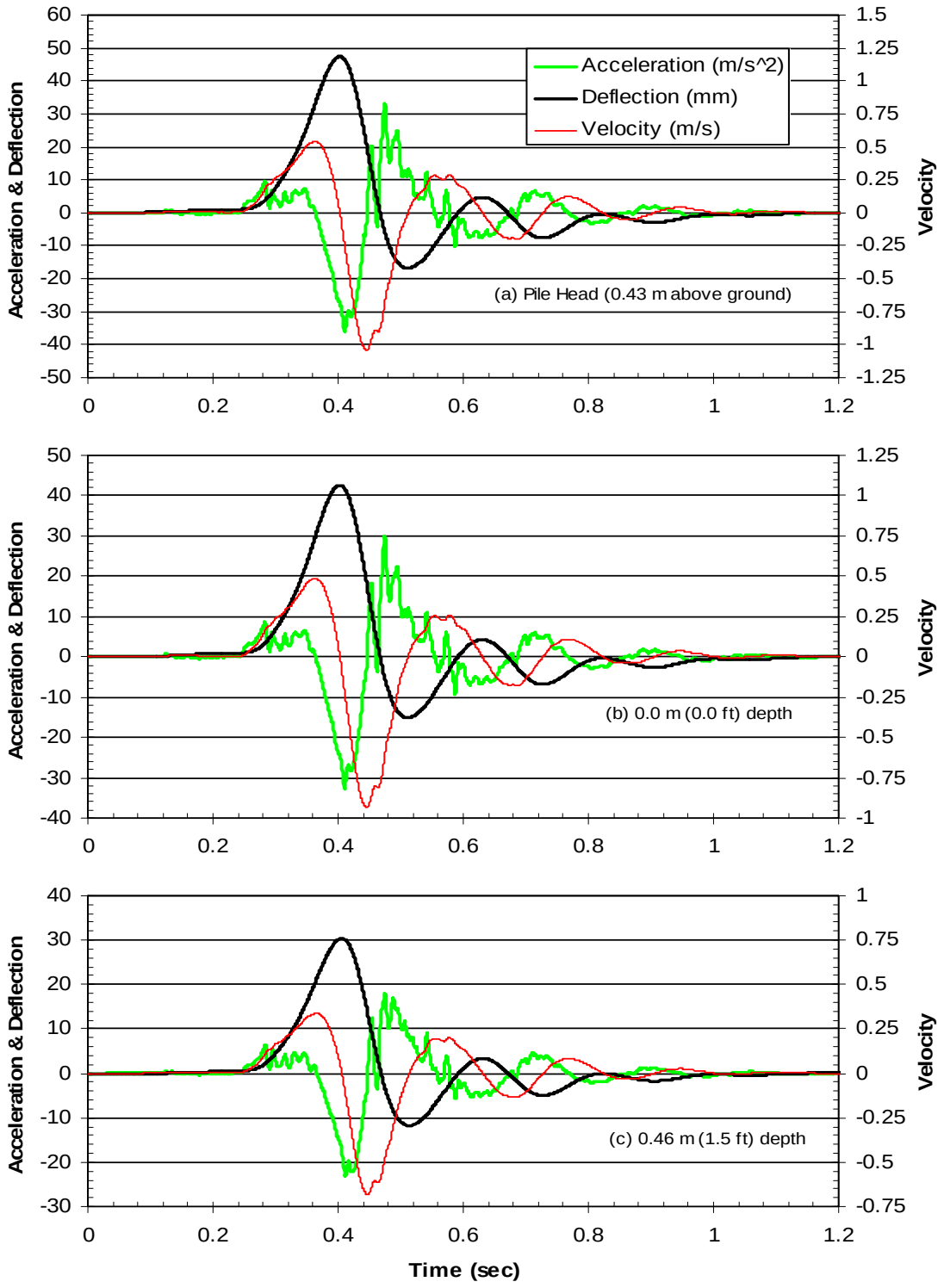

Figure A.37: 9-pile group, test 3—accelerometer time histories at (a) pile head, (b)0.0m (0ft), and (c) 0.46m (1.5ft) depths.

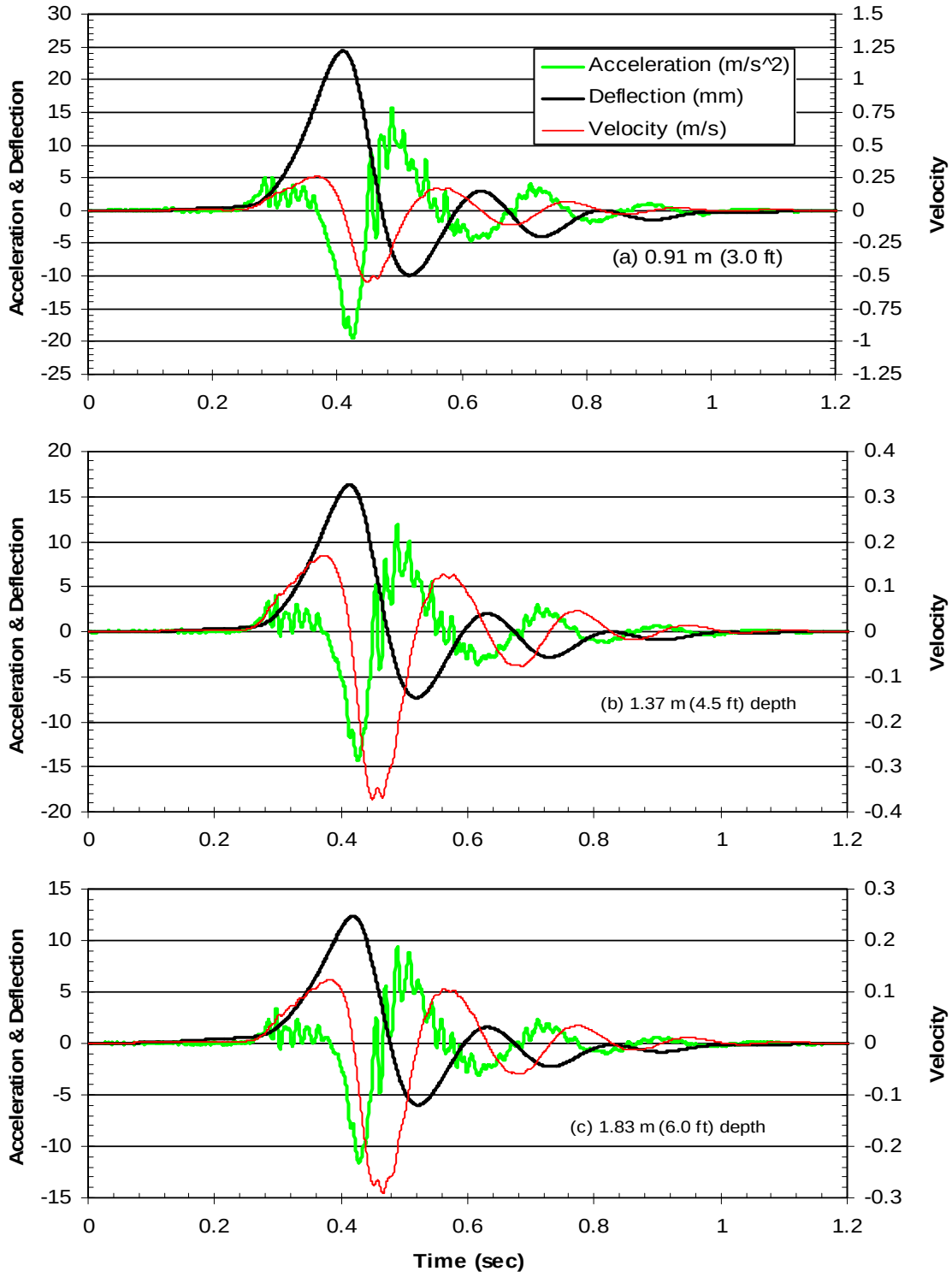

Figure A.38: 9-pile group, test 3—accelerometer time histories at (a) 0.91m (3.0ft), (b)1.37m (4.5ft), and (c) 1.83m (6.0ft) depths.

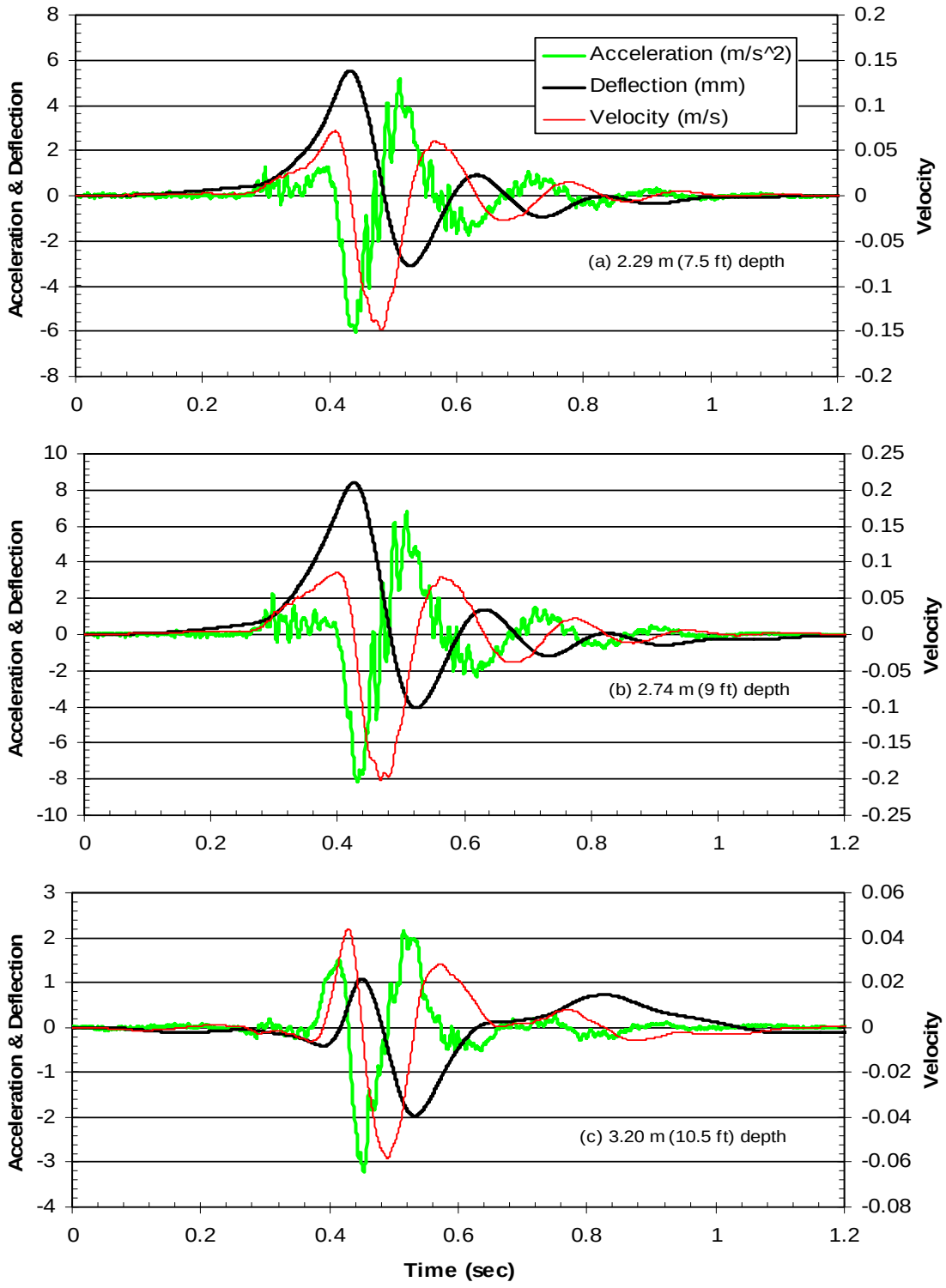

Figure A.39: 9-pile group, test 3—accelerometer time histories at (a) 2.29m (7.5ft), (b)2.74m (9.0ft), and (c) 3.20m (10.5ft) depths.

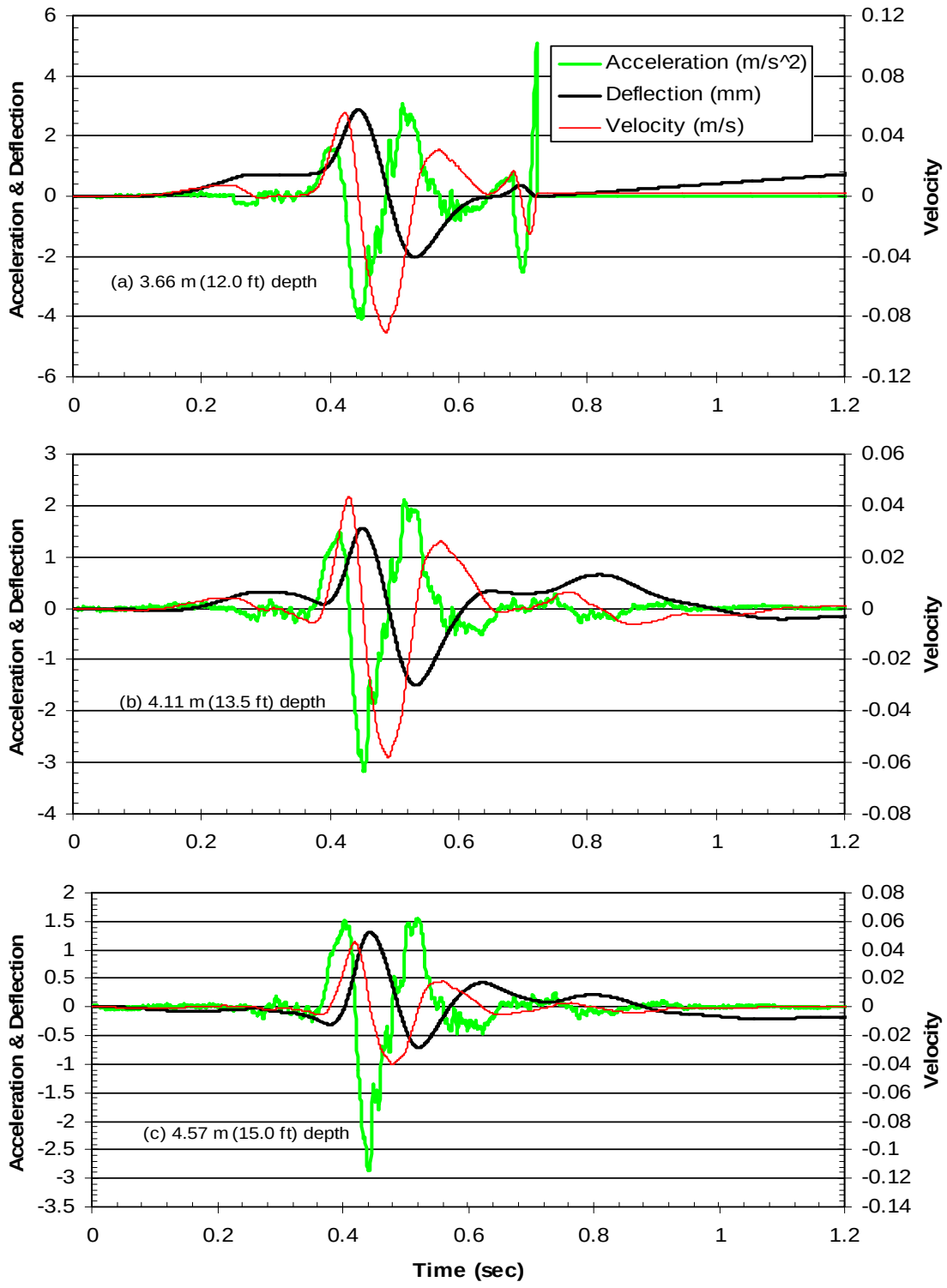

Figure A.40: 9-pile group, test 3—accelerometer time histories at (a) 3.66m (12.0ft), (b) 4.11m (13.5ft), and (c) 4.57m (15.0ft) depths.

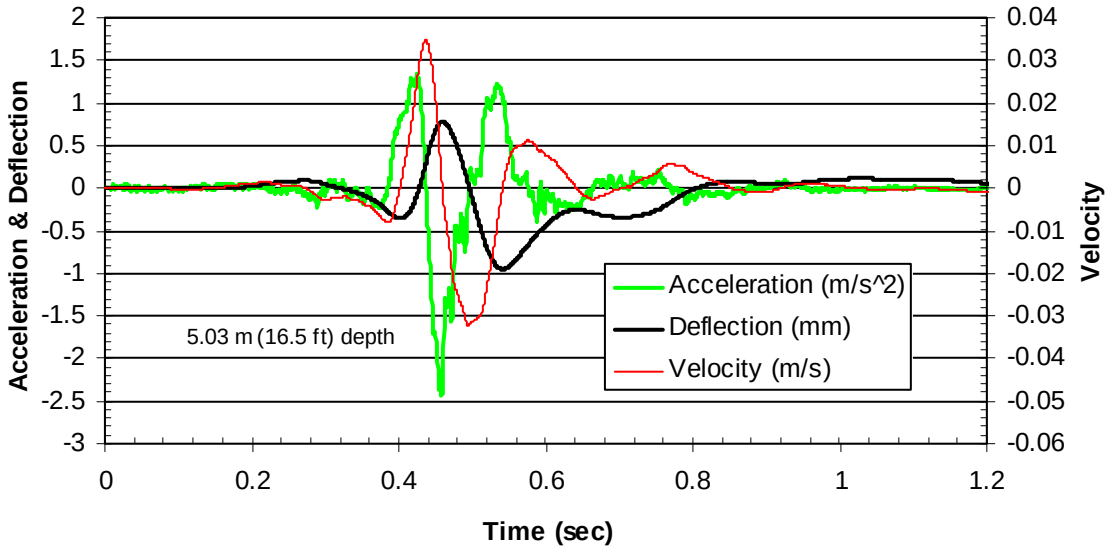

Figure A.41: 9-pile group, test 3—accelerometer time history at 5.03m (16.5ft) depths.

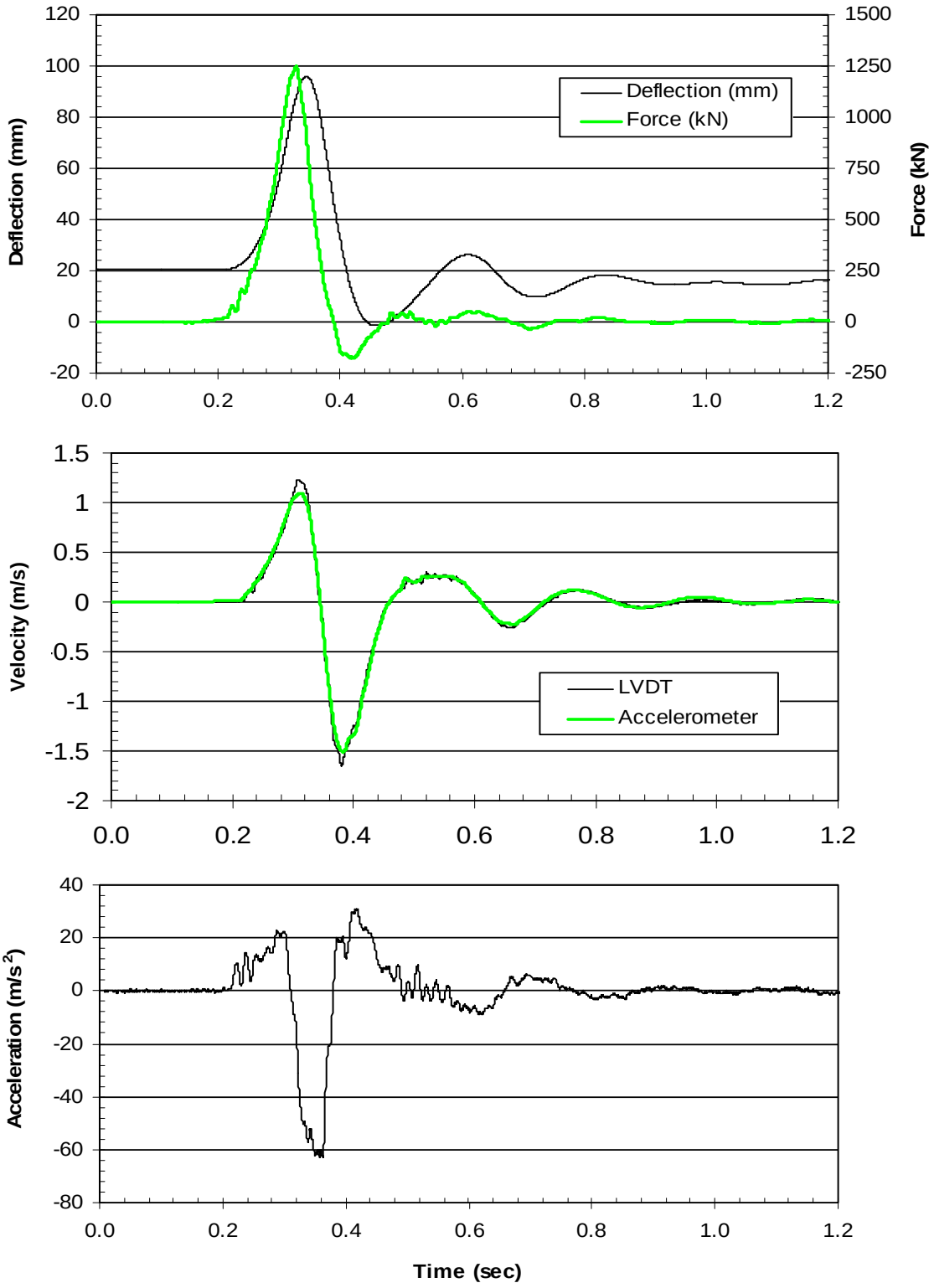

Figure A.42: 9-pile group, test 4, 64 mm (2.5 in) target—LVDT time histories at pile head.

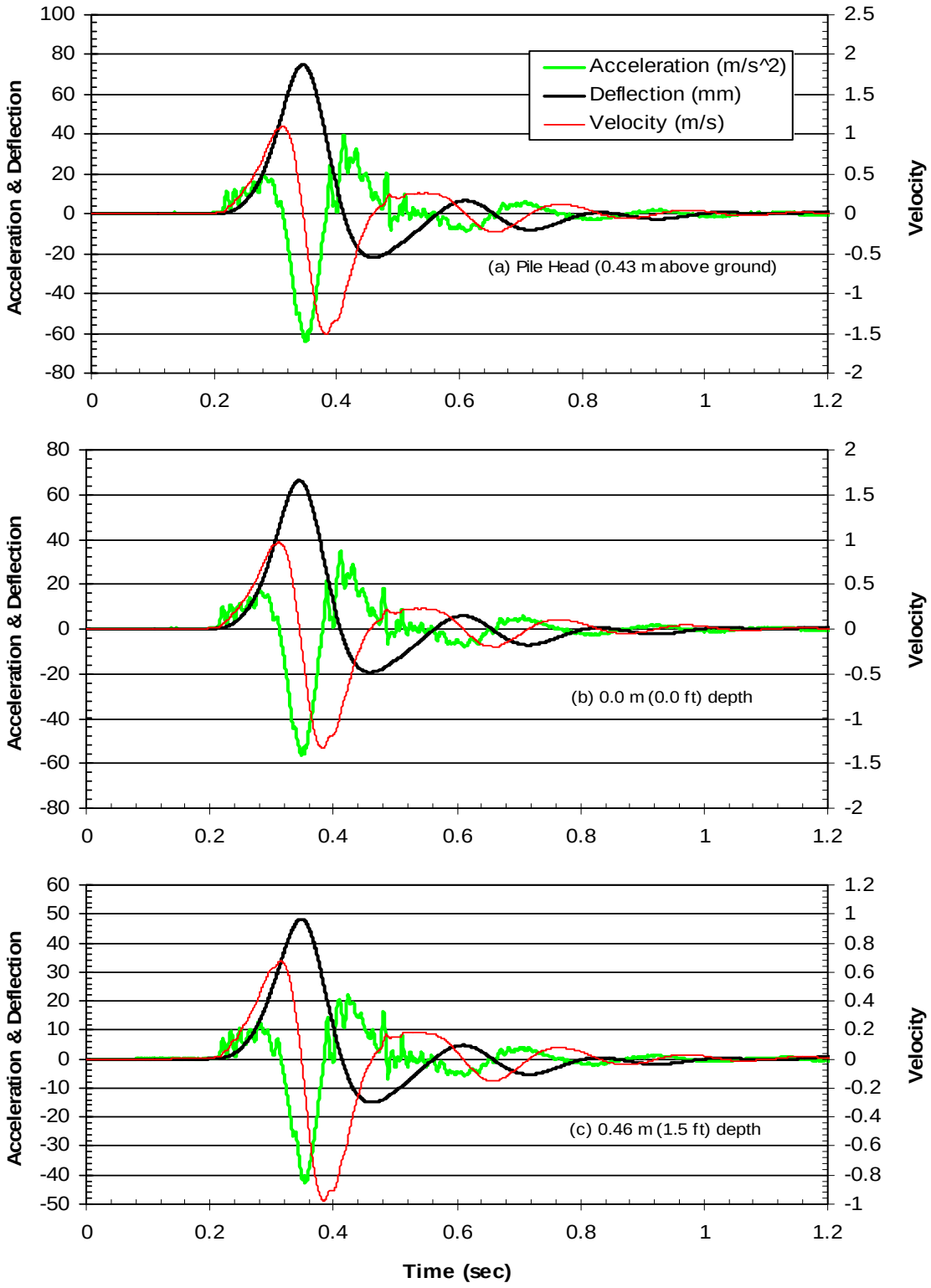

Figure A.43: 9-pile group, test 4—accelerometer time histories at (a)pile head, (b)0.0m (0ft), and (c) 0.46m (1.5ft) depths.

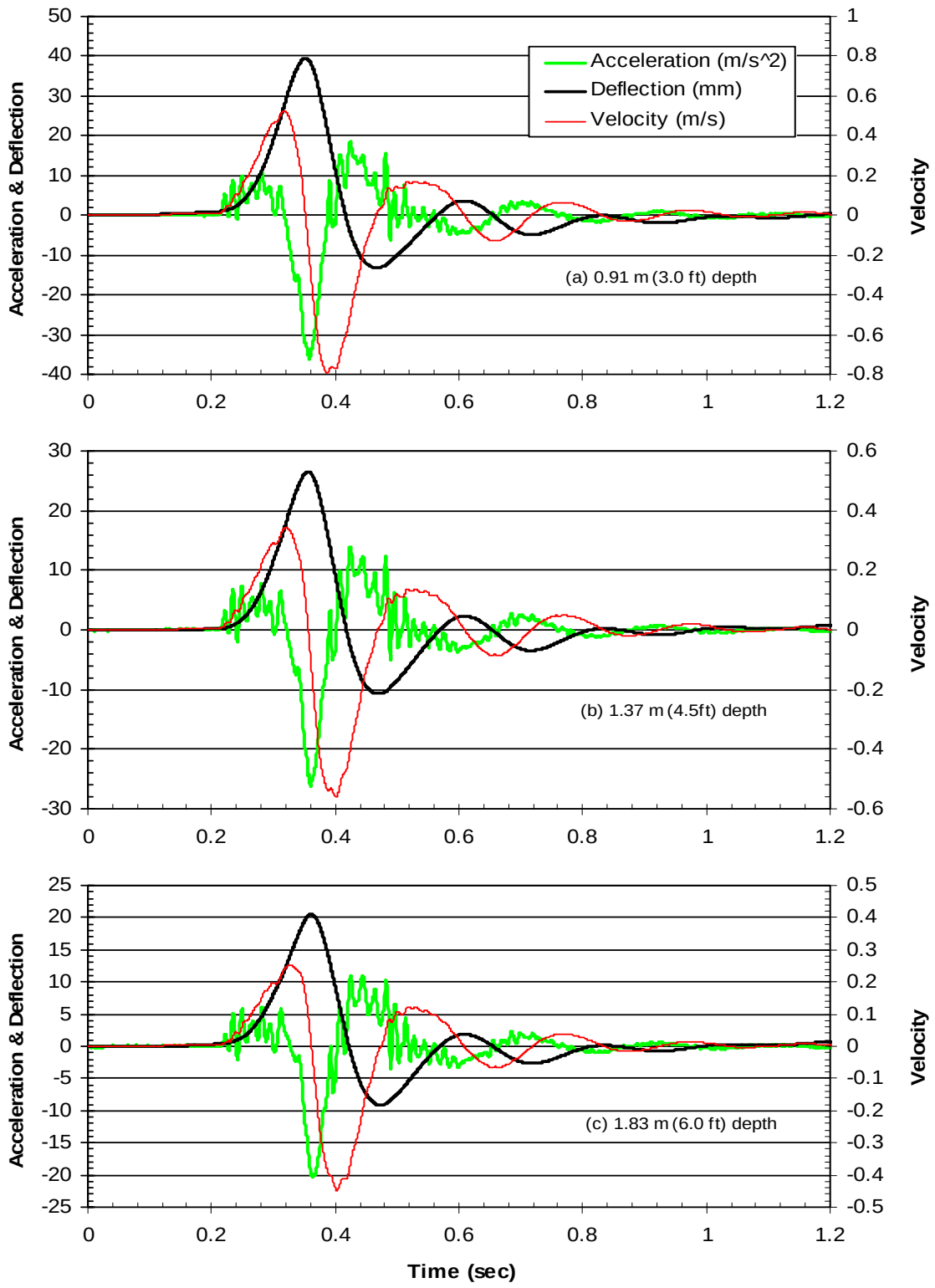

Figure A.44: 9-pile group, test 4—accelerometer time histories at (a) 0.91 (3.0ft), (b)1.37m (4.5ft), and (c) 1.83m (6.0t) depths.

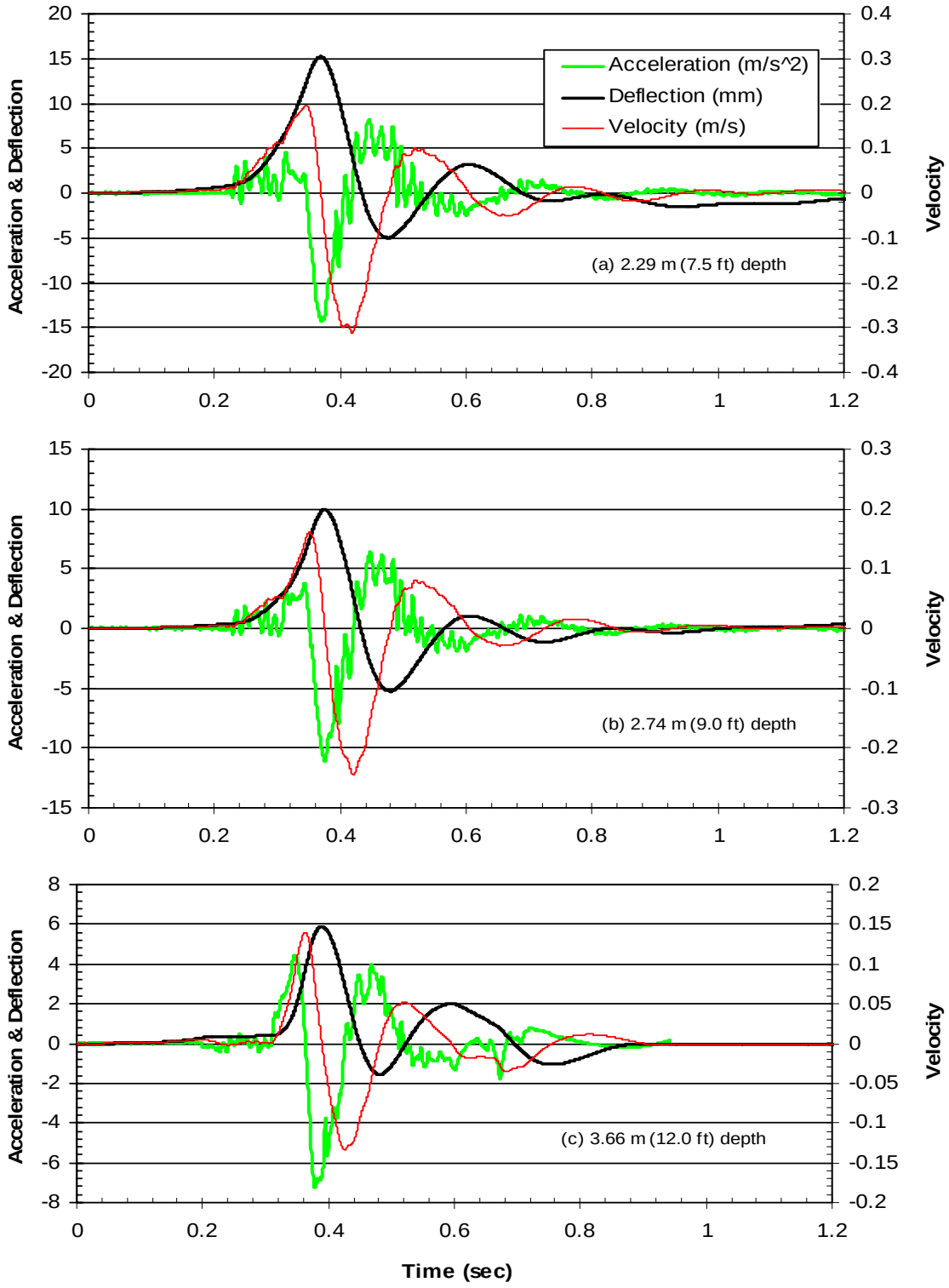

Figure A.45: 9-pile group, test 4—accelerometer time histories at (a) 2.29m (7.5ft), (b)2.74m (9.0ft), and (c) 3.20m (10.5ft) depths.

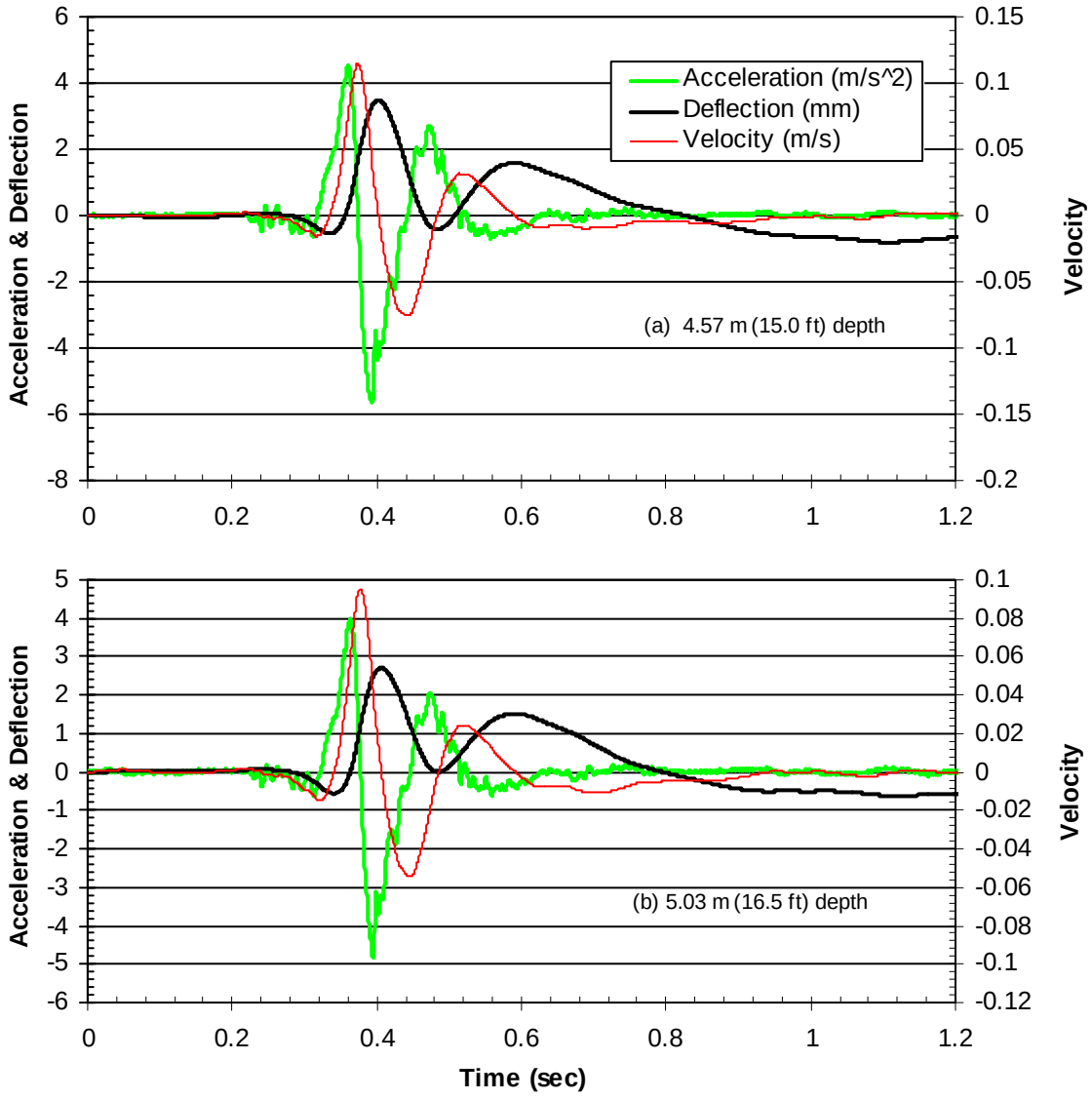

Figure A.46: 9-pile group, test 4—accelerometer time histories at (a) 4.57m (15.0ft) and (b) 5.03m (16.5ft) depths.

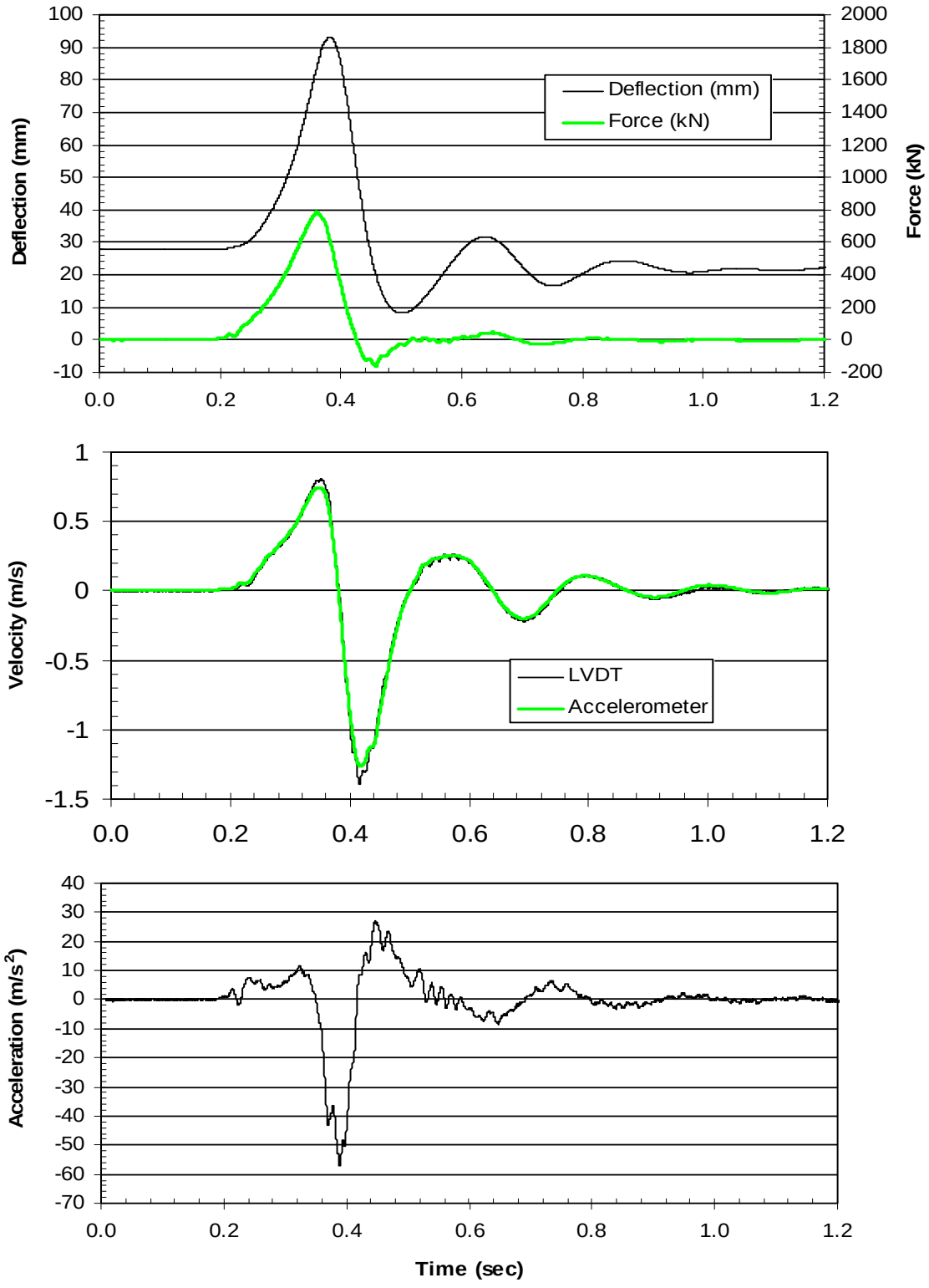

Figure A.47: 9-pile group, test 5, 99 mm (3.75 in) target—LVDT time histories at pile head.

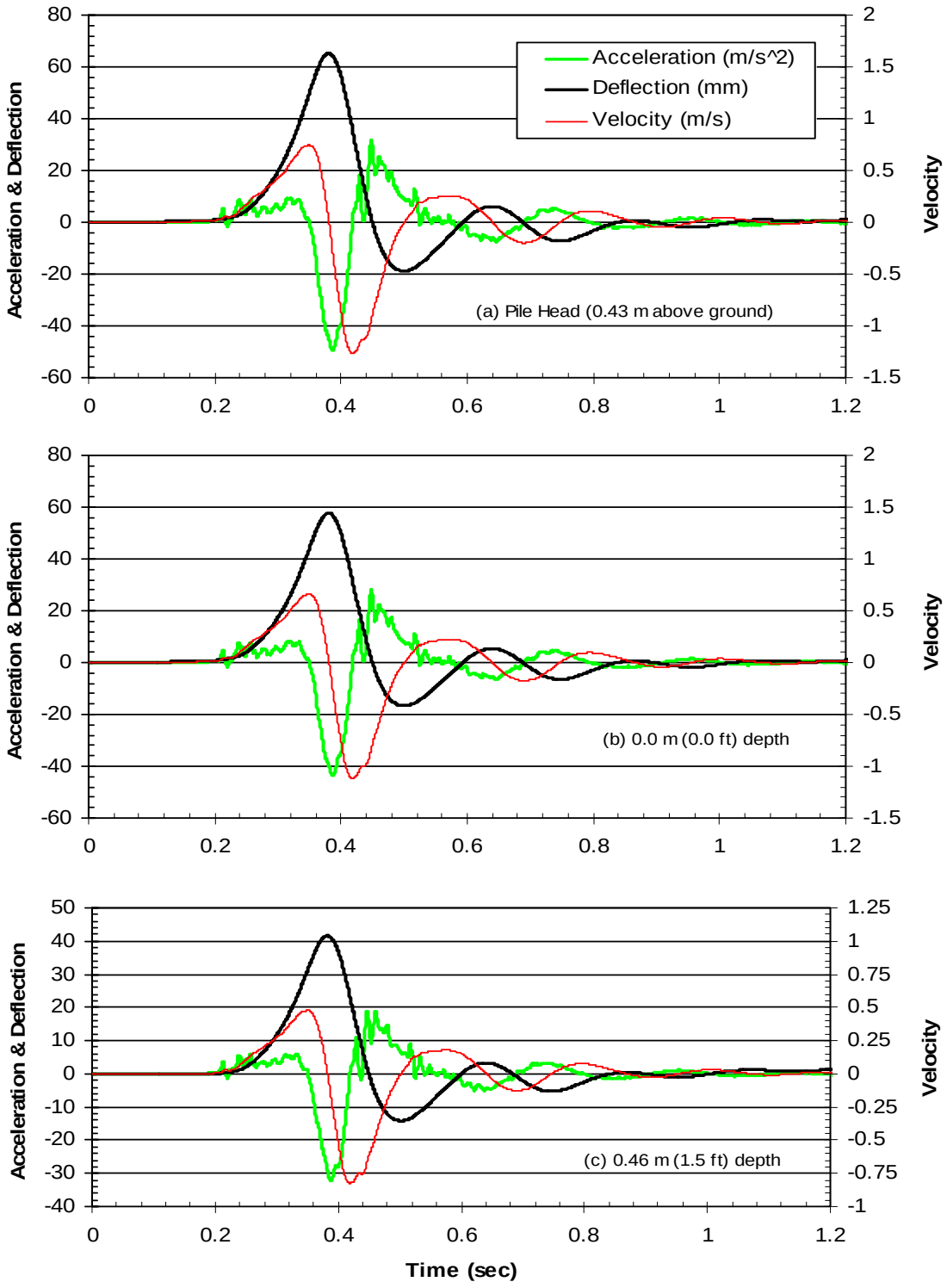

Figure A.48: 9-pile group, test 5—accelerometer time histories at (a) pile head, (b)0.0m (0ft), and (c) .046m (1.5ft) depths.

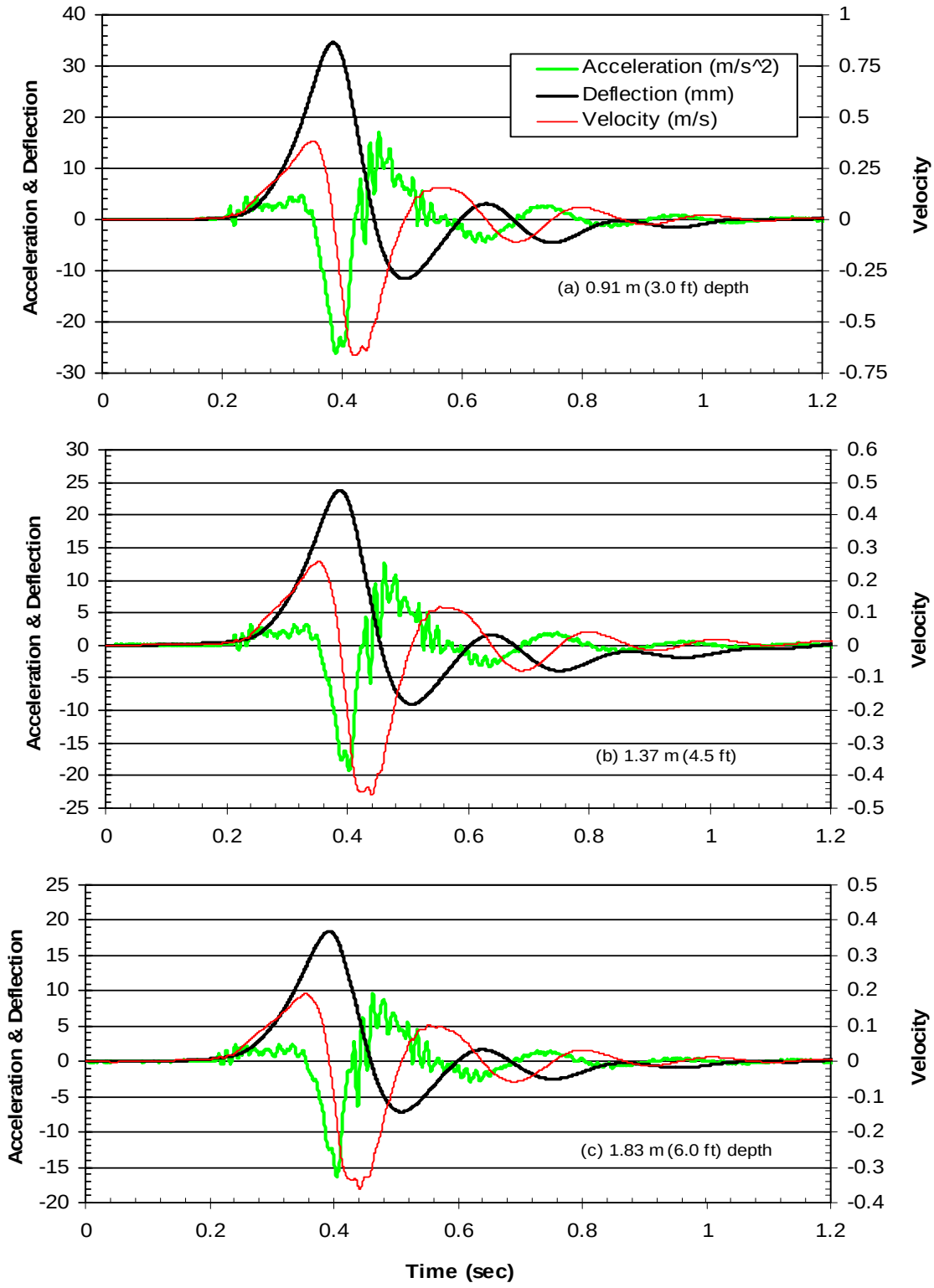

Figure A.49: 9-pile group, test 5—accelerometer time histories at (a) 0.91m (3.0ft), (b)1.37m (4.5ft), and (c) 1.83m (6.0ft) depths.

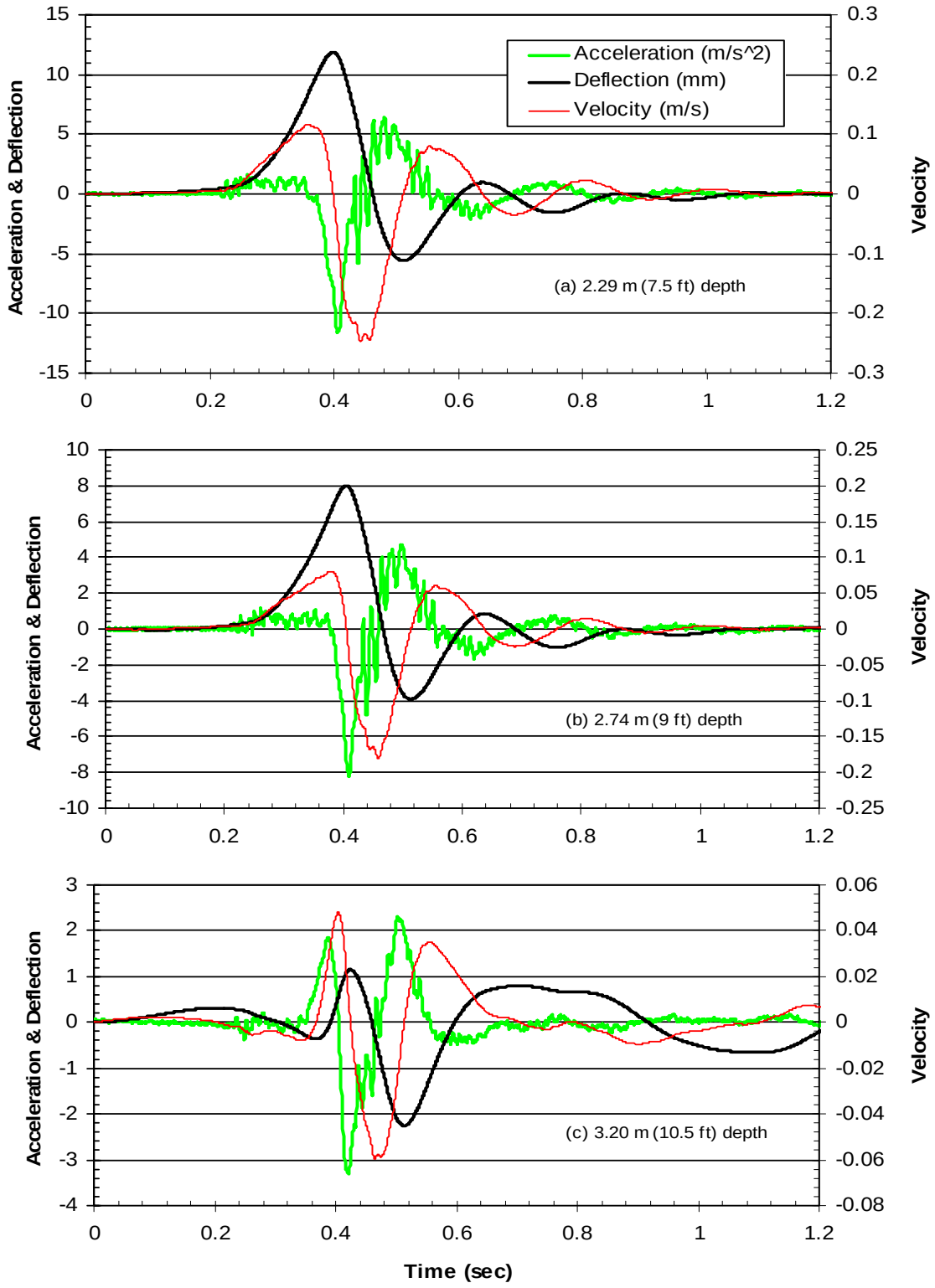

Figure A.50: 9-pile group, test 4—accelerometer time histories at (a) 2.29m (7.5ft), (b)2.74m (9.0ft), and (c) 3.20m (10.5ft) depths.

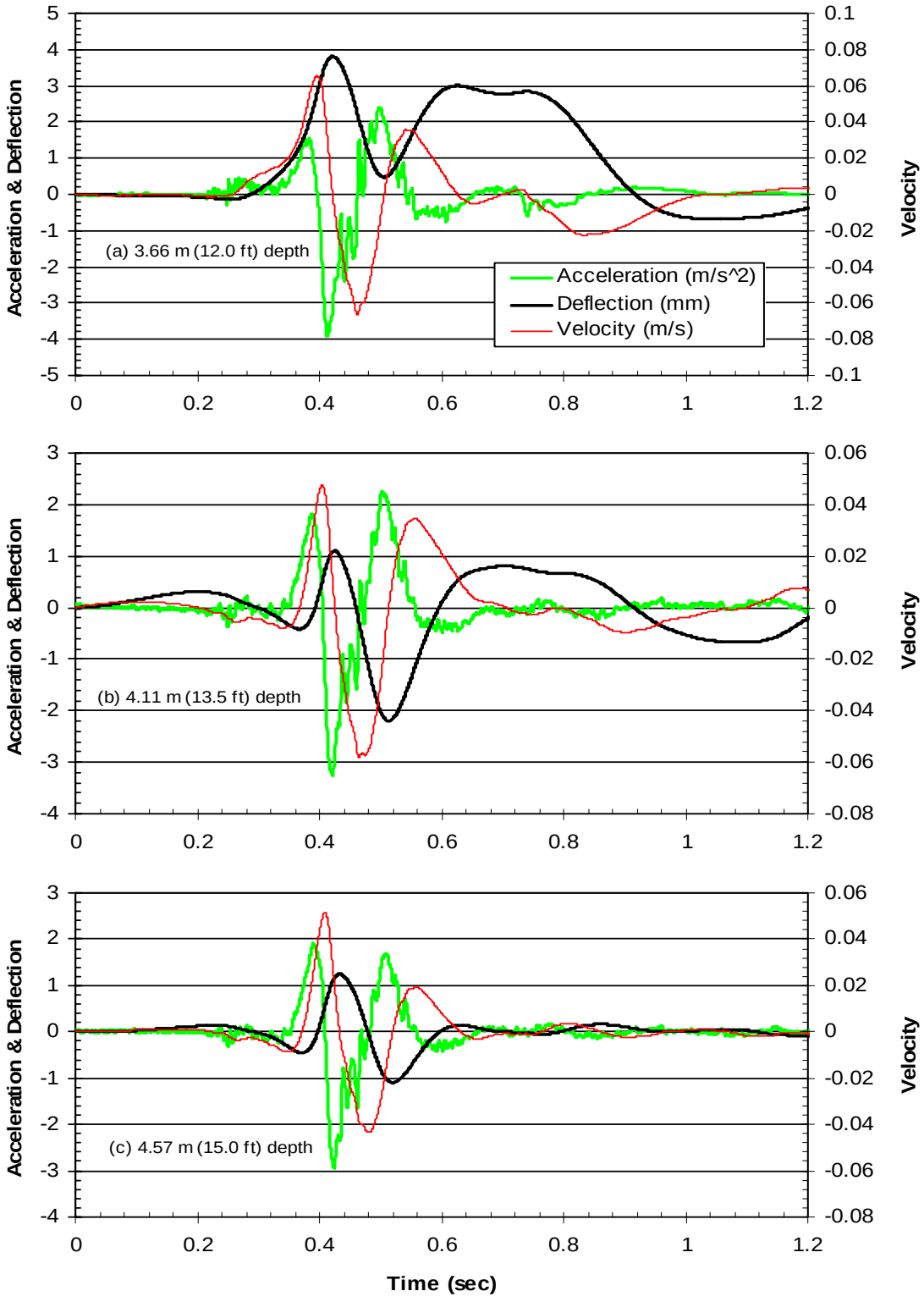

Figure A.51: 9-pile group, test 5—accelerometer time histories at (a) 3.66m (12.0ft), (b) 4.11m (13.5ft), and (c) 4.57m (15.0ft) depths.

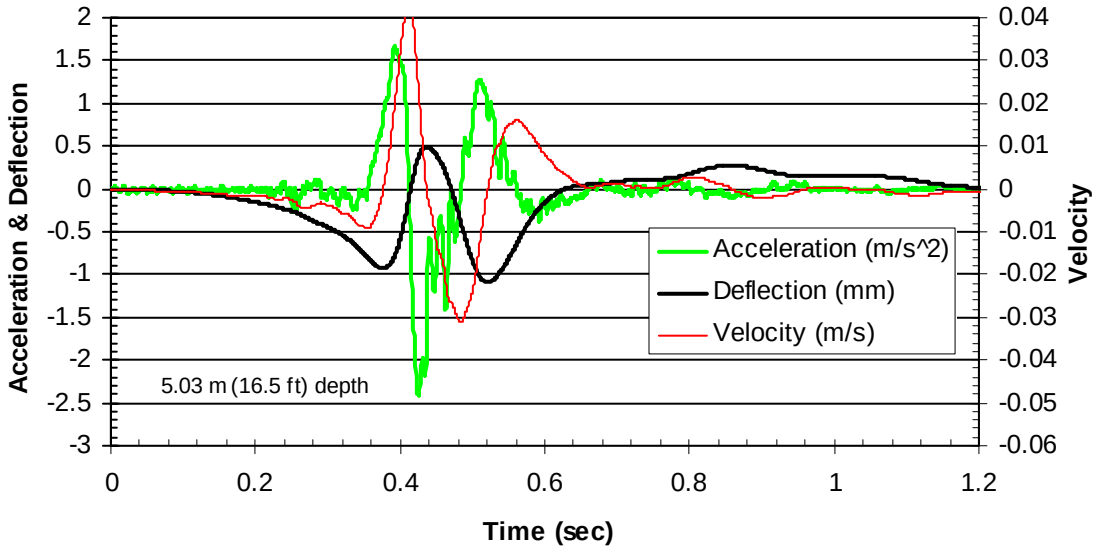

Figure A.52: 9-pile group, test 5—accelerometer time history at 5.03m (16.5ft) depth.